The TsdA family of thiosulfate dehydrogenases/tetrathionate reductases

Dissertation

zur

Erlangung des Doktorgrades (Dr. rer. nat.)

der

Mathematisch-Naturwissenschaftlichen Fakultät

der

Rheinischen Friedrich-Wilhelms-Universität Bonn

vorgelegt von

Julia Kurth

aus Düren

Bonn, Dezember 2016

Angefertigt mit Genehmigung der Mathematisch-Naturwissenschaftlichen Fakultät der
Rheinischen Friedrich-Wilhelms-Universität Bonn

1. Gutachterin: PD Dr. Christiane Dahl

2. Gutachter: Prof. Dr. Uwe Deppenmeier

Tag der Promotion: 22.03.2017

Erscheinungsjahr: 2017

Table of contents

I. Summary

TsdA enzymes are a phylogenetically widespread family of periplasmic *c*-type diheme cytochromes which catalyse both thiosulfate oxidation and tetrathionate reduction. The reaction directionality varies between enzymes isolated from different bacteria (**Chapter 1**) and is in line with their different physiological functions: TsdA enables the purple sulfur bacteria *Allochromatium vinosum* (*Av*) and *Marichromatium purpuratum* (*Mp*) to use thiosulfate as an electron donor for respiration or photosynthesis whereas the enzyme from the human gut pathogen *Campylobacter jejuni* (*Cj*) allows the organism to use tetrathionate as a terminal electron acceptor.

The bifunctionality of the TsdA enzyme allowed experimental determination of the reduction potential of the tetrathionate/thiosulfate couple $E_{TT/TS}$ (**Chapter 1**). This was very important as calculations from the relevant, constantly reevaluated thermodynamic data had yielded conflicting results. An $E_{TT/TS}$ value of +198 mV was obtained by experimental means which is much more positive than the value of +24 mV widely cited in the field of microbial bioenergetics. As a consequence more free energy is available to be harnessed during the respiratory reduction of tetrathionate to thiosulfate than was previously recognized and dissimilatory tetrathionate reduction is likely to be more prevalent in tetrathionate-containing environments such as the human gut or marine sediments than presently thought.

The TsdA active site heme, Heme 1, shows an unusual His/Cys ligation which appears to be of special importance in sulfur-based energy metabolism. Whereas this heme-ligating cysteine is conserved in TsdAs from different organisms, the ligand constellation of the electron transfer heme, Heme 2, differs depending on the source organism. In the case of *Av*TsdA, methionine ligates Heme 2 iron only in the reduced state. In contrast, in *Cj*TsdA this residue acts as a Heme 2 iron ligand already in the oxidized state (**Chapters 3 and 5**). In the case of *Cj*TsdA, the redox activity of the negative potential heme, Heme 1, reaches down to -650 mV and that of the positive potential heme, Heme 2, up to +300 mV (**Chapter 5**). Moreover, a strong cooperativity between the two TsdA hemes was observed. In addition to the heme-ligating methionine the adjacent amino acids asparagine and lysine also play key roles in the physiological function of *Cj*TsdA (**Chapter 3)**. *In vitro* as well as *in vivo* experiments with *Cj*TsdA revealed that structural differences in the immediate environment of Heme 2 contribute to defining the reaction directionality.

An essential part of the TsdA reaction cycle is the covalent linkage between thiosulfate and the heme-ligating cysteine in the active site (**Chapter 2**) involving electron transfer to or from the TsdA hemes, respectively. In addition, a thiol-disulfide exchange is an important step of the TsdA reaction mechanism. To get a closer insight into the TsdA reaction mechanism, sulfite which was shown to be a competitive inhibitor of TsdA can be used as substrate mimic (**Chapter 5**). Hints were obtained that the covalent linkage of a sulfur species to the active site cysteine is the rate-defining step within the TsdA reaction cycle. Furthermore, a positive shift in the Heme 1 reduction potential is assumed to occur during formation of this covalent bond facilitating electron transfer during the reaction cycle.

The diheme cytochrome *c* TsdB acts as an effective electron acceptor of TsdA *in vitro* when TsdA and TsdB originate from the same source organism. When present, the diheme cytochrome *c* TsdB is the immediate electron acceptor of TsdA-type thiosulfate dehydrogenases (**Chapter 2**). For *Av*TsdA and the *Mp*TsdBA fusion protein the high potential iron-sulfur protein HiPIP was identified as a suitable electron acceptor.

In contrast to all other *tsdA* containing organisms, the *tsdA* gene from *Wolinella succinogenes* is preceded by *tsdC*. TsdC from *W. succinogenes* is a novel and unique membrane attached lipoprotein that directly interacts with TsdA and does not contain prosthetic groups (**Chapter 4**). Similar to *Cj*TsdA, TsdA from *W. succinogenes* predominantly acts as a tetrathionate reductase. In contrast to the situation in *C. jejuni*, a membrane attachment of the tetrathionate reductase by the lipoprotein TsdC seems to be indispensable for tetrathionate reduction in *W. succinogenes*.

Chapter 6 gives a short overview on TsdA enzymes.

II. Introduction

1. Thiosulfate and tetrathionate in microbial physiology

Thiosulfate ($S_2O_3^{2-}$) and tetrathionate ($S_4O_6^{2-}$) are inorganic sulfur compounds that are used by many bacteria as an electron donor or acceptor, respectively. The two sulfur ions are interconverted according to the reaction $2\ S_2O_3^{2} \leftrightarrow\ S_4O_6^{2-} + 2\ e^-$. Thiosulfate and tetrathionate play an important role in the biogeochemical sulfur cycle as shown in Figure 1 (Podgorsek and Imhoff, 1999; Zopfi *et al.*, 2004)

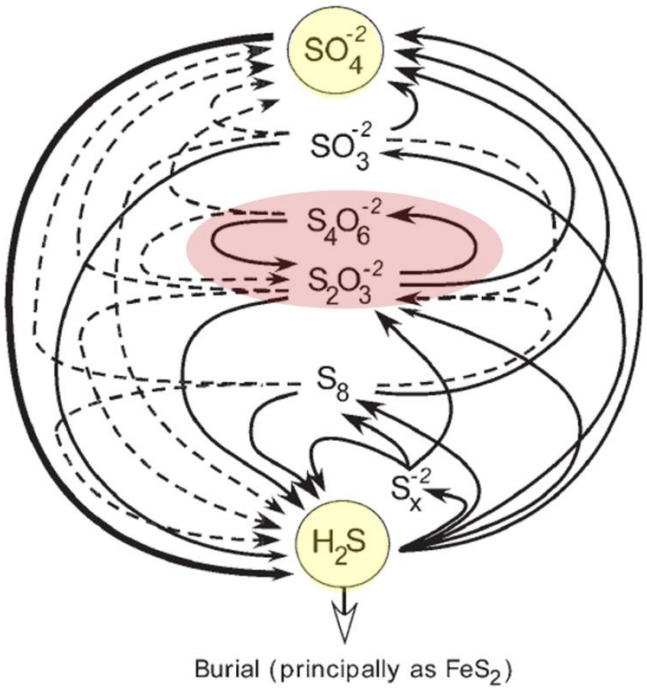

Figure 1: The sedimentary sulfur cycle. Important reductive (left-side, downward arrows) and oxidative (right-side, upward arrows) pathways are shown. Broken lines indicate bacterial disproportionation reactions. The degradation of organic matter through sulfate-reducing bacteria (thick arrow on the left) is very important for the sulfur cycle. The dominant sink for reduced sulfur in marine sediments is represented by burial of iron-sulfur minerals, mostly FeS_2. Figure modified after Zopfi *et al.*, 2004.

Thiosulfate and tetrathionate are reported to be present in most soils (Starkey, 1950). Thiosulfate has also been found in significant quantities at the oxygen-sulfide interfaces of the sea (Sorokin, 1970; Tuttle and Jannasch, 1973a) and even in surface waters of the open ocean (Tilton *et al.*, 1967). Therefore, it is not surprising that heterotrophic or facultatively chemolithotrophic bacteria which oxidize thiosulfate appear to be widespread in the marine environment (Tuttle and Jannasch, 1972; Tuttle and Jannasch, 1976).

In a complex web of competing chemical and biological reactions, most of the sulfide produced in surface marine sediments is oxidized back to sulfate via intermediate sulfur

compounds like thiosulfate and tetrathionate (Zopfi *et al.*, 2004; Figure 1). Tetrathionate is produced by considerable numbers of sulfur oxidizing bacteria in marine sediments (Podgorsek and Imhoff, 1999). In their habitat, these bacteria are important for oxidation of reduced sulfur compounds like thiosulfate with tetrathionate as an important oxidation product. In natural marine and brackish water sediments a net oxidation of sulfide to sulfur occurs in the presence of catalytic amounts of thiosulfate and tetrathionate due to combined bacterial action and chemical reactions (Podgorsek and Imhoff, 1999; Figure 2). Tetrathionate is a quite unstable sulfur compound and a chemical reaction with sulfide leads to production of the more stable compounds thiosulfate and sulfur (Figure 2).

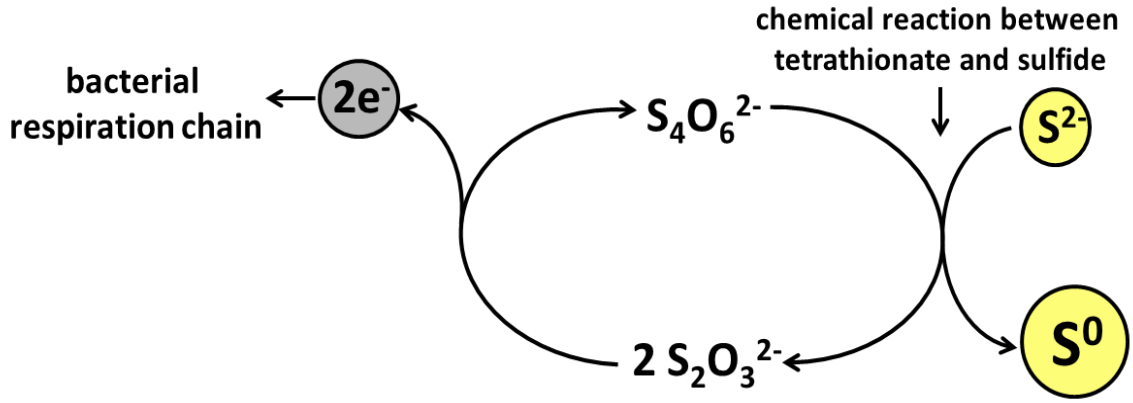

Figure 2: The tetrathionate cycle. The bacterial thiosulfate oxidation to tetrathionate in combination with the chemical reactions between sulfide and tetrathionate leads to a cyclic reaction sequence (Roy and Trudinger, 1970). The formation of elemental sulfur results in an accumulation of sulfur in marine sediments. Such a cycle has been proposed on the basis of pure culture studies with *Catenococcus thiocyclus* by Sorokin *et al.*, 1996. Figure modified after Podgorsek and Imhoff, 1999.

The rapid reduction of tetrathionate back to thiosulfate has the effect that the biological oxidation of thiosulfate is the rate-limiting step in the oxidative turnover of sulfur compounds in the sea (Tuttle and Jannasch, 1973a; Zopfi *et al.*, 2004).

2. Role of thiosulfate as electron donor

Thiosulfate can either be an intermediate product during oxidation of reduced sulfur compounds or it is used as electron donor in course of photosynthetic or respiratory electron transport chains. The ability to utilize reduced sulfur compounds as electron donors for anaerobic phototrophic and aerobic or anaerobic chemotrophic growth is phylogenetically widespread (Dahl, Friedrich, *et al.*, 2008). There are several chemoorganoheterotrophic bacteria that are able to oxidize reduced sulfur compounds like sulfide, thiosulfate and sulfur with tetrathionate as sole final product (Sorokin, 1996). The utilization of thiosulfate as an electron donor for aerobic growth is well documented among a number of bacteria, especially for the genus *Thiobacillus* (Barrett and Clark, 1987).

Tetrathionate-forming thiosulfate:acceptor oxidoreductases were found to be present in various chemotrophic bacteria like the sulfur-oxidizing bacteria *Thiobacillus thioparus* (Lyric and Suzuki, 1970)*, Thermithiobacillus tepidarius* (f. *Thiobacillus tepidarius*) (Lu and Kelly, 1988)*, Halothiobacillus neapolitanus* (Trudinger, 1961)*, Thiobacillus* sp. W5 (Visser *et al.*, 1997), which was shown to belong into the genus *Halothiobacillus* and is closely related to *H. neapolitanus* (Sievert *et al.*, 2000)*, Acidiphilium acidophilum* (f. *Thiobacillus acidophilus*) (Meulenberg *et al.*, 1993), *Acidithiobacillus thiooxidans* (Nakamura *et al.*, 2001)*, Acidithiobacillus ferrooxidans* (Silver and Lundgren, 1968; Janiczek *et al.*, 2007; Kikumoto *et al.*, 2013) as well as in *Alcaligenes* sp. (Hall and Berk, 1972), *Advenella mimigardefordensis* (f. *Tetrathiobacter kashmirensis*) (Dam *et al.*, 2007)*, Pseudomonas aeruginosa* (Schook and Berk, 1979) and other pseudomonads (Tuttle *et al.*, 1983; Sorokin *et al.*, 1999). In addition to those bacterial enzymes, tetrathionate-forming thiosulfate oxidoreductases are present in the thermoacidophilic archaeon *Acidianus ambivalens* (f. *Desulfurolobus ambivalens*) (Müller *et al.*, 2004), in a haloarchaeon (Sorokin *et al.*, 2005) and in the yeast *Rhodoturula* sp. (Kurek, 1985). In most cases the relevant enzyme has been purified from the organism, but it has not been characterized in detail.

Thiosulfate does not only play a role in microbial respiratory chains, but also in bacterial photosynthesis: There are several anoxygenic phototrophic bacteria that can use inorganic sulfur compounds like thiosulfate as electron donors for reductive carbon dioxide fixation during photolithoautotrophic growth (Brune, 1989; Frigaard and Dahl, 2009). The formation of tetrathionate from thiosulfate has been described for the green sulfur bacterium *Chlorobium limicola* (f. *C. thiosulfatophilum*) (Kusai and Yamanaka, 1973), the purple non-sulfur bacteria *Rhodopseudomonas palustris* (Schleifer *et al.*, 1981) and *Rhodopila globiformis* (Then and Trüper, 1981) as well as for the purple sulfur bacterium *Allochromatium vinosum* (f. *Chromatium vinosum*) (Smith, 1966; Knobloch *et al.*, 1981; Schmitt *et al.*, 1981; Hensen *et al.*, 2006; Denkmann *et al.*, 2012). The latter can oxidize thiosulfate either to tetrathionate or sulfate. Tetrathionate is the main product of thiosulfate oxidation under acidic conditions (Smith, 1966).

As described above tetrathionate production from thiosulfate is performed by a number of microorganisms. However, this reaction is not as bioenergetically favored as sulfate production from thiosulfate (Thauer *et al.*, 1977). Thiosulfate oxidation to tetrathionate is energetically even less favorable than previously thought as revealed by the latest determination of the tetrathionate/thiosulfate reduction potential $E_{TT/TS}$ (Kurth *et al.*, 2015, **Chapter 1**). The calculated values for $E_{TT/TS}$ stated in literature range from +24 to +300 mV versus SHE (Standard hydrogen electrode) (Cobble *et al.*, 1972; Kaprálek, 1972; Thauer *et al.*, 1977; Williamson and Rimstidt, 1992). This variation is due to the irreversible nature of the thiosulfate/tetrathionate interconversion at an inert electrode (Bard *et al.*, 1985; Pourbaix

and Pourbaix, 1992) precluding a direct measurement of $E_{TT/TS}$. Catalytic protein film electrochemistry with a bifunctional thiosulfate oxidizing and tetrathionate reducing enzyme provided a direct measure for $E_{TT/TS}$ (Kurth *et al.*, 2015; **Chapter 1**). The determined value is +198 mV vs. SHE, which is much more positive than the value of +24 mV (Thauer *et al.*, 1977) widely cited in the field of microbial bioenergetics. As a consequence less free energy is available to be harnessed during the respiratory oxidation of thiosulfate to tetrathionate than was previously recognized. Nonetheless, thiosulfate is used as electron donor by many bacteria as mentioned before. It is assumed that electrons from the thiosulfate oxidation are fed into the respiratory chain at the level of cytochrome *c* (Drozd, 1977; Visser et al., 1997).

2.1. Thiosulfate-oxidizing enzymes

There are several ways of oxidizing thiosulfate. One possibility is the oxidation of thiosulfate to sulfate without the transient release of reaction intermediates. This reaction is catalyzed by the periplasmic Sox system, a multienzyme complex. The Sox sulfur oxidation enzyme system is widely distributed among sulfur-oxidizing bacteria that oxidize thiosulfate to sulfate (Meyer *et al.*, 2007). The Sox-mediated oxidation of thiosulfate to sulfate without the appearance of sulfur deposits as intermediates occurs in several facultatively chemo- or photolithotrophic organisms (Appia-Ayme *et al.*, 2001; Friedrich *et al.*, 2001). A mechanism for this reaction has been postulated for *Paracoccus pantotrophus* by Friedrich and coworkers (Friedrich *et al.*, 2001; Figure 3).

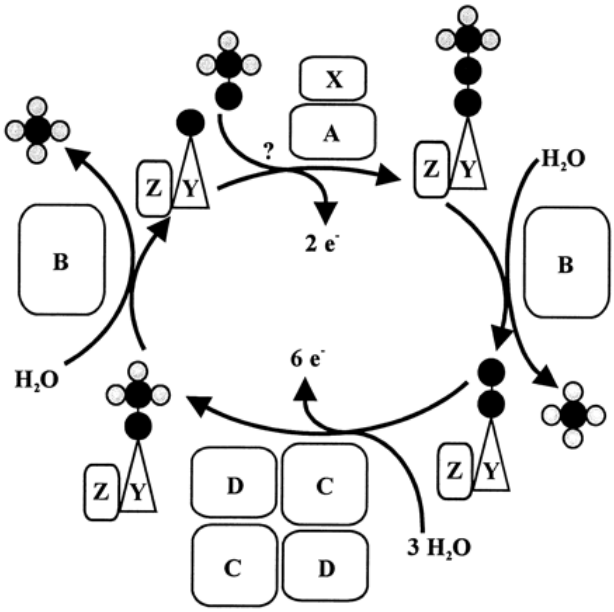

Figure 3: Model of Sox mechanism of thiosulfate oxidation in *P. pantotrophus*. SoxXA catalyzes a two-electron oxidation in which the sulfane sulfur of thiosulfate is linked to a cysteine residue of SoxY to produce SoxY-thiocysteine-S-sulfate. SoxB hydrolyzes sulfate from the thiocysteine-S-sulfate residue to give S-thiocysteine. SoxCD then oxidizes the outer sulfur atom to SoxY-cysteine-S-sulfate. Finally, sulfate is again hydrolyzed and removed by SoxB to regenerate the cysteine residue of SoxY (Friedrich *et al.*, 2001). Full circles represent sulfur atoms, whilst oxygen atoms are shown as open circles. Figure taken from Friedrich *et al.*, 2001.

The Sox-mediated oxidation of thiosulfate to sulfate involving formation of sulfur globules occurs in many environmentally important sulfur oxidizers including the phototrophic green and purple sulfur bacteria and free-living and symbiotic chemotrophic sulfur oxidizers like *Beggiatoa* or *Thiothrix* (Dahl, 1999; Dahl and Prange, 2006). For the purple sulfur bacterium *Allochromatium vinosum* it was shown that the intermediary formation of sulfur globules is related to the lack of *soxCD* genes, the products of which are proposed to oxidize the sulfane sulfur bound to SoxY (Hensen *et al.*, 2006). In *A. vinosum* the sulfane sulfur is assumed to be transferred to sulfur globules instead.

Another way for thiosulfate oxidation to proceed besides sulfate formation via the Sox multienzyme complex is the formation of tetrathionate catalyzed by thiosulfate:acceptor oxidoreductases. As mentioned above such an enzyme was purified and characterized from several phototrophic and chemotrophic bacteria. To date there are two different enzymes known to catalyze the aforementioned reaction: A soluble thiosulfate:ferricytochrome *c* oxidoreductase (EC 1.8.2.2) and a membrane-bound thiosulfate:quinone oxidoreductase (EC 1.8.5.2). In most cases, genes encoding the relevant enzymes have not been identified until now. A membrane-bound thiosulfate-oxidizing and quinone-reducing enzyme so far has only been purified and characterized from the thermoacidophilic archaeon *Acidianus ambivalens* (f. *Desulfurolobus ambivalens*) (Müller *et al.*, 2004).

In the case of the soluble thiosulfate:ferricytochrome *c* oxidoreductases the described characteristics vary considerably depending on the source organisms. All of the described enzymes can use ferricyanide as electron acceptor *in vitro*. In addition, enzymes from most organisms are able to reduce either mammalian cytochrome *c* (Trudinger, 1961; Lyric and Suzuki, 1970; Hall and Berk, 1972; Schook and Berk, 1979; Lu and Kelly, 1988; Meulenberg *et al.*, 1993) and/or native cytochrome *c* (Trudinger, 1961; Hall and Berk, 1972; Kusai and Yamanaka, 1973; Schook and Berk, 1979; Knobloch *et al.*, 1981; Schleifer *et al.*, 1981; Schmitt *et al.*, 1981; Then and Trüper, 1981; Tuttle *et al.*, 1983; Kurek, 1985; Lu and Kelly, 1988; Visser *et al.*, 1997). For the thiosulfate oxidoreductase from the phototrophic bacteria *A. vinosum* and *R. palustris* (Knobloch *et al.*, 1981) as well as from the chemotrophic bacteria *T. tepidarius* (Lu and Kelly, 1988), *A. thiooxidans* (Nakamura *et al.*, 2001) and *Thiobacillus* sp. W5 (Visser *et al.*, 1997) a periplasmic localization of the enzyme has been described. Moreover, the availability and type of prosthetic group differs from enzyme to enzyme. The thiosulfate oxidizing enzymes from *A. acidophilum* (Meulenberg *et al.*, 1993), *Thiobacillus* sp. W5 (Visser *et al.*, 1997), *A. thiooxidans* (Nakamura *et al.*, 2001) and *A. vinosum* (Hensen *et al.*, 2006) are cytochromes, whereas the enzyme from *T. thioparus* (Lyric and Suzuki, 1970) binds two molecules non-heme iron and for the other characterized enzymes no prosthetic group was described. Furthermore, there is a huge difference in the molecular weight and number of subunits of the enzymes. The enzyme from *A. acidophilum*

exhibits an $\alpha_2\beta_2$ structure with two 20 kDa and two 24 kDa subunits (Meulenberg *et al.*, 1993), that of *Thiobacillus* sp. W5 an $\alpha_2\beta_2$ structure with two 27 kDa and two 33 kDa subunits (Visser *et al.*, 1997), that of *T. tepidarius* an α_3 structure with three 45 kDa subunits (Lu and Kelly, 1988) and that of *R. palustris* an α_2 structure with two 48 kDa subunits (Schleifer *et al.*, 1981). The molecular weight of enzyme monomers varies from about 30 kDa in *A. vinosum* (Schmitt *et al.*, 1981; Hensen *et al.*, 2006) and *A. thiooxidans* (Nakamura *et al.*, 2001) to 115 kDa in *T. thioparus* (Lyric and Suzuki, 1970). The heterogeneity of organisms with soluble thiosulfate:ferricytochrome *c* oxidoreductase and the diversity of the structure of various characterized enzymes lead to the conclusion that this enzyme class has evolved by convergent evolution (Visser *et al.*, 1997).

There are only two thiosulfate oxidoreductases that have been characterized on a molecular genetic level so far: One of these enzymes is the periplasmic thiosulfate dehydrogenase TsdA first studied from the purple sulfur bacterium *A. vinosum* (*Av*TsdA) (Denkmann *et al.*, 2012) and the other enzyme is the membrane-bound tetrathionate-forming thiosulfate:quinone oxidoreductase from the archaeon *A. ambivalens* (Figure 4). The latter consists of a 28 kDa (DoxA) and a 16 kDa (DoxD) subunit (Müller *et al.*, 2004). A mixture of caldariella quinone, sulfolobus quinone and menaquinone was non-covalently bound to the protein, but no other cofactors were detected. It has been shown that caldariella quinone shuttles electrons between the thiosulfate oxidoreductase and the terminal quinol oxidase (Müller *et al.*, 2004).

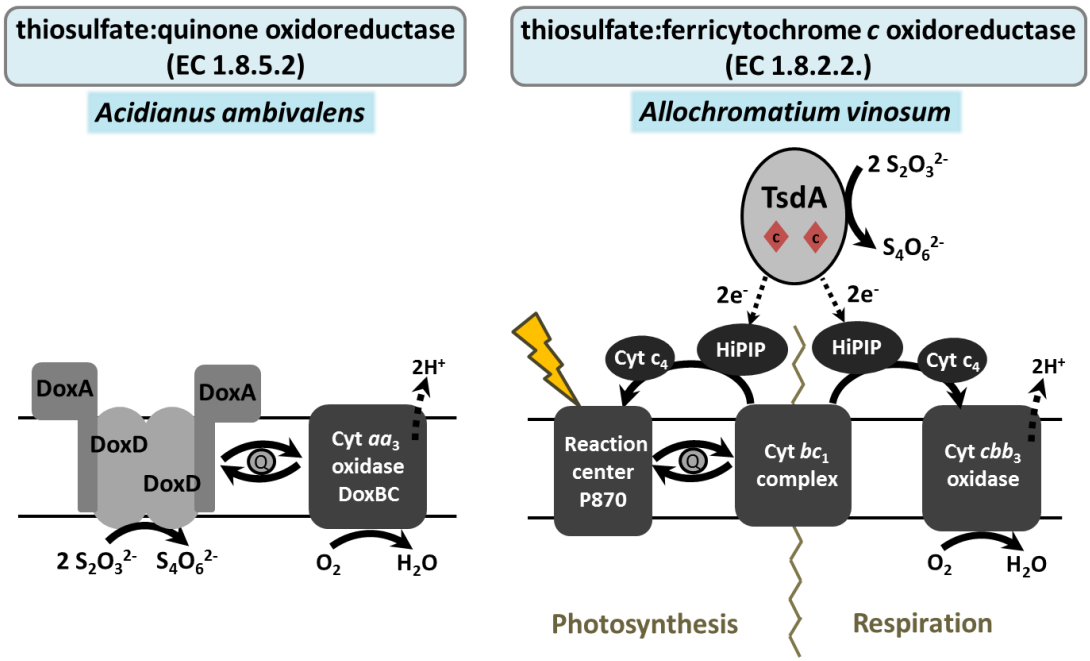

Figure 4: Thiosulfate:acceptor oxidoreductases. A model for the membrane-bound thiosulfate-oxidizing and quinone-reducing enzyme from *A. ambivalens* (Müller *et al.*, 2004) and for the periplasmic thiosulfate dehydrogenase TsdA from *A. vinosum* (Brito *et al.*, 2015; Kurth, Brito *et al.*, 2016) is shown. Those two enzymes are the only thiosulfate:acceptor oxidoreductases characterized on a molecular genetic level so far.

In contrast to this membrane-bound enzyme, the periplasmic thiosulfate dehydrogenase TsdA from *A. vinosum* is a diheme *c*-type cytochrome (Hensen *et al.*, 2006; Denkmann *et al.*, 2012). This enzyme enables *A. vinosum* to use the electrons from thiosulfate-oxidation for photosynthesis (Kurth, Brito *et al.*, 2016; **Chapter 2**, Figure 4).

The thiosulfate-oxidizing enzyme from *A. vinosum* has been studied over several decades (Smith, 1966; Fukumori and Yamanaka, 1979; Knobloch *et al.*, 1981; Schmitt *et al.*, 1981; Hensen *et al.*, 2006), but the gene *tsdA* (Alvin_0091) encoding this enzyme was only identified in 2012 (Denkmann *et al.*, 2012). This gene has been found to be very widespread not only among all branches of the *Proteobacteria* but also in Gram-positive bacteria like *Brevibacillus brevis* or *Lysinibacillus sphaericus* (Denkmann *et al.*, 2012). Besides TsdA from *A. vinosum*, pronounced thiosulfate-oxidizing activity has been demonstrated for the relevant enzyme from another phototrophic γ-proteobacterium, *Marichromatium purpuratum* (Kurth *et al.*, 2015; Kurth, Brito *et al.*, 2016; **Chapters 1 and 2**), for the enzymes from the chemotrophic β-proteobacteria *Thiomonas intermedia* (Denkmann *et al.*, 2012) and *Sideroxydans lithotrophicus* (Kurth, Brito *et al.*, 2016; Kurth, Schuster *et al.*, 2016; **Chapters 2 and 4**) as well as for the enzymes from the chemotrophic γ-proteobacteria *Pseudomonas stutzeri* and *Psychrobacter arcticus* (Denkmann *et al.*, 2012).

With regard to the wide distribution of TsdA, enzymes from several bacteria that have been described to oxidize thiosulfate and form tetrathionate might belong to the TsdA family. For example, the thiosulfate-oxidizing and tetrathionate-forming ability of several pseudomonads (Schook and Berk, 1979; Tuttle, 1980; Sorokin *et al.*, 1999) might be linked to the TsdA enzyme, as *Pseudomonas stutzeri* possesses a *tsdA* gene encoding an active TsdA enzyme (Denkmann *et al.*, 2012). In addition, *R. palustris* has been shown to produce a thiosulfate-oxidizing enzyme (Schleifer *et al.*, 1981) and possesses a gene, RPA2013, that encodes a tetraheme cytochrome *c* with a C-terminus bearing 43% sequence identity to Alvin_0091. The *H. neapolitanus* gene Hneap_1476 encodes a 31 kDa (without signal peptide) diheme cytochrome *c* exhibiting 37 % sequence identity to Alvin_0091. *H. neapolitanus* as well as the closely related bacterium *Thiobacillus* sp. W5 produce thiosulfate-oxidizing enzymes (Trudinger, 1961; Visser *et al.*, 1997) that therefore might belong to the TsdA family. While there are several formerly described thiosulfate-oxidizing enzymes that can be related to TsdA, there are also tetrathionate-forming thiosulfate oxidoreductases that do not belong to the TsdA or DoxAD family. For example, the gram-positive bacteria *Bacillus megaterium* and *Bacillus globigii,* which have been shown to oxidize thiosulfate to tetrathionate (Mason and Kelly, 1988), do not contain a *tsdA* or *doxAD* homologous gene (Denkmann *et al.*, 2012).

2.2. Electron acceptors for thiosulfate dehydrogenases

In the late 1990s Visser and colleagues described the thiosulfate dehydrogenase from the *H. neapolitanus* related strain *Thiobacillus* sp. W5 as a heterotetramer consisting of two different heme *c* containing subunits of about 33 and 27 kDa (Visser *et al.*, 1997). The genome of *H. neapolitanus* possesses a *tsdA* homologue, Hneap_1476, which is predicted to encode a 31 kDa (without signal peptide; without hemes) diheme cytochrome *c*. This gene is immediately preceded by the gene Hneap_1477 that is predicted to encode a 20 kDa (without signal peptide; without hemes) diheme cytochrome *c*. In a number of organisms, including *Thiomonas intermedia, Pseudomonas stutzeri* and *Sideroxydans lithotrophicus,* the *tsdA* gene is immediately preceded by a gene encoding another diheme cytochrome *c*, *tsdB* (Denkmann *et al.*, 2012). A strong interaction between TsdA and TsdB was verified (Denkmann *et al.*, 2012; Kurth, Brito *et al.*, 2016).

In subsequent experiments the redox properties and the interaction of TsdA and TsdB were analyzed in more detail (Kurth, Brito *et al.*, 2016; **Chapter 2**). Spectrophotometric experiments in combination with enzymatic assays in solution revealed that TsdB acts as an effective electron acceptor of TsdA *in vitro* when TsdA and TsdB originate from the same source organism. As TsdA covers a range from -300 mV to +150 mV and TsdB is redox active between -100 to +300 mV electron transfer between those cytochromes is feasible.

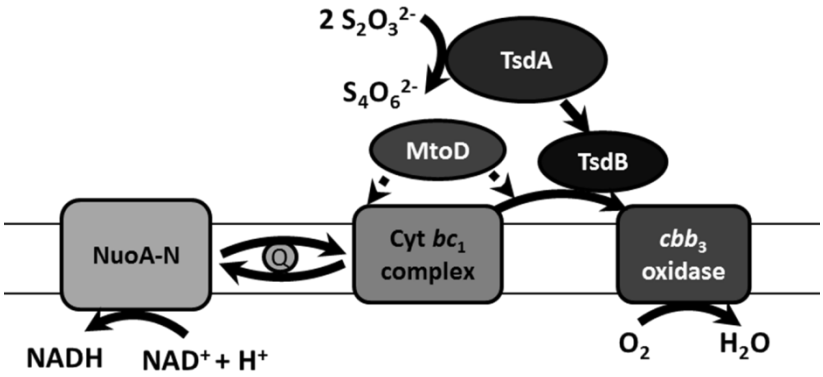

Figure 5: Role of periplasmic electron transfer proteins in aerobic respiration of *S. lithotrophicus* and *T. intermedia.* Both organisms contain genes for NuoA-N (Slit_1070-1083, Tint_2255-2268), cytochrome bc_1 complex (Slit_0130-0132, Tint_2192-2194) and cbb_3 oxidase (Slit_0411-0414, Tint_1070-1073). For *S. lithotrophicus* it is assumed that MtoD (Slit_2498) can transfer electrons to cbb_3 oxidase and the cytochrome bc_1 complex (Beckwith *et al.*, 2015). Figure extracted from Kurth, Brito *et al.*, 2016.

For the chemotrophic bacteria *Thiomonas intermedia* and *Sideroxydans lithotrophicus* it is assumed that there is either a direct interaction between TsdB and cbb_3 oxidase or that MtoD or an MtoD-like protein serves as electron shuttle to the respiratory terminal oxidase (Kurth, Brito *et al.*, 2016; Figure 5).

The anoxygenic phototrophic purple sulfur bacterium *Marichromatium purpuratum* possesses a *tsdB-tsdA* gene-fusion in its genome. The three-dimensional structure of the TsdB-TsdA fusion protein from *Marichromatium purpuratum* (*Mp*TsdBA) was solved by X-ray crystallography (Kurth, Brito *et al.*, 2016; **Chapter 2**) providing insights into internal electron transfer.

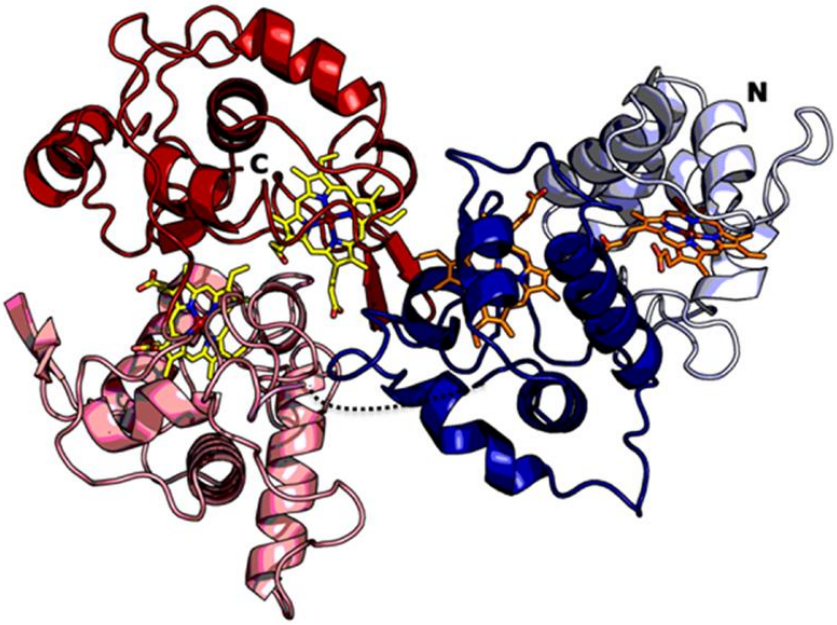

Figure 6: Crystal structure of *Mp*TsdBA. Overall fold with TsdB N-terminal domain depicted in blue and TsdA C-terminal domain in red; the two shades in each domain represent the respective sub-domains. The heme prosthetic groups are colored by atom type (orange or yellow for carbon, blue for nitrogen, red for oxygen and dark red for iron). Figure extracted from Kurth, Brito *et al.*, 2016.

In several bacteria such as *A. vinosum*, TsdB is not present, precluding a general and essential role of TsdB in TsdA related electron transfer. A candidate for accepting electrons from *Av*TsdA is the high potential iron-sulfur protein HiPIP. In 1979 Fukumori and Yamanaka showed that *Av*TsdA rapidly reduces HiPIP *in vitro* (Fukumori and Yamanaka, 1979). The reduction potential of HiPIP from *A. vinosum* is +350 mV (Bartsch, 1978) and therefore more positive than that of *Av*TsdA, covering a range from -300 mV to +150 mV, which makes electron transfer from TsdA to HiPIP feasible (Kurth, Brito *et al.*, 2016; **Chapter 2**). The purple sulfur bacteria *A. vinosum* and *M. purpuratum* both encode HiPIP in their genome. *Av*TsdA and *Mp*TsdBA were shown to react efficiently with HiPIP *in vitro* identifying HiPIP as a suitable electron acceptor for those proteins (Kurth, Brito *et al.*, 2016). Thus, HiPIP is the most likely electron carrier between Tsd(B)A and the reaction center during growth in the light or the terminal oxidase during oxygen respiration in organisms containing HiPIP (Kurth, Brito *et al.*, 2016; **Chapter 2;** Figure 7).

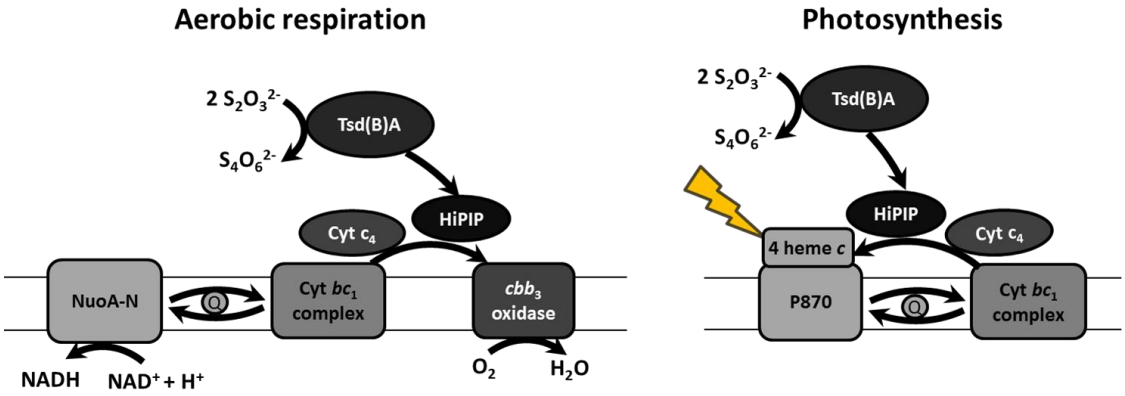

Figure 7: Role of periplasmic electron transfer proteins in aerobic respiration or photosynthesis of *A. vinosum* and *M. purpuratum.* Both organisms contain genes for NuoA-N (Alvin_2418-2430 and Alvin_2412, Marpu_04365-04430), cytochrome bc_1 complex (Alvin_0068-0070, Marpu_01465-01475) and cbb_3 oxidase (Alvin_0781-0784, Marpu_02795-02810). Moreover, *A. vinosum* and *M. purpuratum* can gain energy by photosynthetic growth. HiPIP can transfer electrons to the photosynthetic reaction center (Kennel *et al.*, 1972; Bartsch, 1991) as well as to cbb_3 oxidase (Hochkoeppler, Kofod, *et al.*, 1995; Bonora *et al.*, 1999). Cytochrome c_4 also is known to transfer electrons to the photosynthetic reaction center (Ohmine *et al.*, 2009) as well as to cbb_3 oxidase (Chang *et al.*, 2010; Arai *et al.*, 2014; Barco *et al.*, 2015) in some bacteria. Figure extracted from Kurth, Brito *et al.*, 2016.

3. Role of tetrathionate as electron acceptor

As mentioned before, thiosulfate and tetrathionate are reported to be present in most soils (Starkey, 1950) and in the marine environment (Tilton *et al.*, 1967; Sorokin, 1970; Tuttle and Jannasch, 1973a; Podgorsek and Imhoff, 1999). As thiosulfate is converted to tetrathionate and the produced tetrathionate then undergoes bacterial tetrathionate reduction and chemical reactions (Podgorsek and Imhoff, 1999), any thiosulfate containing environment is potentially suitable for tetrathionate reduction. Because of the close linkage between thiosulfate oxidation and tetrathionate reduction in certain environments, it is not surprising that some bacteria are able to oxidize thiosulfate and to reduce tetrathionate as well. This ability has been described for the marine pseudomonad strain 16B (Tuttle, 1980), for a heterotrophic bacterium isolated from soil (Trudinger, 1967) and for some heterotrophic bacteria isolated from aquatic environments (Sorokin, 1992), for example.

For sulfate-reducing bacteria tetrathionate reduction is less well studied than the reduction of sulfate and sulfite. In sulfate-reducing bacteria tetrathionate is completely reduced to sulfide (Barrett and Clark, 1987). For a *Desulfovibrio* strain (a strain now designated as *Desulfovibrio vulgaris*) it has been shown that the organism quantitatively reduces tetrathionate to sulfide with hydrogen as reductant indicating that tetrathionate can serve as an electron acceptor for sulfate-reducing bacteria (Postgate, 1951). Tetrathionate reduction is energetically more favorable than sulfate reduction. Thus, tetrathionate might be a profitable electron acceptor when the electron donating substrate is limited, which is the typical situation in most sediments (Zopfi *et al.*, 2004).

Pollock and coworkers discovered the reduction of tetrathionate in facultatively anaerobic bacteria of the intestinal tract such as *Salmonella* or *Proteus* (Pollock *et al.*, 1942; Pollock and Knox, 1943). It was suggested that tetrathionate acts as an alternative electron acceptor to O_2 when using hydrogen as electron donor and that under anaerobic conditions tetrathionate would favor the growth of those organisms which can reduce it (Pollock and Knox, 1943). In 1973 Tuttle and Jannasch reported dissimilatory reduction of tetrathionate by facultatively anaerobic marine bacteria (Tuttle and Jannasch, 1973b). Kaprálek observed that tetrathionate reduction by anaerobically grown *Citrobacter* causes a significant rise in specific growth rate and molar growth yield (Kaprálek, 1972). The ability to reduce tetrathionate is widespread among Enterobacteriaceae and *Salmonella*, *Citrobacter* and *Proteus* strains are usually tetrathionate reductase-positive (Papavassiliou *et al.*, 1969). Furthermore, the enzymatic reduction of tetrathionate by facultative anaerobic bacteria was studied in more detail by Pichinoty and Bigliardi-Rouvier (Pichinoty and Bigliardi-Rouvier, 1963). The synthesis of an irreversible tetrathionate reductase in facultative anaerobic bacteria including *Escherichia intermedia* was found to be suppressed by oxygen (Pichinoty and Bigliardi-Rouvier, 1962; Pichinoty and Bigliardi-Rouvier, 1963).

As mentioned before, the recently determined value of the thiosulfate/tetrathionate reduction potential $E_{TT/TS}$ is +198 mV, which is much more positive than the value of +24 mV (Thauer *et al.*, 1977) widely cited in the field of microbial bioenergetics.

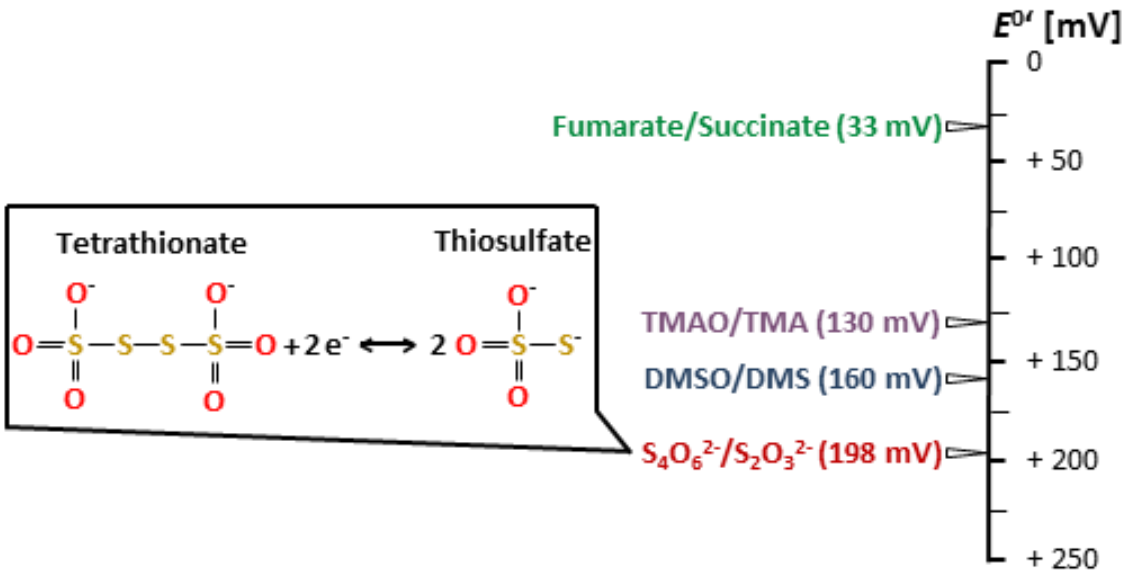

Figure 8: Reduction potential of the tetrathionate/thiosulfate couple ($E_{TT/TS}$). $E_{TT/TS}$ is shown in comparison to other redox couples with reduction potentials between +25 and +200 mV that are relevant for bacterial respiratory chains. Figure taken from Kurth *et al.*, 2015.

The re-determined $E_{TT/TS}$ value is more positive than the corresponding E_m values for several prevalent terminal respiratory electron-acceptor couples at neutral pH (Figure 8). For this reason, tetrathionate appears to be a quite favorable electron acceptor for bacterial

respiration. As oxidative phosphorylation can be facilitated by both trimethylamine oxide reduction (Barrett and Kwan, 1985) and fumarate reduction (Miki and Lin, 1975), it can be assumed that tetrathionate with a more positive reduction potential can serve as an electron acceptor for oxidative phosphorylation in tetrathionate-reducing bacteria.

Thiosulfate and tetrathionate have gained increased attention with regard to the mammalian gut in recent years. First it was discovered that thiosulfate is produced during the detoxification of highly toxic thiols: Hydrogen sulfide and methanethiol produced by gut bacteria are oxidized to thiosulfate as a specialized function of the colonic mucosa (Furne *et al.*, 2001). Secondly it was shown that reactive oxygen species generated during inflammation in the gut react with sulfur compounds like thiosulfate to form tetrathionate (Winter *et al.*, 2010). It has been shown that the human gut pathogen *Salmonella enterica* serotype *typhimurium* (*S. typhimurium*) induces host-driven production of tetrathionate that allows the pathogen to use tetrathionate as an electron acceptor resulting in a growth advantage for this organism over the competing microbiota in the inflamed gut (Winter *et al.*, 2010). In addition to *Salmonella*, tetrathionate also stimulates growth of the microaerophilic human gut pathogen *Campylobacter jejuni* (Liu *et al.*, 2013). It is suggested that the ability to trigger intestinal inflammation and the ability to use tetrathionate as electron acceptor is crucial for the biology of *S. typhimurium* (Winter *et al.*, 2010) and maybe further intestinal pathogens. In addition, for marine microbiota tetrathionate represents a more favorable electron acceptor than the highly abundant compounds dimethyl sulfoxide and trimethylamine oxide (Barrett and Kwan, 1985) at neutral pH. Dissimilatory tetrathionate reduction is likely to be more prevalent than presently thought in tetrathionate-containing environments such as the human gut or marine sediments (Kurth *et al.*, 2015; **Chapter 1**).

3.1. Tetrathionate-reducing enzymes

As mentioned before, the ability to reduce tetrathionate has been described for several bacteria. At this stage not much was known about the enzymes catalyzing tetrathionate reduction. For the tetrathionate-reducing enzyme from the marine pseudomonad 16B it has been assumed that the enzyme is a reversible thiosulfate oxidase/tetrathionate reductase (Tuttle, 1980; Whited and Tuttle, 1983), but the enzyme has not been characterized in detail.

Until now there are three types of tetrathionate reductases that have been characterized on a molecular genetic level (Figure 9): The molybdoprotein Ttr from *S. typhimurium* (Hensel *et al.*, 1999), the octaheme tetrathionate reductase OTR from *Shewanella oneidensis* (Mowat *et al.*, 2004) and the diheme cytochrome *c* TsdA from *C. jejuni* (Liu *et al.*, 2013; Kurth *et al.*, 2015; Kurth, Butt *et al.*, 2016; **Chapters 1 and 3**).

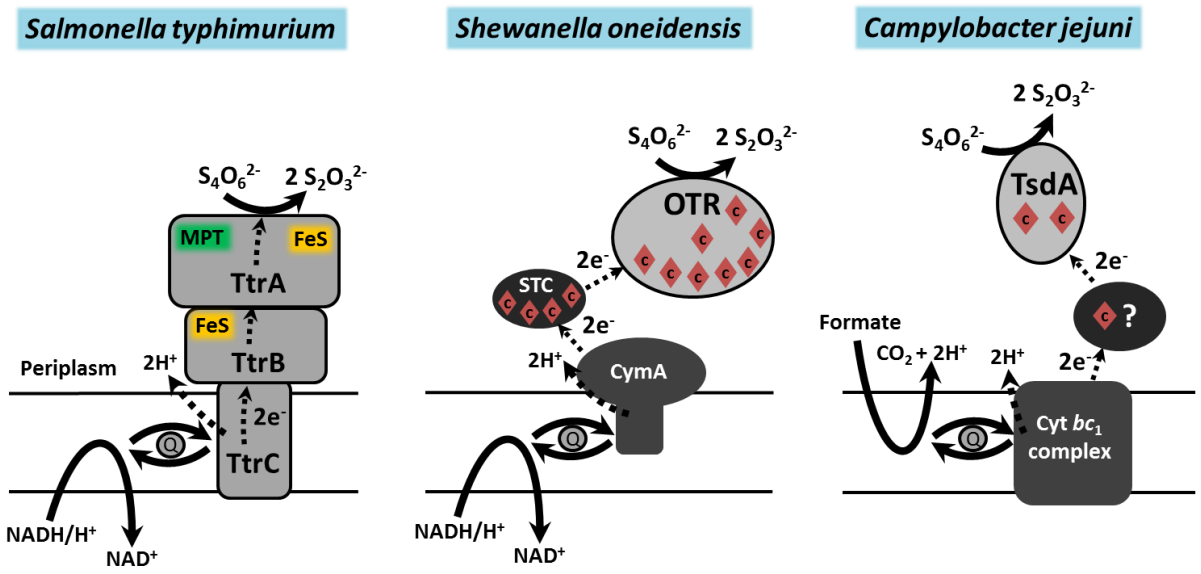

Figure 9: The three types of tetrathionate reductases. The molybdoenzyme Ttr (Hensel *et al.*, 1999), the octaheme tetrathionate reductase OTR (Mowat *et al.*, 2004) and the diheme cytochrome *c* TsdA from *C. jejuni* (Liu *et al.*, 2013) are shown. The tetrathionate reducing pathway of *C. jejuni* is depicted as described in Liu *et al.*, 2013 and that of *S. oneidensis* is shown as described in Alves *et al.*, 2015. STC: small tetraheme cytochrome that accepts electrons from the tetraheme *c*-type cytochrome CymA and distributes them to a number of terminal oxidoreductases (Alves *et al.*, 2015).

In the 1970s Oltmann and coworkers already found the tetrathionate reductase from *Proteus mirabilis* to be membrane-bound (Oltmann *et al.*, 1974) and to contain a molybdenum cofactor (Oltmann *et al.*, 1979). Besides tetrathionate reduction, this enzyme has also been described to catalyze the reduction of thiosulfate and trithionate (Oltmann and Stouthamer, 1975). Later the tetrathionate reductase from *S. typhimurium* was also identified as a molybdenum containing enzyme (Hinojosa-Leon *et al.*, 1986). The *ttrRSBCA* gene locus has been shown to be required for tetrathionate respiration in *S. typhimurium* (Hensel *et al.*, 1999). TtrA, TtrB and TtrC have been found to form the three subunits of the membrane-bound tetrathionate reductase (Figure 9). TtrA contains a molybdopterin guanine dinucleotide cofactor and a [4Fe-4S] cluster, TtrB binds four [4Fe-4S] clusters, and TtrC is an integral membrane protein containing a quinol oxidation site. TtrA and TtrB have been predicted to be anchored by TtrC to the periplasmic face of the cytoplasmic membrane (Hensel *et al.*, 1999).

In 2004 Mowat and coworkers isolated a soluble cytochrome from *S. oneidensis* that contains eight covalently attached heme groups and catalyzes tetrathionate reduction. This octaheme tetrathionate reductase (OTR) comprises one heme group with an unusual lysine-ligation of the heme iron. This heme has been assumed to be the active site of the enzyme (Mowat *et al.*, 2004). Besides tetrathionate the enzyme can reduce nitrite and hydroxylamine as well (Atkinson *et al.*, 2007). The small tetraheme cytochrome (STC) has been shown to accept electrons from CymA and distribute them to a number of terminal oxidoreductases

including OTR (Alves *et al.*, 2015; Figure 9). As mentioned before, tetrathionate reduction is present in several sulfate-reducing bacteria. Some of those bacteria, including *Desulfovibrio vulgaris* and *Candidatus* Desulfococcus oleovorans, encode proteins with high similarity to *S. oneidensis* Otr (46 to 48 % identity on the sequence basis).

Recently it was shown that tetrathionate stimulates growth of the microaerophilic human gut pathogen *Campylobacter jejuni* under oxygen limited conditions (Liu *et al.*, 2013). The reduction of tetrathionate could be linked to the diheme cytochrome *c* TsdA (C8J_0815) that acts as a thiosulfate dehydrogenase in *A. vinosum* (Denkmann *et al.*, 2012). Therefore, TsdA was identified as a bifunctional enzyme. Besides *C. jejuni*, genes homologous to *tsdA* are present in a number of known pathogens from the α-, β-, γ- and ε-proteobacteria, and include other gastrointestinal mucosal pathogens such as *Campylobacter curvus*, *Helicobacter felis*, *Arcobacter butzleri* and *Laribacter hongkongensis,* as well as many strains and species of the zoonotic pathogen *Brucella* and of the respiratory pathogen *Bordetella* (Liu *et al.*, 2013). TsdA might act as a tetrathionate reductase in those organisms as well. Thus the tetrathionate reductase TsdA might enable several pathogenic intestinal bacteria to utilize tetrathionate as electron acceptor resulting in a growth advantage as described for *S. typhimurium* (Winter *et al.*, 2010). The reversible thiosulfate oxidase/tetrathionate reductase from the pseudomonad strain 16B (Tuttle, 1980; Whited and Tuttle, 1983) might also belong to the TsdA family, as the *tsdA* gene is present in several pseudomonads and *P. stutzeri* has been shown to encode a functional TsdA enzyme (Denkmann *et al.*, 2012).

3.2. Electron donors for TsdA-type tetrathionate reductases

In *C. jejuni* electrons delivered by a typical low potential electron donor like formate can be shuttled via the formate dehydrogenase and the menaquinone pool to the bc_1 complex. From there electrons might be transferred to a monoheme cytochrome *c* donating the electrons to the periplasmic TsdA (Liu et al., 2013; Figure 9). A monoheme cytochrome *c* has been identified as a feasible electron donor/acceptor of *C. jejuni* TsdA (*Cj*TsdA) (Liu *et al.*, 2013; Kurth, Butt *et al.*, 2016; **Chapter 3**).

The ε-proteobacterium *W. succinogenes* is a non-pathogenic bacterium closely related to *C. jejuni* and possesses a *tsdA* homologue in its genome (Denkmann *et al.*, 2012). In contrast to all other *tsdA* possessing organisms, the *tsdA* gene from *W. succinogenes* is preceded by a gene predicted to encode a membrane associated lipoprotein (TsdC) which does not show any significant sequence similarity to proteins from other organisms. Motifs for the binding of prosthetic groups which could mediate electron transfer are not apparent. In a study on TsdAC from *W. succinogenes* (Kurth, Schuster *et al.*, 2016; **Chapter 4**) it was shown that TsdC is a novel and unique membrane attached lipoprotein that directly interacts

with TsdA. Both proteins were co-purified from *W. succinogenes* membranes and it was unambiguously shown, that TsdC is necessary for full catalytic activity of TsdA. Similar to *Cj*TsdA, TsdA from *W. succinogenes* (*Ws*TsdA) acts predominantly as a tetrathionate reductase. But in contrast to the situation in *C. jejuni*, a membrane attachment of the tetrathionate reductase by the lipoprotein TsdC seems to be indispensable for tetrathionate reduction in *W. succinogenes*. It is assumed that the TsdAC complex enables *W. succinogenes* to use tetrathionate as an additional substrate for anaerobic respiration and that this complex might interact either with the quinone pool directly or with the bc_1 complex by attachment of TsdA to the membrane (Kurth, Schuster *et al.*, 2016; **Chapter 4**; Figure 10).

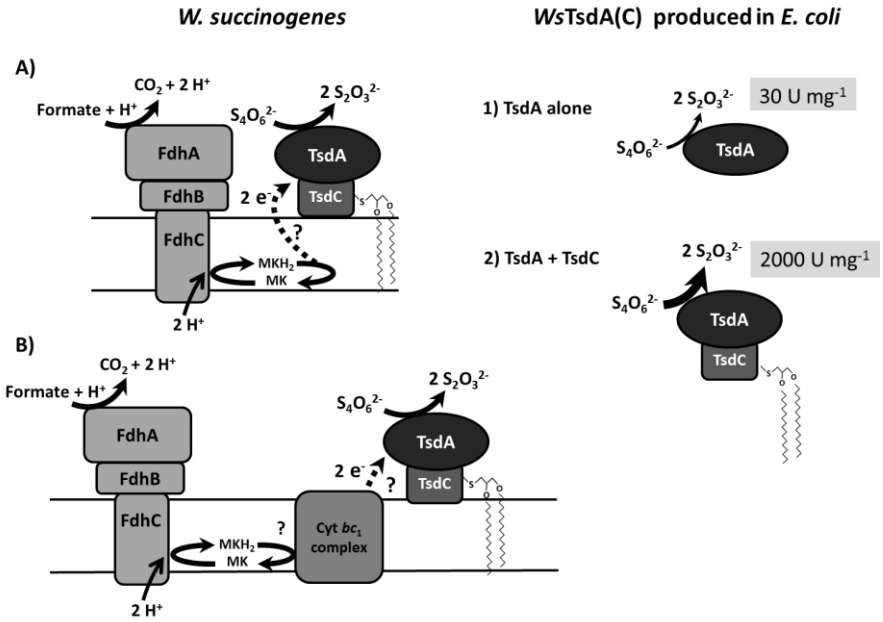

Figure 10: Putative role of TsdA(C) in *W. succinogenes* and characteristics of TsdA(C) produced recombinantly in *E. coli*. Values for V_{max} are rounded values measured in enzyme activity assays. Figure taken from Kurth, Schuster *et al.*, 2016.

4. The diheme cytochrome *c* TsdA

4.1. Structural features and heme ligation

Sequence analysis revealed that a strong structural similarity exists between TsdA and SoxA proteins (Denkmann *et al.*, 2012). SoxA is a subunit of SoxXA, which is part of the thiosulfate-oxidizing multienzyme complex in several bacteria and catalyzes the formation of a sulfur-sulfur bond between thiosulfate and a cysteine residue (Friedrich *et al.*, 2001), as described before. The X-ray structure of *Av*TsdA revealed that there indeed is close structural similarity between the N-terminal domain of TsdA and SoxA (Brito *et al.*, 2015; Figure 11) implying structural and possibly also functional analogy. Moreover, it has been shown that TsdA contains two very similar typical class I *c*-type cytochrome domains wrapped around two hemes.

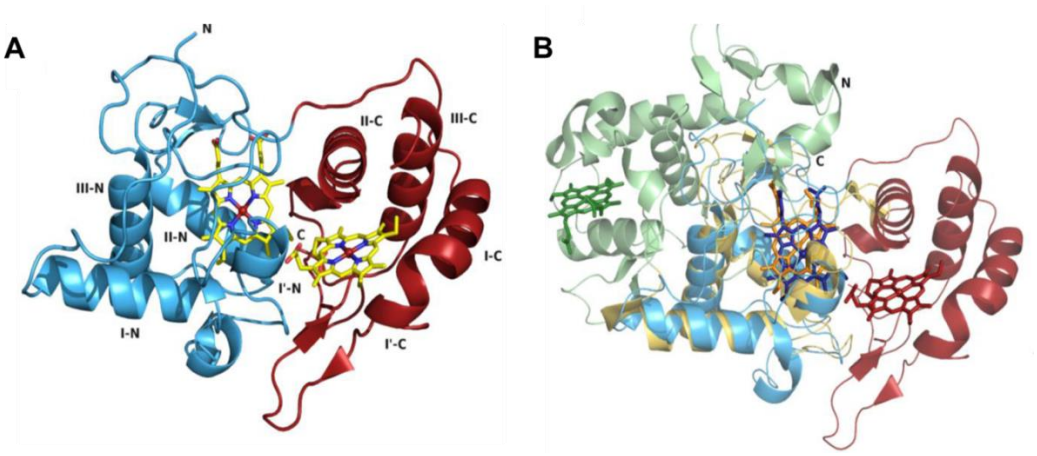

Figure 11: TsdA structure and comparison with SoxA. A) TsdA overall fold with N-terminal domain represented in blue and C-terminal domain in red; the heme prosthetic groups are colored by atom type (yellow for carbon, blue for nitrogen, red for oxygen and dark red for iron). B) Structural superposition of *A. vinosum* TsdA with *Rhodovulum sulfidophilum* SoxA for which the N-terminal domain is shown in green (corresponding heme group in dark green), and the C-terminal domain in yellow (corresponding heme group in orange). Figure extracted from Brito *et al.*, 2015.

In *c*-type cytochromes like TsdA a covalent thioether linkage is formed between two vinyl side chains of the heme and two cysteine residues of the apoprotein. A histidine serves as a proximal axial ligand to the iron of the heme molecule. In six-coordinated *c*-type cytochromes the distal axial ligand is most commonly a second histidine or a methionine (Reedy and Gibney, 2004). Remarkably, TsdA enzymes exhibit an axial histidine/cysteine ligation of the central iron atom for the active site heme, Heme 1 (Brito *et al.*, 2015; Kurth, Brito *et al.*, 2016; Kurth, Butt *et al.*, 2016; **Chapters 2, 3 and 5**; Figure 12). The His/Cys-ligated heme equivalent to TsdA Heme 1 has been shown to participate in the SoxXA catalyzed reaction (Cheesman *et al.*, 2001; Dambe *et al.*, 2005; Kilmartin *et al.*, 2011). This type of ligation is rare among prokaryotes and appears to be of special importance in sulfur-based energy metabolism. The first protein for which such a ligation was discovered is the SoxXA protein of *Rhodovulum sulfidophilum* (Cheesman *et al.*, 2001).

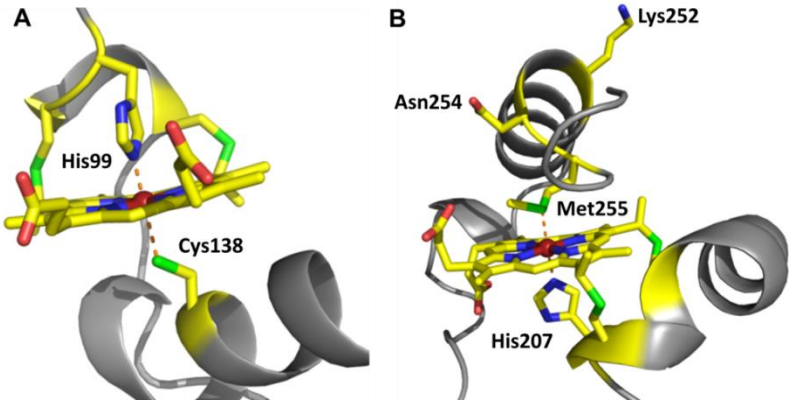

Figure 12: Heme coordination of "as isolated" *Cj*TsdA. A) Heme 1 is coordinated by His^{99} and Cys^{138}. B) Heme 2 is coordinated by His^{207} and Met^{255}. Cartoon representation is shown in pale grey with heme moieties and coordinating amino acid residues shown in sticks and colored by atom type (yellow for carbon, blue for nitrogen, red for oxygen, dark red for iron and green for sulfur). Figure is also shown in Chapter 5.

Other examples for His/Cys-ligated hemes in *c*-type cytochromes are the DsrJ protein from *A. vinosum* (Grein *et al.*, 2010) and *Desulfovibrio desulfuricans* (Pires *et al.*, 2006), the green heme protein (GHP) from *Halochromatium salexigens* (van Driessche *et al.*, 2006), a triheme cytochrome *c* from *R. sulfidophilum* (Alric *et al.*, 2004), and the PsbV2 cytochrome from the cyanobacterium *Thermosynechococcus elongatus* (Suga *et al.*, 2013).

For *Av*TsdA and *Cj*TsdA it has been shown that the Heme 1 iron-ligating cysteine is essential for catalysis, that the substrate-binding site is in the vicinity of Heme 1 and that a transient movement of the Sγ atom of the Heme 1 iron-ligating cysteine out of the iron coordination sphere occurs, which seems to be involved in the TsdA reaction cycle (Brito *et al.*, 2015; Kurth, Butt *et al.*, 2016; **Chapters 3 and 5**). Whereas the heme-ligating cysteine is conserved in TsdA enzymes (Denkmann *et al.*, 2012) and indeed serves as sixth heme iron ligand of the active site heme in *Av*TsdA (Brito *et al.*, 2015), *Mp*TsdBA (Kurth, Brito *et al.*, 2016) and *Cj*TsdA (Kurth, Butt *et al.*, 2016; **Chapters 3 and 5**), the ligand constellation of the electron transfer heme, Heme 2, differs depending on the source organism.

For *Cj*TsdA it was shown that methionine is ligating Heme 2 iron in the oxidized state and that the adjacent amino acids asparagine and lysine play a key role in the physiological function of TsdA as well (Kurth, Butt *et al.*, 2016; **Chapters 3 and 5;** Figure 12). Both, the Heme 1 iron-ligating cysteine and the Heme 2 iron-ligating methionine are indispensable for efficient function of *Cj*TsdA *in vitro* and *in vivo.* In contrast to *Cj*TsdA, the sixth heme iron ligand of *Av*TsdA Heme 2 is a lysine in the oxidized state, but it changes to methionine upon reduction (Brito *et al.*, 2015).

The crystal structure of *Mp*TsdBA revealed that this tetraheme cytochrome *c* contains three hemes with axial His/Met ligation, while the active site heme exhibits the His/Cys coordination typical for TsdA active sites (Kurth, Brito *et al.*, 2016; **Chapter 2**). The TsdB subunit from the *Mp*TsdBA fusion protein as well as the TsdB protein serving as electron acceptor in various organisms was shown to bind two His/Met-ligated hemes.

In the study on the effect of the *Cj*TsdA heme environment on catalysis (Kurth, Butt *et al.*, 2016) as well as in the study on *Av*TsdA heme ligation (Brito *et al.*, 2015), alterations in the Heme 2 environment were shown to influence catalysis at the active site heme. For both enzymes changes in Heme 2 environment were shown to affect substrate affinity of TsdA (Brito *et al.*, 2015; Kurth, Butt *et al.*, 2016). Moreover, an exchange of Lys^{252} in vicinity of *Cj*TsdA Heme 2 led to an immense increase in substrate inhibition by tetrathionate (Kurth, Butt *et al.*, 2016). Those observations indicate strong cooperativity between the two TsdA hemes. This conclusion was confirmed by nIR-MCD spectroscopy and analysis of the redox properties (**Chapter 5**) revealing that exchange of the Heme 2 iron ligand Met^{255} by glycine influences Heme 1 iron ligation and redox properties thereof. The strong cooperativity

between the TsdA hemes might be due to structural changes. X-ray crystallization of *Av*TsdA revealed that each TsdA heme is embedded in one of two very similar typical class I *c*-type cytochrome domains (Brito *et al.*, 2015). There might be some flexibility between those domains resulting in structural changes and rearrangement of the Heme groups.

4.2. Redox properties

Analyzing the redox properties of TsdA enzymes is crucial to understanding the catalysis and reaction mechanism of these enzymes. In general His/Cys-ligated hemes are characterized by a very negative midpoint potential as shown for the corresponding heme in SoxA and DsrJ (Pires *et al.*, 2006; Reijerse *et al.*, 2007; Kappler *et al.*, 2008; Bradley *et al.*, 2012). Values of -400 mV and -432 mV have been reported for the SoxXA His/Cys-ligated active site heme (Reijerse *et al.*, 2007; Bradley *et al.*, 2012). Using nIR-MCD and UV-vis spectroscopy of *Cj*TsdA in the presence of the mild reductant ascorbate it was shown that Heme 1 exhibits the more negative reduction potential and Heme 2 the more positive potential (**Chapter 5**). The redox potential of Heme 1 was shown to be more negative than -81 mV and its redox activity reaches down to -650 mV. Thus, the redox properties observed for TsdA Heme 1 fit to those of other His/Cys-ligated hemes.

His/Met-ligated hemes like TsdA Heme 2 usually exhibit a quite positive reduction potential as soft ligands such as methionine stabilize reduced iron resulting in a positive E_m value (Reedy and Gibney, 2004; Reedy *et al.*, 2008). This was confirmed for *Cj*TsdA Heme 2: The redox potential of Heme 2 was shown to be more positive than -81 mV and the heme was redox active up to +300 mV (**Chapter 5**).

For *Av*TsdA Heme 2 a ligand switch has been described (Brito *et al.*, 2015) that is expected to affect the redox potential of the appropriate heme (Reedy and Gibney, 2004; Reedy *et al.*, 2008). Heme 2 is predicted to be more positive in potential in the His/Met than in the His/Lys-ligated state (Brito *et al.*, 2015). Moreover, it was supposed that in case of *Av*TsdA the ligand change from lysine to methionine upon reduction guides the catalytic electron transfer event such that the gate for the back reaction is closed upon reduction of Heme 2, because the positive redox potential of the His/Met-ligated heme hinders its re-oxidation.

*Cj*TsdA exhibits a range of redox activity between -650 mV and +300 mV (**Chapter 5**). In comparison, *Av*TsdA was found to be redox active in a narrower range between -300 mV and +150 mV (Kurth, Brito *et al.*, 2016; **Chapter 2**). However, the reduction potential of Heme 1 appears to be quite negative in both proteins as expected for His/Cys-ligated hemes. As the E_m of +198 mV for the thiosulfate/tetrathionate couple (Kurth *et al.*, 2015) is relatively positive in comparison to the reduction potential of TsdA Heme 1 that lies far below -81 mV, electron transfer from thiosulfate oxidation to the active site heme appears quite difficult.

Electrochemistry with *Cj*TsdA bound on a SnO_2 electrode in the presence of sulfite (**Chapter 5**) pointed to a solution of this problem: The reduction potential of Heme 1 becomes more positive after binding of sulfite to Sγ of the Heme 1 iron-ligating cysteine. Thiosulfate is assumed to have a similar effect on the reduction potential of Heme 1 as sulfite, because of the structural similarities of the two compounds.

4.3. Reaction mechanism

An important finding in regard to the TsdA reaction mechanism was revealed by the *Mp*TsdBA crystal structure: A thiosulfate ion was found to be covalently bound to Sγ of the active site heme-ligating cysteine (Kurth, Brito *et al.*, 2016; **Chapter 2**; Figure 13). This finding unambiguously proves that catalysis of Tsd(B)A enzymes and very probably also that of the closely related SoxXA proteins involves formation of a covalent adduct between thiosulfate and Sγ of the active site cysteine. The obtained result supports the reaction mechanism proposed by Grabarczyk and colleagues for *Av*TsdA that includes a redox reaction in which a thiosulfate molecule is covalently bound to the active site cysteine as an essential step in the catalytic cycle (Grabarczyk *et al.*, 2015). A rhodanese-like reaction cycle has already been depicted and discussed for SoxXA, but could not be unambiguously proven before (Bamford *et al.*, 2002; Hensen *et al.*, 2006).

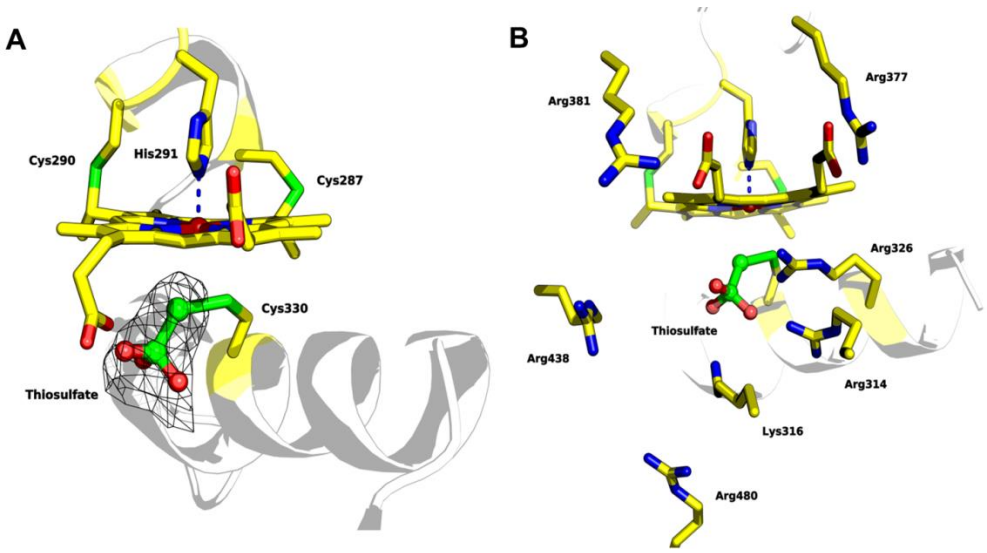

Figure 13: Heme coordination of "as isolated" *Mp*TsdBA. A) The *Mp*TsdBA active site heme with Sγ of Cys^{330} covalently bound to thiosulfate, displayed in ball and stick, and electron density depicted as a black mesh. B) Active site heme with positively charged residues surrounding the substrate cleft. Colors of atoms: yellow for carbon, blue for nitrogen, red for oxygen, dark red for iron and green for sulfur. Figure taken from Kurth, Brito *et al.*, 2016.

The importance of the active site cysteine for the SoxA and TsdA reaction mechanism has already been described some years ago. For SoxA it has been reported several times that the cysteine residue acting as heme ligand exhibits high flexibity (Pires *et al.*, 2006; Kilmartin

et al., 2011; Kappler and Maher, 2013). In case of TsdA the flexibility of the active site cysteine was observed by the movement of Sγ of the Heme 1 iron-ligating cysteine out of the heme coordination sphere (Brito *et al.*, 2015). Moreover, the active site region of TsdA was found to be comparable to that described for SoxA (Bamford *et al.*, 2002; Kappler *et al.*, 2004; Dambe *et al.*, 2005; Kilmartin *et al.*, 2011). Similar to SoxA several positively charged amino acids surround the substrate binding pocket in *Av*TsdA (Brito *et al.*, 2015) and *Mp*TsdBA (Kurth, Brito *et al.*, 2016; **Chapter 2**; Figure 13B) which are expected to create a strong positive electrostatic field suited for binding the anionic substrate thiosulfate.

A covalent linkage between thiosulfate and Sγ as seen in the *Mp*TsdBA crystal structure (Kurth, Brito *et al.*, 2016) is also supported by UV-vis spectroscopy, spectroelectrochemical experiments and protein film voltammetry with *Cj*TsdA in presence of sulfite (**Chapter 5**) indicating that such a bond is not an artifact resulting from protein crystallization but also occurs in solution. The cysteine S-thiosulfonate intermediate involved in the TsdA reaction mechanism is assumed to be formed when the first thiosulfate molecule is positioned in the substrate binding pocket (Grabarczyk *et al.*, 2015; Kurth, Brito *et al.*, 2016; **Chapter 2**; Figure 13). This reaction intermediate is supposed to be stabilized by positively charged amino acid side chains in the active site (Grabarczyk *et al.*, 2015; Kurth, Brito *et al.*, 2016; Figure 13B). Formation of the cysteine S-thiosulfonate releases two electrons which immediately reduce the iron atoms of the two hemes in TsdA to the Fe^{II} state. After an external electron acceptor causes re-oxidation of the hemes, a thiol-disulfide exchange reaction most likely occurs that involves an attack of the second thiosulfate ion on the thiosulfonate group (Grabarczyk *et al.*, 2015). During tetrathionate reduction the central sulfur-sulfur bond of the tetrathionate ion first has to be cleaved by attack of Sγ of the active site cysteine (Kurth, Butt *et al.*, 2016). This reaction most likely releases the first thiosulfate and forms a cysteine S-thiosulfonate group. The second thiosulfate is reductively released from this intermediate after heme reduction by an external electron donor.

To get further insight into the TsdA reaction mechanism sulfite was used as a substrate mimic in UV-vis spectroscopy, spectroelectrochemical experiments and protein film voltammetry with *Cj*TsdA (**Chapter 5**). Sulfite is known to be a strong inhibitor of thiosulfate oxidizing-enzymes (Lyric and Suzuki, 1970; Schook and Berk, 1979; Meulenberg *et al.*, 1993; Hensen *et al.*, 2006) and was shown to be a competitive inhibitor of TsdA in both catalytic directions (**Chapter 5**). Sulfite causes a movement of *Cj*TsdA Cys^{138} Sγ out of the Heme 1 iron coordination sphere and forms a covalent bond with this sulfur atom (**Chapter 5**) similar to the effect caused by thiosulfate (Brito *et al.*, 2015; Kurth, Brito *et al.*, 2016). Moreover, the experiments led to the assumption that the covalent linkage of a sulfur species to Cys^{138} Sγ is the rate-defining step in TsdA catalysis (Figure 14). In contrast, the thiol-disulfide exchange reaction is assumed to occur fast.

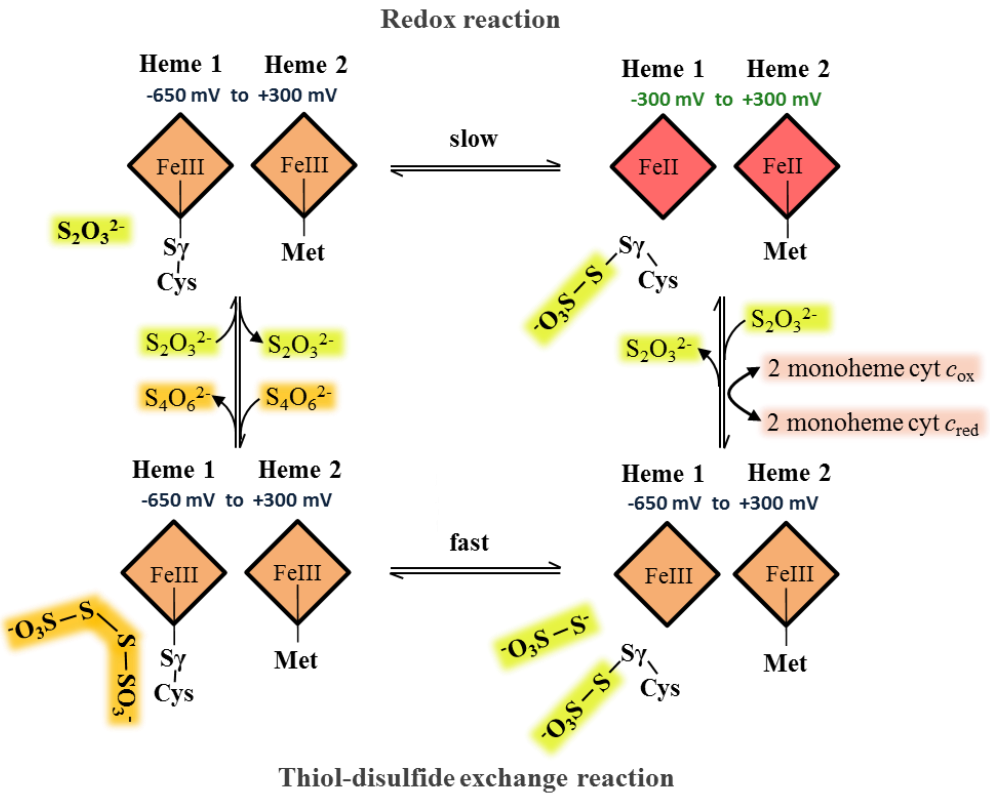

Figure 14: Model of *Cj*TsdA reaction mechanism. In case of *Cj*TsdA the sixth axial heme ligand of the active site heme, Heme 1, is Cys[138] and of the electron transfer heme, Heme 2, Met[255]. Hints were obtained that covalent linkage of thiosulfate to the Cys[138] Sγ leads to a positive increase of the Heme 1 reduction potential (Chapter 5). Moreover, it is supposed that the redox reaction involving Cys[138] S-thiosulfonate formation is the rate-determining step in *Cj*TsdA catalysis. The thiol-disulfide exchange is assumed to occur fast. A monoheme cytochrome has been shown to be the most likely electron acceptor/donor of *Cj*TsdA (Liu *et al.*, 2013). This figure is also shown in Chapter 5.

The obtained findings regarding the TsdA redox properties especially helped with understanding the reaction mechanism of this enzyme (**Chapter 5**). As mentioned before, binding of a sulfur species to the Sγ of the Heme 1 iron-ligating cysteine leads to a positive increase of the heme's reduction potential. This finding supports the hypothesis that the active site cysteine acts as a switch (Brito *et al.*, 2015): It could keep the heme in a low redox potential oxidized state, but would be a weak enough ligand that it could be moved out of the coordination sphere when thiosulfate enters the active site, thus leading to a strong increase in the heme's redox potential (Brito *et al.*, 2015). The observed positive increase in the reduction potential of Heme 1 is assumed to occur during movement of the heme-ligating cysteine Sγ out of the Heme 1 iron coordination sphere and formation of a cysteine S-thiosulfonate group (**Chapter 5**). The increase in redox potential might facilitate electron transfer from thiosulfate to Heme 1 before passing electrons to an external electron acceptor via Heme 2 (Figure 14). In the tetrathionate-reducing direction an increase in the Heme 1 reduction potential might facilitate electron transfer from Heme 2 to Heme 1 as the redox potential of the negative potential Heme 1 converges to that of the positive potential Heme 2.

4.4. Reaction directionality

All TsdA enzymes characterized so far have been identified as bifunctional enzymes. However, they exhibit very different catalytic properties *in vitro* and differ in reaction directionality (Liu *et al.*, 2013; Brito *et al.*, 2015; Kurth *et al.*, 2015; Kurth, Butt *et al.*, 2016; **Chapter 1**). Enzyme activity assays with redox dyes have identified TsdA from *A. vinosum* as thiosulfate dehydrogenase and TsdA from *C. jejuni* as tetrathionate reductase (Liu *et al.*, 2013; Brito *et al.*, 2015; Kurth, Butt *et al.*, 2016). The catalytic bias of different TsdA proteins has been studied in detail by protein film electrochemistry (PFE). PFE is a good method for mechanistic studies of redox enzymes and was developed and described in detail in the 1990s (Armstrong, 1990; Armstrong *et al.*, 1993; Hirst *et al.*, 1996; Armstrong *et al.*, 1997). Redox proteins can be induced to interact directly with an electrode and display reversible electrochemistry giving the possibility of using dynamic electrochemical methods, such as cyclic voltammetry, to examine the functional properties of redox-active centers in proteins ranging from a rapid image of the redox chemistry of centers in a protein to the determination of equilibrium and kinetic constants for coupled reactions (Armstrong *et al.*, 1993).

Protein film electrochemistry with TsdA enzymes (Kurth *et al.*, 2015; Kurth, Butt *et al.*, 2016; **Chapters 1 and 3**) was performed using a non-isothermal three-electrode cell configuration (Anderson *et al.*, 2001) with a graphite working electrode, a Ag/AgCl reference electrode and a platinum counter electrode. In those experiments the TsdA enzymes were adsorbed onto graphite electrodes, which ensure direct electron transfer between electrode and substrate via the active site of the enzyme. The electrode serves both an electron-accepting and an electron-donating function depending on the potential applied to the electrode. The graphite electrode with the adsorbed enzyme was placed in an electrochemical cell containing buffer and thiosulfate, tetrathionate or equimolar concentrations of both substrates. The advantage of this method is that the same reaction is assayed in the forward and the reverse direction in experiments with TsdA in a solution containing equimolar concentrations of thiosulfate and tetrathionate. Any differences in rate that may be introduced by using different redox dyes for the two different directions in colorimetric assays are eliminated. By changing the electrode potential, the redox state of the enzyme is altered, and the voltammogram, i.e. the plot of current against electrode potential, depicts the substrate turnover of the enzyme. The magnitude of current is proportional to the turnover rate. As the electroactive coverage is unknown, a specific activity of the TsdA catalyzed reaction cannot be determined with this method. Figure 15 shows a voltammogram of *Cj*TsdA adsorbed on a graphite electrode and placed in a solution with equimolar thiosulfate and tetrathionate concentrations. The negative catalytic currents indicate tetrathionate reduction and its positive counterparts thiosulfate oxidation.

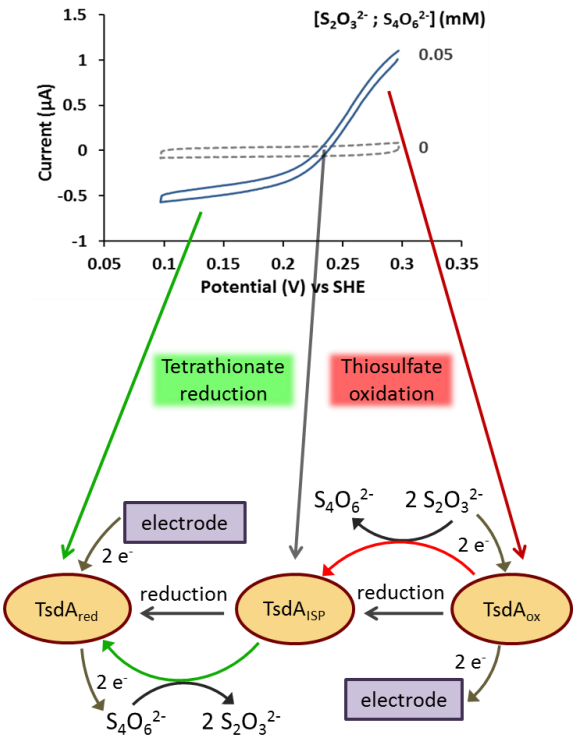

Figure 15: Explanation of protein film voltammetry with *Cj*TsdA. The protein is adsorbed on a graphite electrode and placed in a solution containing ammonium acetate buffer pH 5 (100 mM ammonium acetate, 50 mM NaCl) and equimolar concentrations of thiosulfate and tetrathionate. The scan rate is 10 mV s^{-1} and the electrode rotates with 500 rpm. When a potential above +0.24 V vs. SHE is applied to the electrode, TsdA is oxidized by the electrode and able to catalyze thiosulfate oxidation. This yields in an electron transfer from thiosulfate via TsdA to the electrode and a positive catalytic current is measured. At the isosbestic point (~+0.24 V vs. SHE) the rate of thiosulfate oxidation equals that of tetrathionate reduction. When a potential below +0.24 V vs. SHE is applied to the electrode, TsdA is reduced by accepting electrons from the electrode and those electrons are used for tetrathionate reduction. During this process electrons are transferred from the electrode via TsdA to tetrathionate and a negative catalytic current is measured. ISP: isosbestic point, SHE: Standard hydrogen electrode.

The catalytic bias of different TsdA proteins was analyzed in detail by protein film cyclic voltammetry with the enzymes adsorbed on graphite electrodes in the presence of equimolar concentrations of thiosulfate and tetrathionate (Kurth *et al.*, 2015; **Chapter 1;** Figure 16).

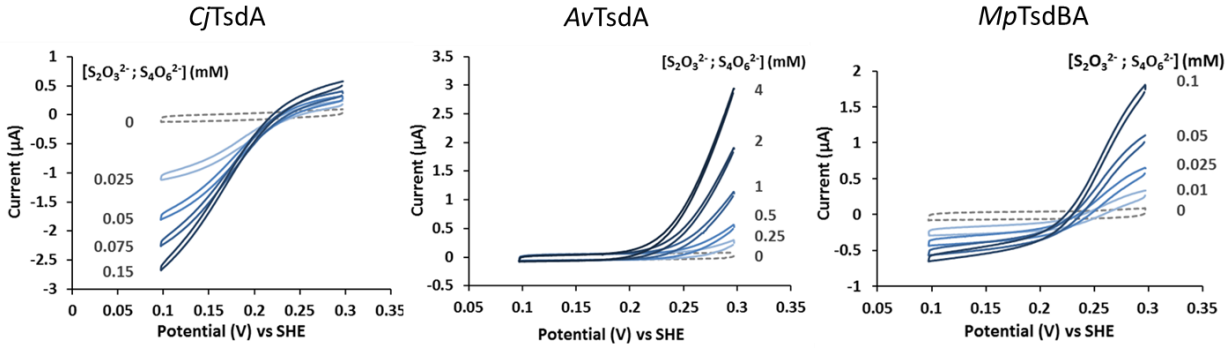

Figure 16: Representative protein film cyclic voltammetry of *Cj*TsdA, *Av*TsdA and *Mp*TsdBA. Cyclic voltammetry was performed in solutions containing equal concentrations of thiosulfate and tetrathionate as indicated (blue continuous lines) and prior to substrate addition (gray broken lines). Scan rate 10 mV s^{-1}, electrode rotation 500 rpm in 100 mM ammonium acetate, 50 mM NaCl, pH 5 at 25 °C for *Mp*TsdBA and *Av*TsdA and at 42 °C for *Cj*TsdA. Figure modified after Kurth *et al.*, 2015.

In accordance with colorimetric activity assays, *Cj*TsdA appears clearly biased toward tetrathionate reduction and *Av*TsdA as well as *Mp*TsdBA are strongly biased toward thiosulfate oxidation (Kurth *et al.*, 2015) fitting to the *in vivo* function of those enzymes described before. As *Cj*TsdA and *Mp*TsdBA catalyze rapid bidirectional interconversion of tetrathionate and thiosulfate those enzymes could be used for determination of the reduction potential of the tetrathionate/thiosulfate couple (Kurth *et al.*, 2015).

To establish factors that influence the reaction directionality of TsdA, the impact of structural differences in the immediate environment of one or both hemes in *Cj*TsdA on the enzyme's adaptation to tetrathionate reduction was analyzed (Kurth, Butt *et al.*, 2016; **Chapter 3**). Therefore the enzyme activities of recombinant *Cj*TsdA variants were characterized to elucidate whether the heme-ligating amino acids alter the catalytic properties of the enzyme and whether both or only one catalytic direction are affected. In addition, the redox properties of the *Cj*TsdA wildtype and variant proteins with changes in the Heme 1 and Heme 2 amino acid environment were set in context to their catalytic properties.

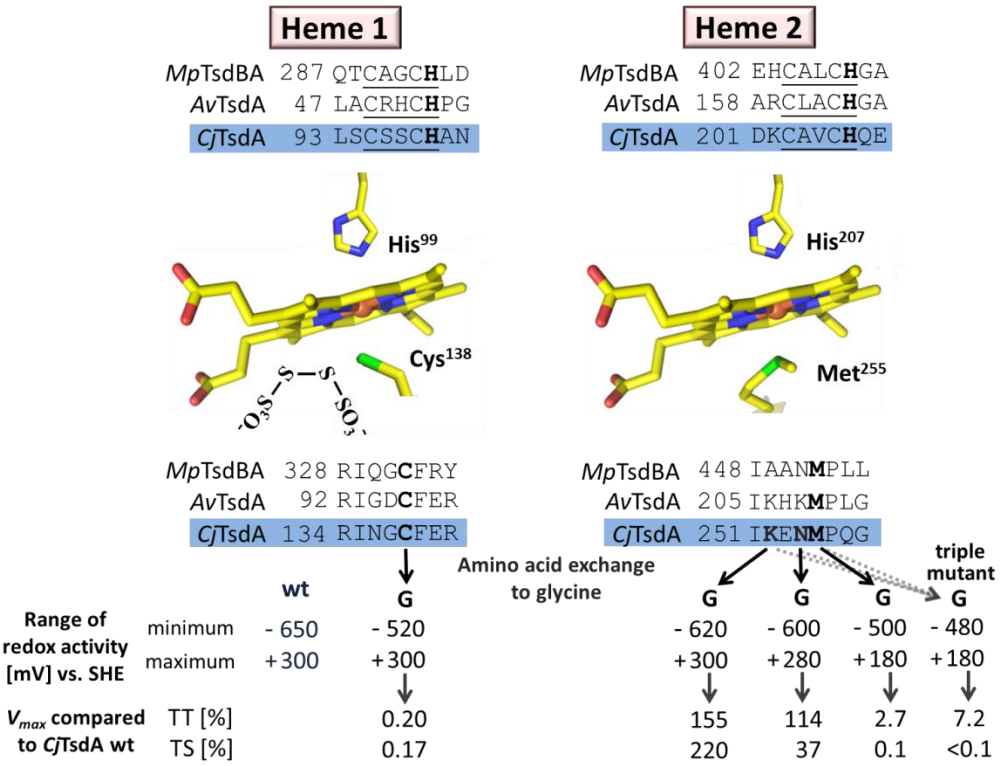

Figure 17: Impact of changes in *Cj*TsdA Heme 1 and Heme 2 environment on redox properties and catalytic activity. Relevant sequence alignments are shown for TsdA from *C. jejuni* (*Cj*TsdA), *A. vinosum* (*Av*TsdA) and the TsdBA fusion protein from *M. purpuratum* (*Mp*TsdBA). In the central left panel a tetrathionate molecule is shown in vicinity of the active site Heme 1 iron-ligating cysteine, based on the *Av*TsdA crystal structure (Brito *et al.*, 2015). Amino acid numbers in the central panels refer to *Cj*TsdA. In the lower part of the figure, changes in the environments of Heme 1 and Heme 2 are indicated which were introduced by site directed mutagenesis. The effects of these changes on the range of redox activity (Chapter 5) in comparison to that of the wildtype protein are shown. The impact of these alterations on maximal reaction velocity are listed as percent of V_{max} for the wildtype enzyme in the tetrathionate-reducing (TT) and the thiosulfate-oxidizing (TS) direction. Figure modified after Kurth, Butt *et al.*, 2016 and also shown in Chapter 5.

Exchange of the Heme 1 iron-ligating cysteine (Cys^{138}) did not alter the reaction directionality of TsdA (Kurth, Butt *et al.*, 2016; **Chapter 3**; Figure 17). In contrast, exchange of the Heme 2 iron-ligating methionine (Met^{255}) by glycine led to a strong impairment in both catalytic directions, however thiosulfate oxidation was more strongly effected than tetrathionate reduction. In the case of *Cj*TsdA M255G the reduction potential of Heme 2 has become more negative (**Chapter 5**). Simultaneously the reduction potential of Heme 1 has become more positive indicating that the Heme 1 ligation is affected when Met^{255} is exchanged by glycine which is also observed in nIR-MCD spectra (**Chapter 5**). The alteration in the redox properties of one or both hemes might influene the observed changes in reaction directionality of *Cj*TsdA M255G in comparison to the wildtype protein.

Replacement of the asparagine (Asn^{254}) or the lysine (Lys^{252}) residue adjacent to the Heme 2 iron-ligating methionine by glycine led to the largest changes in *Cj*TsdA reaction directionality (Kurth, Butt *et al.*, 2016; **Chapter 3**; Figure 17) demonstrating the importance of those amino acid residues for functionality of the enzyme. The reaction directionality of the *Cj*TsdA K252G variant shifted toward thiosulfate oxidation and that of the N254G variant toward tetrathionate reduction. The observed changes in reaction directionality of those variants are not caused by altered redox properties of the TsdA hemes (**Chapter 5**; Figure 17). Thus, the differences in the enzyme's reaction directionality are not assumed to be significantly influenced by the reduction potentials of the hemes.

In vitro as well as *in vivo* experiments with *Cj*TsdA revealed that structural differences in the immediate environment of Heme 2 contribute to defining the reaction directionality of TsdA (Kurth, Butt *et al.*, 2016; **Chapter 3**). However, it was also shown that the heme environment is not the main determinant of TsdA reaction directionality: When heme ligands in *Cj*TsdA were adapted to the situation in *Av*TsdA, the enzyme did not show a stronger bias to thiosulfate oxidation than wildtype *Cj*TsdA. For this reason the reaction directionality of the enzyme has to be determined by other factors. Studies on the catalytic bias of hydrogenases have indicated that the reaction directionality of those enzymes is not mainly determined by redox properties of the active site, but rather by steps which occur on sites of the proteins that are remote from the active site, such as proton transfer, intramolecular electron transfer, reorganization energy, substrate release or lid opening (Abou Hamdan *et al.*, 2012; Hexter *et al.*, 2014). As mentioned before, there is a strong cooperativity between the two TsdA hemes. Thus, structural rearrangements inside the enzyme, probably concerning the heme groups, might influence the enzyme's reaction directionality.

III. Aims of this thesis

Enzymes of the thiosulfate dehydrogenase TsdA family are diheme *c*-type cytochromes that are widespread among bacteria. The TsdA enzyme of the purple sulfur bacterium *Allochromatium vinosum* (*Av*) acts as a thiosulfate dehydrogenase and has been intensively studied over the last few years. This enzyme enables *A. vinosum* to use thiosulfate as electron donor for photosynthesis. In the human gut pathogen *Campylobacter jejuni* (*Cj*) TsdA has instead been described as enabling the use of tetrathionate as an additional electron acceptor for anaerobic respiration. Unlike *Av*TsdA, *Cj*TsdA was lacking a detailed biochemical and biophysical analysis.

The aims of this thesis were:

- Analysis of the reaction directionality of TsdA enzymes from different organisms
- Further insight into the TsdA reaction mechanism revealed by structural, kinetic, spectroscopic, electrochemical and spectroelectrochemical characterization of *Cj*TsdA
- Determination of the reduction potential of TsdA enzymes as well as that of the tetrathionate/thiosulfate couple
- Analysis of electron accepting and electron donating units of TsdA

IV. Publications included in this thesis

Chapter 1

Kurth, J.M., Dahl, C., and Butt, J.N. (2015) Catalytic protein film electrochemistry provides a direct measure of the tetrathionate/thiosulfate reduction potential. *J Am Chem Soc* **137**: 13232–13235.

Chapter 2

Kurth, J.M., Brito, J.A., Reuter, J., Flegler, A., Koch, T., Franke, T., Klein E.-M., Rowe S.F., Butt J.N., Denkmann K., Pereira I.A.C., Archer M., Dahl C. (2016) Electron accepting units of the diheme cytochrome *c* TsdA, a bifunctional thiosulfate dehydrogenase/tetrathionate reductase. *J Biol Chem* **291**: 24804–24818.

Chapter 3

Kurth, J.M., Butt, J.N., Kelly, D.J., and Dahl, C. (2016) Influence of haem environment on the catalytic properties of the tetrathionate reductase TsdA from *Campylobacter jejuni*. *Biosci Rep* **36**: e00422.

Chapter 4

Kurth, J.M., Schuster, A., Seel, W., Herresthal, S., Simon, J., and Dahl, C. (2016) TsdC, a unique lipoprotein from *Wolinella succinogenes* that enhances tetrathionate reductase activity of TsdA. *FEMS Microbiol Lett* **submitted**.

Chapter 1

Catalytic protein film electrochemistry provides a direct measure of the tetrathionate/thiosulfate reduction potential

Introduction & Summary

Thiosulfate and tetrathionate can be used as electron donor or acceptor in bacterial respiratory chains. In addition, the oxidation of thiosulfate is of industrial importance. Thiosulfate is for example used in volumetric analysis of oxidizing agents and bleach neutralization during water treatment. The tetrathionate/thiosulfate interconversion is not reversible at inert electrodes and this prevents experimental determination of the thiosulfate/tetrathionate reduction potential $E_{TT/TS}$ by conventional methods. The values for $E_{TT/TS}$ stated in the literature rely on calculations from thermodynamic data that themselves underwent several re-evaluations and modifications over the last decades. Accordingly, reported $E_{TT/TS}$ values span a large window of 250 mV.

Protein film electrochemistry with enzymes from the TsdA family clearly revealed that those enzyme exhibit different reaction directionalities in dependence of the source organism. The enzymes from the purple sulfur bacteria *Allochromatium vinosum* and *Marichromatium purpuratum* were shown to be biased toward thiosulfate oxidation while the enzyme from the human gut pathogen *Campylobacter jejuni* is adapted to catalyzing tetrathionate reduction. The use of these bifunctional TsdA enzymes catalyzing the interconversion of the tetrathionate/thiosulfate couple enabled an experimental determination of $E_{TT/TS}$. With this method a value of +198 mV vs. SHE was determined. This value is much higher than the value of +24 mV (Thauer *et al.*, 1977) most widely cited in the field of microbial bioenergetics. Thus, tetrathionate is a better electron acceptor than previously thought and the role of bacterial tetrathionate reduction in tetrathionate containing environments like the human gut and marine sediments has previously been underestimated.

Chapter 1

Catalytic protein film electrochemistry provides a direct measure of the tetrathionate/thiosulfate reduction potential

This research was reproduced with permission from:

Kurth, J.M., Dahl, C., and Butt, J.N. (2015) Catalytic protein film electrochemistry provides a direct measure of the tetrathionate/thiosulfate reduction potential. *J Am Chem Soc* **137**: 13232–13235.

http://pubs.acs.org/doi/abs/10.1021/jacs.5b08291

Author contributions

- JMK performed all experiments

- JMK wrote the paper together with CD and JNB

JACS
JOURNAL OF THE AMERICAN CHEMICAL SOCIETY

Communication

pubs.acs.org/JACS

Catalytic Protein Film Electrochemistry Provides a Direct Measure of the Tetrathionate/Thiosulfate Reduction Potential

Julia M. Kurth,[*,†] Christiane Dahl,[†] and Julea N. Butt[*,‡]

[†]Institut für Mikrobiologie & Biotechnologie, Rheinische Friedrich-Wilhelms-Universität Bonn, Meckenheimer Allee 168, D-53115 Bonn, Germany

[‡]Centre for Molecular and Structural Biochemistry, School of Chemistry, and School of Biological Sciences, University of East Anglia, Norwich Research Park, Norwich NR4 7TJ, United Kingdom

Supporting Information

ABSTRACT: The tetrathionate/thiosulfate interconversion is a two-electron process: $S_4O_6^{2-} + 2\ e^- \leftrightarrow 2\ S_2O_3^{2-}$. Both transformations can support bacterial growth since $S_2O_3^{2-}$ provides an energy source, while $S_4O_6^{2-}$ serves as respiratory electron acceptor. Interest in the corresponding $S_2O_3^{2-}$ oxidation also arises from its widespread use in volumetric analysis of oxidizing agents and bleach neutralization during water treatment. Here we report protein film electrochemistry that defines the reduction potential of the $S_4O_6^{2-}/S_2O_3^{2-}$ couple. The relevant interconversion is not reversible at inert electrodes. However, facile reduction of $S_4O_6^{2-}$ to $S_2O_3^{2-}$ and the reverse reaction are catalyzed by enzymes of the thiosulfate dehydrogenase, TsdA, family adsorbed on graphite electrodes. Zero-current potentials measured with different enzymes, at three pH values, and multiple $S_4O_6^{2-}$ and $S_2O_3^{2-}$ concentrations together with the relevant Nernst equation resolved the tetrathionate/thiosulfate reduction potential as +198 ± 4 mV versus SHE. This potential lies in the ∼250 mV window encompassing previously reported values calculated from parameters including the free energy of formation. However, the value is considerably more positive than widely used in discussions of bacterial bioenergetics. As a consequence anaerobic respiration by tetrathionate reduction is likely to be more prevalent than presently thought in tetrathionate-containing environments such as marine sediments and the human gut.

There are numerous sulfur oxoacids, and many of those compounds have industrial significance.[1] Perhaps the most well-known is sulfuric acid. This chemical is a key constituent of lead-acid batteries and the production of phosphate fertilizers. However, other sulfur oxoanions are valuable reducing agents. A case in point is thiosulfate ($S_2O_3^{2-}$). This ion instantly neutralizes bleach in a reaction frequently exploited during water treatment and paper making. The final products of the reaction are tetrathionate ($S_4O_6^{2-}$), higher polythionates, and sulfate.[2] Tetrathionate is formed by oxidative conjugation of two molecules of thiosulfate with two electrons released in the corresponding half-reaction (eq 1):

$$S_4O_6^{2-} + 2e^- \leftrightarrow 2S_2O_3^{2-} \quad (1)$$

This half-reaction also underpins the widespread use of thiosulfate in analytical chemistry whereby stoichiometric reaction with I_2 produces 2 I^-. The corresponding color change is widely used for volumetric analysis of oxidizing agents in aqueous solutions of ecological and recreational interest. However, in other contexts, e.g., the extraction of gold and silver by ammoniacal thiosulfate leaching, the oxidation of thiosulfate to tetrathionate is detrimental and aims to be minimized.[3]

In addition to the industrial and analytical importance of the thiosulfate/tetrathionate interconversion, this reaction has considerable significance in the global biogeochemical cycling of sulfur.[4−6] Certain prokaryotes in aquatic and terrestrial habitats obtain energy by the oxidation of thiosulfate to tetrathionate. Other prokaryotes use the reverse reaction, namely tetrathionate reduction, to support anaerobic respiration. In this latter context two prominent examples are the human gut pathogens *Salmonella typhimurium*[7] and *Campylobacter jejuni*.[8] *S. typhimurium* reduces tetrathionate produced by vertebrate intestinal mucosa during inflammation, and this may confer a competitive growth advantage on the pathogen by supporting increased transmission through the faecal-oral route.[7]

The processes mentioned above have focused attention on the reduction potential ($E_{TT/TS}$) of the tetrathionate/thiosulfate couple. Pourbaix (reduction potential-pH) diagrams including this value have been presented.[3,9] $E_{TT/TS}$ is also included in redox towers. These compare the reduction potentials of different redox couples as a guide to the respiratory electron-transfer processes that may support bacterial colonization of a particular environment. However, there is ambiguity in the $E_{TT/TS}$ values that appear in such resources as they span a window exceeding 250 mV; from +24 to +300 mV versus SHE.[10−13] This variation stems largely from the irreversible nature of the thiosulfate/tetrathionate interconversion at an inert electrode.[9,14] The resulting behavior is inconsistent with the relevant Nernst equation, and this precludes direct measurement of $E_{TT/TS}$. As a consequence previously reported values relied completely on calculations from relevant thermodynamic data. However, free energies of formation for thiosulfate and tetrathionate are themselves constantly re-evaluated and published values cover ranges from approx-

Received: August 6, 2015
Published: October 5, 2015

DOI: 10.1021/jacs.5b08291
J. Am. Chem. Soc. 2015, 137, 13232−13235

imately −510 to −600 kJ mol^{-1} and −1020 to −1055 kJ mol^{-1}, respectively.[12,15−18] Over the last four decades, an $E_{TT/TS}$ value of +24 mV has been most widely cited in the field of microbiology. This value was calculated based on free energies of formation published in the 1950s[15,17] and released in a highly influential seminal work on energy conservation in chemotrophic anaerobic bacteria.[10]

In order to address this situation by providing a direct measure of $E_{TT/TS}$ we have performed catalytic protein film electrochemistry of enzymes from the thiosulfate dehydrogenase, TsdA, family.[19] The TsdA proteins are *c*-type cytochromes carrying two heme groups.[19,20] An axial histidine/cysteine ligation of the central iron atom is characteristic for the active site heme. This type of ligation is rare among prokaryotes and appears to be of special importance in sulfur-based energy metabolism.[20] In many cases, TsdA is accompanied by another diheme cytochrome *c* (TsdB) that serves as the redox partner for TsdA.[19] In some instances, TsdA and TsdB form a fusion protein. All TsdA enzymes characterized to date catalyze both the oxidation of thiosulfate to tetrathionate and the reduction of tetrathionate to thiosulfate at measurable rates.[8,19] This reversibility is of crucial importance for the work presented here.

Samples of the purified TsdA enzymes from *Campylobacter jejuni* (*Cj*) and *Allochromatium vinosum* (*Av*) as well as the TsdBA fusion protein from *Marichromatium purpuratum* (*Mp*) were adsorbed as separate electrocatalytically active films on graphite electrodes. Cyclic voltammetry revealed clear catalytic currents when the enzyme-coated electrodes were placed in pH 5 solutions of equimolar tetrathionate and thiosulfate, Figure 1. These currents were absent when either the enzyme or the substrates were omitted from the experiment. Thus, the catalytic currents arise exclusively from enzyme-catalyzed tetrathionate reduction and/or thiosulfate oxidation and with that catalysis sustained by direct electron exchange between the enzyme and electrode.

For *Cj*TsdA the reductive (negative) catalytic currents have significantly larger magnitude than their oxidative (positive) counterparts, Figure 1A. As a consequence, it is immediately apparent that *Cj*TsdA is biased toward tetrathionate reduction relative to thiosulfate oxidation. By contrast *Mp*TsdBA displays higher catalytic rates for thiosulfate oxidation than tetrathionate reduction which reveals this enzyme's bias to oxidative catalysis, Figure 1B. However, *Av*TsdA displays the greatest bias toward thiosulfate oxidation of the enzymes studied here, Figure 1C. No evidence could be found for reductive catalysis by *Av*TsdA, and this was despite all three enzymes displaying comparable current magnitudes for thiosulfate oxidation. This agrees with results from colorimetric solution assays of *Av*TsdA activity that found a strong bias toward thiosulfate oxidation with very low specific activity for tetrathionate reduction.[8,20] Electrochemical resolution of catalytic reduction by *Av*TsdA is most likely to be precluded by the intrinsically low rate of tetrathionate reduction combined with low electrocatalytic coverage of the electrode by the enzyme. Indeed, none of the enzymes display detectable nonturnover waves in the absence of substrate, and this is consistent with low electrocatalytically active enzyme populations.

At high overpotentials the majority of the catalytic waves from all three enzymes fail to attain values that are independent of driving force for the relevant reaction. This is behavior that suggests heterogeneously oriented enzyme molecules displaying a range of interfacial electron-transfer kinetics.[21] Never the

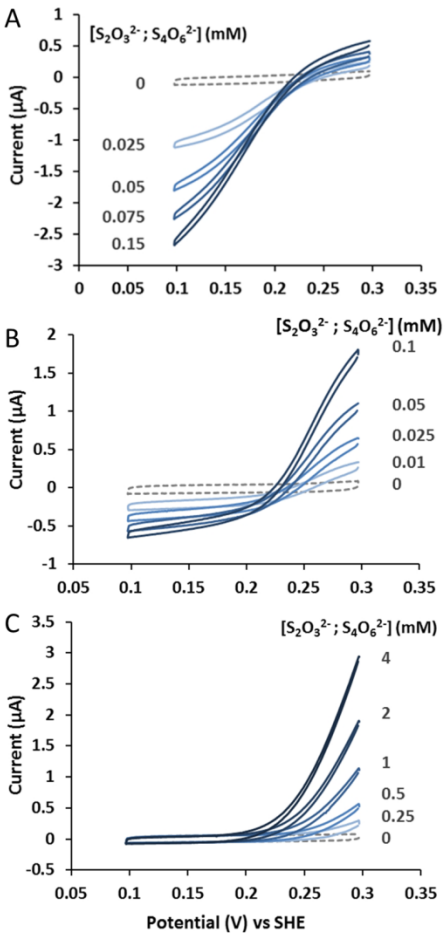

Figure 1. Representative protein film cyclic voltammetry of (A) *Cj*TsdA, (B) *Mp*TsdBA, and (C) *Av*TsdA in solutions containing equal concentrations of thiosulfate and tetrathionate as indicated (blue continuous lines) and prior to substrate addition (gray broken lines). Scan rate 10 mV s^{-1}, electrode rotation 500 rpm in 100 mM ammonium acetate, 50 mM NaCl, pH 5 at 25 °C for *Mp*TsdBA and *Av*TsdA and at 42 °C for *Cj*TsdA.

less, it is clear that films of *Cj*TsdA and *Mp*TsdBA catalyze rapid bidirectional interconversion of tetrathionate and thiosulfate. By visualizing such catalysis, the protein film electrochemistry defines a zero-current potential (E_{ZCP}) from which $E_{TT/TS}$ can be calculated using the relevant Nernst eq (eq 2):

$$E_{TT/TS} = E_{ZCP} - \frac{RT}{2F} \ln\left(\frac{[S_4O_6^{2-}]}{[S_2O_3^{2-}]^2}\right) \quad (2)$$

where *R*, *F*, and *T* have their usual meaning.[22−24] A number of factors contribute to defining catalytic bias,[25,26] but their resolution for the TsdA enzymes lies beyond the scope of the present work.

Values for E_{ZCP} were obtained by two methods as detailed in the Supporting Information. In one approach E_{ZCP} was defined as the points of intersection for cyclic voltammograms recorded in the presence and absence of substrates (averaged for each scan direction), e.g., Figure 1A,B. In the second approach the

DOI: 10.1021/jacs.5b08291
J. Am. Chem. Soc. 2015, 137, 13232−13235

potential required to maintain zero current through the cell was measured directly. For all experiments the thiosulfate/tetrathionate mixtures were prepared immediately prior to use and with concentrations chosen to minimize the likelihood of any significant reaction between tetrathionate and thiosulfate.[27,28] Measurements by the second method were typically complete within 3 min, while those using the first method took ~15 min. No systematic differences were detected between E_{ZCP} values determined by the two approaches so the initial substrate concentrations were taken as those defining E_{ZCP}. The corresponding values of $E_{TT/TS}$ lie between +187 and +205 mV versus SHE, Figure 2 (black solid circles and triangles).

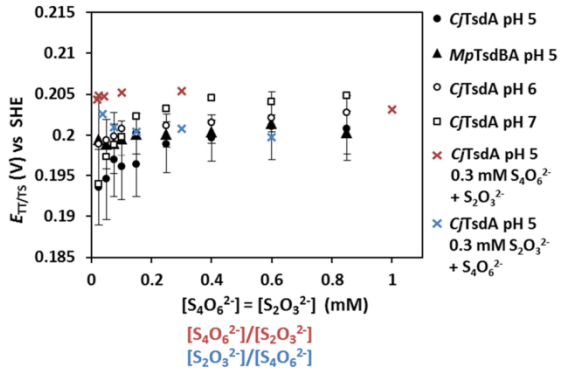

Figure 2. Values for the formal potential of the tetrathionate/thiosulfate couple, $E_{TT/TS}$, defined by protein film electrochemistry. Equal concentrations of $S_2O_3^{2-}$ and $S_4O_6^{2-}$ (black: symbols and *x*-axis title). Different concentrations of $S_2O_3^{2-}$ with $[S_4O_6^{2-}]$ = 0.3 mM (red: "×" and *x*-axis title). Different concentrations of $S_4O_6^{2-}$ with $[S_2O_3^{2-}]$ = 0.3 mM (blue: "×" and *x*-axis title). See text for details. Error bars were generated when at least two independent measurements were made.

Our analysis makes two assumptions. First, that the enzymes are true catalysts, changing the rate of attainment of equilibrium but not the position of equilibrium. Second, that the activities of thiosulfate and tetrathionate equate to their respective concentrations under our experimental conditions. Further experiments performed with *Cj*TsdA confirmed the validity of our approach. Thiosulfate was introduced to a solution that contained 0.3 mM tetrathionate but initially no thiosulfate, Figure 3A. Cyclic voltammetry quantified an increase in the ratio of oxidative relative to reductive catalysis on increasing the thiosulfate concentration from 0.3 to 12 mM. In addition E_{ZCP} was displaced by approximately −100 mV. In a separate experiment the tetrathionate concentration was increased from 0.05 to 0.5 mM in a solution containing initially 0.3 mM thiosulfate, Figure 3B. Here E_{ZCP} was displaced by approximately +30 mV. However, for both data sets the values of $E_{TT/TS}$ calculated from eq 2 were essentially independent of the thiosulfate:tetrathionate ratio, Figure 2 (red and blue "×"). The values were also in accord with those defined from the measurements with equal concentrations of both substrates.

The cyclic voltammograms presented above contain a wealth of information on the catalytic properties of TsdA enzymes. For example, thiosulfate is seen to inhibit tetrathionate reduction, Figure 3A, and tetrathionate to inhibit thiosulfate oxidation, Figure 3B. However, these features of the catalytic properties of *Cj*TsdA will be described more fully elsewhere (manuscript in

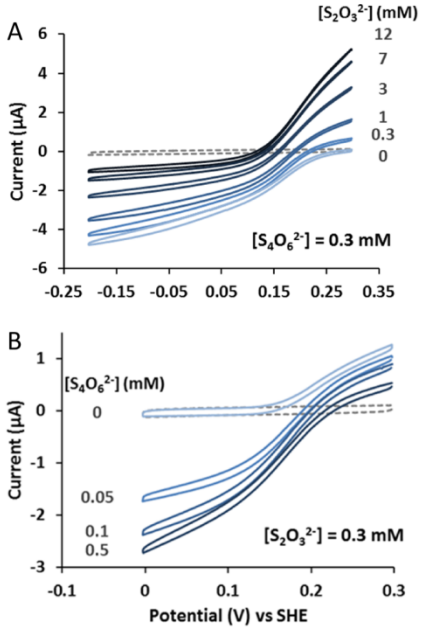

Figure 3. Protein film cyclic voltammetry for *Cj*TsdA in (A) 0.3 mM $S_4O_6^{2-}$ and (B) 0.3 mM $S_2O_3^{2-}$ with increasing concentration of the second substrate as indicated. Cyclic voltammetry recorded prior to substrate addition (gray broken lines). Scan rate 10 mV s^{-1}, electrode rotation, 500 rpm in 100 mM ammonium acetate, 50 mM NaCl, pH 5, 42 °C.

preparation). Here we retain a focus on the experimental resolution of $E_{TT/TS}$ and a final series of experiments that address the pH dependence of this parameter. Neither thiosulfate nor tetrathionate change their protonation state between pH 5 and 7.[9] As a consequence $E_{TT/TS}$ will be independent of pH in this range. Measurements in solutions of equal concentrations of thiosulfate and tetrathionate with *Cj*TsdA at pH 6 or at pH 7 generated $E_{TT/TS}$ values with the predicted behavior, Figure 2 (open circles and squares). Taking the average of the 111 data points represented in Figure 2, we determine a value for $E_{TT/TS}$ of +198 ± 4 mV versus SHE.

The range of oxidation states (−2 to +8) available to sulfur and the abundance of compounds containing multiple sulfurs with different oxidation states leads to a rich and complex chemistry of aqueous sulfur oxoanions.[1,2,29] By exploiting enzymes as selective catalysts for the tetrathionate/thiosulfate interconversion, we have been able to provide experimental resolution of a key thermodynamic parameter contributing to the description of such systems. The experimentally measured value of $E_{TT/TS}$ lies within the range of values calculated previously.[10−13] However, it is 174 mV more positive than the value of +24 mV[10] widely cited in the construction of redox towers. As a consequence more free energy is available to be harnessed during the respiratory reduction of tetrathionate than was previously recognized. At + 198 mV the formal reduction potential of the tetrathionate/thiosulfate couple is more positive than the corresponding values for several prevalent terminal respiratory electron-acceptor couples at neutral pH. These include fumarate/succinate (+33 mV),[10] trimethylamine oxide/trimethylamine (+130 mV),[30] and dimethyl sulfoxide/dimethylsulfide (+160 mV).[31] This can explain why *Salmonella enterica* grows by oxidation of propanediol or ethanolamine in

DOI: 10.1021/jacs.5b08291
J. Am. Chem. Soc. 2015, 137, 13232−13235

the presence of tetrathionate, but not dimethyl sulfoxide, trimethylamine oxide, or fumarate, as terminal respiratory electron acceptor. This is despite *S. enterica* having capacity to respire on these alternate terminal electron acceptors when more reduced electron donor(s) such as glycerol are used.[32] Indeed tetrathionate may provide the respiratory electron acceptor in many more contexts than presently recognized. The lifestyles of pathogenic and commensal gut bacteria may benefit from respiratory reduction of the tetrathionate produced in the human intestine during inflammation.[6] In addition, for marine microbiota at neutral pH, the tetrathionate in sediments represents a more favorable electron acceptor than the high abundance compounds dimethyl sulfoxide and trimethylamine oxide.[33]

An exact, experimentally achieved $E_{TT/TS}$ value as provided here will also contribute to a better understanding of industrial applications involving thiosulfate. One prominent example is the use of thiosulfate instead of the hazardous cyanide as a lixiviant for gold. Despite extensive research work in this area, neither commercialization of the thiosulfate processes nor full knowledge of the underlying mechanism have been achieved.[5,34,35] This is due largely to the complexity of the chemical reactions accompanying the process and which include the formation of tetrathionate and other polythionates from the oxidation of thiosulfate in aqueous solutions.

■ ASSOCIATED CONTENT

Supporting Information

The Supporting Information is available free of charge on the ACS Publications website at DOI: 10.1021/jacs.5b08291.

Overproduction, purification and preparation of the thiosulfate dehydrogenases. Electrochemical procedures, resolution of E_{ZCP} and quantification of catalytic bias resolved from Figure 1 (PDF)

■ AUTHOR INFORMATION

Corresponding Authors

*j.butt@uea.ac.uk

*julia-kurth@gmx.de

Notes

The authors declare no competing financial interest.

■ ACKNOWLEDGMENTS

We thank Jula Reuter for cloning pET_marpuDRAFT_1194, Alexander Flegler for preparation of *Mp*TsdBA and *Av*TsdA, Sam Rowe and Colin Lockwood for assistance with the electrochemical measurements, and Myles Cheesman for helpful discussion. Funding was from the Deutsche Forschungsgemeinschaft (DA 351/7-2) to C.D., a scholarship to J.M.K. from the Aventis Foundation awarded by the Association of the Chemical Industry (scholarship 700051) and the UK Biotechnology and Biological Sciences Research Council grants K009885 and L022176 to J.N.B.

■ REFERENCES

(1) Harding, C.; Janes, R.; Johnson, D. *Elements of the P Block*; Royal Society of Chemistry: Cambridge, 2002.
(2) Varga, D.; Horváth, A. K.; Nagypál, I. *J. Phys. Chem. B* **2006**, *110*, 2467−2470.
(3) Aylmore, M. G.; Muir, D. M. *Miner. Eng.* **2001**, *14*, 135−174.
(4) Trudinger, P. A. *J. Bacteriol.* **1967**, *93*, 550−559.
(5) Barrett, E. L.; Clark, M. A. *Microbiol. Rev.* **1987**, *51*, 192−205.
(6) Podgorsek, L.; Imhoff, J. F. *Aquat. Microb. Ecol.* **1999**, *17*, 255−265.
(7) Winter, S. E.; Thiennimitr, P.; Winter, M. G.; Butler, B. P.; Huseby, D. L.; Crawford, R. W.; Russell, J. M.; Bevins, C. L.; Adams, L. G.; Tsolis, R. M.; Roth, J. R.; Bäumler, A. J. *Nature* **2010**, *467*, 426−429.
(8) Liu, Y. W.; Denkmann, K.; Kosciow, K.; Dahl, C.; Kelly, D. J. *Mol. Microbiol.* **2013**, *88*, 173−188.
(9) Pourbaix, M.; Pourbaix, A. *Geochim. Cosmochim. Acta* **1992**, *56*, 3157−3178.
(10) Thauer, R. K.; Jungermann, K.; Decker, K. *Bacteriol. Rev.* **1977**, *41*, 100−180.
(11) Kaprálek, F. *J. Gen. Microbiol.* **1972**, *71*, 133−139.
(12) Cobble, J. W.; Stephens, H. P.; McKinnon, I. R.; Westrum, E. F. *Inorg. Chem.* **1972**, *11*, 1669−1674.
(13) Williamson, M. A.; Rimstidt, J. D. *Geochim. Cosmochim. Acta* **1992**, *56*, 3867−3880.
(14) Bard, A. J.; Parsons, R.; Jordan, J. *Standard potentials in aqueous solution*; Marcel Dekker: New York, 1985.
(15) Mel, H. C.; Hugus, Z. Z.; Latimer, W. M. *J. Am. Chem. Soc.* **1956**, *78*, 1822−1826.
(16) Wagman, D. D.; Evans, W. H.; Parker, V. B.; Schumm, R. H.; Halow, I.; Bailey, S. M.; Churney, K. L.; Nuttall, R. L. *J. Phys. Chem. Ref. Data, Suppl.* **1982**, *11*, Supplement No. 2, pp 2-1−2-392.
(17) Latimer, W. M. *Oxidation potentials*, 2nd ed.; Prentice-Hall: New York, 1952.
(18) Oelkers, E. H.; Helgeson, H. C.; Shock, E. L.; Sverjensky, D. A.; Johnson, J. W.; Pokrovskii, V. A. *J. Phys. Chem. Ref. Data* **1995**, *24*, 1401−1560.
(19) Denkmann, K.; Grein, F.; Zigann, R.; Siemen, A.; Bergmann, J.; van Helmont, S.; Nicolai, A.; Pereira, I. A. C.; Dahl, C. *Environ. Microbiol.* **2012**, *14*, 2673−2688.
(20) Brito, J. A.; Denkmann, K.; Pereira, I. A. C.; Archer, M.; Dahl, C. *J. Biol. Chem.* **2015**, *290*, 9222−9238.
(21) Léger, C.; Jones, A. K.; Albracht, S. P. J.; Armstrong, F. A. *J. Phys. Chem. B* **2002**, *106*, 13058−13063.
(22) Hirst, J.; Sucheta, A.; Ackrell, B. A. C.; Armstrong, F. A. *J. Am. Chem. Soc.* **1996**, *118*, 5031−5038.
(23) Zu, Y.; Shannon, R. J.; Hirst, J. *J. Am. Chem. Soc.* **2003**, *125*, 6020−6021.
(24) Parkin, A.; Seravalli, J.; Vincent, K. A.; Ragsdale, S. W.; Armstrong, F. A. *J. Am. Chem. Soc.* **2007**, *129*, 10328−10329.
(25) Hexter, S. V.; Esterle, T. F.; Armstrong, F. A. *Phys. Chem. Chem. Phys.* **2014**, *16*, 11822−11833.
(26) Abou Hamdan, A.; Dementin, S.; Liebgott, P. P.; Gutierrez-Sanz, O.; Richaud, P.; De Lacey, A. L.; Roussett, M.; Bertrand, P.; Cournac, L.; Léger, C. *J. Am. Chem. Soc.* **2012**, *134*, 8368−8371.
(27) Zhang, H.; Jeffrey, M. I. *Inorg. Chem.* **2010**, *49*, 10273−10282.
(28) Fava, A.; Bresadola, S. *J. Am. Chem. Soc.* **1955**, *77*, 5792−5794.
(29) Xu, L.; Horváth, A. K. *J. Phys. Chem. A* **2014**, *118*, 6171−6180.
(30) Jones, C. W. *Bacterial respiration and photosynthesis*; Thomas Nelson and Sons, Ltd.: Walton-on-Thames, England, 1982.
(31) Wood, P. M. *FEBS Lett.* **1981**, *124*, 11−14.
(32) Price-Carter, M.; Tingey, J.; Bobik, T. A.; Roth, J. R. *J. Bacteriol.* **2001**, *183*, 2463−2475.
(33) Barrett, E. L.; Kwan, H. S. *Annu. Rev. Microbiol.* **1985**, *39*, 131−149.
(34) Grosse, A. C.; Dicinoski, G. W.; Shaw, M. J.; Haddad, P. R. *Hydrometallurgy* **2003**, *69*, 1−21.
(35) Feng, D.; Van Deventer, J. S. J. *Hydrometallurgy* **2010**, *105*, 120−126.

DOI: 10.1021/jacs.5b08291
J. Am. Chem. Soc. 2015, 137, 13232−13235

SUPPORTING INFORMATION.

Catalytic Protein Film Electrochemistry Provides a Direct Measure of the Tetrathionate/Thiosulfate Reduction Potential

Julia M. Kurth*[1], Christiane Dahl[1], Julea N. Butt*[2]

[1]Institut für Mikrobiologie & Biotechnologie, Rheinische Friedrich-Wilhelms-Universität Bonn, Meckenheimer Allee 168, D-53115 Bonn, Germany.

[2]Centre for Molecular and Structural Biochemistry, School of Chemistry and School of Biological Sciences, University of East Anglia, Norwich Research Park, Norwich NR4 7TJ, U.K.

OVERPRODUCTION AND PURIFICATION OF RECOMBINANT THIOSULFATE DEHYDROGENASES

The *c8j_0815* (*tsdA*) gene was amplified from the *C. jejuni* 81116 genome with primers pET-N-TsdACj_fw (CCGGATCCTTAGATCCAAATTTG) and pET-N-TsdACj_rev (CCGAAGCTTCTACTTCTTGATCA) carrying BamHI and HindIII restriction sites, respectively. The digested PCR product was cloned into a modified pET22b vector encoding an N-terminal Strep-tag (pETStrepDsrJ), resulting in pET-N-Strep-TsdACj. pETStrepDsrJ (Fabian Grein, Bonn, unpublished work) contains the *A. vinosum dsrJ*[1] gene with a sequence encoding a N-terminal Strep-tag between the NcoI and HindIII sites of pET22b (Novagen). A BamHI site resides between the Strep-tag and DsrJ encoding sequences.

Single colonies of *E. coli* BL21(DE3) containing pET-N-Strep-TsdACj and pEC86[2] were inoculated in 800 ml batches of LB medium containing 100 mg ml^{-1} ampicillin and 25 mg ml^{-1} chloramphenicol and incubated at 37 °C and 180 rpm. Cells were harvested by centrifugation after 15 to 17 h, resuspended in 100 mM Tris-HCl, pH 8.0, and lysed by sonication. Insoluble material was removed by centrifugation; 17 700 *g* for 30 min at 4 °C. Then *Cj*TsdA (37103 Da; without signal peptide, with hemes) was purified by Strep-Tactin affinity chromatography according to the manufacturer's instructions (IBA GmbH, Göttingen, Germany).

The *marpu_02550* (*tsdBA*) gene was amplified from the *M. purpuratum* 984 genome with primers MarpuDR1194_for (CGGAGGGATCCTCATATGACGCATCTC) and MarpuDR1194_rev (GACCTGCTCGAGATCCTTGGC) carrying NdeI and XhoI restriction sites, respectively. The fragment was cloned into pET-22b(+) (Novagen) containing the sequence for a C-terminal His-tag, resulting in pET_marpuDRAFT_1194. 700 ml batches of LB medium with 100 mg ml^{-1} ampicillin and 25 mg ml^{-1} chloramphenicol were inoculated (2 % v/v) with a preculture of *E. coli* BL21 (DE3) cells containing pET_marpuDRAFT_1194 and pEC86[2]. Cultures were grown at 37 °C and 180 rpm until an OD_{600} of 0.6 was reached, followed by overnight incubation at 25 °C and 180 rpm. The cells were harvested by centrifugation, resuspended in 50 mM NaH_2PO_4, 300 mM NaCl, 10 mM imidazole; pH 7.5 and lysed by sonication. Insoluble material was removed by centrifugation; 17 700 *g* for 30 min at 4 °C. *Mp*TsdBA (58151 Da; without signal peptide, with hemes) was purified via nickel-chelate affinity chromatography according to the manufacturer's instruc-

tions (Qiagen, Hilden, Germany). *Av*TsdA (28142 Da; without signal peptide, with hemes) was overproduced and purified as described previously[3].

The purity of the proteins was assessed by sodium dodecyl sulfate-polyacrylamide gel electrophoresis (SDS-PAGE) performed as described in Dahl *et al*. (2005)[4] and heme staining in acrylamide gels was done as described by Thomas *et al*. (1976)[5]. The proteins used for electrochemistry were judged to be at least 95 % pure on the basis of SDS-PAGE, SI Fig. 1. Protein concentrations were determined with the BCA-Kit from Pierce (Rockford, USA). Aliquots of the purified proteins were stored frozen at -80 °C.

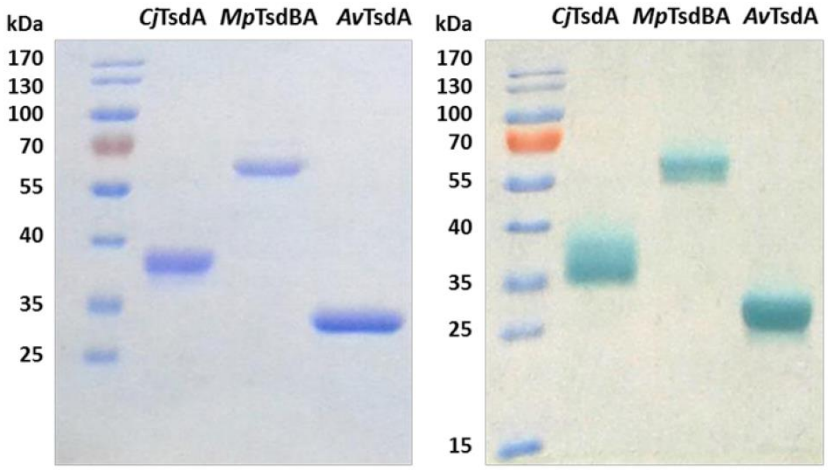

SI Figure 1: SDS-PAGE demonstrating purity of samples used for protein film electrochemistry. Gels loaded with 3 to 6 µg *Cj*TsdA, *Mp*TsdBA and *Av*TsdA as indicated. Protein visualized by Coomassie blue staining (left panel) and heme staining (right panel).

PROTEIN FILM ELECTROCHEMISTRY

Reagents were of Analar quality or higher and the water was of resistivity > 18 MΩ cm. Stock solutions of $Na_2S_2O_3$ (0.5 M) and $Na_2S_4O_6$ (0.5 M) were prepared as needed for each day of experiments by dissolution of the required mass in an appropriate volume of water. Solutions for electrochemical analysis were prepared immediately prior to measurement by appropriate dilution of the stock solution(s) into the desired buffer-electrolyte. The buffer-electrolyte at pH 5 was 100 mM ammonium acetate, 50 mM NaCl, at pH 6 was 50 mM potassium phosphate, 50 mM NaCl and at pH 7 was 50 mM HEPES, 50 mM NaCl. For *Av*TsdA, higher current magnitudes were observed when 2 mM neomycin was included in the enzyme solution used to coat the electrode and in the electrochemical cell.

Protein-film electrochemistry was performed using a previously described non-isothermal three-electrode cell configuration[6]. The reference electrode was Ag/AgCl, saturated KCl. Measured potentials were converted to values vs SHE by addition of 197 mV. Immediately prior to use pyrolytic graphite edge working electrodes (3 mm diameter) were polished with an aqueous slurry of 0.3 μm Al_2O_3, sonicated, rinsed and dried with a tissue. The polished electrode was exposed to a solution of the desired enzyme; 103 μM *Cj*TsdA in 50 mM HEPES pH 7, 50 mM NaCl or 60 μM *Mp*TsdBA in 20 mM Tris-HCl pH 7.5, 150 mM NaCl or 129 μM *Av*TsdA in 50 mM Bis-Tris pH 6.5, 2 mM neomycin. After ca. 3 minutes the enzyme solution was removed from the electrode surface, which was then rinsed with room temperature buffer-electrolyte to remove any loosely bound enzyme. Excess buffer-electrolyte was carefully removed from the electrode with a tissue taking care not to dry the electrode surface. The electrode was then placed in the electrochemical cell and measurement commenced. Electrochemical measurements were performed with an Autolab electrochemical analyzer under the control of GPES software. Electrode rotation was with an EG&G Model 636 electrode rotator. Catalytic currents were independent of electrode rotation at ≥ 500 rpm and so free from limitation by mass transfer of substrate (product) to (from) the adsorbed enzyme. For these conditions the catalytic currents of the forward and reverse sweeps were essentially superimposable and proved to be remarkably robust. There was no detectable loss of magnitude over 30 minutes of continuous cyclic voltammetry. The electrochemical sample was maintained at 42 °C for studies of *Cj*TsdA because this is the optimal growth temperature of *C. jejuni*. Measurements with *Mp*TsdBA and *Av*TsdA were performed with the sample at 25 °C.

Values for $E_{TT/TS}$ were derived from measurements made in the presence of *Cj*TsdA or *Mp*TsdBA since both enzymes displayed clear catalytic currents for thiosulfate oxidation and tetrathionate reduction. The catalytic bias of both enzymes at pH 5 is quantified in SI Figure 2. Values for $E_{TT/TS}$ were calculated using the Nernst equation and E_{ZCP} values measured in a range of conditions. From cyclic voltammetry, E_{ZCP} values were defined from the points of intersection of voltammograms recorded in the presence and absence of substrates and averaged for each scan direction (as an example see SI Figure 3). E_{ZCP} values were also measured directly with the electrochemical analyzer operated in the galvanostat mode. Values of $E_{TT/TS}$ calculated from these two methods conform very well (SI Figure 4). For Figure 2 of the main text and in reporting the error range, average values and standard deviations were calculated from the appropriate data sets in Microsoft Excel 2010.

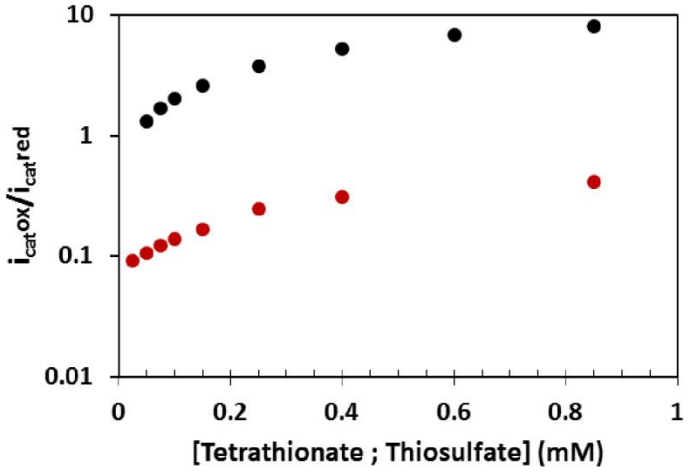

SI Figure 2. The catalytic bias of *Cj*TsdA (red) and *Mp*TsdBA (black) at pH 5 in equal concentrations of tetrathionate and thiosulfate. The catalytic current magnitudes were measured at +275 mV for thiosulfate oxidation (i_{cat}ox) and +175 mV for tetrathionate reduction (i_{cat}red). These values were extracted from the cyclic voltammograms of Figure 1 that were performed with a scan rate of 10 mV s^{-1} and electrode rotation at 500 rpm. Buffer-electrolyte 100 mM ammonium acetate, 50 mM NaCl, pH 5 at 42 °C for *Cj*TsdA and 25 °C for *Mp*TsdAB.

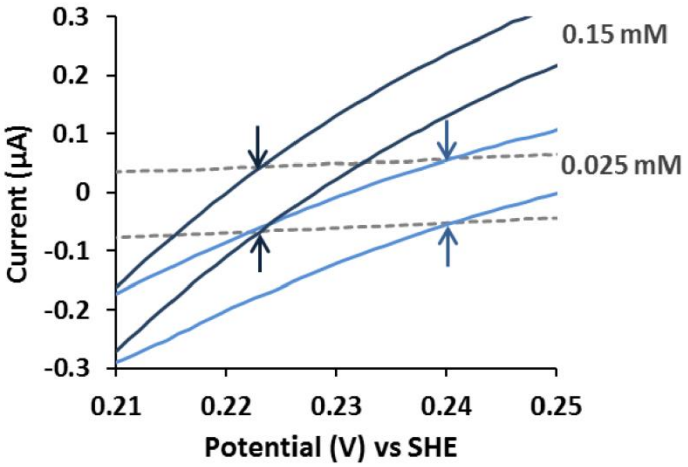

SI Figure 3. Representative protein film cyclic voltammetry of *Cj*TsdA in solutions containing equal concentrations of thiosulfate and tetrathionate as indicated (blue continuous lines) and prior to substrate addition (grey broken line). The points of zero current for each scan direction are indicated with arrows and the corresponding E_{ZCP} values are 0.223 V at 0.15 mM substrates and 0.240 V at 0.025 mM substrates. Scan rate 10 mV s^{-1}, electrode rotation 500 rpm in 100 mM ammonium acetate, 50 mM NaCl, pH 5 at 42 °C. This graphic is an extract of Figure 1 of the main text.

S4

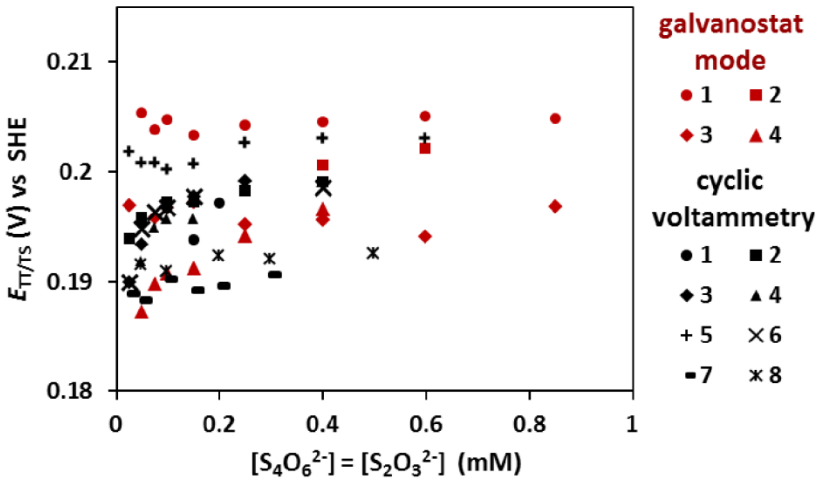

SI Figure 4. $E_{TT/TS}$ values defined by protein film electrochemistry of *Cj*TsdA at pH 5 and equal concentrations of $S_2O_3^{2-}$ and $S_4O_6^{2-}$. The E_{ZCP} values used for calculation of $E_{TT/TS}$ were either measured by cyclic voltammetry (black symbols) or directly with the electrochemical analyzer operated as a galvanostat (red symbols).The average $E_{TT/TS}$ value determined by cyclic voltammetry is 196 ± 4 mV and the average value derived from measurements in the galvanostat mode is 198 ± 5 mV.

REFERENCES

(1) Grein, F.; Venceslau, S. S.; Schneider, L.; Hildebrandt, P.; Todorovic, S.; Pereira, I. A. C.; Dahl, C. *Biochemistry* **2010**, *49*, 8290–8299.
(2) Arslan, E.; Schulz, H.; Zufferey, R.; Künzler, P.; Thöny-Meyer, L. *Biochem. Biophys. Res. Commun.* **1998**, *251*, 744–747.
(3) Denkmann, K.; Grein, F.; Zigann, R.; Siemen, A.; Bergmann, J.; van Helmont, S.; Nicolai, A.; Pereira, I. A. C.; Dahl, C. *Environ. Microbiol.* **2012**, *14*, 2673–2688.
(4) Dahl, C.; Engels, S.; Pott-Sperling, A. S.; Schulte, A.; Sander, J.; Lübbe, Y.; Deuster, O.; Brune, D. C. *J. Bacteriol.* **2005**, *187*, 1392–1404.
(5) Thomas, P. E.; Ryan, D.; Levin, W. *Anal. Biochem.* **1976**, *75*, 168–176.
(6) Anderson, L. J.; Richardson, D. J.; Butt, J. N. *Biochemistry* **2001**, *40*, 11294–11307.

Chapter 2

Electron accepting units of the diheme cytochrome *c* TsdA, a bifunctional thiosulfate dehydrogenase/tetrathionate reductase

Introduction & Summary

The widespread enzyme TsdA enables the purple sulfur bacterium *Allochromatium vinosum* (*Av*) to use thiosulfate as electron donor for phototrophic growth. Previously, it has been shown that in some bacterial sulfur oxidizers like *Sideroxydans lithotrophicus* and *Thiomonas intermedia* the *tsdA* gene is immediately preceded by *tsdB* encoding another diheme cytochrome *c* that might be able to accept electrons from TsdA. However, TsdB is not always present and the question arose which other and/or additional redox carrier(s) can accept electrons from TsdA and feed them into photosynthetic and respiratory electron transport chains.

Here, a strong interaction between TsdA and TsdB was found to be present when both proteins originate from the same source organism and TsdB was indeed proven to act as effective electron acceptor of TsdA *in vitro*. Therefore, it is concluded that organisms encoding not only TsdA but also TsdB in their genomes use TsdB as an effective electron acceptor for TsdA. The purple sulfur bacterium *Marichromatium purpuratum* (*Mp*) contains a TsdBA fusion protein. For *Av*TsdA and *Mp*TsdBA the periplasmic high potential iron-sulfur protein (HiPIP) was identified as the electron acceptor that mediates electron flow during anoxygenic photosynthesis and aerobic respiration. The *Mp*TsdBA crystal structure revealed a thiosulfate ion being covalently bound to the Sγ atom of the active site heme-ligating cysteine. This observation was a breakthrough regarding the reaction mechnanism of the TsdA catalyzed reaction as it proves that a cysteine S-thiosulfonate intermediate is formed as a central reaction intermediate.

Chapter 2

Electron accepting units of the diheme cytochrome *c* TsdA, a bifunctional thiosulfate dehydrogenase/tetrathionate reductase

This research was originally published in the Journal of Biological Chemistry:

Kurth, J.M., Brito, J.A., Reuter, J., Flegler, A., Koch, T., Franke, T., Klein E.-M., Rowe S.F., Butt J.N., Denkmann K., Pereira I.A.C., Archer M., Dahl C. (2016) Electron accepting units of the diheme cytochrome *c* TsdA, a bifunctional thiosulfate dehydrogenase/tetrathionate reductase. *J Biol Chem* **291**: 24804–24818.

http://www.jbc.org/content/291/48/24804.full

Author contributions

- JMK analyzed and compiled the data for all experiments except the *Mp*TsdBA crystallization and determination of reduction potentials
- JMK wrote the paper together with CD, JAB and MA
- JMK produced and analyzed the proteins from *S. lithotrophicus*

THE JOURNAL OF BIOLOGICAL CHEMISTRY VOL. 291, NO. 48, pp. 24804–24818, November 25, 2016

Electron Accepting Units of the Diheme Cytochrome *c* TsdA, a Bifunctional Thiosulfate Dehydrogenase/Tetrathionate Reductase*◆

Received for publication, August 19, 2016, and in revised form, September 22, 2016 Published, JBC Papers in Press, September 30, 2016, DOI 10.1074/jbc.M116.753863

Julia M. Kurth[‡1,2], José A. Brito[§1,3], Jula Reuter[‡4], Alexander Flegler[‡], Tobias Koch[‡], Thomas Franke[‡], Eva-Maria Klein[‡5], Sam F. Rowe[¶6], Julea N. Butt[¶7], Kevin Denkmann[‡8], Inês A. C. Pereira[§], Margarida Archer[§9], and Christiane Dahl[‡10]

From the [‡]Institut für Mikrobiologie & Biotechnologie, Rheinische Friedrich-Wilhelms-Universität Bonn, 53115 Bonn, Germany, the [§]Instituto de Tecnologia Química e Biológica António Xavier, Universidade Nova de Lisboa (ITQB-UNL), 2780-157 Oeiras, Portugal, and the [¶]Centre for Molecular and Structural Biochemistry, School of Chemistry and School of Biological Sciences, University of East Anglia, Norwich Research Park, Norwich NR4 7TJ, United Kingdom

Edited by Ruma Banerjee

The enzymes of the thiosulfate dehydrogenase (TsdA) family are wide-spread diheme *c*-type cytochromes. Here, redox carriers were studied mediating the flow of electrons arising from thiosulfate oxidation into respiratory or photosynthetic electron chains. In a number of organisms, including *Thiomonas intermedia* and *Sideroxydans lithotrophicus*, the *tsdA* gene is immediately preceded by *tsdB* encoding for another diheme cytochrome. Spectrophotometric experiments in combination with enzymatic assays in solution showed that TsdB acts as an effective electron acceptor of TsdA *in vitro* when TsdA and TsdB originate from the same source organism. Although TsdA covers a range from −300 to +150 mV, TsdB is redox active between −100 and +300 mV, thus enabling electron transfer between these hemoproteins. The three-dimensional structure of the TsdB-TsdA fusion protein from the purple sulfur bacterium *Marichromatium purpuratum* was solved by X-ray crystallography to 2.75 Å resolution providing insights into internal electron transfer. In the oxidized state, this tetraheme cytochrome *c* contains three hemes with axial His/Met ligation, whereas heme 3 exhibits the His/Cys coordination typical for TsdA active sites. Interestingly, thiosulfate is covalently bound to Cys^{330} on heme 3. In several bacteria, including *Allochromatium vinosum*, TsdB is not present, precluding a general and essential role for electron flow. Both *Av*TsdA and the *Mp*TsdBA fusion react efficiently *in vitro* with high potential iron-sulfur protein from *A. vinosum* (E_m +350 mV). High potential iron-sulfur protein not only acts as direct electron donor to the reaction center in anoxygenic phototrophs but can also be involved in aerobic respiratory chains.

* This work was supported by Deutsche Forschungsgemeinschaft Grant Da 351/7-2; Fundação para a Ciência e Tecnologia through iNOVA4Health Research Unit, LISBOA-01-0145-FEDER-007344, co-funded by Fundação para a Ciência e a Tecnologia do Ministério para a Ciência e Ensino Superior (FCT/MCES) and Fonds Européen de Developpement Économique et Régional (FEDER) under the PT2020 Partnership Agreement through the Research and Development Unit; UID/Multi/04551/2013 (GreenIT); BioStruct-X Proposal 1493; MostMicro Unit by Project LISBOA-01-0145-FEDER-007660 (Microbiologia Molecular, Estrutural e Celular) funded by FEDER funds through COMPETE2020-Programa Operacional Competitividade e Internacionalização (POCI), and by National Funds through FCT.

◆ This article was selected as a Paper of the Week.

The atomic coordinates and structure factors (code 5LO9) have been deposited in the Protein Data Bank (http://wwpdb.org/).

[1] Both authors contributed equally to this work.

[2] Recipient of Scholarship 700051 funded by the Aventis Foundation and awarded by the Fonds der Chemischen Industrie.

[3] Recipient of Fundação para a Ciência e a Tecnologia Fellowship SFRH/BPD/79224/2011.

[4] Present address: Rheinische Friedrich-Wilhelms-Universität Bonn, Institut für Pharmazeutische Mikrobiologie, Meckenheimer Allee 168, 53115 Bonn, Germany.

[5] Present address: Rheinische Friedrich-Wilhelms-Universität Bonn, Institut für Virologie, Siegmund-Freud-Str. 25, 53127 Bonn, Germany.

[6] Supported by a studentship from the Biotechnology and Biological Sciences Research Council, United Kingdom.

[7] Supported by a Royal Society Leverhulme Trust Senior Research Fellowship.

[8] Present address: Dunn Labortechnik GmbH, Thelenberg 6, 53567 Asbach, Germany.

[9] Awarded FCT Investigator IF/00656/2014. To whom correspondence may be addressed. Tel.: 351-214-469-747; Fax: 351-214-433-644; E-mail: archer@itqb.unl.pt.

[10] To whom correspondence may be addressed. Tel.: 49-228-732119; Fax: 49-228-737576; E-mail: chdahl@uni-bonn.de.

The bifunctional thiosulfate dehydrogenase/tetrathionate reductase TsdA is present in various organisms of different proteobacterial genera (1). In the diheme cytochrome *c* from the purple sulfur bacterium *Allochromatium vinosum*, an axial histidine/cysteine ligation of the central iron atom has been firmly established for the active site heme (2). This type of ligation is rare among prokaryotes, usually leads to a low redox potential of the corresponding heme (3–6), and appears to be of special importance in sulfur-based energy metabolism. TsdA proteins catalyze the reversible formation of a sulfur-sulfur bond between the sulfane atoms of two thiosulfate molecules, yielding tetrathionate and releasing two electrons. TsdA enzymes of various source organisms exhibit different catalytic bias (7). Although the enzyme from the sulfur oxidizer *A. vinosum* is strongly adapted to catalyzing thiosulfate oxidation (2), TsdA from *Campylobacter jejuni* acts primarily as a tetrathionate reductase and enables the organism to use tetrathionate as an alternative electron acceptor for anaerobic respiration (8).

At present, it is largely unclear which redox carriers mediate the flow of electrons arising from thiosulfate oxidation into respiratory or photosynthetic electron chains. In several organ-

isms, including *Thiomonas intermedia*, *Sideroxydans lithotrophicus,* and *Pseudomonas stutzeri*, *tsdA* is immediately preceded by a gene encoding another diheme cytochrome, TsdB (1). TsdB itself is not reactive with thiosulfate but accepts electrons from TsdA even when TsdA and TsdB do not originate from the same organism (1). Kinetic data that quantitatively describe the interaction between TsdA and TsdB have not been published so far. In the anoxygenic phototrophic purple sulfur bacterium *Marichromatium purpuratum*, TsdA and TsdB form a fusion protein with TsdB constituting the N-terminal domain (7). TsdBA fusion proteins are also encoded in other members of the family Chromatiaceae, *i.e. Thiorhodococcus* sp. AK35 (D779_1816), *Thiocystis violascens* (Thivi_3993), *Thiorhodococcus drewsii* (ThidrDRAFT_3922), and *Thioflaviococcus mobilis* (Thimo_0460). However, TsdBA fusions are not a common trait in purple sulfur bacteria. In *A. vinosum*, a *tsdB* gene is not present (1).

In *A. vinosum,* the protein with the closest relationship to *T. intermedia* or *P. stutzeri* TsdB is Alvin_2879. This cytochrome c_4 (previously cytochrome $c_{553(550)}$) is membrane-bound (possibly via the hydrophobic protein Alvin_2880) and has a positive redox potential of +330 mV (9). Another candidate for accepting electrons from TsdA in purple anoxygenic phototrophic bacteria is the high potential iron-sulfur protein (HiPIP).[11] *A. vinosum* and *M. purpuratum* produce HiPIP, and as this protein has a quite positive reduction potential (+350 mV (10)) it would be well suited as an electron acceptor for TsdA. This proposal is corroborated by a previous report where a protein preparation with thiosulfate dehydrogenase activity from *A. vinosum* reduced HiPIP *in vitro* (11).

Here, we study Tsd(B)A enzymes from dedicated sulfur oxidizers and characterize in detail the interaction of TsdA with TsdB. Additionally, we pose the following question. Which proteins serve as immediate electron acceptors for either TsdA alone or the TsdBA fusion protein (when present)? It is furthermore intended to derive models for the electron flow involved.

Results

Characterization of TsdA and TsdB—UV-visible electronic absorbance spectroscopy, X-ray diffraction, and activity assays have revealed a number of characteristic features of *Av*TsdA (1, 2, 12). However, the electrochemical window in which the hemes are redox active remained unknown. To gain insight into this property, we mapped out the redox activity of *Av*TsdA adsorbed as an electroactive film on optically transparent mesoporous nanocrystalline SnO_2 electrodes. The spectrum of the enzyme-coated electrode equilibrated at +302 mV contained features typical of ferric *c*-type hemes superimposed on a small contribution from light scattering by the electrode material (Fig. 1). The Soret maximum at 406 nm and broad lower intensity features in the $\alpha\beta$-region are typical of those displayed by solutions of oxidized *Av*TsdA (1). When the electrode potential was lowered to −648 mV in 50-mV steps with a spectrum recorded after a 60-s pause at each desired potential (Fig. 1), those features were replaced with peaks having maxima at 418, 523, and 553 nm, which are typical of dithionite-reduced enzyme (1). Variation of the Soret intensity at 418 nm with electrode potential revealed that the hemes were reduced between approximately +150 and −350 mV (Fig. 1, *inset, closed squares*).

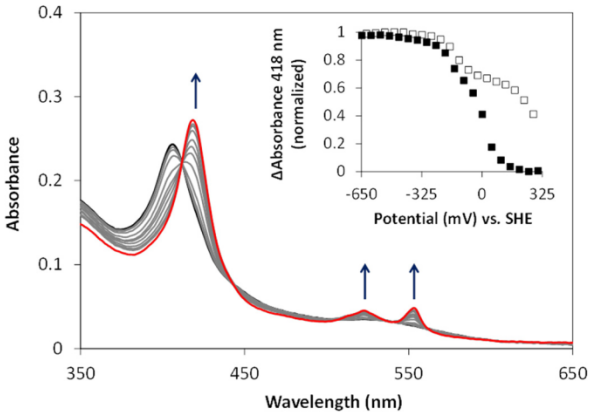

FIGURE 1. **Redox activity of *Av*TsdA adsorbed on a mesoporous nanocrystalline SnO_2 electrode.** Electronic absorbance was recorded with the electrode poised at +302 mV (*black*), +152 to −298 mV at 50-mV intervals (*gray*), and −648 mV (*red*). All potentials are quoted *versus* the standard hydrogen electrode (*SHE*). The *arrows* indicate increases in absorbance as the electrode potential was lowered. *Inset* shows the normalized change in absorbance at 418 nm against the applied potential as the enzyme was reduced (*closed squares*) and re-oxidized (*open squares*).

The response of reduced *Av*TsdA to a stepwise increase of the electrode potential was assessed in a similar manner. The potential was raised in 50-mV steps, and the spectra were recorded after a 60-s pause at each potential (Fig. 1, *inset, open squares*). Between −648 and −98 mV, the variation in Soret intensity with the applied potential was very similar to that recorded on reduction. However, further increase of potential revealed significantly less oxidation than anticipated from the behavior seen on reduction of the enzyme. Importantly, spectra typical of the fully oxidized enzyme were measured after the electrode was poised at +302 mV for ~30 min. It was concluded that electrodic redox cycling of adsorbed *Av*TsdA was fully reversible but that full reduction occurred more quickly than complete re-oxidation. Further experiments confirmed that this behavior persisted over multiple rounds of reduction and re-oxidation. The spectral changes induced by variation of potential between −648 and −98 mV were rapidly reversed and accounted for ~35% of the change in absorbance at 418 nm when spectra of the fully oxidized and fully reduced forms of the enzyme were compared. By contrast, variations of electrode potential between −98 and +302 mV showed rapid reduction and much slower reoxidation, and the associated changes in absorbance accounted for ~65% of the total seen on full redox cycling of the enzyme. It was concluded that the slow reoxidation associated with higher potential redox event(s) was not a consequence of reversible redox events that occurred at lower potentials. Detailed inspection of the spectra provided no indication for the presence of high-spin ferric- or ferrous-heme.

The hysteretic nature of the plot of absorbance *versus* potential prevented Nernstian analysis to define the heme reduction

[11] The abbreviations used are: HiPIP, high potential iron-sulfur protein; PDB, Protein Data Bank; BisTris, 2-[bis(2-hydroxyethyl)amino]-2-(hydroxymethyl)propane-1,3-diol; r.m.s.d., root mean square deviation.

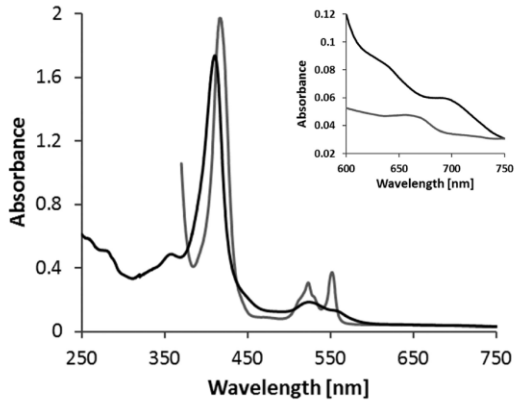

FIGURE 2. **UV-visible spectra of TsdB from *S. lithotrophicus*.** As the protein is partly reduced in the "as isolated" state, up to 170 μM ferricyanide were added to record the oxidized spectrum (*black line*). For full reduction of the protein, sodium dithionite was added (*gray line*). 100 mM Tris buffer, pH 8.0, with 150 mM NaCl and 2.5 mM desthiobiotin was used, and spectra are normalized to 750 nm. The oxidized spectrum exhibits a 700-nm peak indicating methionine as heme iron ligand. Protein concentration was 6 μM in the overview and 29 μM in the blowup.

potentials. Nevertheless, some further conclusions regarding the redox activity of *Av*TsdA can be proposed in light of the crystal structures reported (2, 12). The fully oxidized diheme cytochrome *Av*TsdA contains His/Cys coordination in heme 1 and His/Lys in heme 2. His/Cys-ligated hemes are typically distinguished from other low-spin *c*-type hemes by having much lower reduction potentials and smaller changes in extinction coefficient associated with the Fe(III)/(II) couple (4, 13). As a consequence, we propose that reduction of His/Cys-ligated heme 1 occurs reversibly between approximately −100 and −350 mV. Reduction of His/Lys-ligated heme 2 is proposed to occur between approximately +150 and −100 mV. *Av*TsdA X-ray structures reveal that this reduction is accompanied by a switch of Lys by Met as axial distal ligand to ferrous-heme 2 (2). Such a change of ligation would be expected to raise the reduction potential of heme 2. If the Met ligand is replaced slowly by Lys upon enzyme oxidation, this would account for the hysteretic nature of the redox behavior displayed by *Av*TsdA.

In contrast to TsdAs, TsdB proteins are not well characterized. The most closely related characterized cytochromes on a sequence level belong to the diheme cytochromes of the c_4 family (1). The recombinant TsdB protein from *T. intermedia* indeed binds two heme groups of 616.5 Da as the mass of 21,792.5 Da determined by MALDI-TOF mass spectrometry almost exactly matched the mass of 21,783.3 Da predicted for the mature recombinant protein, including Strep tag and two hemes. The same held true for recombinant *S. lithotrophicus* TsdB (measured mass, 22,864 Da, and predicted mass, 22,835 Da). UV-visible spectroscopy of pure recombinant TsdB from *S. lithotrophicus* is shown in Fig. 2. The spectrum conforms to that of *Ti*TsdB (1).

A sequence alignment of various TsdB proteins (Fig. 3) reveals two conserved methionine residues but no conserved histidines or cysteines indicating that both hemes of TsdB have axial coordination by His/Met. This is underpinned by the 700-nm peak in the spectrum, which is characteristic for methionine as the sixth axial heme iron ligand (14) and corroborated by the *Mp*TsdBA crystal structure determined herein (see below). A shift of the Soret band from 411 to 417 nm upon reduction was observed. Moreover, there is a distinct δ band at 359 nm in the oxidized protein spectrum. In the reduced state, the α band was detected at 552 nm and the β band at 523 nm. A split α band characteristic for a number of c_4-type cytochromes, including those from purple sulfur bacteria, was not observed (9, 15). The UV-visible spectrum for oxidized TsdB exhibited a low intensity high spin feature at 620 nm similar to that noted for cytochrome c_4 from *P. stutzeri* (16). Obviously, the ferric form of TsdB holds a small fraction of high-spin heme probably caused by weakening of the Fe-S bond at one of the two hemes with concomitant partial dissociation of the methionine and formation of an Fe-aquo bond just as outlined for the *P. stutzeri* cytochrome (16).

The reduction potential of *Ti*TsdB was determined by potentiometry with a gold electrode (Fig. 4). The potential changes determined upon reduction and reoxidation of TsdB match well. The two hemes are redox active between −100 and +300 mV. Hysteresis was not observed, consistent with both hemes being His/Met-ligated. Ligand changes are not apparent.

TsdB Is an Electron-transferring Unit Tightly Interacting with TsdA—The interaction of TsdA and TsdB proteins was analyzed for the recombinant proteins from *S. lithotrophicus*. Upon analytical gel permeation chromatography *Sl*TsdA alone eluted at a volume corresponding to a molecular mass of 65 kDa, indicating dimerization of the protein under the conditions applied (monomer, 33,042 Da). In contrast, *Sl*TsdB behaved as a 22-kDa monomer (predicted molecular mass, 22,835 Da). When both proteins were produced simultaneously in *Escherichia coli* and purified employing the Strep tag attached to TsdA, a preparation was obtained that exhibited two heme stainable polypeptides. In size, these exactly matched *Sl*TsdB and *Sl*TsdA (Fig. 5). The co-purification of the two proteins is evidence for significant interaction between them. Upon size exclusion chromatography, *Sl*TsdA and *Sl*TsdB co-eluted again in fractions corresponding to a mass of 108 kDa, indicating formation of an $\alpha_2\beta_2$ heterodimer.

Characterization of the TsdBA Fusion Protein from M. purpuratum—The protein encoded by *tsdB-tsdA* gene fusion in *M. purpuratum* provides an exceptional possibility to study the complete tetraheme cytochrome for catalytic properties and internal electron transfer. A sequence alignment of *Mp*TsdBA with combined TsdB and TsdA sequences from *S. lithotrophicus* and *T. intermedia* shows significant similarity between the N-terminal region of *Mp*TsdBA and TsdB (amino acids 1–199 of *Mp*TsdBA and *Ti*TsdB share 45% sequence identity) and between the C-terminal region of *Mp*TsdBA and TsdA (amino acids 224–518 of *Mp*TsdBA compared with *Av*TsdA or *Ti*TsdA, 39 and 50% sequence identity, respectively). The heme distal ligands cysteine and methionine of TsdA as well as the two putative heme-ligating methionines are strictly conserved (Fig. 3). Therefore, we predicted *Mp*TsdBA to contain three His/Met ligated and one His/Cys ligated heme. UV-visible spectroscopy of *Mp*TsdBA protein is shown in Fig. 6. The presence of His/Met-ligated hemes in *Mp*TsdBA is substantiated by the 700-nm peak in the spectrum of the oxidized

```
MpTsdBA          PFERGRTLAEQGDAARGIVACAGCHRADGGGDEALGAARLAGLEPAYLATQIERFRAGQR   60
SlTsdB+TsdA      --ADEARNITLQGNKQGAPACQSCHGTDGGGTPSAGIPRLAGLNAAYIEQQLKNFRAGKR   58
TiTsdB+TsdA      ------------AAPPEAASCIACHGAGGMGNPAAGYPRLAGLPEQYLADQLRYFADGAR   48
                                :* .** : * *  : *  *****   *:  *:. *  * *

MpTsdBA          SHPVMSPWAERLTPVDIAAVSAYYGALAPASN-ARAPSDVDAAAGRALAETGDWPERDLP   119
SlTsdB+TsdA      SNPIMQPIADLLTETEVTQVAAYYAALPVPLTTPQGADPALLRKGEAIATVGDWS-HEIP   117
TiTsdB+TsdA      NNAIMSGMAKPLSAAQVTALATYYSKLKPSGKPAPMPTGAAAAEGERLALRGDWE-KGIP   107
                 .. :*.  *. *: .::: :::**. *    .        .    *. :*  ***  : :*

MpTsdBA          ACVRCHGPGGVGAGAVFPPLAGQPYSYLLAQLQAWGTGRRHGEPMAIMGAVAGRLDADEQ   179
SlTsdB+TsdA      ACFQCHGPNGKGIAPHFPAIAGQSALYISNQIEAWKSGTRSNDPAGIMKSVADKLSPEQI   177
TiTsdB+TsdA      ACIRCHGPGAVGVGENFPALVGQSAAYIEAQIKAWKDGSRSGDPLGIMHTVALRMTDAQT   167
                 **.:**** . * .  ** :.**   *:  *::**  * *  :* .** :** ::   :

MpTsdBA          RALAAYFATRPLAVADPADDLPDPSPPPATASVSTPAMTVAGANAVVPEHLGAVPAGRAE   239
SlTsdB+TsdA      EAVSAYLADQQSTNGNQK-------------------------------ASETSTPTAA   205
TiTsdB+TsdA      QAVAQWLAAQPLSPTKSASAKH--------------------ADAPMAPPKSEINAAVG   206
                 .*:: ::* :  :  .                                        .

MpTsdBA          AASRFTPPSRDALPEGPLGEMVRLGARLFRHTNTDPRSAPHVGNDQTCAGCHLDNGRRAD   299
SlTsdB+TsdA      KALVFTPPNDEEIPNNEFGKIVRQGKNIFEDTQH--YAKQYVGNSLNCVNCHLASGRKEN   263
TiTsdB+TsdA      TGAKFTPPPESAIPDDDFGKMVKLGRDIMLDTPK--YAKDYVGNTLSCVNCHTDAGRMAG   264
                  .  ****  . :*:  :*::*: *  :: .*     :  :***  .*. **   **

MpTsdBA          ASPMWAAWVAYPAYRGKNQRVDTMAERIQGCFRYSMNAQDSVSGQVPETNGLVLDALQSY   359
SlTsdB+TsdA      SSPLWAAYVRYPAYRAKNNKVNTYEERIQGCFKYSLNGK------APAVDSPEMVALVTY   317
TiTsdB+TsdA      SAPLWAAYVSYPAYRGKNKKVNTFEERLQGCFKFSQNGK------APPLGSKTLVALESY   318
                 ::*:***:* *****.**::*:*  **:****::* *.:      .*   .  : ** :*

MpTsdBA          IFWLATGAPTGDTAMSGRGYPRLQPPAEGFDRTRGAALYAEHCALCHGAEGEGLLVDGEV   419
SlTsdB+TsdA      SYWLATGAPVGA-KLKGAGYPEVPKPGLIPDANRGKTVFVENCQVCHGSNGEGKKVDGKY   376
TiTsdB+TsdA      SYWLSKGLPVDE-KVAGRGYPNLPEPQQAPDYVRGQKVYEAKCILCHAANGEGQYVNGET   377
                  :**:.* *.    : * ***.:  *    *  **  ::  .* :**.::***  *:*:

MpTsdBA          VFPPLWGPRSYNWGAGMHRVDTAAAFIAANMPLLDTVRLTPQEAWDVAAYINAHERPQDP   479
SlTsdB+TsdA      IFPPLWGSESFNWGAGMHRINTAAAFIKANMPLSKGGTLTDQEAWDVATFVMSHERPQDP   436
TiTsdB+TsdA      VFPPLWGPKSFNWGAGMGSYKNAAKFIYANMPYGMSYSLSPQEAWDVAYFMDAQERPQDP   437
                 :****** .*:******   ..** ** ****      *: ******* :: ::******

MpTsdBA          RFDGSVERTAARFHASPFDLYGEPLGVDGAVLGQGVAKD--          518
SlTsdB+TsdA      RFKGNVAQTKKEYHDENC-RYGETV--NGKVLGGKHQTAAK          474
TiTsdB+TsdA      RWQGSVAATRAKFHDSKFSLYGTKV--NGKLLGDIGAPKPR          476
                 *:.*.*  *  .:* .    **  :  :* :**
```

FIGURE 3. **Sequence alignment of *Mp*TsdBA and *Sl*TsdB + TsdA as well as *Ti*TsdB + TsdA.** Sequence comparison of TsdBA fusion protein of *M. purpuratum* (MARPU_02550) with the combined sequence of TsdB and TsdA from *S. lithotrophicus* (Slit_1877 and Slit_1878) and *T. intermedia* (Tint_1893 and Tint_2892). All signal peptide sequences were removed. Heme-binding motifs are indicated by *gray boxes*, and putative distal heme ligands are marked by *black edging*. Strictly conserved residues are marked with *asterisks*. TsdA sequences of *S. lithotrophicus* and *T. intermedia* start after the gap at amino acids 195 and 189, respectively.

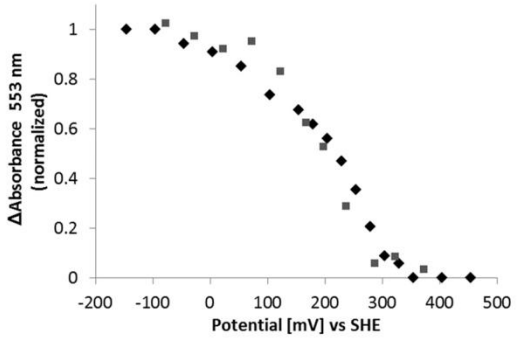

FIGURE 4. **Determination of *Ti*TsdB reduction potential by potentiometry with a gold electrode.** Potentiometric determination of redox potentials of both TsdB hemes. Applied potential according to normalized values of the α-peak (553 nm) is shown. Reduction of TsdB (*black diamonds*) and re-oxidation of the protein (*gray squares*) was measured. 10 μM TsdB in phosphate buffer, pH 5.0, was used. *SHE*, standard hydrogen electrode.

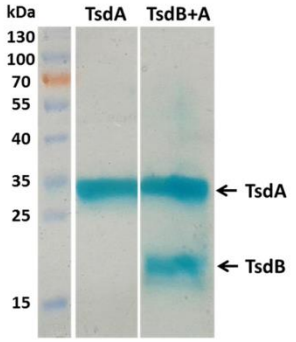

FIGURE 5. **Analysis of purified *Sl*TsdA and *Sl*TsdB + A by SDS-PAGE.** 10–15 μg of *Sl*TsdA and *Sl*TsdB + A obtained after Strep tag affinity chromatography were loaded per lane on a 12.5% gel and stained for presence of heme. In case of *Sl*TsdB + A, both proteins were produced simultaneously in *E. coli* and purified on the basis of a Strep tag attached to TsdA.

protein. This absorption band is characteristic for methionine as heme iron ligand (14). A shift of the Soret band from 413 to 420 nm was observed upon reduction. Moreover, there is a distinct δ band at 363 nm in the oxidized protein spectrum. The α band is located at 553 nm, and the β band resides at 524 nm.

The partly reduced spectrum exhibits a low intensity high spin feature at 620 nm similar to *Av*TsdA (2). The $A_{413\ nm}/A_{280\ nm}$ for pure oxidized *Mp*TsdBA is 3.4.

Crystal Structure Determination and Model Quality of MpTsdBA—To compare structural features of TsdA and TsdBA, to get a closer look into ligation of the four heme

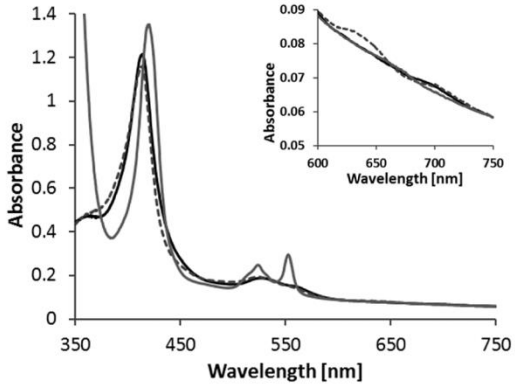

FIGURE 6. **UV-visible spectra of *Mp*TsdBA.** As the protein is slightly reduced in the "as isolated" state, 60 μM ferricyanide were added to record the oxidized spectrum (*black line*). For partial (*gray broken line*) and full reduction (*gray line*) of the protein, 0.33 and 5 mM sodium dithionite were added, respectively. 100 mM ammonium acetate buffer, pH 5, with 200 mM NaCl was used, and spectra are normalized to 750 nm. The oxidized spectrum exhibits a 700-nm peak indicating methionine as heme iron ligand and the partially reduced protein exhibits a feature at 630 nm. Protein concentration was 3.3 μM.

groups and to see how TsdA and TsdB domains are linked to each other, we have determined the X-ray structure of *Mp*TsdBA by Fe-SAD. Crystals belong to the hexagonal space group *H*32 with cell dimensions $a = b = 159.75$ Å and $c = 393.09$ Å. There are two molecules in the asymmetric unit corresponding to a Matthews coefficient (17) of 2.8 $Å^3$ Da^{-1} and a solvent content around 56%. The "as isolated" structure was refined to 2.75 Å resolution with R_{cryst} of 15.7% and R_{free} of 19.8% using a 141°-sweep of data with overall better statistics. Data collection and refinement statistics are depicted in Table 1. The high R_{meas} values observed for both sweeps are due, first, to the fine binning that autoPROC implements during data reduction, and second, to the fact that the crystal has some regions in the rotational space that are of bad quality. This is perfectly clear in the plots R_{meas} *versus* image number output by autoPROC (data not shown), highlighting that the high R_{meas} values are due to the crystal quality and not radiation damage. No evidence for radiation damage is also observed in a $m|F_o| - m|F_o|$ map calculated using both data sweeps (data not shown). *Mp*TsdBA is numbered without taking into account its 23-amino acid signal peptide that is removed upon transport into the periplasm. The model comprises the following residues of the mature recombinant protein: Pro^1–Leu^{191} and Arg^{237}–Val^{515} (chain A) and Pro^1–Ala^{192} and Ala^{240}–Ala^{516} (chain B), eight heme molecules, two thiosulfate ions, two chloride ions, seven ethylene glycols, two 1,2-propanediols and one triethylene glycol, and 113 water molecules. Electron density maps are of good quality except for the C-terminal His tag and the disordered loop connecting TsdB and TsdA domains. This region (45 amino acid residues long in chain A and 47 in chain B) has a predicted loop-like secondary structure and is not included in the final model, because no electron density was observed. Moreover, some parts of the map are somewhat "noisy" with positive and negative difference map peaks in the solvent region that could not be modeled.

Overall Fold and Similar Structures of MpTsdBA—*Mp*TsdBA is organized into two domains, an N-terminal TsdB domain and a C-terminal TsdA domain (Fig. 7*A*). Each domain includes two subdomains that are related by a pseudo-2-fold symmetry axis. Each subdomain consists of four α-helices surrounding a heme group, the typical class I *c*-type cytochrome topology. This has been previously reported for the *Av*TsdA crystal structure (2, 12) and is also observed for the *M. purpuratum* N-terminal TsdB domain. The four subdomains superimpose with r.m.s.d. of 1.3–3.0 Å for ~70 aligned Cα atoms corresponding to sequence similarities between 10 and 38%.

The final model coordinates were submitted to the DALI server (18), showing no similar structures to the complete *Mp*TsdBA arrangement. However, several hits structurally match each domain of the enzyme separately. The highest matches to *Mp*TsdB domain were cytochrome c_4 from *P. stutzeri* (PDB code 1M6Z), cytochrome c_{552} from *Acidithiobacillus ferroxidans* (PDB code 1H1O), the cytochrome subunit of flavocytochrome *c* sulfide dehydrogenase from *A. vinosum* (PDB code 1FCD), and flavocytochrome *c* from *Thermochromatium tepidum* (PDB code 3VRD), with *Z*-scores of 22.7 to 17.5, r.m.s.d. of 2.0–2.4 Å, and sequence identities between 30 and 23%.

The highest hit for the *Mp*TsdA domain was *Av*TsdA (4V2K and 4WQ9) with a Z-score of 30.6 (with 20% sequence identity and r.m.s.d. of 1.4 and 1.2 Å, respectively), followed by SoxAX from *Rhodovulum sulfidophilum* (2OZ1), the SoxD subunit of SoxCD from *Paracoccus pantotrophus* (2XTS), and the SoxA subunits of SoxAX from *Starkeya novella* (3OA8) and *P. pantotrophus* (2C1D). Z-scores ranged from 12–7.4 and r.m.s.d.s from 2.1 to 4.7 Å.

Heme Coordination in the "As Isolated" MpTsdBA—The *Mp*TsdBA crystal structure shows four heme groups per chain packed as a wire with closest iron-to-iron distances between 15 and 19 Å and shortest edge-to-edge distances of 3.5 to 6.6 Å (Fig. 7, *B* and *C*). This agrees well with other multiheme cytochrome structures that show edge-to-edge distances of 4–8 Å (19, 20).

The four hemes are covalently bound to the polypeptide chain through thioether bonds formed by cysteine residues Cys^{21} and Cys^{24} for heme 1, Cys^{121} and Cys^{124} for heme 2, $Cys^{287}$and Cys^{290} for heme 3, and Cys^{402} and Cys^{405} for heme 4 (Fig. 8, *A*–*D*). Moreover, the structure confirmed the spectroscopic evidence gathered showing that this tetraheme cytochrome *c* has three hemes (hemes 1, 2, and 4) with His/Met coordination (Fig. 8, *A*, *B*, and *D*). Axial ligation by histidine and cysteine is typical for the active site of TsdA proteins (2, 12). Indeed, heme 3 exhibits axial ligation by His^{291}, and the Sγ atom of Cys^{330} is located in close vicinity to the heme iron such that it could serve as the sixth ligand. However, the 2.9 Å distance between the sulfur and the iron atom precludes direct ligation (Fig. 8, *C*, *E*, and *F*). It has been shown earlier that the Sγ atom of the corresponding active site cysteine (Cys^{96}) in TsdA from *A. vinosum* can adopt two different conformations by rotation of the cysteine Cα–Cβ bond. Therefore, the sulfur atom switches between iron-ligating and iron-non-ligating states (2). The non-ligating conformation has been proposed as

TABLE 1
Data reduction and refinement statistics for *Mp*TsdBA structure

	142.65°-sweep data set (refinement)	Full 360° data set (Fe-SAD phasing)
PDB code	5LO9	
Data collection		
Synchrotron	ESRF (Grenoble, France)	
Beamline	ID-29	
Wavelength (Å)	1.7236	
Space group	*H*32	
Unit cell		
a, *b*, *c* (Å)	159.75, 159.75, 393.09	159.89, 159.89, 392.99
α, β, γ (o)	90.0, 90.0, 120.0	
Resolution range[a] (Å)	113.13–2.75 (2.76–2.75)	130.99–2.82 (2.83–2.82)
Total no. of reflections	377,526 (2187)	891,650 (6064)
No. of unique reflections	50,199 (461)	49,983 (442)
Completeness (%)	99.0 (87.8)	99.6 (94.2)
Anomalous completeness (%)	98.7 (84.8)	99.6 (94.1)
Multiplicity	7.5 (4.7)	19.0 (13.7)
Anomalous multiplicity	3.9 (2.5)	9.9 (7.0)
$\langle I/\sigma(I)\rangle$	14.9 (2.0)	15.4 (2.4)
R_{meas}[b] (%)	11.7 (70.6)	25.5 (184.7)
R_{pim} (%)	5.7 (41.8)	8.1 (69.2)
$CC_{1/2}$[c] (%)	99.7 (63.8)	99.4 (75.7)
Refinement		
R_{cryst}[d] (%)	15.7 (25.9)	
R_{free}[e] (%)	19.8 (30.0)	
No. of non-H atoms		
Protein	7028	
Ligands	330	
Waters	113	
r.m.s.d. bonds (Å)	0.013	
r.m.s.d. angles (°)	1.50	
Protein residues	Pro[1]–Leu[191] and Arg[237]–Val[515] (chain A), Pro[1]–Ala[192] and Ala[240]–Ala[516] (chain B)	
Ramachandran plot		
Most favored (%)	97.6	
Allowed (%)	2.4	
Outliers (%)	0	
Rotamer outliers (%)	0.9	
Clashscore	2.69	
MolProbity score[f]	1.28	
B-Factors (Å^2)		
Protein	52.04	
Ligands/ions	50.43	
Waters	45.06	

[a] Information in parentheses refers to the last resolution shell.
[b] $R_{meas} = \Sigma_h\Sigma_l|I_{hl} - \langle I_h\rangle|/\Sigma_h\Sigma_l\langle I_h\rangle$, where I_{hl} is the Ith observation of reflection *h* and $\langle I_h\rangle$.
[c] $CC_{1/2}$ is as described previously (57).
[d] $R_{cryst} = \Sigma_h||F_{obs(h)}| - |F_{calc(h)}||/\Sigma_h|F_{obs(h)}|$, where $F_{obs(h)} - F_{calc(h)}$ are the observed and calculated structure factors for reflection h, respectively.
[e] R_{free} was calculated as R_{factor} but using only 5% of reflections randomly selected and omitted from refinement.
[f] MolProbity score provides a single number that represents the central MolProbity protein quality statistics; it is a log-weighted combination of clashscore, Ramachandran not favored and bad side-chain rotamers, giving one number that reflects the crystallographic resolution at which those values would be expected.

an essential intermediate step in the catalytic cycle, possibly involving covalent attachment of a substrate molecule (2, 12).

Remarkably, in the "as isolated" structure of *Mp*TsdBA a thiosulfate ion is indeed covalently bound to Cys^{330}. A *polder* map supporting the modeling of the thiosulfate ion is depicted in Fig. 8*E*. The thiosulfate is oriented such that the S1-S2 plane points toward the heme plane, and the S2 atom lies 2.06 Å away from the Sγ atom of Cys^{330}, thus being within covalent bond distance. Thiosulfate was refined to 66% occupancy in chain A and 72% in chain B. The Sγ of Cys^{330} (full occupancy) superposes well with the Sγ atom of Cys^{96} in *Av*TsdA with bisulfite (PDB code 4WQB). Here, the Sδ of persulfurated Cys^{96} superimposes with S2 of thiosulfate in the *Mp*TsdBA structure. In both structures, these ligand-bound cysteines are not coordinating the heme. Noteworthy, some continuity in the electron density maps is still seen on heme 3, even though Cys^{330} is not ligated to the heme iron. We expect *Mp*TsdBA Cys^{330} to coordinate the heme when no ligand/substrate is present, similar to what is observed in *Av*TsdA crystal structures (2, 12).

The thiosulfate substrate lies in a cleft accessible from the solvent to Cys^{330} and heme 3. This cavity is delineated by the side chains of positively charged residues Arg^{314}, Lys^{316}, Arg^{326}, Arg^{438}, and Arg^{480} (Fig. 8*F*), which have been previously proposed to be involved in the orientation and stabilization of the substrate for catalysis (2, 12). Some positive electron density ($m|F_o| - D|F_c|$) is present near the substrate, although no density is observed in $2m|F_o| - D|F_c|$ maps (even at low contours). This electron density is observed between the Nζ atom of Lys^{316} and the plane formed by the three oxygen atoms of the thiosulfate ion (although independent from the density observed for the thiosulfate ion itself). Because this electron density was not amenable to refinement, nothing was included in the final 3D structure. Furthermore, heme 3 seems to display another residual conformation with one of the propionates alternating between this cavity and a cleft above the heme plane delineated by Arg^{377}, Arg^{381}, and the N main chain atoms of Gly^{378} and Tyr^{379}. This motion is illustrated by the different conformation modeled for heme 3 in both chains, either pointing toward the

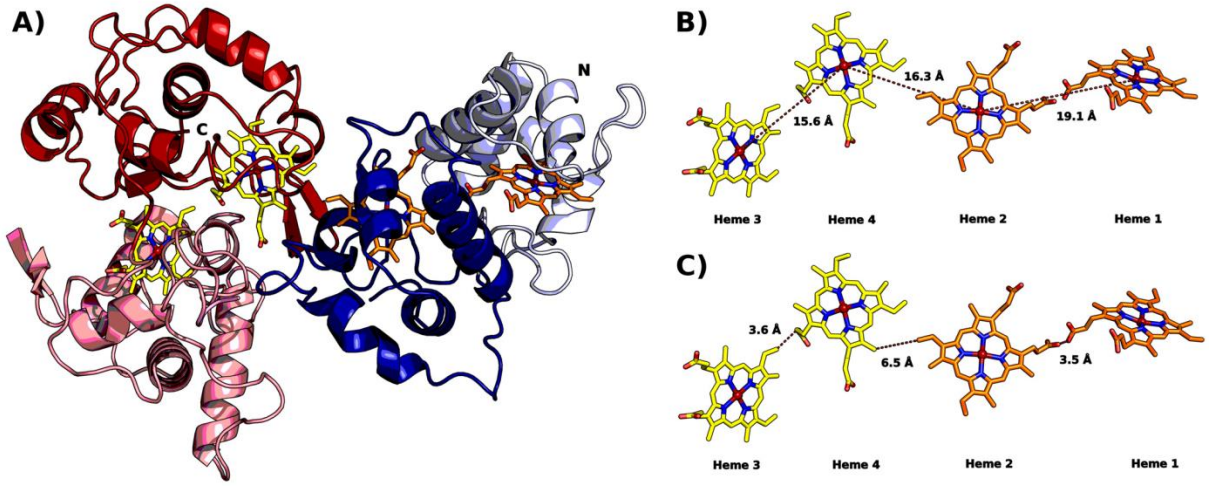

FIGURE 7. **X-ray structure of *Mp*TsdBA and heme arrangement.** *A,* overall fold with TsdB N-terminal domain (residues 1–193) depicted in *blue* and TsdA C-terminal domain (residues 240–516) in *red*; the two shades in each domain represent the respective sub-domains (1–90 and 91–193 for TsdB and 240–377 and 378–516 for TsdA). The heme prosthetic groups are colored by atom type (*orange* or *yellow* for carbon, *blue* for nitrogen, *red* for oxygen, and *dark red* for iron). *B,* Fe-to-Fe distances; *C,* closest edge-to-edge distances.

active site cavity, in chain A (Fig. 8*E*), or toward the cleft above the heme plane, in chain B (Fig. 8, *C* and *F*). However, this possible alternate conformation could not be properly refined, and therefore it was not added to the crystallographic model.

Reactivity with External Electron Acceptors—To test different electron acceptors for TsdA and TsdBA, we performed enzyme activity assays with TsdB from *T. intermedia, A. vinosum* cytochrome c_4 (Alvin_2879), and *A. vinosum* HiPIP as electron acceptors. All three potential electron acceptors were produced as recombinant proteins in *E. coli*.

Previously, it had been shown that TsdB from *T. intermedia* is not reactive with thiosulfate but that it is instantaneously reduced when TsdA is added in the presence of thiosulfate (1). Here, we succeeded in obtaining quantitative kinetic data for a homologous system by analyzing electron transfer between TsdA and TsdB from *S. lithotrophicus.* Just as *Ti*TsdB, *Sl*TsdB alone is not reduced by addition of thiosulfate. An enzyme activity assay with *Sl*TsdA as the catalyst and *Sl*TsdB as the electron acceptor resulted in a specific activity of 6.3 units mg^{-1} for *Sl*TsdA. $S_{0.5}$ for thiosulfate was determined to be 0.04 mM. This unambiguously identified *Sl*TsdB as an effective electron acceptor for TsdA from the same organism. However, a heterologous approach yielded a different result; with 0.6 units mg^{-1} the specific activity of *Av*TsdA with TsdB from *T. intermedia* amounted to only one-tenth that determined for the homologous system, whereas $S_{0.5}$ for thiosulfate (0.03 mM) resided in a similar range.

In a further series of experiments, *Av*TsdA activity was tested with Cyt c_4 originating from the same host. It should be noted that the recombinant cytochrome was electrophoretically pure and that it exhibited exactly the same spectral features as Cyt c_4 purified from *A. vinosum* cells, including the characteristic split α-band (9). The specific activity of *Av*TsdA with *Av*Cyt c_4 as the electron acceptor amounted to 0.6 units mg^{-1} and was thus not found to be higher than with TsdB from a different source organism. Therefore, we exclude those diheme cytochromes as efficient electron acceptors for *Av*TsdA *in vitro* as well as *in vivo*.

HiPIP from *A. vinosum*, a protein with a positive reduction potential (+350 mV (10)), was tested as another potential candidate for accepting electrons from *Av*TsdA as well as from *Mp*TsdBA. Indeed, both thiosulfate dehydrogenases reacted efficiently with *A. vinosum* HiPIP (Fig. 9 and Table 2). *Av*TsdA exhibited a higher V_{max} with HiPIP as electron acceptor, whereas *Mp*TsdA featured an especially low $S_{0.5}$ value for thiosulfate when the reaction was measured with HiPIP as electron acceptor. In both cases, $S_{0.5}$ for thiosulfate was much lower with HiPIP than with ferricyanide as the electron acceptor indicating cooperativity between the electron-transferring heme 2 and the active site heme 1. *A. vinosum* and *M. purpuratum* both encode HiPIP in their genome, and both thiosulfate dehydrogenases exhibit substantial specific activity with HiPIP as electron acceptor *in vitro*, leading us to conclude that HiPIP also serves as an efficient *in vivo* electron acceptor for Tsd(B)A in both organisms.

Discussion

In our approach to find suitable electron acceptors for TsdA-type thiosulfate dehydrogenases, we first focused on TsdB, a diheme cytochrome encoded upstream of TsdA in a number of different organisms. As demonstrated here for the proteins from *S. lithotrophicus* and earlier for those from *T. intermedia* (1), TsdA and TsdB enzymes interact strongly with each other and form an $\alpha_2\beta_2$ heterodimer. The same arrangement has been described for thiosulfate dehydrogenase from *Halothiobacillus neapolitanus* (21), which consists of heme *c* binding subunits of 27 and 33 kDa conforming in size with TsdA and TsdB, respectively.

In this work, a redox range of −300 to +150 mV was determined for *Av*TsdA, whereas *Ti*TsdB is redox active between −100 and +300 mV. Generalizing this finding, we state that the

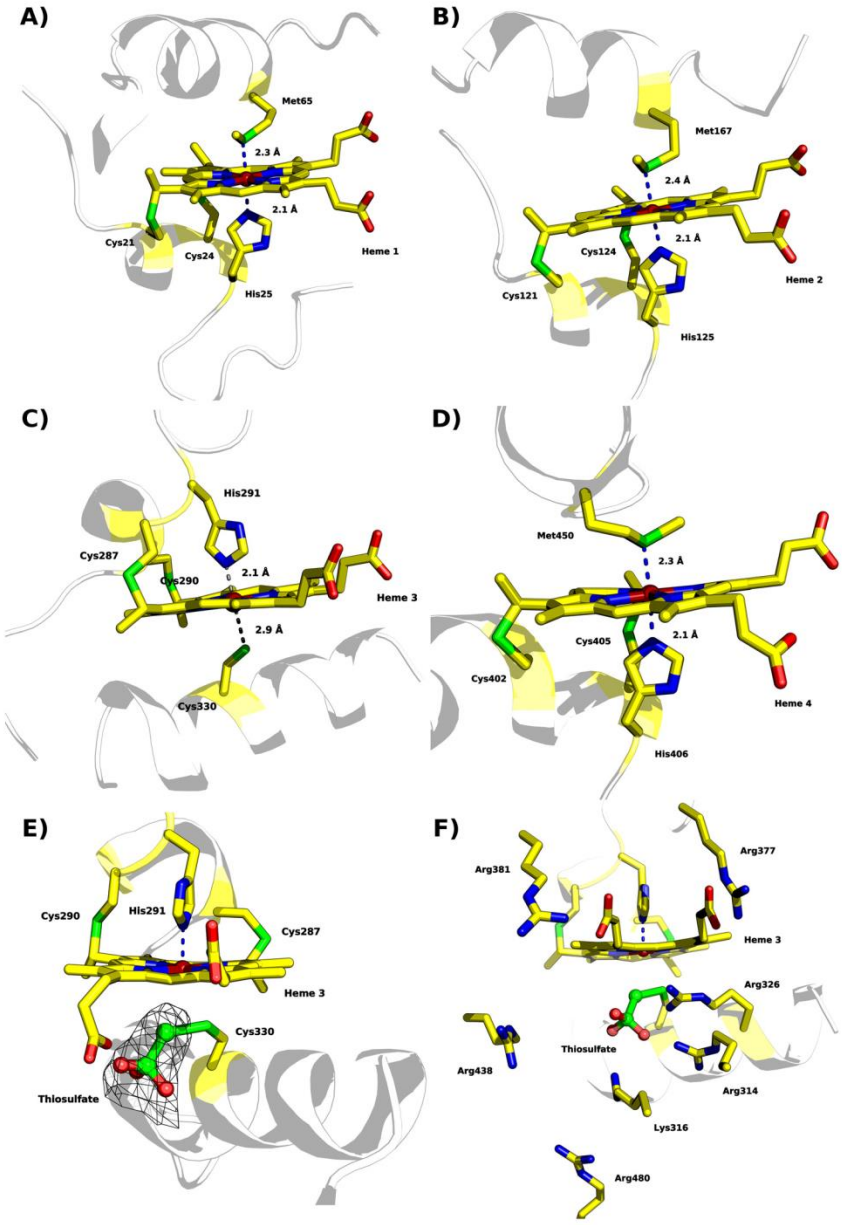

FIGURE 8. **Heme coordination of "as isolated" *Mp*TsdBA (PDB code 5LO9).** *A*, heme 1 is coordinated by His^{25} and Met^{65}. *B*, heme 2 is coordinated by His^{125} and Met^{167}. *C*, heme 3 is ligated to His^{291} but not to Cys^{330}. The distance of Sγ to the heme iron is 2.9 Å and thus not close enough for direct ligation. Thiosulfate covalently bound to Sγ of Cys^{330} is not shown here for clarity. Presence of thiosulfate is illustrated in detail in *E* and *F*. *D*, Heme 4 is ligated by His^{406} and Met^{450}. *E*, heme 3 with Sγ of Cys^{330} covalently bound to thiosulfate, displayed in *ball and stick*, and *polder* map electron density contoured at 6σ level depicted as a *black mesh*. *F*, heme 3 in a similar view as in *E* but with positively charged residues surrounding the substrate cleft depicted as *sticks*. Scheme representation is shown in *pale gray* with heme moieties and coordinating amino acid residues shown as *sticks;* color code as in Fig. 7 with sulfur atoms in *green*.

overall reduction potential of TsdB is more positive than that of TsdA, which should enable electron flow from TsdA to TsdB. Indeed, reduction of *Ti*TsdB by *Av*TsdA had been shown previously (1) and was verified here for the proteins from *S. lithotrophicus*. Enzyme activity assays further revealed *Sl*TsdB as an effective electron acceptor for *Sl*TsdA but not for *Av*TsdA. This was not surprising as *A. vinosum* does not contain a gene encoding TsdB (Table 3).

In *A. vinosum*, the gene with strongest similarity to *tsdB* is Alvin_2879. The encoded high potential diheme cytochrome c_4 has been suggested to play a role in transferring electrons to the photosynthetic reaction center (9). The *M. purpuratum* genome also encodes a protein (Marpu_15750) with high similarity to *A. vinosum* Cyt c_4 (78% identity on the sequence basis; see Table 3). In the anoxygenic phototroph *Rubrivivax gelatinosus*, a related cytochrome c_4 indeed has an established func-

tion as an alternative electron donor to the photosynthetic reaction center (22). It was therefore feasible to assume that electrons generated by thiosulfate oxidation could be shuttled to the reaction center via cytochrome c_4 in purple sulfur bacteria. However, the very low specific activity of *Av*TsdA with *A. vinosum* cytochrome c_4 essentially precludes such a role (Fig. 10).

In many anoxygenic photosynthetic bacteria, the periplasmic high potential iron-sulfur protein is well known to shuttle electrons between the cytochrome bc_1 complex and the photosynthetic reaction center during cyclic electron flow (23–26). This function has also been firmly established for the protein from *A. vinosum* (24, 27). Here, we demonstrate that HiPIP is a suitable electron acceptor for Tsd(B)A from *A. vinosum* and *M. purpuratum in vitro*, identifying this protein as the most likely electron carrier between the thiosulfate-oxidizing enzyme and the reaction center during growth in the light. It should be noted that a direct interaction between Tsd(B)A and the photosynthetic reaction center cannot be completely excluded so far.

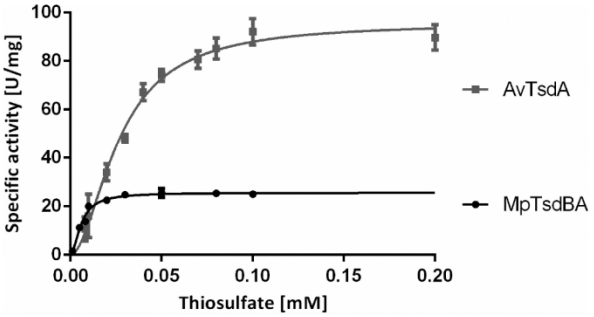

FIGURE 9. **Thiosulfate oxidation catalyzed by *Av*TsdA and *Mp*TsdBA with HiPIP as electron acceptor.** Enzyme assays with *Av*TsdA were performed in 100 mM ammonium acetate buffer, pH 5, at 30 °C with 8 nM enzyme. Activity measurements with *Mp*TsdBA were performed in 100 mM ammonium acetate buffer, pH 5.2, with 200 mM NaCl at 25 °C and with 3.9 nM enzyme. In both assays 10 μM HiPIP and 40 μM ferricyanide were used. A change in absorbance was measured at 480 nm. *v versus* [S] plots were fitted to the Hill equation.

TABLE 2

Thiosulfate oxidation of *Av*TsdA and *Mp*TsdBA with ferricyanide and HiPIP

Enzyme assays with *Av*TsdA were performed in 100 mM ammonium acetate buffer, pH 4, at 30 °C with 8 nM enzyme. Activity measurements with *Mp*TsdBA were performed in 100 mM ammonium acetate buffer, pH 5.2, with 200 mM NaCl at 25 °C and with 3.9 nM enzyme. In assays with HiPIP as electron acceptor, 10 μM HiPIP and 40 μM ferricyanide were used, and absorbance at 480 nm was followed. In activity assays with ferricyanide as electron acceptor, 1 mM ferricyanide was used, and the absorbance at 420 nm was measured. The units for V_{max} are μmol min^{-1} mg protein^{-1}. *v versus* [S] plots were fitted to the Hill equation.

Electron acceptor	Enzyme	V_{max}	$S_{0.5}$	k_{cat}	$k_{cat}/S_{0.5}$
		units mg^{-1}	μM	s^{-1}	$mM^{-1}\ s^{-1}$
Ferricyanide	*Av*TsdA	31,419 ± 2408	835 ± 119	14,091	16,875
	*Mp*TsdBA	3011 ± 108	179 ± 21	2794	15,611
HiPIP	*Av*TsdA	96 ± 3	27 ± 2	43	1595
	*Mp*TsdBA	26 ± 1	6 ± 0	24	4000

Many purple sulfur bacteria, including *A. vinosum*, are capable of chemolithotrophic growth on reduced sulfur compounds and oxygen under microaerobic conditions (28). Accordingly, cbb_3 as well as ubiquinol oxidases are encoded in their genomes. Although the standard reduction potential of the thiosulfate/tetrathionate couple (+198 mV (7)) appears too positive to feed electrons directly into the quinone pool, and from there to oxygen, delivery of electrons originating from the thiosulfate to tetrathionate conversion to cbb_3 oxidase is certainly feasible. In fact, HiPIP has been reported to be involved in bacterial respiratory chains (29, 30) and is a prime candidate for electron transport between Tsd(B)A and the terminal oxidase in those organisms where it is present. However, in chemotrophs like *T. intermedia* or *S. lithotrophicus*, the situation must be different because these bacteria do not contain HiPIP. In fact, for these organisms, it is not exactly established so far which periplasmic proteins deliver electrons to cbb_3 oxidase, regardless of the electron donor oxidized. For *S. lithotrophicus* it is assumed that the *c*-type cytochrome MtoD (Slit_2498) can transfer electrons stemming from iron oxidation to cbb_3 oxidase and the cytochrome bc_1 complex (31). In the *T. intermedia* genome, there are two *c*-type cytochromes (Tint_2575 and Tint_3060) with 36 and 42% sequence identity to *S. lithotrophicus* MtoD, respectively, which may serve a similar function. It may be possible that thiosulfate dehydrogenase delivers electrons to the MtoD(-like) cytochrome, which then shuffles the electrons to the terminal oxidase.

Nevertheless, an alternative scenario is also possible when we consider the similarity between TsdB and cytochromes of the c_4-type (about 49% sequence identity between *Ti*TsdB and Cyt c_4 from *Achromobacter xylosoxidans* or *Pseudomonas protegens*). Cytochromes of the c_4-type have been reported to donate electrons to cbb_3-type cytochrome *c* oxidases in various oxygen-respiring bacteria (32–34), and we therefore consider the possibility that TsdB serves as a direct electron donor to cbb_3 oxidase at least in tetrathionate-forming thiosulfate oxidizers that neither contain HiPIP nor any cytochrome c_4 homolog except TsdB.

We have determined the first three-dimensional structure of *M. purpuratum* TsdBA, where TsdA is fused with its electron acceptor TsdB. It showed heme arrangement with characteristic class I *c*-type cytochrome topology, unveiling their relative heme spatial disposition and providing insights into the electron flow during enzymatic reaction. In the *Mp*TsdBA structure, a thiosulfate ion is covalently bound to Sγ of Cys^{330} in heme 3, although the protein was produced in and purified from *E. coli* without the addition of thiosulfate to media or buffers. This implies high affinity of the enzyme to thiosulfate, which is possibly present in the complex growth medium in

TABLE 3

Occurrence of genes encoding TsdA and putative electron acceptors in the genome sequenced organisms relevant to this study

Organism	TsdA	TsdB	Cyt c_4	HiPIP
A.vinosum DSM 180^T	Alvin_0091		Alvin_2879	Alvin_2274
M. purpuratum 984 (DSM 1591^T)	Marpu_02550 (TsdBA fusion)	Marpu_15750	Marpu_11560	
S. lithotrophicus ES-1 (ATCC 700298^T)	Slit_1878	Slit_1877		
T. intermedia K12 (DSM 18155^T)	Tint_2892	Tint_2893		

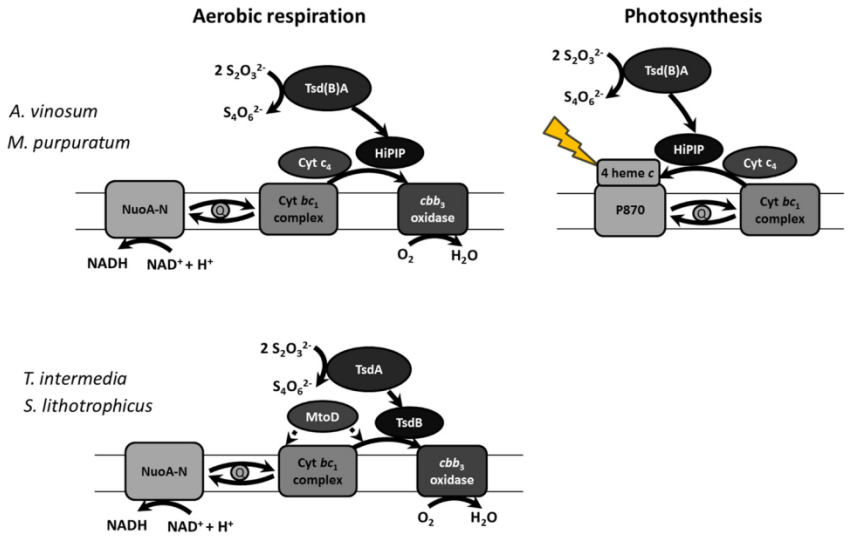

FIGURE 10. **Role of periplasmic electron transfer proteins in aerobic respiration or photosynthesis of *A. vinosum*, *M. purpuratum*, *S. lithotrophicus*, and *T. intermedia*.** All organisms contain genes for NuoA-N (Alvin_2418–2430 + Alvin_2412, Marpu_04365–04430, Slit_1070–1083, and Tint_2255–2268), the cytochrome bc_1 complex (Alvin_0068–0070, Marpu_01465–01475, Slit_0130–0132, and Tint_2192–2194), and cbb_3 oxidase (Alvin_0781–0784, Marpu_02795–02810, Slit_0411–0414, and Tint_1070–1073). Moreover, *A. vinosum* and *M. purpuratum* can gain energy by photosynthetic growth. HiPIP can transfer electrons to the photosynthetic reaction center (23, 24) as well as to cbb_3 oxidase (29, 30). Cytochrome c_4 also is known to transfer electrons to the photosynthetic reaction center (22) as well as to cbb_3 oxidase (32–34) in some bacteria. For *S. lithotrophicus*, it is assumed that MtoD (Slit_2498) can transfer electrons to cbb_3 oxidase and the cytochrome bc_1 complex (31).

very low concentrations. It should be noted that recombinant *Av*TsdA and also several SoxA proteins have been isolated with the active site cysteine in a partially or fully persulfurated state (2, 35–37). This has been interpreted as indication for temporary binding of thiosulfate and subsequent incomplete catalysis. Just as proposed here, thiosulfate was assumed to originate from the *E. coli* growth medium (2).

Regardless of its source, the covalent attachment of a complete thiosulfate molecule to the *Mp*TsdBA active site cysteine strongly supports the hypothesis that tetrathionate formation from two thiosulfate molecules proceeds via a rhodanese-like reaction mechanism involving a thiosulfate transfer reaction with a thiosulfate molecule covalently bound to the active site cysteine as an essential intermediate in the catalytic cycle (2, 12). This type of mechanism has been illustrated in detail by Grabarczyk *et al.* (12) for TsdA from *A. vinosum*. A rhodanese-like reaction cycle has also repeatedly been depicted and discussed for the closely related SoxXA protein, but it could not be unambiguously proven before (4, 35). The *Mp*TsdBA structure provides conclusive evidence that the reactions catalyzed by TsdA as well as SoxXA enzymes indeed involve a cysteine *S*-thiosulfonate intermediate that is formed once the first thiosulfate molecule is positioned in the substrate binding pocket by positively charged amino acid side chains (Arg^{314}, Lys^{316}, Arg^{326}, and Arg^{438} in *Mp*TsdBA, Fig. 8*F*). The latter also stabilized the cysteine *S*-thiosulfonate group once it had formed. Formation of the cysteine *S*-thiosulfonate releases two electrons that reduce the iron atoms of the two hemes in TsdA to the Fe(II) state. Heme reoxidation by an external electron acceptor is then likely to be followed by a thiol-disulfide exchange reaction that proceeds via an attack of the sulfane atom of a second thiosulfate molecule on the thiosulfonate group (12).

We conclude that catalysis of thiosulfate oxidation by Tsd(B)A enzymes and very probably also that by SoxXA proteins involves formation of a covalent adduct between the sulfane sulfur atom of thiosulfate and the Sγ of the active site cysteine. When present, TsdB is the immediate electron acceptor of TsdA. TsdB is very likely able to transfer electrons directly to the cbb_3 terminal oxidase. In organisms containing HiPIP, this electron carrier is likely to act as an additional shuttle not only between Tsd(B)A and the terminal oxidase during oxygen respiration but also between Tsd(B)A and the photosynthetic reaction center during photolithotrophic growth in the light.

Experimental Procedures

Bacterial Strains, Plasmids, and Growth Conditions—Table 4 lists the bacterial strains and plasmids used for this study. *E. coli* BL21 (DE3) was used for recombinant protein production and was grown in LB medium. *E. coli* DH5α was used for molecular cloning.

Recombinant DNA Techniques—All general molecular genetics techniques were described earlier (38). Restriction enzymes, T4 ligase, and *Pfu* DNA polymerase were obtained from Thermo Scientific (Schwerte, Germany) and used according to the manufacturer's instructions. Oligonucleotides for cloning were obtained from Eurofins MWG (Ebersberg, Germany).

Construction of Expression Plasmids—*A. vinosum tsdA* and *T. intermedia tsdB* genes coding for the mature proteins without the signal peptides were amplified and cloned as described

TABLE 4
***E. coli* strains and plasmids used in this study**

Strains and plasmids	Description	Ref. or source
Strains		
E. coli DH5α	F^- φ80d *lacZ*ΔM15 Δ(*lacZYA-argF*)*U169 recA1 endA1hsdR17* (rk^- mk^+) *supE44* λ^- *thi-1 gyrA relA1*	56
E. coli BL21 (DE3)	F^- *ompT hsdS*$_B$ ($r_B^-m_B^-$) *gal dcm met*(DE3)	Novagen
Plasmids		
pEC86	Cm^r, product from pEC66 and pACYC184 with *E. coli ccmABCDEFGH* genes	40
pET-22b (+)	Ap^r, T7 promoter, lac operator, C-terminal His tag, pelB leader	Novagen
pASK-IBA3 plus	Ap^r, *tetA* promoter/operator, C-terminal Strep tag	IBA (Göttingen)
pET_ MarpuDRAFT_1194	Ap^r, *tsdA* from *M. purpuratum* (Marpu_02550) was cloned into pET-22b (+) with NdeI and XhoI, C-terminal His tag	7
pASK-IBA*Tint_tsdB*	Ap^r; *tsdB* from *T. intermedia* cloned into pASK-IBA3 plus with BsaI, C-terminal Strep tag	1
pASK-IBA3plus-*slit1877*	Ap^r; *tsdB* from *S. lithotrophicus* (Slit_1877) cloned into pASK-IBA3 plus with BsaI, C-terminal Strep tag	This study
pASK-IBA3plus-*slit1878*	Ap^r; *tsdA* from *S. lithotrophicus* (Slit_1878) cloned into pASK-IBA3 plus with BsaI, C-terminal Strep tag	This study
pASK-IBA3plus-*slit1877-slit1878*	Ap^r; *tsdBA* from *S. lithotrophica* (Slit_1877-Slit_1878) cloned into pASK-IBA3 plus with BsaI, C-terminal Strep tag	This study
pET-soxXAK-Strep	Ap^r, *soxXAK*, including fragment cloned into pET-22b(+) together with C-terminal Strep tag by use of XbaI and HindIII	This study
pET-Alvin2274-C-Strep	Ap^r, *hip* gene coding for HiPIP from *A. vinosum* (Alvin_2274) cloned into pET-soxXAK-Strep with NdeI and NcoI, C-terminal Strep tag	This study
pPR-IBAAvtsdA	Ap^r; *tsdA* from *A. vinosum* (Alvin_0091) cloned into pASK-IBA3, C-terminal Strep tag	1
pASK-IBA3plus_Alvin_2879	Ap^r; Alvin_2879 from *A. vinosum* cloned into pASK-IBA3 plus with BsaI, C-terminal Strep tag	This study

earlier (1). The *tsdA* gene (Slit_1878), the *tsdB* gene (Slit_1877), and the *tsdBA* gene combination (Slit_1877-Slit1878) from *S. lithotrophicus* ES-1 (ATCC 700298^T) were amplified from genomic DNA with primers Slit1877_fw/Slit1877_rev, Slit1878_fw/Slit1878_rev, and Slit1877_fw/Slit1878_rev (Table 5), respectively. The native signal peptides encoding sequences were included in all three cases. The *tsdBA* gene fusion (Marpu_02550) from *M. purpuratum* 984 (DSM 1591^T) was amplified without its original signal peptide encoding sequence using primers MarpuDR1194_for/MarpuDR1194_rev. The gene Alvin_2879, encoding a cytochrome c_4 with similarity to TsdB, was amplified with primers 2879+Sp-for and 2879-rev such that the signal peptide-encoding sequence was included. The HiPIP-encoding *hip* (Alvin_2274) gene (39) was amplified without the signal peptide-encoding sequence applying primers Alvin2274-C-strep_for/Alvin2274-C-strep_rev. Chromosomal DNA from *A. vinosum* DSM 180^T served as the template. For cloning of *SltsdB*, *SltsdA*, *SltsdB-tsdA*, and Alvin_2879, primers included BsaI restriction sites, and the digested PCR products were cloned into BsaI-digested pASK-IBA3plus (IBA, Göttingen) resulting in vectors pASK-IBA3plus-slit1877, pASK-IBA3plus-slit1878, pASK-IBA3plus-slit1877-slit1878, and pASK-IBA3plus_Alvin_2879. For the cloning of *MptsdBA* into pET-22b(+) (Novagen), the restriction enzymes NdeI and XhoI were used yielding plasmid pET_MarpuDRAFT_1194. Plasmid pET-Alvin2274 was constructed by cloning *Avhip* into a modified pET-22b(+) vector (pET-soxXAK-strep) encoding a C-terminal Strep tag. This vector had previously been constructed in the course of cloning the *A. vinosum soxXAK* genes. PCR primers with NdeI (XAK-NdeI-for) and NcoI (XAK-NcoI-rev) sites were used, and the resulting fragment was cloned into pET-22b(+). The XbaI/NcoI fragment of the resulting plasmid was cloned into pASK-IBA3. XbaI and HindIII served for excising the *soxXAK* genes together with the Strep tag-encoding sequence. The XbaI/HindIII fragment was cloned between the XbaI and HindIII sites of pET22b(+) giving pET-soxXAK-strep. Replacing the *soxXAK* genes in this construct by *Avhip* yielded *A. vinosum* HiPIP fused to a C-terminal Strep tag.

Overproduction, Purification, and Preparation of Recombinant Proteins—*Av*TsdA and *Ti*TsdB were produced as described before (1). For production of *S. lithotrophicus* TsdA, *Sl*TsdB and the simultaneous production of *Sl*TsdB and *Sl*TdsA *E. coli* BL21(DE3) cells containing pASK-IBA3plus-slit1877, pASK-IBA3plus-slit1878, or pASK-IBA3plus-slit1877-slit1878 and pEC86 (40) were cultured in 700 ml of LB media supplemented with 100 μg ml^{-1} ampicillin and 25 μg ml^{-1} chloramphenicol at 37 °C and 180 rpm after inoculation with an overnight pre-inoculum in a (1:50) dilution. At an $OD_{600\ nm}$ of 0.4 to 0.6, 200 ng ml^{-1} anhydrotetracycline were added, and the appropriate culture was switched to 25 °C and 90 rpm in case of TsdB production. Cells were harvested after 18 h. *Mp*TsdBA and HiPIP were produced in *E. coli* BL21(DE3) cells containing pET_MarpuDRAFT_1194 or pET-Alvin2274 and pEC86 (40). After 2 or 0.5% inoculation with a pre-culture, the cells were grown in 700 ml of LB medium containing 100 μg ml^{-1} ampicillin and 25 μg ml^{-1} chloramphenicol at 37 °C and 180 rpm. At an $OD_{600\ nm}$ of 0.5 to 0.6, the cultures were switched to 25 °C and 120 rpm for about 18 h. For production of *Av*Cyt c_4 (Alvin_2879), *E. coli* BL21(DE3) cells containing pASK-IBA3plus_Alvin_2879 and pEC86 (40) were cultured in 400 ml of LB medium, 100 μg ml^{-1} ampicillin, and 25 μg ml^{-1} chloramphenicol at 37 °C and 180 rpm after 2% inoculation with a preculture. At $OD_{600\ nm}$ ~0.5, 200 ng ml^{-1} anhydrotetracycline were added, and the culture was switched to 25 °C and 90 rpm for 18 h. Harvested cells were resuspended in 100 mM Tris-HCl buffer, pH 8.0, containing 150 mM NaCl and lysed by sonication. After removal of insoluble cell material by centrifugation (10,000 × *g* for 25 min at 4 °C), *Sl*TsdA, *Sl*TsdB, *Sl*TsdB + TsdA, *A. vinosum* cytochrome c_4 (Alvin_2879), and *Av*TsdA were purified by Strep-Tactin (IBA, Göttingen, Germany) affinity chromatography according to the manufacturer's instructions. *Mp*TsdBA was purified by nickel-chelate (Qiagen, Hilden, Germany) affinity chromatography according to the manufacturer's instructions and then subjected to a size-exclusion chromatography step performed on a HiLoad 16/60 Superdex 75-pg column (GE Healthcare) using an ÄKTApuri-

TABLE 5
Primers used in this study

Primer	Sequence 5′–3′	Ref.
MarpuDR1194_for	CGGAGGGATCCTCATATGACGCATCTC	7
MarpuDR1194_rev	GACCTGCTCGAGATCCTTGGC	7
Slit1877_fw	ATGGTAGGTCTCAAATGAAGCAAATATTACTAGCAGCATTAAC	This study
Slit1877_rev	ATGGTAGGTCTCAGCGCTTTTCTGGTTTCCATTGGTTGATTGT	This study
Slit1878_fw	ATGGTAGGTCTCAAATGAAGAATCCCATCGCTATCGCCAT	This study
Slit1878_rev	ATGGTAGGTCTCAGCGCTCTTTGCTGCAGTCTGGTGCTTTC	This study
XAK-NdeI-for	GGAGATTTCATATGCCGTTGAACGTCTCACACCG	This study
XAK-NcoI-rev	ATGGCTCCATGGTATCGAGACCGATCGAGC	This study
Alvin2274-C-strep_for	GCCCATATGTCCGCTCCCGCCAAT	This study
Alvin2274-C-strep_rev	CAACGGCCCATGGCCGGCCTTCAG	This study
2879+Sp-for	ATGGTAGGTCTCAAATGAAGAAGACTTGGCTGACAACGGT	This study
2879-rev	ATGGTAGGTCTCAGCGCTCTTCGACAGGCCCTGGATGTAC	This study

fier system (GE Healthcare). The column was equilibrated with 20 mM Tris-HCl buffer, pH 7.5, and 150 mM NaCl. TsdB and TsdA from *S. lithtrophicus* were analyzed by the same procedure either separately or as a mixture of both proteins. In this case, the Superdex 75 column was equilibrated with 100 mM Tris-HCl buffer, pH 7.5, and 150 mM NaCl. The column was calibrated with the molecular weight marker kit MW-GF-70 (GE Healthcare). All purified proteins were desalted with 5 ml of HiTrap Desalting columns (GE Healthcare) and concentrated with Amicon Ultra-15 centrifugal filter units (Merck Millipore). Recombinant *S. lithotrophicus* proteins were stored in 100 mM sodium acetate buffer pH 5 at −70 °C, *A. vinosum* Cyt c_4 in 20 mM Tris-HCl buffer, pH 7.5, at 4 °C, *Mp*TsdBA in 20 mM Tris-HCl buffer, pH 7.5, with 150 mM NaCl at −70 °C, and HiPIP in 20 mM Tris-HCl, pH 7, at 4 °C. The concentration of purified proteins was determined with the BCA kit from Pierce. For assessment of purity, SDS-PAGE was performed, and the proteins were visualized either by Coomassie or heme staining techniques.

UV-visible Spectroscopy with TsdA in Solution—UV-visible spectra were recorded between 250 and 750 nm with an Analytik Jena Specord 210 (Analytik Jena, Jena, Germany).

Assay of Thiosulfate Oxidase Activity with Ferricyanide—Thiosulfate-dependent ferricyanide reduction was measured by following the decrease in absorbance at 420 nm (ϵ = 1.09 mM^{-1} cm^{-1}). Enzyme activity measurements with *Av*TsdA at pH 4 are described in Ref. 2. Activity measurements with *Mp*TsdBA were performed with 1 mM ferricyanide at 25 °C in 100 mM ammonium acetate buffer, pH 5.2, with 200 mM NaCl. Assays were started by addition of TsdA, and data were recorded in a Specord 210 spectrophotometer (Analytik Jena, Jena, Germany). Activity is expressed as micromoles of tetrathionate produced per min and milligram of protein on the basis of one tetrathionate formed per two ferricyanides reduced. In the case of enzymes that use two molecules of the same substrate (here thiosulfate) primary *v versus* [S] plots provide the best way to examine the data (41). Data were fitted to the empirical Hill equation (Equation 1) using GraphPad Prism (version 6; GraphPad).

$$v = \frac{V_{max}[S]^n}{K + [S]^n} \quad \text{(Eq. 1)}$$

The Hill equation resembles the classical Henri-Michaelis-Menten equation; however, the *n* term allows accounting for non-hyperbolic shapes. A substrate concentration $[S]_{0.5}$ can be reported that yields half-maximal velocity and is characteristic of the process. The constant *K*, which is not equivalent to K_m, characterizes enzyme-substrate interaction. The relationship between *K* and $[S]_{0.5}$ is $K = [S]_{0.5}{}^n$.

Assay of Thiosulfate Oxidase Activity with HiPIP—For assays of electron transfer from thiosulfate to the electron acceptor HiPIP, 10 μM HiPIP preoxidized with 40 μM ferricyanide were used. The reaction was started by addition of enzyme and followed by the absorbance decrease at 480 nm. A molar extinction coefficient at 480 nm of 10.7 mM^{-1} cm^{-1} (10) was used. Measurements with *Av*TsdA were performed in 100 mM ammonium acetate buffer, pH 5, at 30 °C and with *Mp*TsdBA in 100 mM ammonium acetate buffer, pH 5.2, with 200 mM NaCl at 25 °C.

Assay of Thiosulfate Oxidase Activity with TsdB or AvCyt c_4—Thiosulfate-dependent reduction of *T. intermedia* TsdB or *A. vinosum* Cyt c_4 was measured by following the increase in absorbance at 417 nm ($\epsilon_{\Delta 417\ nm}$ = 99 mM^{-1} cm^{-1}) for *Ti*TsdB or *Sl*TsdB and at 420 nm ($\epsilon_{\Delta 420\ nm}$ = 55 mM^{-1} cm^{-1} (9)) for *Av*Cyt c_4. The extinction coefficient for TsdB was calculated with the help of the Beer-Lambert law using distinct concentrations of *Ti*TsdB and the differences in absorbance at 417 nm in the reduced and oxidized spectra. A value averaged from measurements with three different protein concentrations was derived. Assays of *Sl*TsdA activity with *Sl*TsdB as electron acceptor were carried out in 100 mM ammonium acetate buffer, pH 4, at 25 °C. *Av*TsdA activity with *Ti*TsdB was assayed in 100 mM ammonium acetate buffer, pH 5, at 30 °C, whereas *Av*TsdA activity with *Av*Cyt c_4 was determined in 100 mM ammonium acetate buffer, pH 5.5, at 25 °C.

Determination of Redox Properties of AvTsdA Adsorbed on a Mesoporous Nanocrystalline SnO_2 Electrode—An optically transparent mesoporous nanocrystalline SnO_2 electrode coated with *Av*TsdA was prepared using the previously described method (42) with adsorption from a solution of 10 μM *Av*TsdA, 2 mM neomycin, 50 mM NaCl, 50 mM HEPES, pH 7. The enzyme-coated electrode was rinsed with 2 mM neomycin, 50 mM NaCl, 50 mM HEPES, pH 7, to remove unbound protein, taken into a N_2-filled chamber (atmospheric O_2 < 2 ppm) and immersed in an anaerobic solution of the same composition within a previously described spectroelectrochemical cell (42). The cell was sealed, removed from the anaerobic chamber, and inserted into a Jasco V650 UV-visible spectrophotometer thermostated at 4 °C and flushed with argon to maintain anaerobic status. Spectral contributions from light

scattering by the electrode were minimized by placing a bare SnO_2 electrode (*i.e.* having no adsorbed enzyme) in the reference beam of the spectrophotometer. The electronic absorbance of the as prepared enzyme-coated electrode revealed features indicative of a mixture of ferric and ferrous hemes. After the electrode had been poised at +302 mV for 45 min, the spectrum revealed that the enzyme had been converted to the fully oxidized all ferric state. To determine the redox activity of *Av*TsdA, the electrode potential was swept from +302 to −648 mV at a scan rate of 5 mV s^{-1} with a pause of 150 s every 50 mV. At 60 s into each pause, a spectrum was measured before the scan continued. Reoxidation of the sample was performed in a similar manner. Spectra are presented after equating absolute absorbance at 600 nm to account for potential dependent changes in the spectral contributions that arise from scattering by the electrode material.

Redox Potentiometry with TsdB in Solution Measured with a Gold Electrode—The reduction potential of *Ti*TsdB was measured with help of a gold-platinum electrode system under anoxic conditions. The electrode extended into a cuvette containing the protein solution (20 μM) and redox mediators (*N,N*-dimethyl-1,4-phenylenediamine, *p*-benzoquinone, trimethylhydroquinone, phenazine, 1,4-naphthoquinone, and 1,2-naphthoquinone at 2 μM each) in 20 mM MOPS buffer, pH 6, and was connected to a potentiometer. *Ti*TsdB was reduced by changing the applied potential from −150 to 450 mV. Subsequential decrease of the potential again to −150 mV led to reoxidation of the protein. A spectrum was recorded every 2 min and potentials converted to values *versus* standard hydrogen electrode.

Crystallization, Data Collection, Structure Determination, and Refinement—*Mp*TsdBA at a concentration of 3.2 mg ml^{-1} in 20 mM BisTris-HCl, pH 6.5, and 150 mM NaCl was crystallized in 10% (w/v) PEG 8000, 0.1 M Tris-HCl, pH 7.0, 0.2 M $MgCl_2$, and 10 mM trimethylamine hydrochloride (as additive) by vapor-diffusion hanging-drop method at 20 °C. Crystallization droplets contained 1.0 μl of protein, 0.8 μl of precipitant, and 0.2 μl of additive and were equilibrated against a 200-μl reservoir solution (26% (w/v) PEG 3350). Crystals were cryoprotected with No. 2 solution of CryoProtX screen (Molecular Dimensions), consisting of 25% (v/v) diethylene glycol, 25% (v/v) 1,2-propanediol, and 25% (v/v) glycerol. X-ray diffraction data were collected at a wavelength of 1.7236 Å on beamline ID-29 of the European Synchrotron Radiation Facility (ESRF, Grenoble, France). Data were indexed and integrated with XDS (43), and the space group was determined with POINTLESS (44) and scaled with AIMLESS (45, 46), all within the autoPROC (47) data processing pipeline. An R_{free} flag was created at this stage corresponding to 5% of the measured reflections of the data set. The structure was determined by single wavelength anomalous dispersion method around the iron edge (Fe-SAD), employing a high multiplicity data collection strategy using the autoSHARP module (48), within the SHARP package (49). Iterative model building and refinement cycles were performed with COOT (50) and BUSTER-TNT (51) (at early stages of refinement), followed by phenix.refine (52), until a complete model was built and refinement convergence achieved. Friedel mates were kept separately and refinement was carried out against I(+)/SIGI(+),I(−)/SIGI(−). A *polder* map (an omit map that excludes the bulk solvent around the omitted region) and $m|F_o| - m|F_o|$ map were calculated within the PHENIX package of programs. The Ramachandran diagram was assessed with RAMPAGE (53), and the model was validated with MolProbity (54) as implemented in PHENIX. All figures were rendered with PyMOL, Schrödinger LLC (55).

Author Contributions—J. M. K., J. A. B., J. N. B., M. A., and C. D. wrote the manuscript. C. D. conceived and coordinated all experiments except the *Mp*TsdBA crystallization and determination of reduction potentials. J. M. K. analyzed and compiled the data for those experiments. J. R. constructed the vector for production of *Mp*TsdBA and T. F. the vector for production of HiPIP. A. F. and J. R. performed activity assays with *Mp*TsdBA, *Av*TsdA, and HiPIP (Fig. 9; Table 2) and recorded UV-visible spectra of *Mp*TsdBA (Fig. 6). T. K. produced *Av*Cyt c_4 and measured activity of *Av*TsdA with this protein. E. K. and J. M. K. produced and analyzed proteins from *S. lithotrophicus* (Figs. 2 and 5). K. D. determined the redox activity of *Ti*TsdB (Fig. 4) under the supervision of I. A. C. P. and S. F. R. examined the redox activity of *Av*TsdA (Fig. 1) under the supervision of J. N. B. J. A. B. crystallized *Mp*TsdBA, processed the X-ray data, determined the crystal structure, and performed model building and refinement (Figs. 7 and 8; Table 1). J. A. B. and M. A. analyzed the crystal structure.

Acknowledgments—We acknowledge Isabel Bento and Ana Maria Gonçalves for collecting the X-ray diffraction data. We also acknowledge Susana Gonçalves and the ID-29 beamline staff at the European Synchrotron Radiation Facility (ESRF; Grenoble, France) for providing assistance in using the beamline. S. lithotrophicus DNA was kindly provided by David Emerson, Bigelow Laboratory for Ocean Sciences, West Boothbay, ME. MALDI-TOF mass spectrometry of TiTsdB and SlTsdB was kindly performed by Michaele Josten and Hans Georg Sahl, Institute for Medical Microbiology, Immunology and Parasitology, University of Bonn, Germany. We thank James Durrant (Imperial College London) for the SnO_2 electrodes.

References

1. Denkmann, K., Grein, F., Zigann, R., Siemen, A., Bergmann, J., van Helmont, S., Nicolai, A., Pereira, I. A., and Dahl, C. (2012) Thiosulfate dehydrogenase: a widespread unusual acidophilic *c*-type cytochrome. *Environ. Microbiol.* **14,** 2673–2688
2. Brito, J. A., Denkmann, K., Pereira, I. A., Archer, M., and Dahl, C. (2015) Thiosulfate dehydrogenase (TsdA) from *Allochromatium vinosum*: structural and functional insights into thiosulfate oxidation. *J. Biol. Chem.* **290,** 9222–9238
3. Pires, R. H., Venceslau, S. S., Morais, F., Teixeira, M., Xavier, A. V., and Pereira, I. A. (2006) Characterization of the *Desulfovibrio desulfuricans* ATCC 27774 DsrMKJOP complex–a membrane-bound redox complex involved in the sulfate respiratory pathway. *Biochemistry* **45,** 249–262
4. Bradley, J. M., Marritt, S. J., Kihlken, M. A., Haynes, K., Hemmings, A. M., Berks, B. C., Cheesman, M. R., and Butt, J. N. (2012) Redox and chemical activities of the hemes in the sulfur oxidation pathway enzyme SoxAX. *J. Biol. Chem.* **287,** 40350–40359
5. Reijerse, E. J., Sommerhalter, M., Hellwig, P., Quentmeier, A., Rother, D., Laurich, C., Bothe, E., Lubitz, W., and Friedrich, C. G. (2007) The unusual redox centers of SoxXA, a novel *c*-type heme-enzyme essential for chemotrophic sulfur-oxidation of *Paracoccus pantotrophus*. *Biochemistry* **46,** 7804–7810
6. Kappler, U., Bernhardt, P. V., Kilmartin, J., Riley, M. J., Teschner, J., McKenzie, K. J., and Hanson, G. R. (2008) SoxAX cytochromes, a new type

of heme copper protein involved in bacterial energy generation from sulfur compounds. *J. Biol. Chem.* **283,** 22206–22214
7. Kurth, J. M., Dahl, C., and Butt, J. N. (2015) Catalytic protein film electrochemistry provides a direct measure of the tetrathionate/thiosulfate reduction potential. *J. Am. Chem. Soc.* **137,** 13232–13235
8. Liu, Y.-W., Denkmann, K., Kosciow, K., Dahl, C., and Kelly, D. J. (2013) Tetrathionate stimulated growth of *Campylobacter jejuni* identifies TsdA as a new type of bi-functional tetrathionate reductase that is widely distributed in bacteria. *Mol. Microbiol.* **88,** 173–188
9. Cusanovich, M. A., and Bartsch, R. G. (1969) A high potential cytochrome *c* from *Chromatium vinosum* chromatophores. *Biochim. Biophys. Acta* **189,** 245–255
10. Bartsch, R. G. (1978) Purification of $(4Fe\text{-}4S)^{1-2-}$ ferredoxins (high-potential iron-sulfur proteins) from bacteria. *Methods Enzymol.* **53,** 329–340
11. Fukumori, Y., and Yamanaka, T. (1979) A high-potential nonheme iron protein (HiPIP)-linked, thiosulfate-oxidizing enzyme derived from *Chromatium vinosum*. *Curr. Microbiol.* **3,** 117–120
12. Grabarczyk, D. B., Chappell, P. E., Eisel, B., Johnson, S., Lea, S. M., and Berks, B. C. (2015) Mechanism of thiosulfate oxidation in the SoxA family of cysteine-ligated cytochromes. *J. Biol. Chem.* **290,** 9209–9221
13. Du, J., Sono, M., and Dawson, J. H. (2011) The H93G myoglobin cavity mutant as a versatile scaffold for modeling heme iron coordination structures in protein active sites and their characterization with magnetic circular dichroism spectroscopy. *Coord. Chem. Rev.* **255,** 700–716
14. Miles, C. S., Manson, F. D., Reid, G. A., and Chapman, S. K. (1993) Substitution of a haem-iron axial ligand in flavocytochrome b_2. *Biochim. Biophys. Acta* **1202,** 82–86
15. Branca, R. M., Bodó, G., Várkonyi, Z., Debreczeny, M., Osz, J., and Bagyinka, C. (2007) Oxygen and temperature-dependent structural and redox changes in a novel cytochrome c_4 from the purple sulfur bacterium *Thiocapsa roseopersicina*. *Arch. Biochem. Biophys.* **467,** 174–184
16. Nissum, M., Karlsson, J.-J., Ulstrup, J., Jensen, P. W., and Smulevich, G. (1997) Resonance Raman characterization of the di-heme protein cytochrome c_4 from *Pseudomonas stutzeri*. *J. Biol. Inorg. Chem.* **2,** 302–307
17. Matthews, B. W. (1968) Solvent content of protein crystals. *J. Mol. Biol.* **33,** 491–497
18. Holm, L., and Rosenström, P. (2010) Dali server: conservation mapping in 3D. *Nucleic Acids Res.* **38,** W545–W549
19. Igarashi, N., Moriyama, H., Fujiwara, T., Fukumori, Y., and Tanaka, N. (1997) The 2.8 Å structure of hydroxylamine oxidoreductase from a nitrifying chemoautotrophic bacterium, *Nitrosomonas europaea*. *Nat. Struct. Biol.* **4,** 276–284
20. Taylor, P., Pealing, S. L., Reid, G. A., Chapman, S. K., and Walkinshaw, M. D. (1999) Structural and mechanistic mapping of a unique fumarate reductase. *Nat. Struct. Biol.* **6,** 1108–1112
21. Visser, J. M., de Jong, G. A., Robertson, L. A., and Kuenen, J. G. (1996) Purification and characterization of a periplasmic thiosulfate dehydrogenase from the obligately autotrophic *Thiobacillus* sp. W5. *Arch. Microbiol.* **166,** 372–378
22. Ohmine, M., Matsuura, K., Shimada, K., Alric, J., Verméglio, A., and Nagashima, K. V. (2009) Cytochrome c_4 can be involved in the photosynthetic electron transfer system in the purple bacterium *Rubrivivax gelatinosus*. *Biochemistry* **48,** 9132–9139
23. Bartsch, R. G. (1991) The distribution of soluble metallo-redox proteins in purple phototrophic bacteria. *Biochim. Biophys. Acta* **1058,** 28–30
24. Kennel, S. J., Bartsch, R. G., and Kamen, M. D. (1972) Observations on light-induced oxidation reactions in the electron transport system of *Chromatium*. *Biophys. J.* **12,** 882–896
25. Nagashima, K. V., Matsuura, K., Shimada, K., and Verméglio, A. (2002) High-potential iron-sulfur protein (HiPIP) is the major electron donor to the reaction center complex in photosynthetically growing cells of the purple bacterium *Rubrivivax gelatinosus*. *Biochemistry* **41,** 14028–14032
26. Lieutaud, C., Nitschke, W., Verméglio, A., Parot, P., and Schoepp-Cothenet, B. (2003) HiPIP in *Rubrivivax gelatinosus* is firmly associated to the membrane in a conformation efficient for electron transfer towards the photosynthetic reaction centre. *Biochim. Biophys. Acta* **1557,** 83–90
27. Verméglio, A., Li, J., Schoepp-Cothenet, B., Pratt, N., and Knaff, D. B. (2002) The role of high-potential iron protein and cytochrome c_8 as alternative electron donors to the reaction center of *Chromatium vinosum*. *Biochemistry* **41,** 8868–8875
28. Kämpf, C., and Pfennig, N. (1980) Capacity of Chromatiaceae for chemotrophic growth. Specific respiration rates of *Thiocystis violacea* and *Chromatium vinosum*. *Arch. Microbiol.* **127,** 125–135
29. Hochkoeppler, A., Jenney, F. E., Jr., Lang, S. E., Zannoni, D., and Daldal, F. (1995) Membrane-associated cytochrome c_γ of *Rhodobacter capsulatus* is an electron carrier from the cytochrome bc_1 complex to the cytochrome *c* oxidase during respiration. *J. Bacteriol.* **177,** 608–613
30. Bonora, P., Principi, I. I., Monti, B., Ciurli, S., Zannoni, D., and Hochkoeppler, A. (1999) On the role of high-potential iron-sulfur proteins and cytochromes in the respiratory chain of two facultative phototrophs. *Biochim. Biophys. Acta* **1410,** 51–60
31. Beckwith, C. R., Edwards, M. J., Lawes, M., Shi, L., Butt, J. N., Richardson, D. J., and Clarke, T. A. (2015) Characterization of MtoD from *Sideroxydans lithotrophicus*: a cytochrome *c* electron shuttle used in lithoautotrophic growth. *Front. Microbiol.* **6,** 332
32. Arai, H., Kawakami, T., Osamura, T., Hirai, T., Sakai, Y., and Ishii, M. (2014) Enzymatic characterization and in vivo function of five terminal oxidases in *Pseudomonas aeruginosa*. *J. Bacteriol.* **196,** 4206–4215
33. Barco, R. A., Emerson, D., Sylvan, J. B., Orcutt, B. N., Jacobson Meyers, M. E., Ramírez, G. A., Zhong, J. D., and Edwards, K. J. (2015) New insight into microbial iron oxidation as revealed by the proteomic profile of an obligate iron-oxidizing chemolithoautotroph. *Appl. Environ. Microbiol.* **81,** 5927–5937
34. Chang, H. Y., Ahn, Y., Pace, L. A., Lin, M. T., Lin, Y. H., and Gennis, R. B. (2010) The diheme cytochrome c_4 from *Vibrio cholerae* is a natural electron donor to the respiratory cbb_3 oxygen reductase. *Biochemistry* **49,** 7494–7503
35. Bamford, V. A., Bruno, S., Rasmussen, T., Appia-Ayme, C., Cheesman, M. R., Berks, B. C., and Hemmings, A. M. (2002) Structural basis for the oxidation of thiosulfate by a sulfur cycle enzyme. *EMBO J.* **21,** 5599–5610
36. Dambe, T., Quentmeier, A., Rother, D., Friedrich, C., and Scheidig, A. J. (2005) Structure of the cytochrome complex SoxXA of *Paracoccus pantotrophus*, a heme enzyme initiating chemotrophic sulfur oxidation. *J. Struct. Biol.* **152,** 229–234
37. Kilmartin, J. R., Maher, M. J., Krusong, K., Noble, C. J., Hanson, G. R., Bernhardt, P. V., Riley, M. J., and Kappler, U. (2011) Insights into structure and function of the active site of SoxAX cytochromes. *J. Biol. Chem.* **286,** 24872–24881
38. Dahl, C., Schulte, A., Stockdreher, Y., Hong, C., Grimm, F., Sander, J., Kim, R., Kim, S.-H., and Shin, D. H. (2008) Structural and molecular genetic insight into a wide-spread bacterial sulfur oxidation pathway. *J. Mol. Biol.* **384,** 1287–1300
39. Brüser, T., Trüper, H. G., and Dahl, C. (1997) Cloning and sequencing of the gene encoding the high potential iron-sulfur protein (HiPIP) from the purple sulfur bacterium *Chromatium vinosum*. *Biochim. Biophys. Acta* **1352,** 18–22
40. Arslan, E., Schulz, H., Zufferey, R., Künzler, P., and Thöny-Meyer, L. (1998) Overproduction of *Bradyrhizobium japonicum c*-type cytochrome subunits of the cbb_3 oxidase in *Escherichia coli*. *Biochem. Biophys. Res. Commun.* **251,** 744–747
41. Segel, I. H. (1993) *Enzyme Kinetics: Behaviour and Analysis of Rapid Equilibrium and Steady-state Enzyme Systems*, Wiley-Interscience, New York
42. Marritt, S. J., Kemp, G. L., Xiaoe, L., Durrant, J. R., Cheesman, M. R., and Butt, J. N. (2008) Spectroelectrochemical characterization of a pentaheme cytochrome in solution and as electrocatalytically active films on nanocrystalline metal-oxide electrodes. *J. Am. Chem. Soc.* **130,** 8588–8589
43. Kabsch, W. (2010) XDS. *Acta Crystallogr. D Biol. Crystallogr.* **66,** 125–132
44. Evans, P. R. (2011) An introduction to data reduction: space-group determination, scaling and intensity statistics. *Acta Crystallogr. D Biol. Crystallogr.* **67,** 282–292
45. Evans, P. (2006) Scaling and assessment of data quality. *Acta Crystallogr. D Biol. Crystallogr.* **62,** 72–82
46. Evans, P. R., and Murshudov, G. N. (2013) How good are my data and what is the resolution? *Acta Crystallogr. D Biol. Crystallogr.* **69,** 1204–1214

47. Vonrhein, C., Flensburg, C., Keller, P., Sharff, A., Smart, O., Paciorek, W., Womack, T., and Bricogne, G. (2011) Data processing and analysis with the autoPROC toolbox. *Acta Crystallogr. D Biol. Crystallogr.* **67,** 293–302
48. Vonrhein, C., Blanc, E., Roversi, P., and Bricogne, G. (2007) Automated structure solution with autoSHARP. *Methods Mol. Biol.* **364,** 215–230
49. de la Fortelle, E., and Bricogne, G. (1997) Maximum-likelihood heavy-atom parameter refinement for multiple isomorphous replacement and multiwavelength anomalous diffraction methods. *Methods Enzymol.* **276,** 472–494
50. Emsley, P., Lohkamp, B., Scott, W. G., and Cowtan, K. (2010) Features and development of Coot. *Acta Crystallogr. D Biol. Crystallogr.* **66,** 486–501
51. Blanc, E., Roversi, P., Vonrhein, C., Flensburg, C., Lea, S. M., and Bricogne, G. (2004) Refinement of severely incomplete structures with maximum likelihood in BUSTER-TNT. *Acta Crystallogr. D Biol. Crystallogr.* **60,** 2210–2221
52. Afonine, P. V., Grosse-Kunstleve, R. W., Echols, N., Headd, J. J., Moriarty, N. W., Mustyakimov, M., Terwilliger, T. C., Urzhumtsev, A., Zwart, P. H., and Adams, P. D. (2012) Towards automated crystallographic structure refinement with phenix.refine. *Acta Crystallogr. D Biol. Crystallogr.* **68,** 352–367
53. Lovell, S. C., Davis, I. W., Arendall, W. B., 3rd., de Bakker, P. I., Word, J. M., Prisant, M. G., Richardson, J. S., and Richardson, D. C. (2003) Structure validation by Cα geometry: ϕ,ψ and Cβ deviation. *Proteins* **50,** 437–450
54. Chen, V. B., Arendall, W. B., 3rd, Headd J. J., Keedy, D. A., Immormino, R. M., Kapral, G. J., Murray, L. W., Richardson, J. S., and Richardson, D. C. (2010) MolProbity: all-atom structure validation for macromolecular crystallography. *Acta Crystallogr. D Biol. Crystallogr.* **66,** 12–21
55. Delano, W. L. (2002) *The PyMOL Molecular Graphics System*, version 1.7.2.1, DeLano Scientific, San Carlos, CA
56. Hanahan, D. (1983) Studies on transformation of *Escherichia coli* with plasmids. *J. Mol. Biol.* **166,** 557–580
57. Karplus, P. A., and Diederichs, K. (2012) Linking crystallographic model and data quality. *Science* **336,** 1030–1033

Chapter 3

Influence of haem environment on the catalytic properties of the tetrathionate reductase TsdA from *Campylobacter jejuni*

Introduction & Summary

For the well studied thiosulfate-oxidizing diheme cytochrome *c* TsdA from *Allochromatium vinosum* (*Av*TsdA) it was shown that the active site heme, Heme 1, exhibits an unusual His/Cys ligation. The electron transfer heme, Heme 2, is ligated by lysine that is replaced by methionine upon reduction. In contrast to *Av*TsdA, TsdA from the human gut bacterium *Campylobacter jejuni* (*Cj*TsdA) enables the organism to use tetrathionate as additional electron acceptor.

Similar to *Av*TsdA, cysteine serves as sixth heme iron ligand of Heme 1 in *Cj*TsdA. Contrary to the heme ligation in *Av*TsdA, Heme 2 iron is already ligated by methionine in the oxidized state in *Cj*TsdA. Cys^{138} and Met^{255} were found to be indispensable for efficient catalytic activity of this enzyme *in vitro* and *in vivo*. Besides Met^{255} further amino acids in close vicinity of Heme 2, namely Asn^{254} and Lys^{252}, influence the catalytic properties of *Cj*TsdA. The Heme 2 environment was found to contribute to defining the reaction directionality of this enzyme *in vitro* as well as *in vivo*.

Chapter 3

Influence of haem environment on the catalytic properties of the tetrathionate reductase TsdA from *Campylobacter jejuni*

This research was originally published in Bioscience Reports:

Kurth, J.M., Butt, J.N., Kelly, D.J., and Dahl, C. (2016) Influence of haem environment on the catalytic properties of the tetrathionate reductase TsdA from *Campylobacter jejuni*. *Biosci Rep* **36**: e00422.

http://www.bioscirep.org/content/36/6/e00422

Author contributions

- JMK performed all experiments

- JMK wrote the paper together with CD

Influence of haem environment on the catalytic properties of the tetrathionate reductase TsdA from *Campylobacter jejuni*

Julia M. Kurth*, Julea N. Butt†, David J. Kelly‡[1] and Christiane Dahl*[1]

*Institut für Mikrobiologie & Biotechnologie, Rheinische Friedrich-Wilhelms-Universität Bonn, D-53115 Bonn, Germany
†Centre for Molecular and Structural Biochemistry, School of Chemistry, and School of Biological Sciences, University of East Anglia, Norwich Research Park, Norwich NR4 7TJ, U.K.
‡Department of Molecular Biology and Biotechnology, The University of Sheffield, Firth Court, Western Bank, Sheffield S10 2TN, U.K.

Synopsis

Bifunctional dihaem cytochrome *c* thiosulfate dehydrogenases/tetrathionate reductases (TsdA) exhibit different catalytic properties depending on the source organism. In the human food-borne intestinal pathogen *Campylobacter jejuni*, TsdA functions as a tetrathionate reductase enabling respiration with tetrathionate as an alternative electron acceptor. In the present study, evidence is provided that Cys^{138} and Met^{255} serve as the sixth ligands of Haem 1 and Haem 2 respectively, in the oxidized *Cj*TsdA wt protein. Replacement of Cys^{138} resulted in a virtually inactive enzyme, confirming Haem 1 as the active site haem. Significantly, TsdA variants carrying amino acid exchanges in the vicinity of the electron-transferring Haem 2 (Met^{255}, Asn^{254} and Lys^{252}) exhibited markedly altered catalytic properties of the enzyme, showing these residues play a key role in the physiological function of TsdA. The growth phenotypes and tetrathionate reductase activities of a series of Δ*tsdA*/**tsdA* complementation strains constructed in the original host *C. jejuni* 81116, showed that *in vivo*, the TsdA variants exhibited the same catalytic properties as the pure, recombinantly produced enzymes. However, variants that catalysed tetrathionate reduction more effectively than the wild-type enzyme did not allow better growth.

Key words: axial haem ligation, cytochrome *c*, reaction directionality, tetrathionate reductase, thiosulfate.

Cite this article as: Bioscience Reports (2016) **36**, e00422, doi:10.1042/BSR20160457

INTRODUCTION

Although tetrathionate ($^{-}O_3S–S–S–SO_3^{-}$) has long been known to be used by some bacteria as an electron acceptor under anaerobic conditions, recent evidence suggests that the biochemical and environmental significance of tetrathionate respiration has been hugely underestimated [1,2]. In a single step requiring input of two electrons, tetrathionate is reduced to two molecules of thiosulfate ($^{-}S–SO_3^{-}$). The midpoint reduction potential of the tetrathionate/thiosulfate couple was only very recently determined by experimental means and found to be +198 mV compared with standard hydrogen electrode (SHE) [1], a value considerably more positive than the calculation-based value of +24 mV cited in many bacterial bioenergetics studies [3]. As a consequence, more free energy is available to be harnessed during the respiratory reduction of tetrathionate than was previously recognized. Furthermore, the high relevance of tetrathionate as an *in vivo* electron acceptor for bacterial pathogenesis is emphasized by the finding that the human intestinal pathogen *Salmonella typhimurium* induces host-driven formation of tetrathionate from thiosulfate by reactive oxygen species produced during inflammation [4]. The tetrathionate thus formed is used as terminal electron acceptor providing *S. typhimurium* with a growth advantage over the majority of the commensal flora lacking the capacity for tetrathionate reduction. Nevertheless, the extent to which this capacity is exploited by other enteric pathogens has yet to be fully appreciated. For example, although it has long been known that *Citrobacter* and *Proteus* species are also able to perform tetrathionate respiration [5], the mechanism and *in vivo* significance of this have not been studied.

In terms of the burden of disease, the microaerophilic food-borne pathogen *Campylobacter jejuni* is responsible for the majority of cases of bacterial gastroenteritis in the Western world, often being far more prevalent than any other enteric bacterium including *Salmonella* [6]. Normally commensal in the

Abbreviations: BHI-S, brain heart infusion medium supplemented with serine; HRP, horseradish peroxidase; SHE, standard hydrogen electrode; TsdA, thiosulfate dehydrogenases/tetrathionate reductases; wt; wild-type.

[1] Correspondence may be addressed to either of these authors (email d.kelly@sheffield.ac.uk or ChDahl@uni-bonn.de).

intestinal tract of chickens, in humans *C. jejuni* causes acute bloody diarrhoea and in some cases the sequelae include neuromuscular paralysis and even death [7,8]. Previously, it was found that some strains of *C. jejuni* are capable of tetrathionate respiration [2] and it was suggested that this plays an important role in growth in the oxygen-limited human intestinal mucosa; the ability to respire tetrathionate is thus relevant for understanding the pathogenicity of the organism [2]. The finding that *C. jejuni* strains are capable of tetrathionate reduction and that this can stimulate growth under oxygen-limited conditions added a further dimension to the complex, branched electron transport pathways employed in this organism. Other alternatives to oxygen as the terminal respiratory electron acceptor include fumarate, nitrite, trimethylamine *N*-oxide and dimethyl sulfoxide [9–11].

Surprisingly, the enzyme catalysing tetrathionate reduction in *C. jejuni* was found to be distinct from other known tetrathionate reductases, i.e. the iron–sulfur molybdoenzyme TtrABC found in *S. typhimurium* [12,13] and the octahaem Otr enzyme from *Shewanella oneidensis* [14]. Instead, the *Campylobacter* enzyme belongs to a novel, widely-distributed class of bifunctional thiosulfate dehydrogenase/tetrathionate reductases (TsdA) residing in the bacterial periplasm. TsdA enzymes represent a distinct type of dihaem *c*-type cytochrome [2,15,16]. An axial histidine/cysteine ligation of the central iron atom has been established for the active site haem (Haem 1) of the enzyme from *Allochromatium vinosum*, *Av*TsdA [15,16] (Figure 1). This type of ligation is rare among prokaryotes and appears to be of special importance in sulfur-based energy metabolism. In *Av*TsdA, Haem 2 exhibits axial His/Lys and His/Met co-ordination in the oxidized and reduced state respectively [16].

Although all TsdA enzymes characterized to date catalyse both the reduction of tetrathionate and the oxidation of two molecules of thiosulfate to tetrathionate at measurable rates, the enzymes from different bacteria still exhibit very different catalytic properties *in vitro* and have been shown to possess differences in reaction directionality using biochemical assays with redox dyes and also electrochemical protein film voltammetry [1,2,15,16]. The extent to which tetrathionate production or thiosulfate oxidation is favoured, is intrinsic to each TsdA. The *A. vinosum* enzyme catalyses tetrathionate reduction at a very low rate that is only measurable in colorimetric solution assays [15,16]. No evidence for reductive catalysis by *Av*TsdA could be found via protein film cyclic voltammetry whereas *Cj*TsdA appeared clearly biased towards tetrathionate reduction relative to thiosulfate oxidation in these experiments [1]. On graphite electrodes, the enzyme from the anoxygenic phototrophic sulfur bacterium *Marichromatium purpuratum*, *Mp*TsdBA, displays higher catalytic rates for thiosulfate oxidation than tetrathionate reduction revealing this enzyme's bias to oxidative catalysis [1]. The enzymatic features measured *in vitro* are in line with the different physiological functions of the TsdA enzymes which can enable either the use of tetrathionate as a terminal electron acceptor as in *C. jejuni* or the use of thiosulfate as an electron donor for respiration or photosynthesis as is the case in *A. vinosum* or *M. purpuratum*.

Very many if not all sequenced *C. jejuni* strains harbour a second *tsdA*-related gene. The corresponding protein CccC from *C. jejuni* strain NCTC 11168 (formerly Cj0037; C8j_0040 in strain 81116) has recently been identified as an efficient electron donor to the *cb*-oxidase [17]. These proteins contain a methionine in place of the probable Haem 1 ligating cysteine in TsdA. In addition, variation is apparent in the vicinity of the probable Haem 2-ligating methionine. Although all bona fide *C. jejuni tsdA* sequences encode an asparagine one residue upstream of the methionine, an alanine is present in the C8j_0040-related sequences. In a previous experimental approach towards the *in vivo* role of TsdA and related proteins in *C. jejuni* 81116, gene inactivation and complementation showed that the protein corresponding to typical TsdA is absolutely essential for growth on tetrathionate under oxygen limitation. A *tsdA* null mutant still had low tetrathionate reductase and thiosulfate dehydrogenase activities and slowly reduced tetrathionate probably due to low activity of CccC (Cj8_0040) as tetrathionate reductase, albeit this did not support growth [2].

There are still significant gaps in our knowledge about the physiological roles and biochemical properties of the proteins of the TsdA family. The enzyme from the sulfur oxidizer *A. vinosum* is the only one for which variants have so far been studied structurally and by UV–Vis spectroscopy. Kinetic characterization was initiated and showed that the replacement of either one of the Haem 2 distal axial ligands lysine or methionine did not render the enzyme catalytically inactive *in vitro* [15,16]. Initial characterization by UV–Vis absorption spectroscopy indicated that TsdA from *C. jejuni* 81116 has similar properties as the protein from *A. vinosum* [2]. However, experimental evidence has so far not been available providing conclusive information about axial haem iron ligation in the *C. jejuni* enzyme. It has therefore not been possible to assess whether structural differences in the immediate environment of one or both haems may be determinants underlying the enzyme's adaptation to catalysis in the tetrathionate-reducing direction [1]. Detailed kinetic data for a TsdA enzyme adapted to tetrathionate reduction is neither available for a wild-type enzyme nor have any variants been produced or analysed. *In vivo* data for performance of enzyme variants in the original host organism are so far not available for any TsdA. In the present study we address these areas, initially by characterization of pure recombinant *Cj*TsdA variants, which have allowed us to assess whether the nature of the haem-ligating residues alters the catalytic properties of the enzyme and whether both or only one catalytic direction(s) are affected. In addition, we have determined by *in vivo* complementation of the *C. jejuni* 81116 *tsdA* null mutant with a set of variant TsdAs, the growth capabilities and tetrathionate reduction rates as well as specific tetrathionate reductase and thiosulfate dehydrogenase activities in crude extracts of the resulting strains.

MATERIALS AND METHODS

Bacterial strains, plasmids and growth conditions

Table 1 lists the bacterial strains and plasmids used for the present study. *Escherichia coli* BL21 (DE3) was used for recombinant

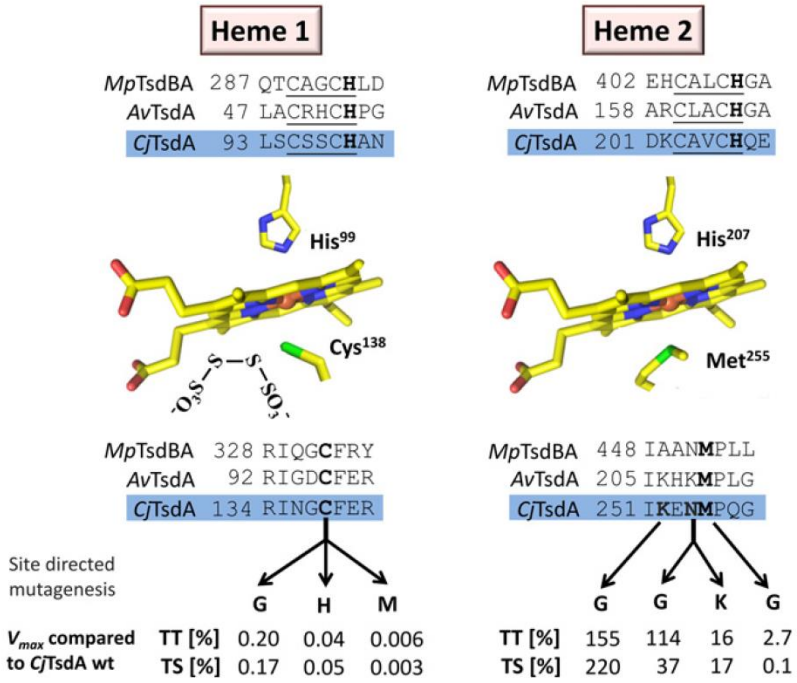

Figure 1 **Schematic overview of Haem 1 and Haem 2 environments in Tsd(B)A proteins**
Relevant sequence alignments are shown for TsdA from *C. jejuni* (*Cj*TsdA), *A. vinosum* (*Av*TsdA) and the TsdBA fusion protein from *M. purpuratum* (*Mp*TsdBA). Amino acid numbers are given for the recombinant proteins without signal peptides. In case of *Cj*TsdA, the sequence of the N-terminal Strep-tag is included. In the central left panel, a tetrathionate molecule is shown in vicinity of the active site Haem 1 iron-ligating cysteine, based on the *Av*TsdA crystal structure [16]. Amino acid numbers in the central panels refer to *Cj*TsdA. In the lower part of the figure, changes in the environments of Haem 1 and Haem 2 are indicated that were introduced by site-directed mutagenesis. The effects of these changes on maximal reaction velocity are listed as percent of V_{max} for the wild-type enzyme in the tetrathionate-reducing (TT) and the thiosulfate-oxidizing (TS) direction.

protein production and was grown in LB medium. *E. coli* DH5α was used for molecular cloning. Wild-type and mutant strains of *C. jejuni* 81116 (NCTC 11828) were used for *in vivo* studies.

Recombinant DNA techniques

All general molecular genetics techniques were described earlier [18]. Restriction enzymes, T4 ligase and *Pfu* or *Phusion* DNA polymerase were obtained from Thermo Scientific or NEB and used according to the manufacturer's instructions. Oligonucleotides for cloning were obtained from Eurofins MWG.

Construction of expression plasmids and site-directed mutagenesis

The *C. jejuni tsdA* gene coding for the mature protein without the signal peptide was amplified and cloned as described earlier [1]. Point mutations were introduced into *tsdA* by overlap extension [19] using standard PCR with *Pfu* DNA polymerase and pET-N-Strep-TsdACj [1] as the template (Table 1). For the TsdA–C138G exchange, two fragments were amplified with the following primers: for the first fragment pET-N-TsdACj_fw and tsdACj-C-Gly_rev, for the second fragment tsdACj-C-Gly_fw and pET-N-TsdACj_rev (Table 2). Both fragments were used as templates for amplification of the complete *tsdA* gene carrying the desired point mutation. In this step, pET-N-TsdACj_fw and pET-N-TsdACj_rev served as primers (Table 2). The resulting fragment was restricted with BamHI and HindIII and cloned into pET-N-Strep-TsdACj resulting in plasmid pET-N-Strep-TsdACj-C138G. The following plasmids were generated applying the same general strategy: pET-N-Strep-TsdACj-C138G, pET-N-Strep-TsdACj-C138H, pET-N-Strep-TsdACj-C138M, pET-N-Strep-TsdACj-M255G, pET-N-Strep-TsdACj-N254G pET-N-Strep-TsdACj-N254K and pET-N-Strep-TsdACj-K252G (Table 1). For construction of pET-N-Strep-TsdACj-KMG, pET-N-Strep-TsdACj-NMG and pET-N-Strep-TsdACj-KNMG pET-N-Strep-TsdACj-M255G was used as template in PCR.

Overproduction, purification and preparation of recombinant TsdA wild-type and variant proteins

Single colonies of *E. coli* BL21(DE3) containing pET-N-Strep-TsdACj or one of the *tsdA* variant expression plasmids in addition to plasmid pEC86 [20] were inoculated in 800 ml batches of LB

Table 1 Strains and plasmids used in the present study

Strains and plasmids	Description	References or sources
Strains		
E. coli DH5α	F$^-$ φ80d *lacZ*ΔM15 Δ(*lacZYA-argF*)*U169 recA1 endA1hsdR17* (rk$^-$ mk$^+$) *supE44* λ^- *thi-1 gyrA relA1*	[37]
E. coli BL21 (DE3)	F$^-$ *ompT hsdS*$_B$ (r_B^- m_B^-) *gal dcm met*(DE3)	Novagen
C. jejuni 81116 (NCTC 11828)	Wild-type	[38]
C. jejuni 81116 Δ*tsdA*	Kan^r; insertion of kanamycin resistance cassette in place of *c8j_0815*	[2]
C. jejuni 81116 Δ*tsdA*/**tsdA* wt	Kan^r, Cm^r; Δ*tsdA* mutant complented with *c8j_0815* in *cj0046* pseudogene locus behind fdxA promotor	The present study
C. jejuni 81116 Δ*tsdA*/**tsdA* CG	Kan^r, Cm^r; Δ*tsdA* mutant complented with *tsdA* C138G in *cj0046* pseudogene locus behind fdxA promotor	The present study
C. jejuni 81116 Δ*tsdA*/**tsdA* MG	Kan^r, Cm^r; Δ*tsdA* mutant complented with *tsdA* M255G in *cj0046* pseudogene locus behind fdxA promotor	The present study
C. jejuni 81116 Δ*tsdA*/**tsdA* NG	Kan^r, Cm^r; Δ*tsdA* mutant complented with *tsdA* N254G in *cj0046* pseudogene locus behind fdxA promotor	The present study
C. jejuni 81116 Δ*tsdA*/**tsdA* KG	Kan^r, Cm^r; Δ*tsdA* mutant complented with *tsdA* K252G in *cj0046* pseudogene locus behind fdxA promotor	The present study
Plasmids		
pEC86	Cm^r, product from pEC66 and pACYC184 with *E. coli ccmABCDEFGH* genes	[20]
pC46-fdxA	*C. jejuni* complementation vector for integration at the *cj0046c* pseudogene locus, expressing cloned genes from the *fdxA* promoter	[39]
pET-N-Strep-TsdACj	Ap^r; N-terminal Strep-tag, f1 origin, T7 Promoter, NcoI-HindIII fragment of PCR amplified *tsdA* in digested pETStrepDsrJ	[1]
pET-N-Strep-TsdACj-C138G	Ap^r; C138G mutation introduced into pET-N-Strep-TsdACj	The present study
pET-N-Strep-TsdACj-C138H	Ap^r; C138H mutation introduced into pET-N-Strep-TsdACj	The present study
pET-N-Strep-TsdACj-C138M	Apr; C138M mutation introduced into pET-N-Strep-TsdACj	The present study
pET-N-Strep-TsdACj-M255G	Ap^r; M255G mutation introduced into pET-N-Strep-TsdACj	The present study
pET-N-Strep-TsdACj-N254G	Ap^r; N254G mutation introduced into pET-N-Strep-TsdACj	The present study
pET-N-Strep-TsdACj-N254K	Ap^r; N254K mutation introduced into pET-N-Strep-TsdACj	The present study
pET-N-Strep-TsdACj-K252G	Ap^r; K252G mutation introduced into pET-N-Strep-TsdACj	The present study
pET-N-Strep-TsdACj-KMG	Ap^r; K252G mutation introduced into pET-N-Strep-TsdACj-M255G	The present study
pET-N-Strep-TsdACj-NMG	Ap^r; N254G mutation introduced into pET-N-Strep-TsdACj-M255G	The present study
pET-N-Strep-TsdACj-KNMG	Ap^r; K252G andN254G mutation introduced into pET-N-Strep-TsdACj-M255G	The present study
pC46-fdxA-0815HIS	Cm^r; *c8j_0815* cloned into pC46-fdxA to produce C-terminal His-tagged TsdA in *C. jejuni*	The present study
pC46-fdxA-TsdACj-C138G	Cm^r, C138G mutation introduced into pC46-fdxA-0815	The present study
pC46-fdxA-TsdACj-M255G	Cm^r, M255G mutation introduced into pC46-fdxA-0815	The present study
pC46-fdxA-TsdACj-N254G	Cm^r, N254G mutation introduced into pC46-fdxA-0815	The present study
pC46-fdxA-TsdACj-K252G	Cm^r, K252G mutation introduced into pC46-fdxA-0815	The present study

medium containing 100 $\mu g \cdot ml^{-1}$ ampicillin and 25 $\mu g \cdot ml^{-1}$ chloramphenicol and incubated at 37 °C and 180 rpm. Cells were harvested by centrifugation after 15 to 17 h, resuspended in 100 mM Tris/HCl buffer (pH 8) containing 150 mM NaCl and lysed by sonication. After removal of insoluble cell material by centrifugation (10 000 ***g*** for 25 min at 4 °C), TsdA or its variants were purified by Strep-Tactin affinity chromatography with a 5 ml StrepTrap HP column (GE Healthcare) according to manufacturer's instructions. Afterwards, a gel filtration chromatography was performed on a HiLoad 16/60 Superdex 75 pg column (GE Healthcare) using an ÄKTApurifier system (GE Healthcare). The column was equilibrated with 20 mM BisTris/HCl buffer, pH 6.5. The purified protein was concentrated with Amicon Ultra-15 30K centrifugal filter units (Merck Millipore) and desalted with a 5 ml HiTrap Desalting column (GE Healthcare). The protein was stored in 50 mM BisTris buffer, pH 6.5 at −70 °C. The concentration of purified protein was determined with the BCA Kit from Pierce. For assessment of purity, SDS/PAGE was performed. Haem staining in acrylamide gels followed an established procedure [21]. Haem content was determined by the pyridine haemochrome method [22].

Construction of *C. jejuni* Δ*tsdA*/**tsdA* complementation strains

The pC46-fdxA-0815HIS complementation vector integrates a copy of the *tsdA* gene at the phenotypically silent *cj0046c* pseudogene locus in *C. jejuni*, with expression driven by the

Table 2 Primer used in the present study

Primer	Sequence 5′–3′	References
pET-N-TsdACj_fw	CCGGATCCTTAGATCCAAATTTG	[1]
pET-N-TsdACj_rev	CCGAAGCTTCTACTTCTTGATCA	[1]
0815-com-F/ATG	GGAGCGTCTCACATGAATAAATTTT CTATAGTTTTAACTTTG	The present study
0815-com-R5XHis	ACGTCTCACATGTTAATGATGATGATGTTTTTTGATCATATTTGTA	The present study
tsdACj-C-Gly_fw	GATCAATGGCGGTTTTGAACGCT	The present study
tsdACj-C-Gly_rev	AGCGTTCAAAACCGCCATTGATC	The present study
tsdACj-C-His_fw	GATCAATGGCCATTTTGAACGCT	The present study
tsdACj-C-His_rev	AGCGTTCAAAATGGCCATTGATC	The present study
tsdACj-C-Met_fw	GATCAATGGCATGTTTGAACGCT	The present study
tsdACj-C-Met_rev	AGCGTTCAAACATGCCATTGATC	The present study
tsdACj-M-Gly_fw	TAAAGAAAATGGTCCTCAAGGTG	The present study
tsdACj-M-Gly_rev	CACCTTGAGGACCATTTTCTTTA	The present study
tsdACj-N-Gly_fw	TATTAAAGAAGGTATGCCTCAAGG	The present study
tsdACj-N-Gly_rev	CCTTGAGGCATACCTTCTTTAATA	The present study
tsdACj-N-Lys_fw	TATTAAAGAAAAGATGCCTCAAGG	The present study
tsdACj-N-Lys_rev	CCTTGAGGCATCTTTTCTTTAATA	The present study
tsdACj-K-Gly_fw	CTTCTTATATTGGCGAAAATATGC	The present study
tsdACj-K-Gly_rev	GCATATTTTCGCCAATATAAGAAG	The present study
tsdACj-NM-Gly_fw	TATTAAAGAAGGTGGTCCTCAAG	The present study
tsdACj-NM-Gly_rev	CTTGAGGACCACCTTCTTTAATA	The present study
tsdACj-KM-Gly_fw	TTCTTATATTGGCGAAAATGGTCC	The present study
tsdACj-KM-Gly_rev	GGACCATTTTCGCCAATATAAGAA	The present study
tsdACj-KNM-Gly_fw	TTATATTGGAGAAGGTGGTCCTC	The present study
tsdACj-KNM-Gly_fw	GAGGACCACCTTCTCCAATATAA	The present study
pC46_TsdA_Mfe_fw	GCCCAATTGAAAATCTAAGTAAAAT	The present study
pC46_TsdA_Cla_rev	TGAATCGATAAGGGAATATAGTATT	The present study
p46-Scr-F	CCACTCCTGAAGATGGAACAC	The present study
p46-Scr-R	ATCATTACAAGAGCTGAAAACCATAC	The present study
Cat-Scr-F	AAAAGTTATACCCAACTCTTTTATATGGAG	The present study
Cj46-Scr-R	GTGCAAGTTTTAGATCAGTTTATGGA	The present study

moderately strong *C. jejuni fdxA* promoter. It was constructed by cloning the amplicon resulting from PCR of genomic DNA of *C. jejuni* strain 81116 with primers 0815-com-F/ATG and 0815-com-R5XHis (Table 2) into the BsmBI site of pC46-fdxA (8). The produced TsdA protein has a C-terminal 5 residue His-tag added, that was used for detection in immunoblots (see below). For the TsdA–C138G exchange, two fragments were amplified from pC46-fdxA-0815 with the following primers: for the first fragment pC46_TsdA_Mfe_fw and tsdACj-C-Gly_fw, for the second fragment tsdACj-C-Gly_rev and pC46_TsdA_Cla_rev (Table 2). Both fragments were used as templates for amplification of the complete *tsdA* gene carrying the desired point mutation. In this step, pC46_TsdA_Mfe_fw and pC46_TsdA_Cla_rev served as primers (Table 2). The resulting fragment was restricted with MfeI and ClaI and cloned into pC46-fdxA resulting in plasmid pC46-fdxA-TsdACj-C138G. The following plasmids were generated applying the same general strategy: pC46-fdxA-TsdACj-M255G, pC46-fdxA-TsdACj-N254G and pC46-fdxA-TsdACj-K255G (Table 1). Plasmids were transformed into the *C. jejuni* 81116 Δ*tsdA* mutant strain [2] by electroporation and transformants were selected on Columbia blood agar plates supplemented with chloramphenicol (20 $\mu g \cdot ml^{-1}$ final concentration). Complementations were confirmed by PCR of genomic DNA with primers pC46F-Scr-F + pC46-Scr-R and Cat-Scr-F + Cj46-Scr-R (Table 2).

Culture conditions for *C. jejuni* growth

Campylobacter jejuni strain 81116 was routinely cultured at 42 °C under microaerobic conditions [10% (v/v) O_2, 5% (v/v) CO_2 and 85% (v/v) N_2] in a MACS growth cabinet (Don Whitley Scientific) on Columbia agar containing 5% (v/v) lysed horse blood and 10 $\mu g \cdot ml^{-1}$ each of amphotericin B and vancomycin. To select *C. jejuni* mutants, kanamycin or chloramphenicol was added at a final concentration of 50 or 20 $\mu g \cdot ml^{-1}$ respectively. Liquid cultures of *C. jejuni* were routinely grown in Mueller-Hinton broth (Oxoid) supplemented with 20 mM L-serine (MH-S) under standard microaerobic conditions (gas concentrations as above), with 50–100 ml of medium contained in 250 ml conical flasks with continuous orbital shaking at 180 rpm. Except

precultures, all cultures contained 50 μM ammonium iron (II) sulfate to induce the *fdxA* promoter in front of *tsdA* in the complementation strains. To study tetrathionate-dependent growth, oxygen-limited cultures were grown in 250 ml of brain heart infusion medium with 20 mM L-serine (BHI-S, brain heart infusion medium supplemented with serine) contained in a 250 ml conical flask with no shaking. In this case, 20 mM sodium formate and 15 mM sodium tetrathionate (final concentrations) were added from filter-sterilized stock solutions. Cultures were maintained in the MACS-VA500 incubator and growth was monitored by measuring absorbance at 600 nm. Values for each growth curve were measured with two independent cultures.

SDS/PAGE and immunoblotting with *C. jejuni* crude cell extract

C. jejuni cells were disrupted by bead beating (Bead Ruptor 12, Omni International) at maximal intensity for 30 s and the crude cell extracts were used for SDS/PAGE. For Western blot analysis, proteins were electroblotted on to nitrocellulose membranes (Amersham Protran 0.45 μm NC, GE Healthcare) for 35 min at 15 V using the Transblot SD semi-dry transfer apparatus (Bio-Rad Laboratories). His-tagged protein was detected with His-tag monoclonal antibody (#70796-3, Novagen) and Goat Anti-Mouse IgG horseradish peroxidase (HRP) Conjugate (#71045-3, Novagen) via the associated peroxidase activity using either chloronaphthol or the SignalFire ECL Reagent kit (Cell Signaling Technology).

Measurement of tetrathionate reduction and thiosulfate respiration rates

Rates of tetrathionate reduction by cell suspensions were measured by adding washed cells to 14 ml 25 mM phosphate buffer (pH 7.4) containing 20 mM sodium formate. Before addition of cells, the buffer was sparged with N_2 for 10 min. The buffer-cell suspension was incubated at 42 °C for 15 min to allow all of the dissolved oxygen to be consumed. Then, sodium tetrathionate was added to 2 mM final concentration and 0.5 ml samples were taken every 2 or 5 min. The cells were immediately removed from these samples by brief centrifugation (12000 × ***g***, 2 min) and the thiosulfate concentration in the supernatants was measured by the method of Urban [23]. Tetrathionate formation rates were calculated by dividing thiosulfate oxidation rates (μmol · min^{-1} · ml^{-1}) by two and dividing the result by the protein content. For determination of the protein content, cell suspensions were first incubated at 100 °C for 20 min. To remove residual thiosulfate and tetrathionate, which interfere with the BCA assay, an acetone precipitation was performed as the next step: 200 μl of cold (− 20 °C) acetone was added to 50 μl of the pre-boiled cell suspension, followed by mixing and incubation at -20 °C for 1 h. BCA standards were treated accordingly. After centrifugation for 15 min at 15000 × ***g***, the supernatant was discarded. The protein pellets were dried by incubation for 25 min at room temperature and subsequently resuspended in 50 μl of H_2O. Protein concentration was determined with the BCA Kit from Pierce.

UV–Vis spectroscopy with TsdA in solution

UV–Vis spectra were recorded with an Analytik Jena Specord 210.

Assay of tetrathionate reductase activity with reduced methyl viologen

Spectrophotometric measurements of tetrathionate reductase activity were performed with recombinant *C. jejuni* TsdA at 42 °C for tetrathionate concentrations up to 0.5 mM and used reduced methyl viologen as electron donor were performed along similar lines as described before [2]. However, in our previous work recombinant enzyme was added to reaction mixtures before these were made anoxic by sparging with argon and addition of 2% titanium (III) citrate oxygen scavenger solution. The assays were started by addition of tetrathionate. Here, enzyme was added to completely oxygen-free reaction mixtures containing tetrathionate and pre-reduced methyl viologen. This improved method yielded 20-fold higher specific tetrathionate reductase activities and thus enabled more precise analysis of kinetic parameters. In addition, the range from 0.01 to 0.5 mM tetrathionate was studied at higher resolution. The assay was carried out in a 1 ml quartz glass cuvette closed with a rubber stopper and purged with N_2 for 10 min. All buffers and solutions were made anoxic by sparging with N_2. The final assay mixture contained 100 mM ammonium acetate buffer, pH 5, 0.3 mM methyl viologen reduced with 1–3 μl of 2% titanium (III) citrate oxygen scavenger solution [24] and different final concentrations of tetrathionate. Enzyme solutions were injected after a relatively stable absorbance at 585 nm was achieved (below 2.0). The rate before addition of enzyme was subtracted from the rate after enzyme addition. Control experiments ensured that reduced methyl viologen was provided at a saturating concentration during all measurements with *Cj*TsdA wt and its derivatives. The specific activity for tetrathionate reductase was calculated using molar absorption coefficient for methyl viologen of 11.8 mM^{-1} · cm^{-1} at 585 nm. For enzyme activity measurements with crude cell extracts, *C. jejuni* 81116 (wt), Δ*tsdA* mutant (Δ*tsdA*) and the different complementation strains (WT, CG, MG, NG, KG) were first disrupted by bead beating (Bead Ruptor 12, Omni International) at maximal intensity for 30 s. Tetrathionate reduction was measured with 0.1 mM tetrathionate. Protein determination was performed with BCA-Kit from Pierce. Activity is expressed as μmol tetrathionate reduced min^{-1} · mg protein^{-1} on the basis of a 1:2 molar ratio of tetrathionate reduced to methyl viologen oxidized.

The activity of TsdA and its variants is inhibited as substrate concentration increases. The K_i values given in Table 4 were derived from fitting complete data sets to the general equation for substrate inhibition (eqn 1) [25] using Graph Pad Prism (version 6; Graph Pad).

$$v = \frac{V_{max}\ [S]}{K_m + [S] + \frac{[S]^2}{K_i}} \quad (1)$$

Kinetic constants other than K_i can be derived from eqn (1). In that case, V_{max} is the maximum enzyme velocity if the substrate did not inhibit enzyme activity.

Table 3 Tetrathionate reduction catalysed by *Cj*TsdA wt and derivatives

Enzyme activity was measured under anoxic conditions at 42 °C in 100 mM ammonium acetate buffer (pH 5) with a saturating concentration of 0.3 mM methyl viologen previously reduced with titanium (III) citrate. Tetrathionate was varied between 0.01 to 0.7 mM. The units for V_{max} are $\mu mol \cdot min^{-1} \cdot mg \cdot protein^{-1}$. Data sets were fitted to the general equation for substrate inhibition [25]. Ligand changes affected either Haem 1 or Haem 2 as indicated.

	TsdA	$V_{max\ measured}$ (units/mg)	V_{max} (units/mg)	K_m (μM)	K_i (μM)
	WT	1316 ± 38	2328 ± 273	74 ± 14	420 ± 100
	C138G	2.63 ± 0.08	3.7 ± 0.5	34 ± 9	810 ± 440
Haem 1	C138H	0.49 ± 0.01	0.5 ± 0.1	24 ± 10	1150 ± 890
	C138M	0.08 ± 0.01	–	–	–
	M255G	35 ± 1	88 ± 13	317 ± 61	570 ± 160
	N254G	1502 ± 136	3284 ± 457	77 ± 15	220 ± 70
	N254K	216 ± 1	2214 ± 918	360 ± 162	20 ± 10
Haem 2	K252G	2045 ± 112	3823 ± 528	69 ± 15	390 ± 130
	NMG	178 ± 3	412 ± 127	113 ± 51	250 ± 130
	KMG	281 ± 1	652 ± 251	151 ± 84	440 ± 300
	KNMG	95 ± 3	129 ± 16	55 ± 14	1620 ± 970

Assay of thiosulfate dehydrogenase activity with horse heart cytochrome *c*

In the article by Liu et al. [2], ferricyanide was used as the artificial electron acceptor during measurements of thiosulfate dehydrogenase activity at pH 4.0. However, a preliminary set of experiments already showed a much lower $S_{0.5}$ value for thiosulfate and a near neutral pH optimum of the reaction when horse heart cytochrome *c* was used as electron acceptor [2]. Therefore, all measurements of thiosulfate dehydrogenase activity were performed with horse heart cytochrome *c* (80 μM; C7752, Sigma–Aldrich) as the electron acceptor at 42 °C in 50 mM BisTris buffer, pH 6.5. Thiosulfate was varied in the range of 0.05–8 mM. Reactions were started by addition of the enzyme and followed by the increase in absorbance at 550 nm. As the reduction of horse heart cytochrome *c* was measured, a molar absorption coefficient at 550 nm of 21.1 $mM^{-1} \cdot cm^{-1}$ [26] was used. The presence of oxygen did not affect these measurements. This was ensured by control reactions with *Cj*TsdA wt and derivatives under anoxic conditions.

In the case of enzymes that use two molecules of the same substrate (here thiosulfate) primary *v* compared with [*S*] plots provide the best way to examine the data [27]. Data were fitted to the empirical Hill eqn (2) using Graph Pad Prism (version 6; Graph Pad).

$$v = \frac{V_{max}[S]^n}{K + [S]^n} \quad (2)$$

The Hill equation resembles the classical Henri–Michaelis–Menten equation; however, the *n* term allows accounting for non-hyperbolic shapes. A substrate concentration $[S]_{0.5}$ can be reported that yields half maximal velocity and is characteristic of the process. The constant *K*, which is not equivalent to K_m, characterizes enzyme–substrate interaction. The relationship between *K* and $[S]_{0.5}$ is $K=[S]_{0.5}{}^n$.

For enzyme activity measurements with crude cell extracts, *C. jejuni* 81116 cells (wild-type), Δ*tsdA* mutant (Δ*tsdA*) and the different complementation strains (WT, CG, MG, NG, KG) were first disrupted by bead beating (Bead Ruptor 12, Omni International) at maximal intensity for 30 s. Thiosulfate oxidation was measured with 2 mM thiosulfate. Protein determination was performed with BCA Kit from Pierce. Activity is expressed as μmol tetrathionate produced per min and mg protein on the basis of one molecule tetrathionate formed per two molecules horse heart cytochrome *c* reduced.

Protein film cyclic voltammetry of *Cj*TsdA wt, N254G and K252G variant

Experiments were performed with a graphite working electrode as described in [1]. Cyclic voltammograms were measured under identical conditions with the freshly polished electrode placed directly into the desired solution, or, coated with enzyme prior to placement in the desired solution. The catalytic currents (i_{cat}) due to the activity of the enzyme were defined by subtraction of the response of the bare electrode from that of the enzyme coated electrode. The dependence of i_{cat} on potential was independent of whether the scan was to more negative, or more positive, potentials.

Statistical analysis

Average values and standard deviations for V_{max} values shown in Tables 3 and 4 as well as for all values shown in Table 5 were calculated from the appropriate data sets using Microsoft Excel 2010. Standard deviations for all further kinetic parameters shown in Tables 3 and 4 were calculated with Graph Pad Prism (version 6; Graph Pad).

RESULTS

Production and characterization of wild-type and variant *Cj*TsdA enzymes

*Cj*TsdA wt and variant proteins (see 'Materials and Methods' section for details of construction) were produced recombinantly

Table 4 Thiosulfate oxidation catalysed by *Cj*TsdA wt and derivatives

Enzyme assays were performed at 42 °C in 50 mM BisTris buffer (pH 6.5) with a saturating concentration of 80 μM horse heart cytochrome *c* as electron acceptor and 0.05–8 mM thiosulfate. The units for V_{max} are $\mu mol \cdot min^{-1} \cdot mg \cdot protein^{-1}$. *v* compared with [S] plots were fitted to the Hill equation. Ligand changes affected either Haem 1 or Haem 2 as indicated; *n*, Hill coefficient.

	TsdA	V_{max} (units/mg)	$S_{0.5}$ (μM)	*n*
	WT	1265 ± 70	280 ± 45	0.87 ± 0.07
	C138G	2.1 ± 0.3	527 ± 273	0.71 ± 0.12
Haem 1	C138H	0.6 ± 0.1	343 ± 205	0.77 ± 0.32
	C138M	0.04 ± 0.01	660 ± 532	0.52 ± 0.13
	M255G	0.7 ± 0.0	162 ± 15	1.07 ± 0.11
	N254G	469 ± 29	194 ± 34	0.94 ± 0.10
	N254K	211 ± 16	157 ± 34	0.95 ± 0.18
Haem 2	K252G	2782 ± 275	330 ± 79	1.24 ± 0.31
	NMG	0.6 ± 0.1	72 ± 27	0.61 ± 0.13
	KMG	0.8 ± 0.1	67 ± 41	0.60 ± 0.18
	KNMG	0.1 ± 0.0	101 ± 29	0.78 ± 0.16

Table 5 Growth rate and doubling time of different *C. jejuni* cultures

Growth parameters were calculated from A_{600} values taken in the exponential phase of the 81116 wt (81116), Δ*tsdA* mutant (Δ*tsdA*) and the different Δ*tsdA*/**tsdA* complementation strains (**tsdA* WT, **tsdA* C138G, **tsdA* M255G, **tsdA* N254G, **tsdA* K252G). Cells were grown under oxygen-limited conditions at 42 °C in almost completely filled 500 ml shake flasks containing BHI-S medium plus 20 mM sodium formate and 15 mM tetrathionate.

Strain	81116	Δ*tsdA*	**tsdA* WT	**tsdA* C138G	**tsdA* M255G	**tsdA* N254G	**tsdA* K252G
μ	0.12 ± 0.01	0.01 ± 0.00	0.24 ± 0.01	0.01 ± 0.00	0.05 ± 0.00	0.25 ± 0.02	0.19 ± 0.02
t_d (h)	5.6 ± 0.4	57.8 ± 14.9	2.9 ± 0.2	52.3 ± 11.1	13.4 ± 1.1	2.8 ± 0.3	3.6 ± 0.3

in *E. coli* BL21 (DE3) containing pEC86 to promote cytochrome *c* synthesis, purified to homogeneity by Strep-tag affinity chromatography and gel filtration. All *Cj*TsdA proteins behaved as homodimers upon analytical gel permeation chromatography (70–76 kDa) and showed the expected size of 37 kDa (exactly: 37103 Da not including the signal peptide, with two covalently bound haems) upon SDS/PAGE (Supplementary Figure S1). Quantification of *Cj*TsdA by the pyridine haemochrome method established that full haem loading had occurred in all cases (1.8–2.2 mol haem per mol protein). Amino acid numbering applies to recombinant protein without signal peptide but including the N-terminal Strep-tag.

Haem ligation in wild-type *Cj*TsdA

On the basis of amino acid sequence comparisons [2,15], the iron atom of *Cj*TsdA Haem 1 is predicted to be in a six-coordinated low spin state. Strictly conserved histidine (His^{99}) and cysteine (Cys^{138}) residues are likely to serve as axial haem iron ligands (Figure 1). Accordingly, a replacement of *Cj*TsdA Cys^{138} by a glycine, an amino acid not capable of haem iron co-ordination, led to a low-intensity spectral feature at 622 nm in the oxidized state indicative of the presence of high-spin haem either with water as a sixth ligand or with five-coordinate iron (Figure 2) [28,29] thus confirming Cys^{138} as the sixth haem ligand of Haem 1.

In *Av*TsdA, Haem 2 exhibits axial His/Lys co-ordination in the oxidized state. A ligand switch from the iron-coordinating Lys^{208} to Met^{209} is observed upon reduction of the enzyme [16]. Although the methionine residue is strictly conserved in all TsdA sequences (residue 255 in *Cj*TsdA), variation is apparent at the position of the lysine, which is located one residue closer to the N-terminus (position 254 in *Cj*TsdA). In *Cj*TsdA, an asparagine (Asn^{254}) is found instead of the lysine in the *A. vinosum* protein (Figure 1). UV–Vis spectroscopy and amino acid replacement clearly revealed that Met^{255} acts as the sixth axial ligand of Haem 2 iron in *Cj*TsdA, at least in the oxidized state. First, a peak at 700 nm, which is characteristic for methionine as haem iron ligand [28], is clearly apparent in the oxidized spectra of *Cj*TsdA wt (Figure 2A) as well as in *Cj*TsdA variants with N254G, K252G and N254K exchanges (Figures 2C and 2E) but no longer present in the spectrum of a variant with a M255G replacement (Figure 2C). Second, the exchange of Met^{255} to the ligation-incompetent glycine leads to appearance of a high-spin haem feature at 622 nm [28,29] in the oxidized spectrum (Figure 2C).

Oxidative and reductive assays – experimental approaches and data analysis procedures

Solution assays with redox dyes yielded the first kinetic parameters for *Cj*TsdA [2]. In the present study, we expanded this work to TsdA variants carrying amino acid replacements in the immediate environment of Haem 1 or Haem 2 (Figures 3 and 4, Tables 3 and 4). In addition, parameters for the wild-type enzyme were reassessed under optimized conditions (cf. Materials and Meth-

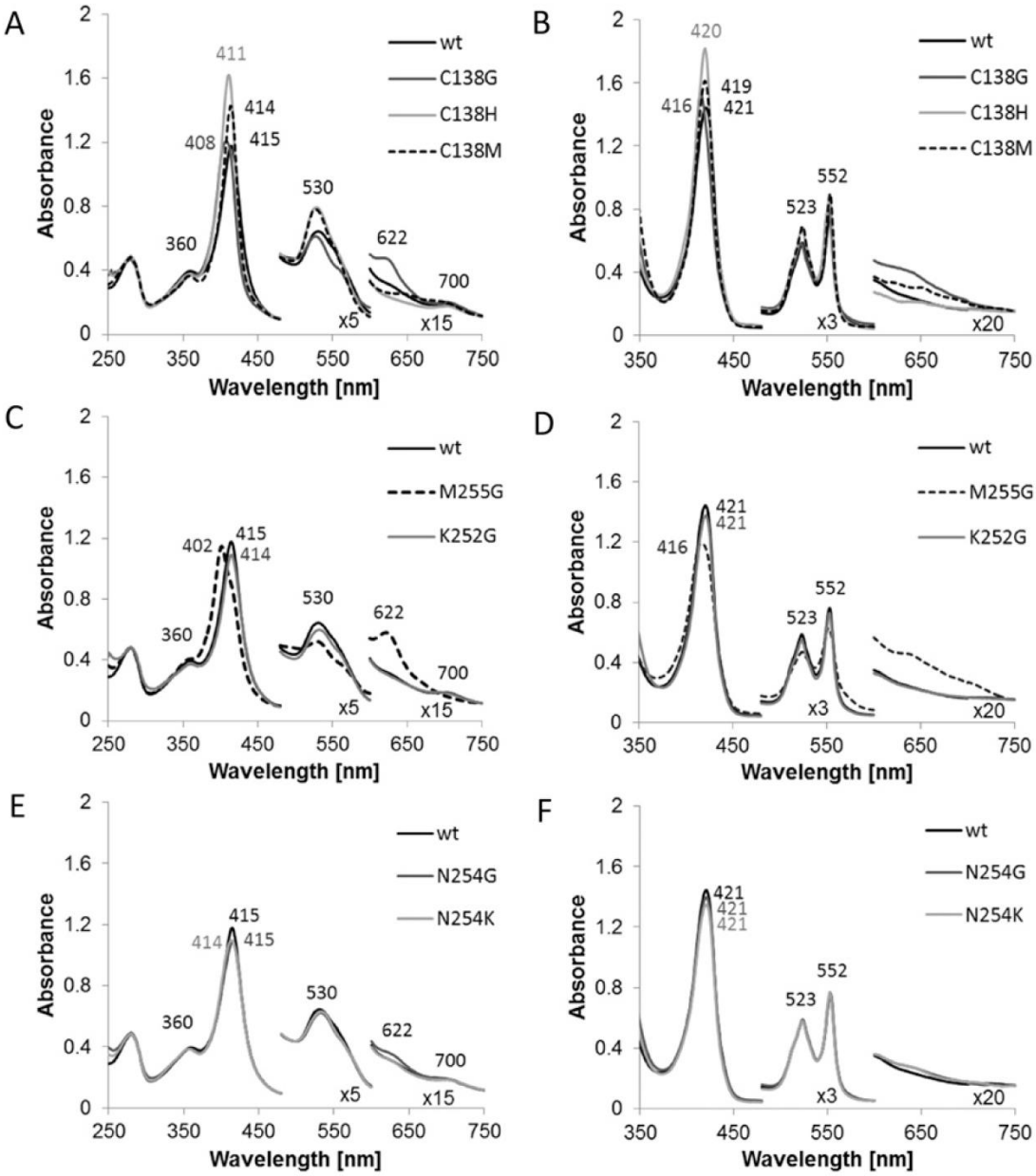

Figure 2 **UV–Vis spectra of *Cj*TsdA wt and variants**

UV–Vis spectra of *Cj*TsdA wt are compared with spectra of variants with affected Haem 1 ligation (**A** and **B**) and with spectra of variants with affected Haem 2 ligation (**C**–**F**). As some of the proteins are partly reduced in the 'as isolated' state, up to 30 μM ferricyanide was added to record the oxidized spectrum (A, C and E). For full reduction of the proteins, 5–16 mM Na-dithionite was added (B, D and F). Thirty millimolars BisTris buffer (pH 6.5) were used and spectra were normalized to 280 nm and 750 nm. For *Cj*TsdA M255G and *Cj*TsdA C138G, a high-spin feature appears at 622 nm in the oxidized state. The oxidized spectrum of TsdA wt and all variants except of M255G exhibits a 700 nm peak indicating methionine as haem iron ligand. Protein concentration: 8 μM.

ods). Before describing specific results, some justification of the choice of assays and methods of data analysis are warranted.

In vivo, one or more of a set of four monohaems cytochrome *c*'s probably serve as the periplasmic electron carrier mediating electron flow between the cytochrome bc_1 complex and the periplasmic TsdA enzyme [2]. This is substantiated by the finding that neither the dihaem cytochrome *c* TsdB, which functions as natural electron acceptor for TsdA in a number of other organisms

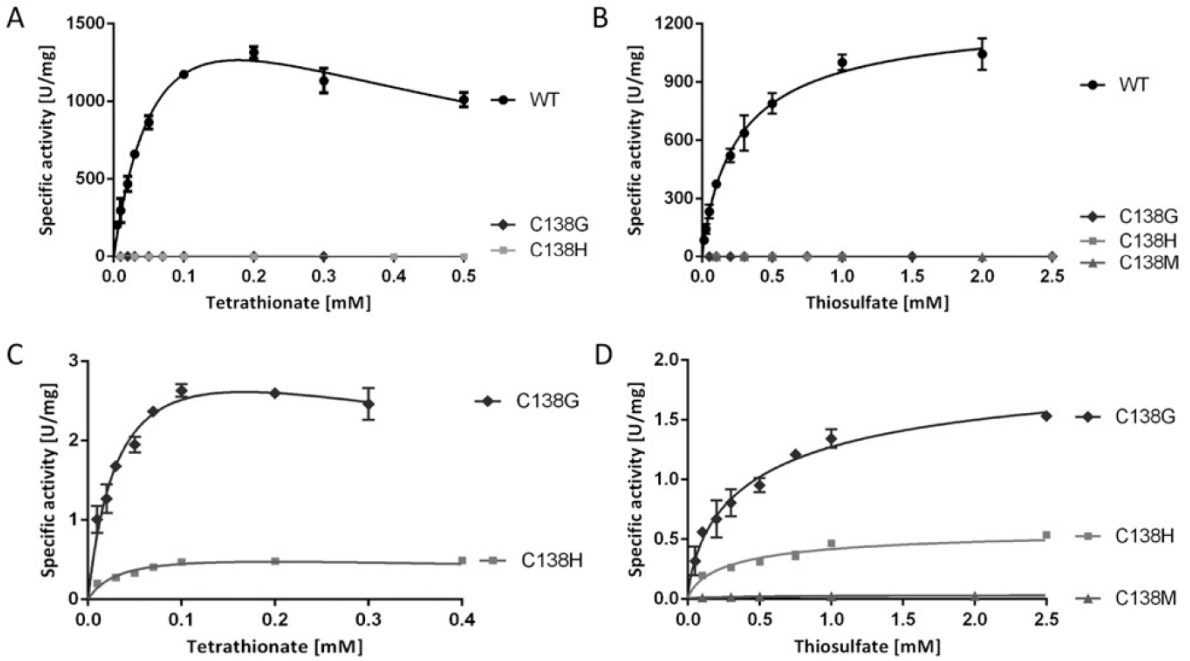

Figure 3 **Enzyme activity assays with TsdA wt and Haem 1 ligation affected variants**

TsdA wt was compared with TsdA C138G, C138H and C138M concerning tetrathionate reduction (**A**) and thiosulfate oxidation (**B**). Tetrathionate reduction (**C**) and thiosulfate oxidation (**D**) of the TsdA C^{138} variants are shown in detail in the panels below. Tetrathionate reduction (A and C) was measured under anoxic conditions at 42 °C in 100 mM ammonium acetate buffer (pH 5) with 0.3 mM methyl viologen previously reduced with titanium (III) citrate. Control measurements showed that methyl viologen was provided at a saturating concentration in all cases. Tetrathionate reduction activity of TsdA C138M was so low that exact kinetic parameters could not be derived with confidence. Different tetrathionate concentrations (0.01–0.7 mM) were used. Thiosulfate oxidation (B and D) was measured at 42 °C in 50 mM BisTris buffer (pH 6.5) with 80 μM horse heart cytochrome *c* as electron acceptor and 0.05–8 mM thiosulfate. Control measurements showed that horse heart cytochrome c was provided at a saturating concentration in all cases.

[15,30] nor the endogenous *Campylobacter* dihaem cytochrome *c* C8j_0040 (Cj0037 or CccC in the reference strain NCTC 11168 [17] is reduced by *Cj*TsdA *in vitro* [2]. As a consequence, all measurements of thiosulfate dehydrogenase activity reported in the present study were performed at pH 6.5 in the presence of 80 μM horse heart cytochrome *c*. In the direction of thiosulfate oxidation, data sets need to be fitted to the Hill equation [27]. Conventional Michaelis–Menten kinetics does not apply because the enzyme catalyses the reaction of two molecules of the same substrate (here thiosulfate). The Hill equation does not yield K_m but a substrate concentration $[S]_{0.5}$ can be reported that yields half maximal velocity and is characteristic of the process. The wt enzyme yielded a V_{max} of 1265 ± 70 U · mg^{-1} and $[S]_{0.5}$ of 280 ± 45 μM.

The assay for tetrathionate reduction used reduced methyl viologen as electron donor. This enzyme activity is inhibited by tetrathionate as a substrate when its concentration is increased (Figure 3). Therefore, data sets have to be fitted to the general equation for substrate inhibition [25], yielding K_i. Kinetic constants other than K_i can also be derived and are tabulated in Table 3. However, in this case V_{max} represents the maximum enzyme velocity and K_m represents the Michaelis–Menten constant only if the substrate did not inhibit enzyme activity. As such, the calculated V_{max} does not yield very useful information for the comparison of different enzyme variants. To circumvent this problem, the highest specific activities actually measured *in vitro* ($V_{max\ measured}$) for *Cj*TsdA and its derivatives are also given in Table 3. The wt enzyme yielded a $V_{max\ measured}$ of 1316 ± 38 U · mg^{-1}. Half maximal apparent reaction velocity was reached at 30 μM tetrathionate, whereas the calculated K_m (disregarding substrate inhibition) was 74 ± 14 μM.

In view of the above considerations, values for the specificity constant K_{cat}/K_m cannot be derived for *Cj*TsdA in a meaningful way for either of the two reaction directions. Furthermore, general use of K_{cat}/K_m as a comparative index for the catalytic effectiveness of enzyme variants has been seriously questioned [31].

Identification of Haem 1 as the active site of *Cj*TsdA

In addition to glycine, the Haem 1 iron-ligating Cys^{138} of *Cj*TsdA was replaced by histidine and methionine (Figure 1). Electronic absorption spectra strongly indicated that histidine and methion-

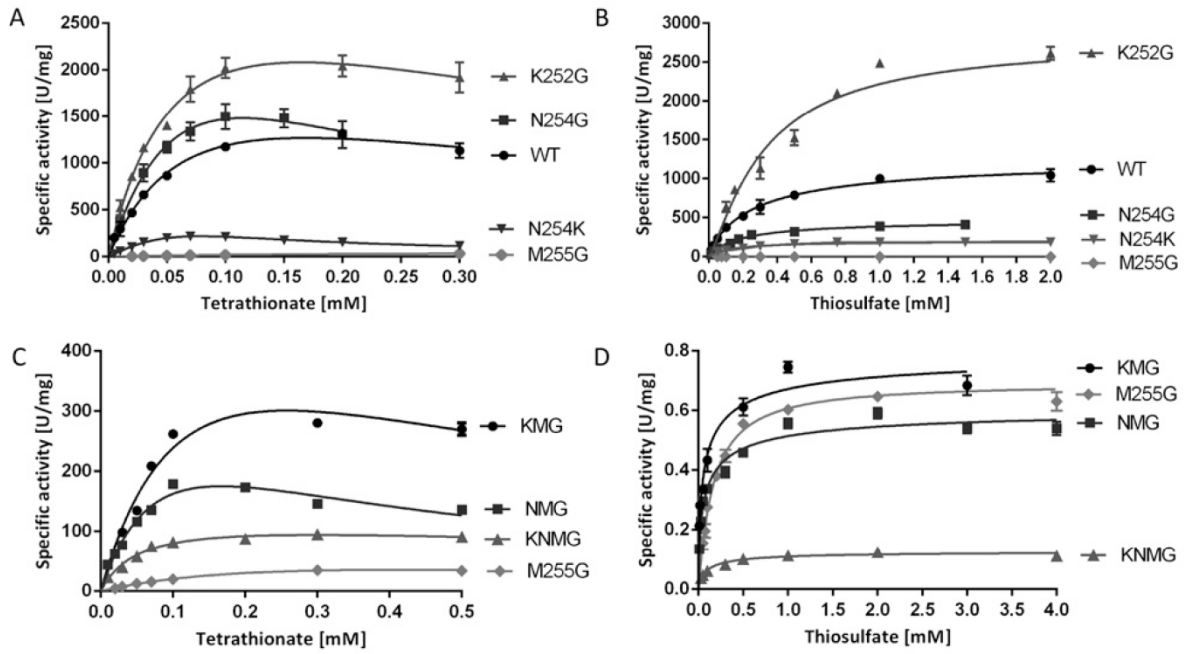

Figure 4 **Enzyme activity assays with TsdA wt and Haem 2 ligation affected variants**
Tetrathionate reduction (**A** and **C**) was measured under anoxic conditions at 42 °C in 100 mM ammonium acetate buffer (pH 5) with 0.3 mM methyl viologen previously reduced with titanium (III) citrate. Different tetrathionate concentrations (0.01–0.7 mM) were used. Thiosulfate oxidation (**B** and **D**) was measured at 42 °C in 50 mM BisTris buffer (pH 6.5) with 80 μM horse heart cytochrome c as electron acceptor and 0.05–8 mM thiosulfate.

ine acted as haem ligands in the *Cj*TsdA C138H and *Cj*TsdA C138M variants respectively. The Soret peaks increased in intensity in the oxidized as well as in the reduced state (Figures 2A and 2B) consistent with replacement of Cys^{138} with the stronger field ligands histidine or methionine [32] and in contrast with the C138G variant a high-spin haem feature was not observed. Exchange of Cys^{138} by glycine, histidine or methionine led to drastic decrease in enzyme activity in all three cases. Tetrathionate reduction and thiosulfate oxidation were equally affected (Figure 3, Tables 3 and 4).

Effect of Haem 2 environment on catalytic properties

As Met^{255} was clearly identified as an important distal ligand of Haem 2 iron, this residue was changed to glycine. Furthermore, Asn^{254} and Lys^{252} were also replaced by glycine (Figure 1). These amino acids are in close vicinity to Haem 2 iron and have theoretical competence for temporary haem ligation. Exchange of Met^{255} had a dramatic effect on catalysis, with V_{max} in the thiosulfate-oxidizing direction reduced by a factor of 1900 as compared with the wild-type protein (Figure 4, Table 4). Thiosulfate oxidation was much more impaired than tetrathionate reduction (Tables 3 and 4, Figure 1). The *Cj*TsdA K252G variant exhibited a higher V_{max} than the wild-type enzyme in both catalytic directions with a significantly stronger improvement in the oxidative direction. In contrast, the *Cj*TsdA N254G variant exhibited virtually unaltered catalytic parameters in the tetrathionate-reducing direction, but a much lower activity in the oxidative direction than the wild-type enzyme (Tables 3 and 4). Thus, the N254G variant appears more adapted to catalysing the reductive direction.

In an attempt to create a haem environment in *Cj*TsdA that resembles the situation in *Av*TsdA, Asn^{254} was replaced by lysine. This variant exhibited especially pronounced substrate inhibition by tetrathionate with a K_i of 0.02 mM as compared with 0.42 mM for the wild-type enzyme (Table 3, Figure 4). As a consequence, the calculated V_{max} exceeded the highest measurable specific activity by a factor of ten. $V_{max\ measured}$ for this variant was 6-fold lower than that for *Cj*TsdA wt. Catalysis in the thiosulfate-oxidizing direction was affected in a comparable manner.

When Asn^{254} or Lys^{252} or both residues were changed in addition to Met^{255}, resulting in the *Cj*TsdA KNG, NMG or KNMG derivatives, highest measured V_{max} increased in the tetrathionate-reducing direction in all three cases when compared with the M255G variant (Table 3, Figure 4C). In contrast, in the thiosulfate-oxidizing direction the activity of the variants carrying double and triple replacements was impaired in a similar manner as observed for the M255G single mutant (Table 4, Figure 4D). This indicates that a lack of Asn^{254} and/or Lys^{252} has a positive

effect on tetrathionate reduction. The triple mutant exhibited the lowest specific activity.

Taken together, the above results indicate that the Haem 2 environment has an impact on the catalytic directionality of *Cj*TsdA. Recently, a catalytic bias towards tetrathionate reduction was demonstrated for *Cj*TsdA by protein film voltammetry in solutions containing equal concentrations of thiosulfate and tetrathionate [1]. In these experiments, the enzyme was adsorbed in an electrocatalytically active form on graphite electrodes such that the electrode serves both an electron-accepting and an electron-donating function depending on the potential. Thus, the same reaction is assayed in the forward and the reverse direction and any differences in rate that may be introduced by using different redox dyes for the two different directions are eliminated. As a consequence, we compared protein film voltammetry of *Cj*TsdA WT with that of the two most active variants with an altered Haem 2 environment, TsdA N254G and K252G, to provide an independent measure of the relative catalytic directionality of these proteins. Cyclic voltammetry was performed in solutions containing tetrathionate and thiosulfate at equal concentration for values between 0.025 mM and 0.15 mM (Figure 5). In each case, the negative catalytic currents (i_{cat}^{red}) that quantify tetrathionate reduction reached greater magnitudes than the positive catalytic currents (i_{cat}^{ox}) that quantify thiosulfate oxidation. To assess catalytic bias, values for i_{cat}^{red} and i_{cat}^{ox} were measured at 0.1 and 0.3 V compared with SHE respectively, where there is equal thermodynamic driving force (0.1 V) for each reaction. For a given substrate concentration, i_{cat}^{ox} (0.3 V)/i_{cat}^{red} (0.1 V) followed the order K252G > WT > N254G (Figure 5, *inset*), which confirms the catalytic directionality deduced from the spectrophotometric assays (Tables 3 and 4). Because the voltammetric experiments were performed in equimolar concentrations of tetrathionate and thiosulfate, the catalytic rate for each reaction is defined by factors that include not just the K_m and V_{max} values for the relevant substrate but also the impact of substrate and production inhibition on each reaction [1]. As a consequence, comparison of the magnitude of i_{cat}^{ox} (0.3 V)/i_{cat}^{red} (0.1V) with a simple counterpart deduced from the spectrophotometric analyses is not warranted.

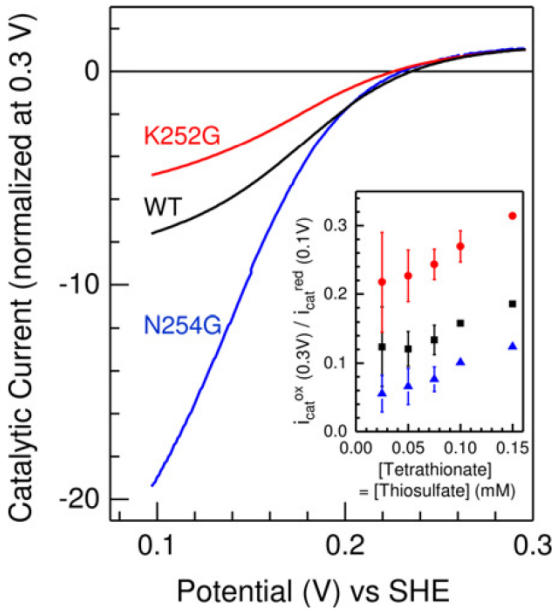

Figure 5 Baseline subtracted protein film cyclic voltammetry of *Cj*TsdA wild-type (black), N254G (blue) and K252G variant (red) in 0.05 mM tetrathionate and 0.075 mM thiosulfate

Inset: The dependence of $i_{cat}^{ox}/i_{cat}^{red}$ on substrate concentration for equimolar substrate concentrations; wild-type (black), N254G (blue) and K252G variant (red), see text for details. Values are the average of two independent measurements, errors show maximum and minimum values, except for N254G at 0.1 and 0.15 mM where single values are presented. Scan rate 10 $mV \cdot s^{-1}$, electrode rotation 500 rpm in 100 mM ammonium acetate, 50 mM NaCl, pH 5 at 42 °C.

Impact of the immediate haem environments on the *in vivo* catalytic properties of *Cj*TsdA

The *in vitro* studies on recombinant *Cj*TsdA and its variants were complemented by analysing the extent to which substitutions of the Haem 1 ligand Cys^{138} and the immediate Haem 2 environment (M255G, N254G and K252G) affect the activity of *Cj*TsdA *in vivo* (i.e with the correct natural physiological electron donor/acceptor) and whether the changes can be correlated to the observations *in vitro*. Selected *Cj*TsdA variants studied above were produced in the original host *C. jejuni* strain 81 116 in order to study the influence of alterations in *Cj*TsdA axial haem ligation on growth and tetrathionate reduction. To investigate the role of Haem 1 ligation, we employed the C138G variant. However, as our major focus was on the effect of changing the environment of Haem 2 on *in vivo* activities, we chose the M255G, N254G and K252G variants for particular attention. The previously constructed *tsdA* deletion mutant [2] was complemented by integration of either the wild-type or the *tsdA* genes encoding these variant proteins at the *cj0046* pseudogene locus, using a vector in which gene expression was driven by the strong *fdxA* (ferredoxin) promoter from *C. jejuni*. Strains with complemented *tsdA* genes produced C-terminally His-tagged *Cj*TsdA enabling Western Blot analysis, thus allowing a comparison of the amounts of wild-type and TsdA variants *in vivo*.

SDS/PAGE analysis of crude cell extracts of *C. jejuni* 81116, the Δ*tsdA* mutant and the Δ*tsdA*/**tsdA* complementation strains did not reveal a specific stained protein band correlating in size with TsdA (37103 Da; without signal peptide, with haems) (Figure 6A). Under the conditions applied, TsdA thus does not appear to be of major abundance in *C. jejuni*. Haem staining (Figure 6B) as well as Western blot analysis (Figures 6C and 6D) clearly revealed that the **tsdA* wt, **tsdA* N254G and **tsdA* K252G complementation strains produced the different TsdA variants in comparable amounts. TsdA M255G was produced in a lower amount and TsdA C138G was hardly detectable. Either these variants are inefficiently produced or are degraded in *C. jejuni*. *C. jejuni* 81116 as well as the Δ*tsdA* mutant do not produce His-tagged protein and were used as negative controls in Western Blot ana-

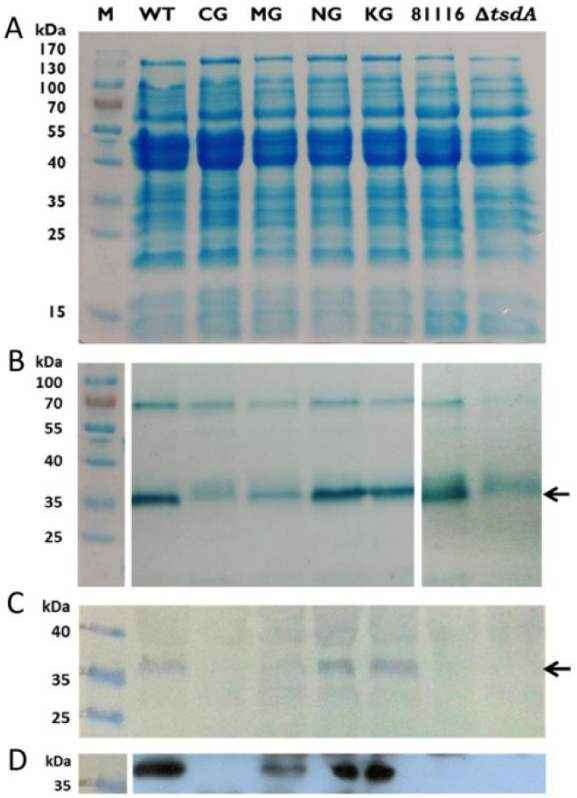

Figure 6 SDS/PAGE of crude cell extracts of *C. jejuni* 81116 wt, Δ*tsdA* mutant and complementation strains

C. jejuni cells of 81116 wt (81116), Δ*tsdA* mutant (Δ*tsdA*) and the different complementation strains (**tsdA* WT, **tsdA* C138G, **tsdA* M255G, **tsdA* N254G, **tsdA* K252G) were disrupted by bead beating and the crude cell extracts were used for SDS/PAGE. Forty micrograms of protein per lane were loaded on the gels for Coomassie staining (**A**) and Western blots (**C** and **D**), and 27 μg of protein per lane was used for haem staining (**B**). For the Western blots, antibody against His-tag was used and the second antibody was a HRP conjugate. The detection was based on the reaction of HRP with chloronaphthol (C) or the interaction between HRP and ECL reagent (D). The 37 kDa protein *Cj*TsdA is marked with an arrow. The approximately 70 kDa haem stained band in panel (B) is the MccA multi-haem sulfite reductase (see text).

lysis. The haem stained gel shows that less TsdA is formed in *C. jejuni* 81116 than in the Δ*tsdA*/**tsdA* wt complementation strain, which suggests that the *fdxA* promoter in front of *tsdA* in the complementation strains is stronger than the natural *tsdA* promoter. For the Δ*tsdA* mutant, a protein was detected after haem staining, which is slightly larger than TsdA (Figure 6B). This band is likely to be C8j_0040, the dihaem cytochrome *c* equivalent to CccC in *C. jejuni* NCTC 11168 [17]. C8j_0040 has detectable sequence homology to TsdA, but does not exhibit clear enzyme activity [2]. The uppermost visible band in the haem stained gels can be unequivocally identified as the 71 kDa protein MccA, a multi-haem sulfite reductase, which is the largest *c*-type cytochrome encoded in the strain 81116 genome [17].

Growth experiments were performed with *C. jejuni* 81116, the Δ*tsdA* mutant and the different Δ*tsdA*/**tsdA* complementation strains to analyse the impact of changes in TsdA haem ligation on the growth of *C. jejuni* with tetrathionate as electron acceptor. The cells were grown under oxygen-limited conditions at 42 °C in almost completely filled 500 ml shake flasks containing BHI-S medium plus 20 mM sodium formate and 15 mM tetrathionate. As a control experiment, *C. jejuni* 81116 and the Δ*tsdA*/**tsdA* wt complementation strain were grown with and without tetrathionate (Figure 7A). As the strains did not grow without added tetrathionate, but did grow with it, we ensured that the growth of the different *C. jejuni* strains used in this experiment is solely supported by tetrathionate as electron acceptor and not by residual oxygen in the medium. The Δ*tsdA* mutant did not grow with tetrathionate (Figure 7A) confirming that TsdA is indispensable for tetrathionate respiration in *C. jejuni*. The Δ*tsdA*/**tsdA* wt complementation strain grew faster than the wild-type strain and exhibited a 2-fold lower doubling time (Table 5) indicating again that the *fdxA* promoter in front of *tsdA* in the complementation strains is stronger than the natural *tsdA* promoter. In accordance, the Δ*tsdA*/**tsdA* wt complementation strain converted 15 mM tetrathionate much faster into 30 mM thiosulfate than the *C. jejuni* 81116 strain (Figure 7B).

As shown in Figure 6, only the **tsdA* wt, **tsdA* N254G and **tsdA* K252G complementation strains produced the respective TsdA variants in similar amounts and are thus comparable between each other. The Δ*tsdA*/**tsdA* NG and **tsdA* KG complementation strains all show growth behaviour (Figures 7C and 7E) and doubling times (Table 5) similar to the Δ*tsdA*/**tsdA* wt complementation strain. Moreover, all these strains converted 15 mM tetrathionate completely into thiosulfate (Figures 7D and 7F). Obviously, growth is not limited by this step of the respiratory chain. The Δ*tsdA*/**tsdA* MG complementation strain showed only very little growth after several hours of incubation (Figure 7C, Table 5) and only small amounts of thiosulfate were produced (Figure 7D). This strain did not produce high amounts of TsdA M255G (Figure 6). The Δ*tsdA*/**tsdA* C138G complementation strain showed a similar growth behaviour as the Δ*tsdA* mutant (Figure 7E, Table 5) and thiosulfate was not formed (Figure 7F).

In order to evaluate the rate of electron transfer to TsdA *in vivo*, the formate-dependent tetrathionate reduction rate over a short time period was determined with resting cells of *C. jejuni* 81116, the Δ*tsdA* mutant and the different Δ*tsdA*/**tsdA* complementation strains (Figure 8A). The Δ*tsdA*/**tsdA* wt, the **tsdA* K252G and the **tsdA* N254G complementation strains did not show large differences in the tetrathionate reduction rate. The *C. jejuni* 81116 strain exhibits a lower tetrathionate reduction rate than the Δ*tsdA*/**tsdA* wt complementation strain, because this strain does not produce as much TsdA as the complementation strains (Figure 8). The Δ*tsdA*/**tsdA* M255G and the **tsdA* C138G complementation strains as well as the Δ*tsdA* mutant do not reduce tetrathionate, as previously discussed.

In a last set of *in vivo* experiments, we used crude cell extracts of the same strains to measure specific enzyme activities (Figure 8B). *C. jejuni* strain 81116 showed much higher tetrathionate reduction than thiosulfate oxidation activity, demonstrating that wild-type *Cj*TsdA works best as a tetrathionate reductase

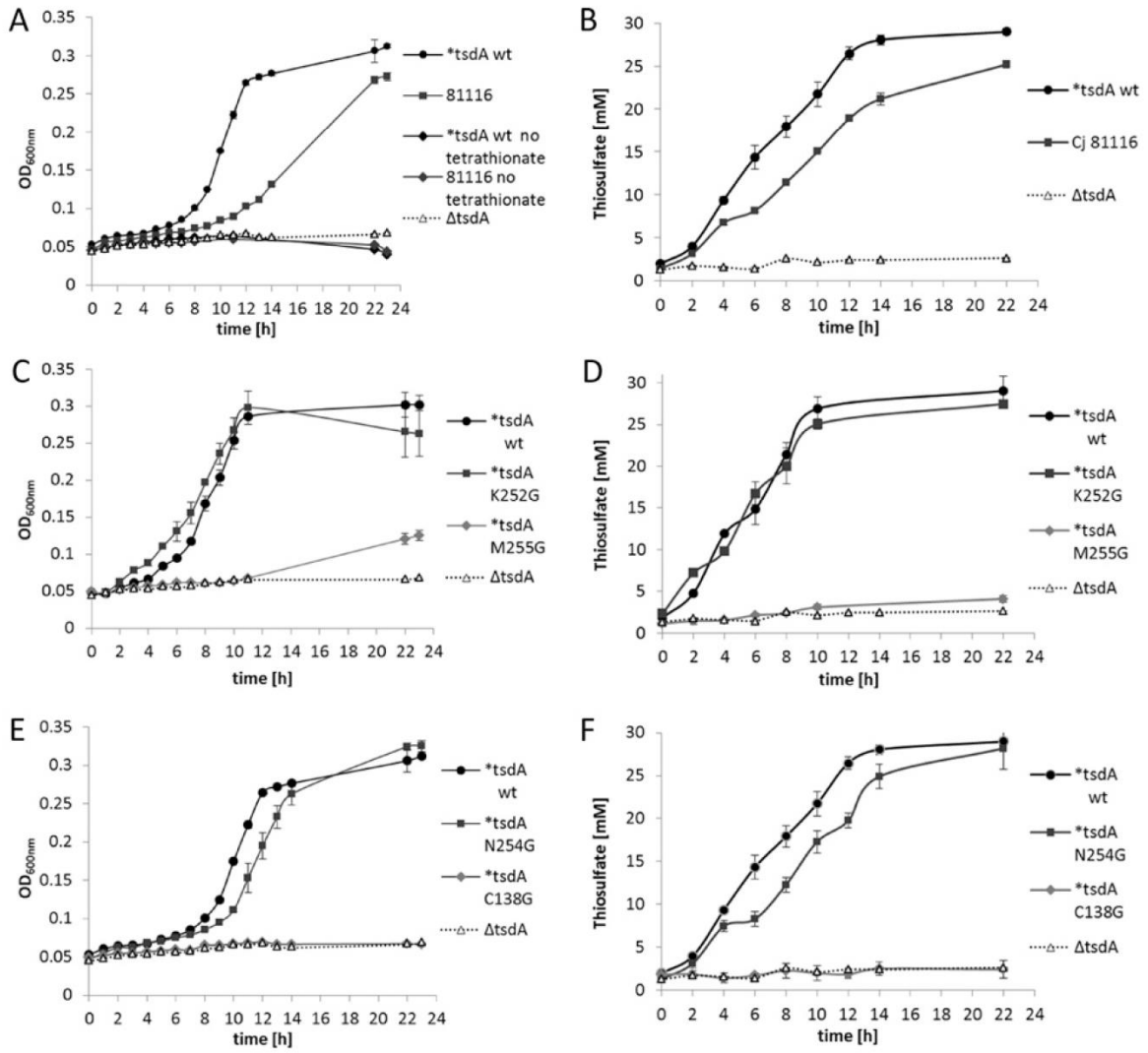

Figure 7 **Anaerobic growth of *C. jejuni* 81116 wt, Δ*tsdA* mutant and complementation strains**

C. jejuni cells of 81116 wt (81116), Δ*tsdA* mutant (Δ*tsdA*) and the different Δ*tsdA*/**tsdA* complementation strains (**tsdA* WT, **tsdA* C138G, **tsdA* M255G, **tsdA* N254G, **tsdA* K252G) were grown under oxygen-limited conditions at 42°C in almost completely filled 500 ml shake flasks containing BHI-S medium plus 20 mM sodium formate and 15 mM tetrathionate. In (**A**, **C** and **E**), the absorbance at 600 nm of the wild-type 81116 strain (closed black circles) is compared with that of an 81116 *tsdA* mutant (open triangles) and the different Δ*tsdA*/**tsdA* complementation strains. In the absence of added tetrathionate [dark grey and black diamonds in (A)], no growth of either strain occurred. In (**B**, **D** and **F**), the conversion of tetrathionate to thiosulfate in each of the culture supernatants at each time point corresponding to the growth curves in (A, C and E) is shown.

and agreeing with earlier results on the pure enzyme [2]. The activities of the Δ*tsdA*/**tsdA* wt complementation strain are higher than those of *C. jejuni* 81116 in both directions, as more TsdA is produced in this strain. The Δ*tsdA* mutant, the Δ*tsdA*/**tsdA* M255G and the **tsdA* C138G complementation strains did not show enzyme activity (Figure 8B), explaining the inability of the respective strains to reduce or to grow on tetrathionate. The N254G and K252G complementation strains showed tetrathionate reductase activity of same order of magnitude as for WT (consistent with expression levels and growth phenotypes).

DISCUSSION

In the present study, we assessed how the nature of the haem environments alters the catalytic properties of the dihaem cytochrome

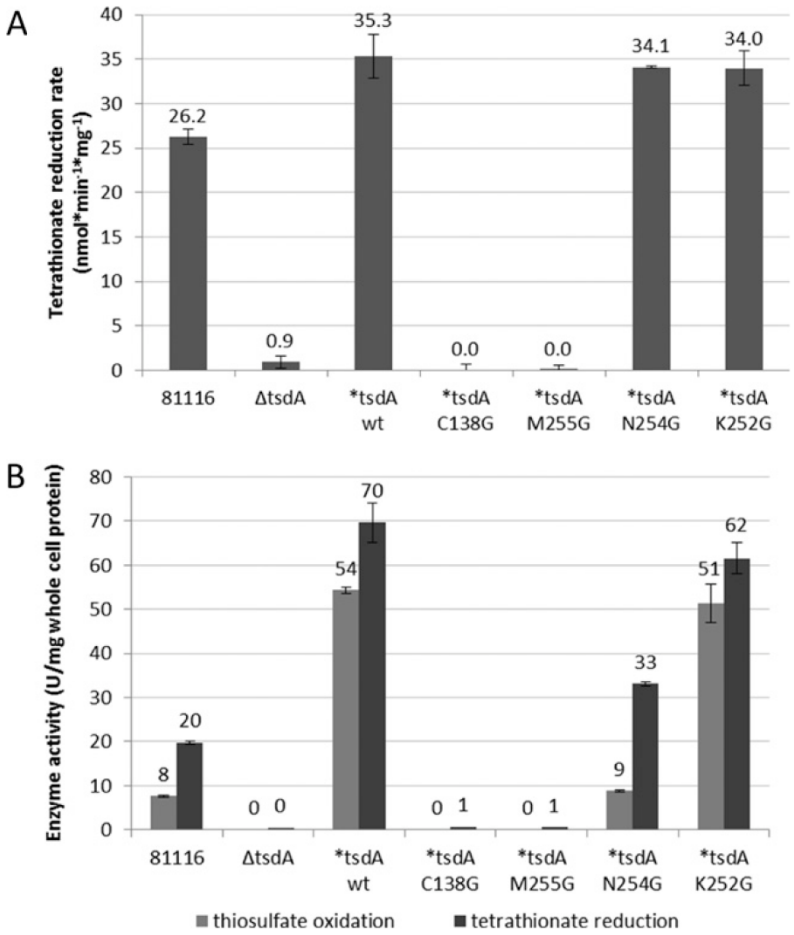

Figure 8 **Determination of tetrathionate reduction rate with whole cells and enzyme activity assays with crude cell extract**

For determination of tetrathionate reduction rate with whole cells (**A**) *C. jejuni* cells of 81116 wt (81116), Δ*tsdA* mutant (Δ*tsdA*) and the different complementation strains (**tsdA* WT, **tsdA* C138G, **tsdA* M255G, **tsdA* N254G, **tsdA* K252G) were incubated at 42°C in 14 ml phosphate buffer (pH 7.4) containing 20 mM sodium formate and 2 mM tetrathionate. The thiosulfate concentrations in the supernatants of samples taken at 2 or 5 min intervals were determined directly after the experiment. For enzyme activity assays with crude cell extract (**B**) *C. jejuni* cells of 81116 wt (81116), Δ*tsdA* mutant (Δ*tsdA*) and the different complementation strains (**tsdA* WT, **tsdA* C138G, **tsdA* M255G, **tsdA* N254G, **tsdA* K252G) were disrupted by bead beating. Tetrathionate reduction was measured anaerobically at 42°C in 100 mM ammonium acetate buffer (pH 5) with 0.3 mM methyl viologen previously reduced with titanium (III) citrate and 0.1 mM tetrathionate. Thiosulfate oxidation was performed at 42°C in 50 mM BisTris buffer (pH 6.5) with 80 μM horse heart cytochrome *c* as electron acceptor and 2 mM thiosulfate.

c tetrathionate reductase/thiosulfate dehydrogenase TsdA *in vivo* and *in vitro* and chose the enzyme from *C. jejuni* as an example. First, we demonstrated without ambiguity that Haem 1 in *Cj*TsdA is axially ligated by a cysteine (Figure 1). Haem 1 constitutes the active site of *Cj*TsdA, as enzyme activity is almost completely abolished in both directions when the Haem 1 ligating Cys^{138} is replaced. Only very recently it has been unambiguously demonstrated that catalysis of thiosulfate oxidation by TsdA and very probably also that by the other *c*-type cytochrome catalysing an oxidative reaction affecting thiosulfate, namely SoxXA, involves formation of a covalent adduct between the sulfane sulfur atom of thiosulfate and the S_γ of the active site cysteine [30]. The finding that the *Cj*TsdA C138G, C138M and C138H variants still exhibit some residual activity shows that the covalent reaction intermediate is not absolutely required for catalysis. In *Cj*TsdA, a change of Cys^{138} to iron-ligation competent histidine or methionine impaired catalysis much more than a replacement by glycine (Figure 1, Table 1), which cannot ligate the haem iron and yields a significant enzyme population containing five-coordinated high-spin haem or high-spin haem with water as a sixth ligand (Figure 2A). This shows that the temporary presence of five-coordinated high-spin haem, which cannot be generated in

the C138H and C138M variants, is an important though not absolutely essential prerequisite for the reaction to proceed. Thus, the concept is strengthened that movement of the Haem 1 ligating cysteine out of the haem iron co-ordination sphere and covalent attachment of thiosulfate to the cysteine's S_γ in this state is a central part of the TsdA reaction cycle [16,33]. The finding that a cysteine S-thiosulfonate intermediate is formed during thiosulfate oxidation catalysed by TsdA in combination with the reaction mechanism proposed by Grabarczyk et al. [34] for *Av*TsdA catalysis led to the conclusion that in case of thiosulfate oxidation formation of the cysteine S-thiosulfonate releases two electrons that reduce the iron atoms of the two haems in TsdA to the Fe(II) state. After haem reoxidation by an external electron acceptor a thiol–disulfide exchange reaction is likely to proceed via an attack of the sulfane atom of a second thiosulfate molecule on the thiosulfonate group. In the tetrathionate-reducing direction, the central sulfur–sulfur bond of the tetrathionate molecule first would be cleaved by attack of the active site cysteine's S_γ atom thus releasing the first thiosulfate molecule and creating the cysteine S-thiosulfonate. From this intermediate, the second thiosulfate would be reductively released with two electrons delivered by an external electron donor via the two TsdA haem groups.

TsdA Haem 2 acts as an electron relay centre and wires the active site to the enzyme's redox partner [16]. An important difference between the tetrathionate-reduction adapted *Cj*TsdA and the thiosulfate-oxidizing enzyme from *A. vinosum*, is indeed apparent at this haem. At *Av*TsdA Haem 2, a ligand change occurs from lysine to methionine upon reduction [16]. In contrast, we found for *Cj*TsdA that the equivalent methionine residue is ligating Haem 2 iron in the oxidized state. The replacement of Met^{255} by glycine led to a strong impairment in both catalytic directions, however the effect on tetrathionate formation was much more severe. The simple attempt to create a haem environment in *Cj*TsdA resembling the situation in *Av*TsdA by exchanging Asn^{254} for lysine did not have the expected effect. As evidenced by UV–Vis spectroscopy, the exchange did not lead to a replacement of Met^{255} as the haem iron ligand by the newly introduced lysine in the oxidized state (Figure 2E). Furthermore, the replacement negatively affected V_{max} in both the tetrathionate-forming and the tetrathionate-reducing direction and did not cause adaptation of TsdA to catalysing thiosulfate oxidation as seen for *Av*TsdA.

Unexpectedly, the largest changes in *Cj*TsdA reaction directionality and catalytic efficiency were observed upon replacing Asn^{254} by glycine instead of lysine and exchanging Lys^{252} to glycine (Figures 1 and 5) demonstrating the importance of those amino acid residues for functionality of the enzyme. The K252G exchange improved *Cj*TsdA, resulting in higher V_{max} in both catalytic directions. However, the reaction directionality of this variant also appeared to shift towards thiosulfate oxidation in solution assays and this was substantiated by protein film electrochemistry. In contrast, the *Cj*TsdA N254G variant exhibited lower specific activity in the oxidative direction than the wild-type enzyme and proved more adapted to catalysing the tetrathionate-reducing direction in electrochemical experiments. These differences might be explicable by altered redox potentials of Haem 2, but more subtle changes in intramolecular electron transfer or reorganization energy might also apply [35,36].

A surprising level of complexity became apparent through the finding that replacement of Asn^{254} by glycine or lysine leads to a much stronger substrate inhibition by tetrathionate than observed for wild-type *Cj*TsdA. This demonstrates that alterations at Haem 2 have an effect on the active site haem and its catalytic properties, indicating interaction between the two haem groups of TsdA. This is corroborated by the finding that the K_m and $S_{0.5}$ values vary between the *Cj*TsdA derivatives with altered Haem 2 ligands (Tables 3 and 4). The same has been observed for *Av*TsdA [16].

Adaptation of a given TsdA to catalyse one or the other reaction direction, i.e. tetrathionate reduction or thiosulfate oxidation should have implications on its function in metabolic networks *in vivo*, i.e. how effectively tetrathionate reduction can be used as an alternative respiratory process. In the present study, we assessed this question by complementing a *C. jejuni* 81116 mutant strain devoid of the *tsdA* gene with TsdA variants exhibiting different specific activity and catalytic adaptation. The C138G variant lacking the active site cysteine was produced in very small amounts (Figure 6) and its specific activity was very low. It was therefore not surprising that this complementation strain was unable to grow with tetrathionate as electron acceptor. The same holds true for the M255G variant, which did not support significant growth with tetrathionate as respiratory electron acceptor. The catalytic properties of TsdA measured in crude cell extracts of the Δ*tsdA/*tsdA* wt complementation strain appear similar to those of pure recombinant TsdA wt (Tables 3 and 4, Figure 8B). Crude extracts of the Δ*tsdA/*tsdA* K252G complementation strain showed activities very similar to the Δ*tsdA/*tsdA* wt complementation strain. For the Δ*tsdA/*tsdA* N254G complementation strain, enzyme activities per mg cell protein were not as high as for the Δ*tsdA/*tsdA* wt complementation strain, but activity in the thiosulfate oxidizing direction was much more negatively affected than tetrathionate reduction. Growth characteristics for the strains complemented with the wild-type enzyme and the *Cj*TsdA N254G and K252G variants did not differ significantly. This was surprising for the *tsdA K252G complementation strain because the TsdA K252G variant clearly exhibited higher specific activity than the wild-type enzyme *in vitro* and was present in similar amounts (Figure 6). We conclude that tetrathionate reduction by TsdA is not the limiting step in the respiratory chain of *C. jejuni* under the conditions applied.

In conclusion, we identified the haem iron ligands of *Cj*TsdA and showed that Haem 2 iron ligation is different to that observed for *Av*TsdA in the oxidized state. The Haem 1 axial ligand cysteine and the Haem 2 iron-ligating methionine are indispensable for efficient enzyme function *in vitro* and *in vivo*. Structural differences in the immediate environment of Haem 2 were shown to contribute to defining the reaction directionality. Ongoing studies in our laboratories aim to gain further understanding of the factors that define the catalytic bias of TsdA enzymes.

AUTHOR CONTRIBUTION

Julia Kurth performed all experiments. Julia Kurth, Christiane Dahl, Julea Butt and David Kelly designed and analysed experiments. Christiane Dahl conceived and co-ordinated the study. David Kelly supervised and co-ordinated the *in vivo* experiments shown in Figures 6 and 7 and Table 5. Julea Butt supervised and co-ordinated the electrochemical experiments shown in Figure 5. Julia Kurth and Christiane Dahl wrote the paper. All authors reviewed the results and approved the final version of the manuscript.

ACKNOWLEDGEMENTS

We thank Yang-Wei Liu for construction of the pC46-fdxA-0815HIS vector and Nitanshu Garg and Michael White for assistance with the experiments performed in Sheffield. This article is dedicated to Christiane Dahl's esteemed academic teacher Hans G. Trüper who passed away on March 9, 2016.

FUNDING

This work was supported by the Deutsche Forschungsgemeinschaft [grant number DA 351/7-2]; the Aventis Foundation and Stiftung Stipendien-Fonds des Verbandes der Chemischen Industrie [grant number 700051 (to J.M.K.)]; and the UK Biotechnology and Biological Sciences Research Council [grant numbers BB/L022176/1 and BB/K009885/1].

REFERENCES

1 Kurth, J., Dahl, C. and Butt, J.N. (2015) Catalytic protein film electrochemistry provides a direct measure of the tetrathionate/thiosulfate reduction potential. J. Am. Chem. Soc. **137**, 13232–13235 CrossRef
2 Liu, Y.W., Denkmann, K., Kosciow, K., Dahl, C. and Kelly, D.J. (2013) Tetrathionate stimulated growth of *Campylobacter jejuni* identifies TsdA as a new type of bi-functional tetrathionate reductase that is widely distributed in bacteria. Mol. Microbiol. **88**, 173–188 CrossRef
3 Thauer, R.K., Jungermann, K. and Decker, K. (1977) Energy conservation in chemotrophic anaerobic bacteria. Bacteriol. Rev. **41**, 100–180
4 Winter, S.E., Thiennimitr, P., Winter, M.G., Butler, B.P., Huseby, D.L., Crawford, R.W., Russell, J.M., Bevins, C.L., Adams, L.G., Tsolis, R.M. et al. (2010) Gut inflammation provides a respiratory electron acceptor for *Salmonella*. Nature **467**, 426–429 CrossRef
5 Oltman, L.F., Claasen, V.P., Kastelein, P., Reijinders, W.N.M. and Stouthammer, A.H. (1979) The influence of tungstate on the formation and activities of four reductases of *Proteus mirabilis*: identification of two new molybdoenzymes, chlorate reductase and tetrathionate reductase. FEBS Lett. **106**, 43–46 CrossRef
6 Havelaar, A.H., Ivarsson, S., Lofdahl, M. and Nauta, M.J. (2013) Estimating the true incidence of campylobacteriosis and salmonellosis in the European Union, 2009. Epidemiol. Infect. **141**, 293–302 CrossRef
7 Blaser, M.J. and Engberg, J. (2008) Clinical aspects of *Campylobacter jejuni* and *Campylobacter coli* infections. *Campylobacter* (Nachamkin, I., Szymanski, G. and Blaser, M.J., eds), pp. 99–121, ASM Press, Washington, DC
8 Jacobs, B.C., van Belkum, A. and Endtz, H.P. (2008) Gullain-Barré syndrome and *Campylobacter* infection. *Campylobacter* (Nachamkin, I., Szymanski, G. and Blaser, M.J., eds), pp. 245–261, ASM Press, Washington, DC
9 Sellars, M.J., Hall, S.J. and Kelly, D.J. (2002) Growth of *Campylobacter jejuni* supported by respiration of fumarate, nitrate, nitrite, trimethylamine-N-oxide, or dimethyl sulfoxide requires oxygen. J. Bacteriol. **184**, 4187–4196 CrossRef
10 Weingarten, R.A., Taveirne, M.E. and Olson, J.W. (2009) The dual functioning fumarate reductase is the sole succinate:quinone reductase in *Campylobacter jejuni* and is required for full host colonization. J. Bacteriol. **191**, 5293–5300 CrossRef
11 Pittman, M.S., Elvers, K.T., Lee, L., Jones, M.A., Poole, R.K., Park, S.F. and Kelly, D.J. (2007) Growth of *Campylobacter jejuni* on nitrate and nitrite: electron transport to NapA and NrfA via NrfH and distinct roles for NrfA and the globin Cgb in protection against nitrosative stress. Mol. Microbiol. **63**, 575–590 CrossRef
12 Hinojosa-Leon, M., Dubourdieu, M., Sanchez-Crispin, J.A. and Chippaux, M. (1986) Tetrathionate reductase from *Salmonella typhimurium*: a molybdenum containing enzyme. Biochem. Biophys. Res. Commun. **136**, 577–581 CrossRef
13 Hensel, M., Hinsley, A.P., Nikolaus, T., Sawers, G. and Berks, B.C. (1999) The genetic basis of tetrathionate respiration in *Salmonella typhimurium*. Mol. Microbiol. **32**, 275–287 CrossRef
14 Mowat, C.G., Rothery, E., Miles, C.S., McIver, L., Doherty, M.K., Drewette, K., Taylor, P., Walkinshaw, M.D., Chapman, S.K. and Reid, G.A. (2004) Octaheme tetrathionate reductase is a respiratory enzyme with novel heme ligation. Nat. Struct. Mol. Biol. **11**, 1023–1024 CrossRef
15 Denkmann, K., Grein, F., Zigann, R., Siemen, A., Bergmann, J., van Helmont, S., Nicolai, A., Pereira, I.A.C. and Dahl, C. (2012) Thiosulfate dehydrogenase: a wide-spread unusual acidophilic c-type cytochrome. Environ. Microbiol. **14**, 2673–2688 CrossRef
16 Brito, J.A., Denkmann, K., Pereira, I.A.C., Archer, M. and Dahl, C. (2015) Thiosulfate dehydrogenase (TsdA) from *Allochromatium vinosum*: structural and functional insights into thiosulfate oxidation. J. Biol. Chem. **290**, 9222–9238 CrossRef
17 Liu, Y.W. and Kelly, D.J. (2015) Cytochrome *c* biogenesis in *Campylobacter jejuni* requires cytochrome *c*6 (CccA; Cj1153) to maintain apocytochrome cysteine thiols in a reduced state for haem attachment. Mol. Microbiol. **96**, 1298–1317 CrossRef
18 Dahl, C., Schulte, A., Stockdreher, Y., Hong, C., Grimm, F., Sander, J., Kim, R., Kim, S.H. and Shin, D.H. (2008) Structural and molecular genetic insight into a wide-spread bacterial sulfur oxidation pathway. J. Mol. Biol. **384**, 1287–1300 CrossRef
19 Horton, R.M. (1995) PCR mediated recombination and mutagenesis: SOEing together tailor-made genes. Mol. Biotechnol. **3**, 93–99 CrossRef
20 Arslan, E., Schulz, H., Zufferey, R., Kunzler, P. and Thöny-Meyer, L. (1998) Overproduction of *Bradyrhizobium japonicum* c-type cytochrome subunits of the cbb_3 oxidase in *Escherichia coli*. Biochem. Biophys. Res. Commun. **251**, 744–747 CrossRef
21 Thomas, P.E., Ryan, D. and Levin, W. (1976) Improved staining procedure for detection of peroxidase-activity of cytochrome P-450 on sodium dodecyl-sulfate polyacrylamide gels. Anal. Biochem. **75**, 168–176 CrossRef
22 Berry, E.A. and Trumpower, B.L. (1987) Simultaneous determination of hemes a, b, and c from pyridine hemochrome spectra. Anal. Biochem. **161**, 1–15 CrossRef
23 Urban, P.J. (1961) Colorimetry of sulfur anions. I. An improved colorimetric method for the determination of thiosulfate. Z. Analyt. Chem. **179**, 415–422 CrossRef
24 Zehnder, A.J.B. and Wuhrmann, K. (1976) Titanium(III) citrate as a nontoxic oxidation-reduction buffering system for culture of obligate anaerobes. Science **194**, 1165–1166 CrossRef
25 Cleland, W.W. (1979) Substrate inhibition. Methods Enzymol. **63**, 500–513 CrossRef

26 van Gelder, B. and Slater, E.C. (1962) The extinction coefficient of cytochrome c. Biochim. Biophys. Acta **58**, 593–595 CrossRef

27 Segel, I.H. (1993) Enzyme Kinetics: Behaviour and Analysis of Rapid Equilibrium and Steady-State Enzyme Systems, Wiley-Interscience, New York

28 Miles, C.S., Manson, F.D.C., Reid, G.A. and Chapman, S.K. (1993) Substitution of a haem-iron axial ligand in flavocytochrome b_2. Biochim. Biophys. Acta **1202**, 82–86 CrossRef

29 Moore, G. R. and Pettigrew, G. W. (1990) Cytochromes c: Evolutionary, Structural and Physicochemical Aspects, Springer-Verlag, Heidelberg

30 Kurth, J.M., Brito, J.A., Reuter, J., Flegler, A., Koch, T., Franke, T., Klein, E.M., Rowe, S.F., Butt, J.N. and Denkmann, K. (2016) Electron accepting units of the diheme cytochrome *c* TsdA, a bifunctional thiosulfate dehydrogenase/tetrathionate reductase. J. Biol. Chem., in the press

31 Eisenthal, R., Danson, M.J. and Hough, D.W. (2007) Catalytic efficiency and k_{cat}/K_M: a useful comparator? Trends Biotechnol. **25**, 247–249 CrossRef

32 Girvan, H.M., Seward, H.E., Toogood, H.S., Cheesman, M.R., Leys, D. and Munro, A.W. (2007) Structural and spectroscopic characterization of P450 BM3 mutants with unprecedented P450 heme iron ligand sets. New heme ligation states influence conformational equilibria in P450 BM3. J. Biol. Chem. **282**, 564–572 CrossRef

33 Bradley, J.M., Marritt, S.J., Kihlken, M.A., Haynes, K., Hemmings, A.M., Berks, B.C., Cheesman, M.R. and Butt, J.N. (2012) Redox and chemical activities of the hemes in the sulfur oxidation pathway enzyme SoxAX. J. Biol. Chem. **287**, 40350–40359 CrossRef

34 Grabarczyk, D.B., Chappell, P.E., Eisel, B., Johnson, S., Lea, S.M. and Berks, B.C. (2015) Mechanism of thiosulfate oxidation in the SoxA family of cysteine-ligated cytochromes. J. Biol. Chem. **290**, 9209–9221 CrossRef

35 Abou Hamdan, A., Dementin, S., Liebgott, P.P., Gutierrez-Sanz, O., Richaud, P., De Lacey, A.L., Rousset, M., Bertrand, P., Cournac, L. and Léger, C. (2012) Understanding and tuning the catalytic bias of hydrogenase. J. Am. Chem. Soc. **134**, 8368–8371 CrossRef

36 Hexter, S.V., Esterle, T.F. and Armstrong, F.A. (2014) A unified model for surface electrocatalysis based on observations with enzymes. Phys. Chem. Chem. Phys. **16**, 11822–11833 CrossRef

37 Hanahan, D. (1983) Studies on transformation of *Escherichia coli* with plasmids. J. Mol. Biol. **166**, 557–580 CrossRef

38 Newell, D.G., McBride, H. and Pearson, A.D. (1984) The identification of outer membrane proteins and flagella of *Campylobacter jejuni*. J. Gen. Microbiol. **130**, 1201–1208

39 Reuter, M. and van Vliet, A.H. (2013) Signal balancing by the CetABC and CetZ chemoreceptors controls energy taxis in *Campylobacter jejuni*. PLoS One **8**, e54390 CrossRef

Received 13 October 2016/25 October 2016; accepted 26 October 2016

Accepted Manuscript online 27 October 2016, doi 10.1042/BSR20160457

SUPPLEMENTARY INFORMATION

Influence of heme environment on the catalytic properties of the tetrathionate reductase TsdA from *Campylobacter jejuni*

Julia M. Kurth[‡1], Julea N. Butt[#], David J. Kelly[§2] and Christiane Dahl[‡3]

From the [‡]Institut für Mikrobiologie & Biotechnologie, Rheinische Friedrich Wilhelms Universität Bonn, D-53115 Bonn, Germany, [§]Department of Molecular Biology and Biotechnology, The University of Sheffield, Firth Court, Western Bank, Sheffield S10 2TN, UK, [#]Centre for Molecular and Structural Biochemistry, School of Chemistry, and School of Biological Sciences, University of East Anglia, Norwich Research Park, Norwich NR4 7TJ, United Kingdom

* Authors for corresdondence: [2]David J. Kelly: E-mail d.kelly@sheffield.ac.uk. Phone +44-114-222-4414 or [3]Christiane Dahl: E-mail ChDahl@uni-bonn.de. Phone +49-228-732119. Fax +49-228-747576.

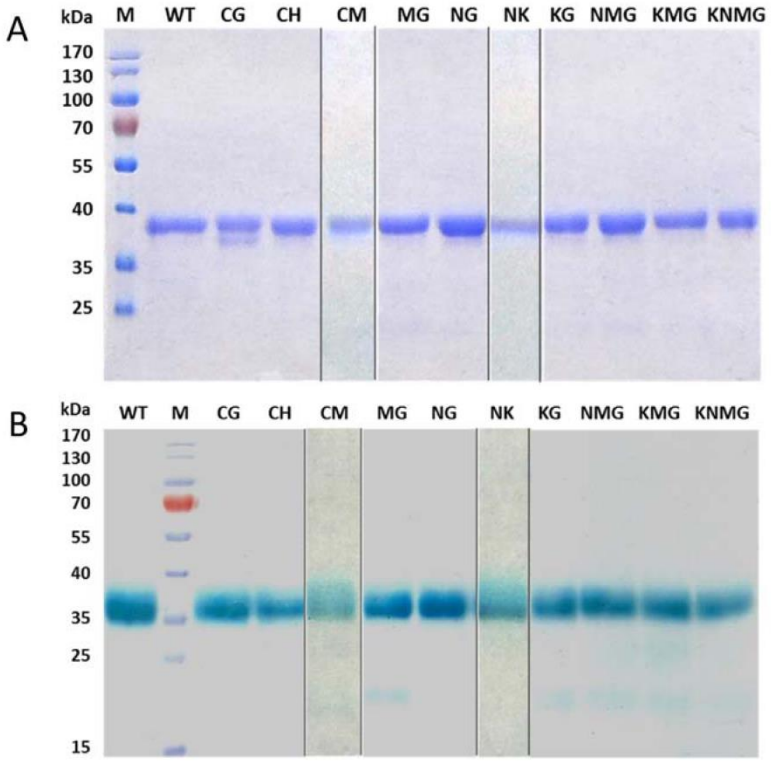

SI Fig. 1. Coomassie blue and heme staining of SDS gels with TsdA wt and variant proteins. Pure, recombinant TsdA wt and mutated proteins (C138G, C138H, C138M, M255G, N254G, N254K, K252G, NMG, KMG, KNMG) were used for SDS-PAGE and loaded on a 12.5 % gel. 5 µg protein per lane were used for Coomassie blue staining and 3 µg for heme staining.

Chapter 4

TsdC, a unique lipoprotein from *Wolinella succinogenes* that enhances tetrathionate reductase activity of TsdA

Introduction & Summary

Wolinella succinogenes belogs to the Epsilonproteobacteria and is closely related to *Camylobacter jejuni*. *C. jejuni* can use tetrathionate as additional electron acceptor. Tetrathionate reduction is catalyzed by the bifunctional diheme cytochrome *c* TsdA. *W. succinogenes* also encodes TsdA in its genome. The situation in *W. succinogenes* is unique because TsdA is closely associated with the unprecedented lipoprotein TsdC encoded immediately downstream of *tsdA* in the same direction of transcription.

TsdC does not show any significant sequence similarity to proteins from other organisms. In this work the protein was unambiguously identified as a lipoprotein: TsdC exhibits a signal peptide typical for lipoproteins and is localized in the membrane fraction of *W. succinogenes* as well as in *Escherichia coli* after recombinant production. Motifs for binding of prosthetic groups that might mediate electron transfer are not apparent in TsdC. The protein was found to form a tight complex with TsdA when purified from *W. succinogenes* as well as from *E. coli* membranes. *Ws*TsdA purified from *E. coli* showed very low specific activities in both catalytic directions. After co-production of TsdC and *Ws*TsdA in *E. coli*, TsdC was found to mediate membrane attachment of TsdA and to ensure its full catalytic activity. This effect was much stronger in the tetrathionate-reducing than in the thiosulfate-oxidizing direction. It is concluded that the TsdAC complex predominantly acts as a tetrathionate reductase *in vivo* similar as observed for TsdA from *C. jejuni*.

Chapter 4

TsdC, a unique lipoprotein from *Wolinella succinogenes* that enhances tetrathionate reductase activity of TsdA

This research was submitted to FEMS Microbiology Letters:

Kurth, J.M., Schuster, A., Seel, W., Herresthal, S., Simon, J., and Dahl, C. (2016) TsdC, a unique lipoprotein from *Wolinella succinogenes* that enhances tetrathionate reductase activity of TsdA. *FEMS Microbiol Lett* **submitted**

https://academic.oup.com/femsle/article-lookup/doi/10.1093/femsle/fnx003

Author contributions

- JMK designed, analyzed and compiled the experiments

- JMK produced and analyzed the proteins from *S. lithotrophicus*

- JMK and CD wrote the paper

TsdC, a unique lipoprotein from *Wolinella succinogenes* that enhances tetrathionate reductase activity of TsdA

Julia M. Kurth[1], Anja Schuster[1†], Waldemar Seel[1$], Stefanie Herresthal[1], Jörg Simon[2], Christiane Dahl[1]

[1] Institut für Mikrobiologie & Biotechnologie, Rheinische Friedrich-Wilhelms-Universität Bonn, Bonn, Germany

[2] Microbial Energy Conversion and Biotechnology, Fachbereich Biologie, Technische Universität Darmstadt, Darmstadt, Germany

Correspondence:

Christiane Dahl, Institut für Mikrobiologie & Biotechnologie, Rheinische Friedrich-Wilhelms-Universität
Meckenheimer Allee 168, D-53115 Bonn, Germany
Fax: +49 228 737576
Tel: +49 228 732119
E-mail: ChDahl@uni-bonn.de

Article type: Original Research Article

[†] Present affiliation: Qiagen GmbH, Qiagen Str. 1, D-40724 Hilden, Germany

[$] Present affiliation: Institut für Ernährungs- und Lebensmittelwissenschaften, Rheinische Friedrich-Wilhelms-Universität, Bonn, Germany

Keywords: tetrathionate reductase, thiosulfate dehydrogenase, *Wolinella succinogenes*, TsdA, cytochrome *c*, lipoprotein

Abstract

The diheme cytochromes *c* of the widespread TsdA family are bifunctional thiosulfate dehydrogenase/tetrathionate reductases. Here, biochemical information was collected about TsdA from the Epsilonproteobacterium *Wolinella succinogenes* (*Ws*TsdA). The situation in *W. succinogenes* is unique since TsdA is closely associated with the unprecedented lipoprotein TsdC encoded immediately downstream of *tsdA* in the same direction of transcription. *Ws*TsdA purified from *Escherichia coli* catalyzed both thiosulfate oxidation and tetrathionate reduction. After co-production of TsdC and *Ws*TsdA in *E. coli*, TsdC was found to mediate membrane attachment of TsdA and to ensure its full catalytic activity. This effect was much stronger in the tetrathionate-reducing than in the thiosulfate-oxidizing direction. It is concluded that the TsdAC complex predominantly acts as a tetrathionate reductase *in vivo*.

Introduction

The widespread diheme cytochromes *c* of the TsdA family are bifunctional thiosulfate dehydrogenase/tetrathionate reductases. The reaction directionality of these enzymes varies dependent on the source organism (Denkmann *et al.* 2012; Kurth *et al.* 2015; Liu *et al.* 2013) (see also Fig. 1). For example, TsdA from the sulfur-oxidizing anoxygenic phototrophic Gammaproteobacterium *Allochromatium vinosum* is strongly adapted to catalyzing thiosulfate oxidation with little capacity for tetrathionate reduction (Brito *et al.* 2015; Kurth *et al.* 2015). In contrast, TsdA from the Epsilonproteobacterium *Campylobacter jejuni* acts primarily as a tetrathionate reductase and enables the organism to use tetrathionate as an alternative electron acceptor for anaerobic respiration (Liu *et al.* 2013). In several thiosulfate-oxidizing organisms the *tsdA* gene is associated with a gene encoding a soluble diheme cytochrome *c*, TsdB that serves as the electron acceptor for TsdA (Denkmann *et al.* 2012; Kurth *et al.* 2016a). Regardless of association with TsdB, all TsdAs characterized to date are soluble proteins that reside in the periplasm (Brito *et al.* 2015; Denkmann *et al.* 2012; Kurth *et al.* 2016a; Kurth *et al.* 2016b; Liu *et al.* 2013).

The non-fermentative Epsilonproteobacterium *Wolinella succinogenes* (*Ws*), a close relative of the human gut pathogen *C. jejuni*, is metabolically versatile and can grow either by microaerobic or anaerobic respiration using fumarate, nitrate, nitrite, nitrous oxide, dimethyl sulfoxide, polysulfide or sulfite as sole terminal electron acceptor (Kern *et al.* 2009; Kern *et al.* 2011; Klimmek *et al.* 2004; Kröger *et al.* 2002; Schumacher *et al.* 1992; Simon 2002; Simon *et al.* 2004). The soluble and membrane-bound cytochromes *b* and *c* involved in energy conservation from these numerous substrates have been studied intensively (Hermann *et al.* 2015; Kern *et al.* 2009; Simon *et al.* 2011). The function of some cytochromes *c*, however, still remained unassigned (Kern *et al.* 2010). Among these is a 40-kDa cytochrome *c* (Ws0009) whose primary sequence is homologous to TsdA proteins and that was previously designated CytA (Kern *et al.* 2010). *Ws*TsdA was detected primarily in the membrane fraction of nitrate- and polysulfide-grown cells (Kern *et al.* 2010). The protein was solubilized and enriched from membranes of polysulfide-grown *W. succinogenes* cells and co-purified with a polypeptide of 16 kDa (Arnold 1999; Supporting Information). Sequencing of the N-terminus and internal peptides by Edman degradation confirmed the identity of TsdA. Furthermore, the 16-kDa protein was unambiguously assigned as Ws0008 (CytB) (Arnold 1999; Baar *et al.* 2003; Kern *et al.* 2010), here named TsdC, which is identified in this work as an unprecedented lipoprotein. The two proteins of the TsdAC complex are encoded by the *tsdAC* gene cluster on the *W. succinogenes* genome (Baar *et al.* 2003).

Here, we set out to collect biochemical information about *W. succinogenes* TsdA and TsdC. The proteins were produced in *Escherichia coli* and both, *Ws*TsdA and TsdC as well as the TsdAC complex were purified. It is demonstrated that the TsdAC complex acts primarily as a tetrathionate reductase and that membrane attachment is achieved by the presence of TsdC. An activity-increasing effect of TsdC on TsdA was found and compared with the effect of TsdB on TsdA activity using the TsdAB system from *Sideroxydans lithotrophicus* as a model.

Material and methods

Bacterial strains, growth conditions and recombinant DNA techniques

The bacterial strains used for this study are listed in Table S1 (Supporting Information). *Escherichia coli* BL21 (DE3) or *E. coli* C43 (DE3) were used for recombinant protein production and were grown in LB medium. *E. coli* DH5α was used for molecular cloning. All general molecular genetic techniques were described earlier (Dahl *et al.* 2008). Restriction enzymes, T4 ligase and *Pfu* DNA polymerase were obtained from Thermo Scientific (Schwerte, Germany) and used according to the manufacturer's instructions. Oligonucleotides for cloning were obtained from Eurofins MWG (Ebersberg, Germany).

Construction of expression plasmids

The plasmids and primers used in this study are listed in Table S1 (Supporting Information). Construction of expression plasmids is described in the Supplementary data file (Supporting Information).

Overproduction, purification and preparation of recombinant proteins

The mature recombinant *Ws*TsdA produced on the basis of plasmid pET-N-2strep-tsdAWs has a predicted molecular mass of 43,388.1 Da (including two heme groups). The recombinant *Ws*TsdA and *Ws*TsdC proteins produced on the basis of plasmid pET-C-2strep-WS0009+0008 have calculated molecular masses of 41,188.9 Da (including two hemes) and 19,014.1 Da, respectively. The proteins were produced in *E. coli* as described for *Cj*TsdA (Kurth *et al.* 2016b). *Ws*TsdC (16,943 Da; without signal peptide) was produced by incubating *E. coli* C43(DE3) containing pET-WS0008 in 400 ml LB medium with 100 μg ml^{-1} ampicillin in 1-L Erlenmeyer flasks. The culture was inoculated 2 % with an overnight pre-culture and shaken with 180 rpm at 30 °C. At an OD_{600nm} of 0.6, 200 ng ml^{-1} anhydrotetracycline were added and the culture was switched to 25 °C. Cells were harvested after 18 h. *S. lithotrophicus* TsdA (*Sl*TsdA), *Sl*TsdB and *Sl*TsdBA were produced as described in (Kurth *et al.* 2016a).

Cell material was resuspended in 100 mM Tris-HCl buffer pH 8 containing 150 mM NaCl and lysed by sonication. After removal of insoluble cell material by centrifugation (10,000 *g* for 25 min at 4°C) the soluble proteins *Ws*TsdA, *Sl*TsdA and *Sl*TsdA plus *Sl*TsdB were purified from the supernatants by Strep-Tactin affinity chromatography according to the manufacturer's instructions (IBA, Göttingen, Germany). When necessary, gel permeation chromatography was performed as described previously (Kurth *et al.* 2016b). Desalting and concentration of the proteins were included as final steps. *Sl*TsdA(B) was stored in 50 mM BisTris, pH 6.5 and *Ws*TsdA in 50 mM HEPES, pH 7.0 containing 50 mM NaCl at -70°C.

As TsdC is a membrane associated protein, the TsdC- and TsdAC-containing *E. coli* cell lysates were first subjected to ultracentrifugation (100,000 *g*, 60 min, 4°C) in order to separate membrane and soluble fractions. The membranes were resuspended in 100 mM Tris-HCl buffer pH 8 containing 1 % Triton X-100 and solubilized for about 18 h by gentle stirring of the protein-detergent solution at 4°C. After a further ultracentrifugation step (100,000 *g*, 45 min, 4°C), the supernatants were applied to Strep tag affinity chromatography as described above. *Ws*TsdAC was stored at -70ºC in 50 mM HEPES, pH 7.0 containing 50 mM NaCl and 0.05 % Triton X-100.

SDS-PAGE, Heme staining and immunoblotting

The concentration of purified proteins was determined with a BCA Kit (Pierce, Rockford, USA). SDS polyacrylamide gel electrophoresis on 12.5 % gels was performed according to established procedures (Laemmli 1970). Gels were either used for Coomassie brilliant blue staining or for heme staining (Thomas *et al.* 1976). For immunoblot analysis recombinant proteins were electroblotted onto nitrocellulose membranes (Amersham Protran 0.45 µm NC, GE Healthcare, Chalfont St Giles, GB) for 35 min at 15 V using the Transblot SD semi-dry transfer apparatus (BioRad, Munich, Germany). Strep-tagged TsdC protein was detected with Strep-Tactin HRP Conjugate (#2-1502-001, IBA, Göttingen, Germany) by using chloronaphthol.

Enzyme activity assays

Thiosulfate-dependent ferricyanide reduction was measured and data were analyzed and fitted to the Hill equation as described previously (Kurth *et al.* 2016a). *Ws*TsdA(C) activity was determined at 39°C in 100 mM ammonium acetate buffer (pH 5.5). Tetrathionate reductase assays with *Ws*TsdA(C) were performed according to the method described in (Kurth *et al.* 2016b) and were carried out in 100 mM ammonium acetate buffer pH 6.5. All enzyme activity measurements with *Sl*TsdA(B) were performed at 20°C in 100 mM ammonium acetate buffer pH 5. More detailed information on activity assays is included in the Supplementary data file (Supporting Information).

UV-vis spectroscopy with TsdA(C) in solution

UV-vis spectra were recorded with an Analytik Jena Specord 210.

Results

Assignment of Ws0009 as a thiosulfate dehydrogenase/tetrathionate reductase (TsdA)

The *tsdA*-like gene from *W. succinogenes* encodes a periplasmic 40-kDa diheme cytochrome *c* (40,028 Da; with hemes; lacking the 21-aa signal peptide). Two Cys-X-X-Cys-His heme *c* binding motifs are present in the sequence. The active site heme (heme 1) is characterized by an unusual His/Cys axial ligation in TsdA enzymes and the respective cysteine residue is also present in the *W. succinogenes* protein (Denkmann *et al.* 2012). Sequence comparisons in conjunction with structural characterization of the related TsdA proteins from *A. vinosum* and *Marichromatium purpuratum* indicate axial His/Met ligation for the electron-transferring heme 2 (Brito *et al.* 2015; Denkmann *et al.* 2012; Kurth *et al.* 2016a).

Recombinant *Ws*TsdA produced in *E. coli* proved to be a soluble protein. It catalyzed thiosulfate oxidation as well as tetrathionate reduction *in vitro*, albeit with comparatively low specific activity of under 30 U mg^{-1} in both directions (Fig. 1A and 1B; Table S2, Supporting Information). This is almost 50-fold lower than observed for the protein from the closely related Epsilonproteobacterium *C. jejuni* (Kurth *et al.* 2016b). Specific activities in the thiosulfate oxidizing direction of Tsd(B)A from *Marichromatium purpuratum* and *A. vinosum* are even higher by factors of one hundred and one thousand, respectively (Kurth *et al.* 2016a). After ultracentrifugation of *E. coli* cell homogenates, more than 90% of the total *Ws*TsdA activity resided in the soluble fraction, in line with the absence of any putative domains for membrane integration or attachment.

Analytical gel permeation chromatography identified *Ws*TsdA as a dimer in solution (data not shown) comparable to the related protein from *C. jejuni* (Kurth *et al.* 2016b). The *W. succinogenes* enzyme exhibited spectral properties typical for the TsdA family of *c*-type cytochromes (Fig. 2A). The Soret band moved from 412 nm to 418 nm upon reduction. In the reduced state α and β peaks resided at 552 and 522 nm. A band at 695 nm characteristic for the His/Met ligation (Miles *et al.* 1993) predicted for heme 2 was observed in the oxidized state. The shoulder apparent around 635 nm is assumed to indicate the presence of a small fraction of high-spin heme probably caused by weakening of the Fe-S bond at heme 1 in TsdA proteins (Brito *et al.* 2015).

TsdC is a membrane-associated lipoprotein

*Ws*TsdC currently has no homologs in any of the available protein databases. Whilst neither transmembrane helices and/or other domains mediating membrane attachment nor prosthetic groups are predicted for *Ws*TsdC, it is among the 18 putative lipoproteins selected for *W. succinogenes* by the algorithm of Babu *et al.* (Babu *et al.* 2006). Accordingly, the *tsdC*-encoded polypeptide starts with a 19-aa type II signal sequence typical for lipoproteins (MKKMKLFMGIVAASLALAG**C**SA; LipoP 1.0 Server, score: 26.4). The sequence perfectly matches the 'lipobox' consensus motif $[LVI]_{-3}$-$[ASTVI]_{-2}$-$[GAS]_{-1}$-C_{+1} with Cys being the first amino acid of the mature lipoprotein (Babu *et al.* 2006; Hayashi *et al.* 1990).

Recombinant *Ws*TsdC was found to be membrane associated and was purified after solubilization from the *E. coli* membrane fraction (Fig. 3D). UV-vis spectroscopy did not provide any evidence for the presence of a prosthetic group. The pure recombinant protein was digested with trypsin and the endoproteinase GluC, followed by mass spectrometric analysis of the resulting peptides (Dr. Marc Sylvester, Mass Spectrometry Service Unit, Institute for Biochemistry and Molecular Biology, University of Bonn). A mass matching the type II signal peptide was not detected showing that it is efficiently cleaved off after transport over the cytoplasmic membrane in the recombinant host. 97.7%

of the other peptides expected for *Ws*TsdC were identified. The amino-terminus of the mature recombinant protein constituted the only exception indicating posttranslational modification just as predicted for a lipoprotein.

*Ws*TsdC mediates membrane attachment of *Ws*TsdA

Co-production of *Ws*TsdA and TsdC in *E. coli* changed the intracellular localization of TsdA. More than 75% of the tetrathionate reductase activity now resided in the membrane fraction and thus co-localized with TsdC (Table 1; Fig. 3). Heme stains of cell fractions (Fig. 3B) supported this finding. Just as observed for TsdC, a considerable portion of TsdA was now present in the membrane fraction (Figs. 3B and C).

Recombinant TsdC co-purifies with *Ws*TsdA and enhances its activity

The low specific activity of the *Ws*TsdA enzyme in comparison with other TsdA enzymes (Brito *et al.* 2015; Kurth *et al.* 2016a; Kurth *et al.* 2016b; Liu *et al.* 2013) indicated that TsdC might be necessary for efficient activity of the *Wolinella* enzyme. In fact, the specific tetrathionate reductase activity in membranes from the *E.coli* strain producing the *Ws*TsdAC combination already amounted to 47 U mg^{-1} protein (Table 1) and was thus higher than that observed for pure recombinant *Ws*TsdA (Table S2, Supporting Information). This finding strongly supports the notion that TsdC had an activating effect on *Ws*TsdA and this assumption was finally verified by analysis of pure recombinant *Ws*TsdAC. Both polypeptides were co-purified upon affinity chromatography exploiting the Strep-tag attached to TsdC (Fig. 4A), indicating that *Ws*TsdA and *Ws*TsdC form a tight complex *in vivo* and *in vitro*. Whilst the presence of TsdC did not significantly alter the spectral properties as compared to TsdA alone (Fig. 2), it had a strong impact on enzymatic activity. The specific activity of pure *Ws*TsdAC amounted to almost 2000 U mg^{-1} in the tetrathionate-reducing direction and was thus more than 40-fold higher than that for pure *Ws*TsdA (Fig. 1A; Table S2, Supporting Information). In the thiosulfate-oxidizing direction, a significant improvement of catalytic activity was also apparent, however, the effect was less drastic (Fig. 1B; Table S2, Supporting Information). It should be noted that the K_m value for tetrathionate amounted to about 70 μM for TsdAC whilst $S_{0.5}$ for thiosulfate was almost 100-fold higher. In conjunction with the more than six fold higher V_{max} in the tetrathionate-reducing than in the thiosulfate-oxidizing direction (Fig. 1A and 1B; Table S2, Supporting Information), *Ws*TsdAC appears to be specifically adapted to catalyzing tetrathionate reduction.

Effect of *Sl*TsdB on *Sl*TsdA activity

Our observation that *Ws*TsdA activity is drastically enhanced by *Ws*TsdC raised the question whether the other known interaction partner of TsdA enzymes, the electron-accepting diheme cytochrome TsdB improves activity in a similar manner. To this end, TsdA and TsdB from *S. lithotrophicus* were purified alone and in combination from *E. coli* (Kurth *et al.* 2016a). On its own, *Sl*TsdA showed 13-fold higher V_{max} in the thiosulfate-oxidizing than in the tetrathionate-reducing direction (Fig. 1C and 1D; Table S3, Supporting Information). When co-purified, TsdAB exhibited approximately twofold increased V_{max} in each of both reaction directions (Fig. 1; Table S3, Supporting Information).

Discussion

In this study we elucidated the enzymatic features of *Ws*TsdA as well as the role of TsdC for TsdA activity. By sequence analysis, mass spectrometry, purification of recombinant *Ws*TsdA, *Ws*TsdC and a combination thereof we established that TsdC from *W. succinogenes* is a novel and unique membrane attached lipoprotein that directly interacts with TsdA. TsdC mediates membrane association of TsdA and drastically enhances its activity.

The identity of TsdC as a lipoprotein is indicated by its membrane localization in *W. succinogenes* (Arnold 1999) as well as in *E. coli* (Fig. 3), the presence of a signal peptide typical for lipoproteins and the posttranstranslational modification of its N-terminus as suggested by our failure to detect any unmodified amino-terminal peptides in a mass spectrometric approach. The observation that the N-terminus of TsdC isolated from *W. succinogenes* was blocked upon Edman degradation (Arnold 1999; Supporting Information) further adds to this notion. The mechanism for lipoprotein biosynthesis and trafficking has been well-characterized in *E. coli* (Masuda *et al.* 2002; Matsuyama *et al.* 1995; Matsuyama *et al.* 1997; Yakushi *et al.* 2000). *W. succinogenes* has the potential to produce all the essential enzymes described for this pathway, i.e. phosphatidylglycerol:prolipoprotein diacylglycerol transferase, Lgt (Ws2111); signal peptidase II, LspA (Ws0819) and apolipoprotein N-acyltransferase, Lnt (Ws0080).

As of November 2016, *W. succinogenes* TsdC does not have sequence similarity to any other protein and database searches did not provide indication for other *tsdA*-related genes being linked with genes encoding membrane-associated proteins. *Ws*TsdA activity is drastically improved by TsdC (Figs. 1 and 5; Table S2, Supporting Information) and this effect is much stronger in the tetrathionate reducing direction than in the thiosulfate oxidizing direction. How this effect is achieved on a molecular basis is currently unclear. Generally, lipoproteins like TsdC play important roles in a wide variety of bacterial physiological processes, including nutrient uptake, transmembrane signal transduction, cell division and virulence (Nakayama *et al.* 2012). Reports about the association of lipoproteins with *c*-type cytochromes are relatively rare but include the finding that the cyanobacterial cytochrome c_{550} PsbV is stabilized by the lipoprotein PsbQ and that this contributes to protection of the catalytic activity of the water oxidation machinery at photosystem II (Kashino *et al.* 2006; Roose *et al.* 2007). In other cases, *c*-type cytochromes have themselves been reported to be lipoproteins, e.g. the cytochrome *c* subunit in the photosynthetic reaction center of *Blastochloris viridis* (formerly *Rhodopseudomonas viridis*) (Weyer *et al.* 1987), the Cu_A and heme *c*-containing subunit II (CtaC) of cytochrome *c* oxidase (cytochrome caa_3) from *Bacillus subtilis* (Bengtsson *et al.* 1999b) or cytochromes c_{551} and CccB from *Bacillus* PS3 and *B. subtilis*, respectively (Bengtsson *et al.* 1999a; Fujiwara *et al.* 1993). The activity improving effect of the electron-transporting TsdB subunit on TsdA as exemplified for the TsdAB complex from *S. lithotrophicus* is far less pronounced than that observed for *Ws*TsdAC. We conclude that the interaction of TsdAC and TsdAB complexes has a different basis on the molecular level.

Enzyme assays in solution showed that the TsdAC complex from *W. succinogenes* was much more adapted to catalyzing tetrathionate reduction than thiosulfate oxidation (Figs. 1 and 5; Table S2, Supporting Information). It therefore appears likely that the *in vivo* function of the complex is tetrathionate reduction (Fig. 5) and it is tempting to speculate that the possession of TsdAC enables *W. succinogenes* to use tetrathionate as an (additional) substrate for anaerobic respiration. The midpoint reduction potential of the tetrathionate/thiosulfate couple is +198 mV (Kurth *et al.* 2015). Thus, electron flow from formate ($E^{o'}$ = -432 mV (Thauer *et al.* 1977)) via the menaquinone pool ($E^{o'}$= -74 mV (Clark 1960; Schnorf 1966)) to tetrathionate would indeed be possible and could support growth (Fig. 5A). The electron transport chain underlying this process could in principle also include the

menaquinol-reactive cytochrome bc_1 complex (Fig. 5B). TsdC might position TsdA in the membrane such that it comes close to the electron-donating units, i.e. formate dehydrogenase or the diheme cytochrome *c* subunit of the cytochrome bc_1 complex. Regardless of such theoretical considerations, it is important to note that Klimmek *et al.* reported *W. succinogenes* to be unable of growth on formate and tetrathionate as sole energy substrates (i.e. in the absence of polysulfides) (Klimmek *et al.* 1991). On the other hand, the organism's ability to grow on polysulfide is well documented. Polysulfide medium is prepared by combining sodium sulfide and tetrathionate (Klimmek *et al.* 1991). We consider the possibility that these two sulfur compounds do not react completely to polysulfides but that some tetrathionate persists that can be used as an additional respiratory electron acceptor. This might only be possible when polysulfides and/or sulfide and tetrathionate are present at the same time. Notably, polysulfide-respiring conditions caused strong induction of TsdA synthesis as compared to fumarate (no TsdA detectable by heme staining) and nitrate respiration (basal amount of TsdA) [11].

Funding

This work was funded by the Deutsche Forschungsgemeinschaft (Grant Da 351/7-2). JMK received scholarship 700051 funded by the Aventis Foundation and awarded by Stiftung Stipendien-Fonds des Verbandes der Chemischen Industrie.

Acknowledgements

We thank Brigitte Arnold, Oliver Klimmek and Melanie Kern for helpful discussions.

Supporting information

Additional supporting information may be found in the online version of this article at the publisher's web site:

Preparation and analysis of TsdAC from *Wolinella succinogenes*

Construction of expression plasmids

Assay of thiosulfate dehydrogenase activity with ferricyanide

Assay of tetrathionate reductase activity with reduced methyl viologen

Table S1. Strains, plasmids and primers used in this study.

Table S2. Tetrathionate reduction and thiosulfate oxidation catalyzed by recombinant *Ws*TsdA or TsdAC.

Table S3. Tetrathionate reduction and thiosulfate oxidation catalyzed by TsdA(B) from *S. lithotrophicus*.

References

Arnold, B. (1999) Die *c*-Cytochrome von *Wolinella succinogenes*. Diplomarbeit. Johann Wolfgang Goethe-Universität Frankfurt.

Baar C, Eppinger M, Raddatz G *et al*. Complete genome sequence and analysis of *Wolinella succinogenes*. *Proc Natl Acad Sci USA* 2003;**100:**11690-5.

Babu MM, Priya ML, Selvan AT *et al*. A database of bacterial lipoproteins (DOLOP) with functional assignments to predicted lipoproteins. *J Bacteriol* 2006;**188:**2761-73.

Bengtsson J, Rivolta C, Hederstedt L *et al*. *Bacillus subtilis* contains two small *c*-type cytochromes with homologous heme domains but different types of membrane anchors. *J Biol Chem* 1999a;**274:**26179-84.

Bengtsson J, Tjalsma H, Rivolta C *et al*. Subunit II of *Bacillus subtilis* cytochrome *c* oxidase is a lipoprotein. *J Bacteriol* 1999b;**181:**685-8.

Brito JA, Denkmann K, Pereira IAC *et al*. Thiosulfate dehydrogenase (TsdA) from *Allochromatium vinosum*: Structural and functional insights into thiosulfate oxidation. *J Biol Chem* 2015;**290:**9222-38.

Clark WM (1960) Oxidation-reduction potentials of organic systems. Williams & Wilkins, Baltimore.

Cleland WW. Substrate inhibition. *Meth Enzymol* 1979;**63:**500-13.

Dahl C, Schulte A, Stockdreher Y *et al*. Structural and molecular genetic insight into a wide-spread bacterial sulfur oxidation pathway. *J Mol Biol* 2008;**384:**1287-300.

Denkmann K, Grein F, Zigann R *et al*. Thiosulfate dehydrogenase: a wide-spread unusual acidophilic *c*-type cytochrome. *Environ Microbiol* 2012;**14:**2673-88.

Fujiwara Y, Oka M, Hamamoto T *et al*. Cytochrome *c*-551 of the thermophilic bacterium PS3, DNA sequence and analysis of the mature cytochrome. *Biochim Biophys Acta* 1993;**1144:**213-9.

Hayashi S, Wu HC. Lipoproteins in bacteria. *J Bioenerg Biomembr* 1990;**22:**451-71.

Hermann B, Kern M, La PL *et al*. The octahaem MccA is a haem c-copper sulfite reductase. *Nature* 2015;**520:**706-9.

Kashino Y, Inoue-Kashino N, Roose JL *et al*. Absence of the PsbQ protein results in destabilization of the PsbV protein and decreased oxygen evolution activity in cyanobacterial photosystem II. *J Biol Chem* 2006;**281:**20834-41.

Kern M, Eisel F, Scheithauer J *et al*. Substrate specificity of three cytochrome c haem lyase isoenzymes from *Wolinella succinogenes*: unconventional haem c binding motifs are not sufficient for haem c attachment by Nrfl and CcsA1. *Mol Microbiol* 2010;**75:**122-37.

Kern M, Klotz MG, Simon J. The *Wolinella succinogenes mcc* gene cluster encodes an unconventional respiratory sulphite reduction system. *Mol Microbiol* 2011;**82:**1515-30.

Kern M, Simon J. Electron transport chains and bioenergetics of respiratory nitrogen metabolism in *Wolinella succinogenes* and other Epsilonproteobacteria. *Biochim Biophys Acta* 2009;**1787:**646-56.

Klimmek, O., Dietrich, W., Dancea, F., Lin, Y.-J., Pfeiffer, S., Löhr, F., Rüterjans, H., Gross, R., Simon, J. and Kröger, A. (2004) Sulfur respiration. In: Respiration in bacteria and archaea (Zannoni, D., Ed.), pp. 217-232. Springer, Dordrecht.

Klimmek O, Kröger A, Steudel R *et al*. Growth of *Wolinella succinogenes* with polysulfide as terminal acceptor of phosphorylative electron transport. *Arch Microbiol* 1991;**155:**177-82.

Kröger A, Biel S, Simon J *et al*. Fumarate respiration of *Wolinella succinogenes*: enzymology, energetics and coupling mechanism. *Biochim Biophys Acta* 2002;**1553:**23-38.

Kurth JM, Dahl C, Butt JN. Catalytic protein film electrochemistry provides a direct measure of the tetrathionate/thiosulfate reduction potential. *J Am Chem Soc* 2015;**137:**13232-5.

Kurth JM, Brito JA, Reuter J *et al*. Electron accepting units of the diheme cytochrome *c* TsdA, a bifunctional thiosulfate dehydrogenase/tetrathionate reductase. *J Biol Chem* 2016a;DOI: 10.1074/jbc.M116.753863 [Epub ahead of print].

Kurth JM, Butt JN, Kelly DJ *et al*. Influence of heme envionment on the catalytic properties of tetrathionate reductase (TsdA) from *Campylobacter jejuni*. *Biosci Rep* 2016b;DOI: 10.1042/BSR20160457 [Epub ahead of print].

Laemmli UK. Cleavage of structural proteins during the assembly of the head of bacteriophage T4. *Nature* 1970;**227:**680-5.

Liu Y-W, Denkmann K, Kosciow K *et al*. Tetrathionate stimulated growth of *Campylobacter jejuni* identifies TsdA as a new type of bi-functional tetrathionate reductase that is widely distributed in bacteria. *Mol Microbiol* 2013;**88:**173-88.

Masuda K, Matsuyama S, Tokuda H. Elucidation of the function of lipoprotein-sorting signals that determine membrane localization. *Proc Natl Acad Sci USA* 2002;**99:**7390-5.

Matsuyama S, Tajima T, Tokuda H. A novel periplasmic carrier protein involved in the sorting and transport of *Escherichia coli* lipoproteins destined for the outer membrane. *EMBO J* 1995;**14:**3365-72.

Matsuyama S, Yokota N, Tokuda H. A novel outer membrane lipoprotein, LolB (HemM), involved in the LolA (p20)-dependent localization of lipoproteins to the outer membrane of *Escherichia coli*. *EMBO J* 1997;**16:**6947-55.

Miles CS, Manson FDC, Reid GA *et al*. Substitution of a haem-iron axial ligand in flavocytochrome b_2. *Biochim Biophys Acta* 1993;**1202:**82-6.

Nakayama H, Kurokawa K, Lee BL. Lipoproteins in bacteria: structures and biosynthetic pathways. *FEBS J* 2012;**279:**4247-68.

Roose JL, Kashino Y, Pakrasi HB. The PsbQ protein defines cyanobacterial Photosystem II complexes with highest activity and stability. *Proc Natl Acad Sci U S A* 2007;**104:**2548-53.

Schnorf, U. (1966) Der Einfluss von Substituenten auf redoxpotential und Wuchseigenschaften von Chinonen. ETH, Zürich.

Schumacher W, Kroneck PMH, Pfennig N. Comparative systematic study on 'Spirillum' 5175, *Campylobacter* and *Wolinella* species. *Arch Microbiol* 1992;**158:**287-93.

Simon J. Enzymology and bioenergetics of respiratory nitrite ammonification. *FEMS Microbiol Rev* 2002;**26:**285-309.

Simon J, Einsle O, Kroneck PM *et al*. The unprecedented *nos* gene cluster of *Wolinella succinogenes* encodes a novel respiratory electron transfer pathway to cytochrome *c* nitrous oxide reductase. *FEBS Lett* 2004;**569:**7-12.

Simon J, Kern M, Hermann B *et al*. Physiological function and catalytic versatility of bacterial multihaem cytochromes c involved in nitrogen and sulfur cycling. *Biochem Soc Trans* 2011;**39:**1864-70.

Thauer RK, Jungermann K, Decker K. Energy conservation in chemotrophic anaerobic bacteria. *Bacteriol Rev* 1977;**41:**100-80.

Thomas PE, Ryan D, Levin W. Improved staining procedure for detection of peroxidase-activity of cytochrome P-450 on sodium dodecyl-sulfate polyacrylamide gels. *Anal Biochem* 1976;**75:**168-76.

Weyer KA, Lottspeich F, Gruenberg H *et al*. Amino acid sequence of the cytochrome subunit of the photosynthetic reaction centre from the purple bacterium *Rhodopseudomonas viridis*. *EMBO J* 1987;**6:**2197-202.

Yakushi T, Masuda K, Narita S *et al*. A new ABC transporter mediating the detachment of lipid-modified proteins from membranes. *Nat Cell Biol* 2000;**2:**212-8.

Figure legends

Fig. 1. Tetrathionate reduction (A,C) and thiosulfate oxidation (B,D) catalyzed by *Ws*TsdA(C) or *Sl*TsdA(B) purified from *E. coli* For thiosulfate oxidation, *v* versus [S] plots were fitted to the Hill equation and for tetrathionate reduction data sets were fitted to the general equation for substrate inhibition (Cleland 1979).

Fig. 2. UV-Vis spectra of purified *Ws*TsdA and *Ws*TsdAC. The proteins were obtained in the fully oxidized state (black curves). For full reduction of the proteins Na-dithionite (4 mM) was added (grey curves). For *Ws*TsdA (A) 50 mM HEPES buffer pH 7 with 50 mM NaCl was used. Spectra for *Ws*TsdAC (B) were recorded in the same buffer containing 0.05 % Triton X-100. Spectra were normalized to 750 nm. The protein peak of TsdAC was obscured by absorbance of the detergent and is therefore not shown. The A_{413nm}/A_{280nm} for pure oxidized *Ws*TsdA was 2.0.

Fig. 3. Analysis of membrane and soluble proteins from *E. coli* cells producing TsdAC (A-C) or TsdC alone (D). Cellular fractions obtained after ultracentrifugation were analyzed on 12.5 % SDS polyacrylamide gels and either stained with Coomassie brilliant blue (A) or developed by heme staining (B) or immunological detection of TsdC using a Strep Tactin HRP conjugate (C and D). Panels A, B and C show cellular fractions obtained from *E. coli* producing both, *Ws*TsdA and *Ws*TsdC. Membranes and soluble proteins analyzed in panel D stem from *E. coli* producing solely *Ws*TsdC. The molecular mass of recombinant TsdC (17 kDa) is slightly smaller than that of TsdC co-produced with TsdA (19 kDa). 10-15 µg protein was loaded in each lane.

Fig. 4. SDS PAGE of purified recombinant TsdAC (A,B), TsdA (C,D), and TsdC (E). 12.5 % SDS polyacrylamide gels were either stained with Coomassie brilliant blue (A,C), developed by heme staining (B,D) or immunological detection of TsdC using a Strep Tactin HRP conjugate (E). 6 to 8 µg TsdA was loaded in each lane. The 90-kDa heme staining band visible for the TsdAC preparation probably originates from a TsdA dimer.

Fig. 5. Putative role of TsdA(C) in *W. succinogenes* and characteristics of TsdA(C) produced recombinantly in *E. coli*. Values for V_{max} are rounded values taken from Table S2**.**

Table 1. Comparison of tetrathionate reductase activity, protein yield and enrichment factor upon TsdAC purification. The tetrathioante reductase activity in the soluble and the membrane fraction obtained after ultracentrifugation of 35 ml *E. coli* crude cell extract is compared with that of pure recombinant TsdAC from *W. succinogens* obtained by affinity chromatography of solubilized membrane proteins using a Streptactin matrix.

Fraction	Volume activity [U/ml]	Total activity [U]	Yield [%]	Specific activity [U/mg]	Enrichment factor
Soluble fraction	91 ± 5	2909 ± 156	23	5 ± 0	-
Membrane fraction	946 ± 41	9461 ± 411	77	47 ± 2	1
Purified TsdAC	6855 ± 123	7609 ± 136	62	1975 ± 35	41

Figure 1

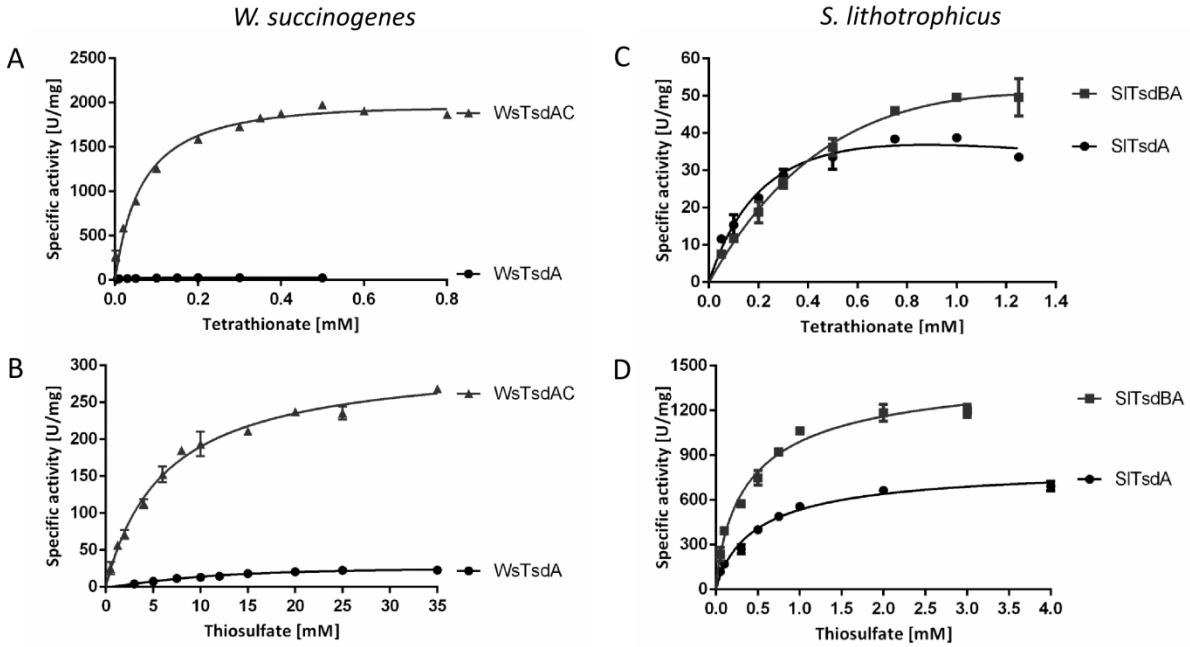
W. succinogenes
S. lithotrophicus
A
B
C
D
Specific activity [U/mg]
Tetrathionate [mM]
Thiosulfate [mM]
WsTsdAC
WsTsdA
SlTsdBA
SlTsdA

Figure 2

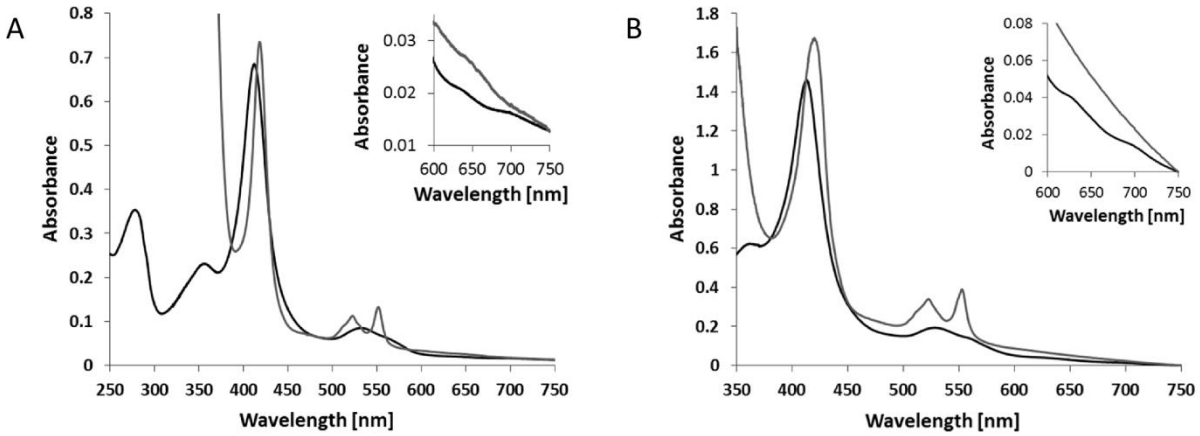

Figure 3

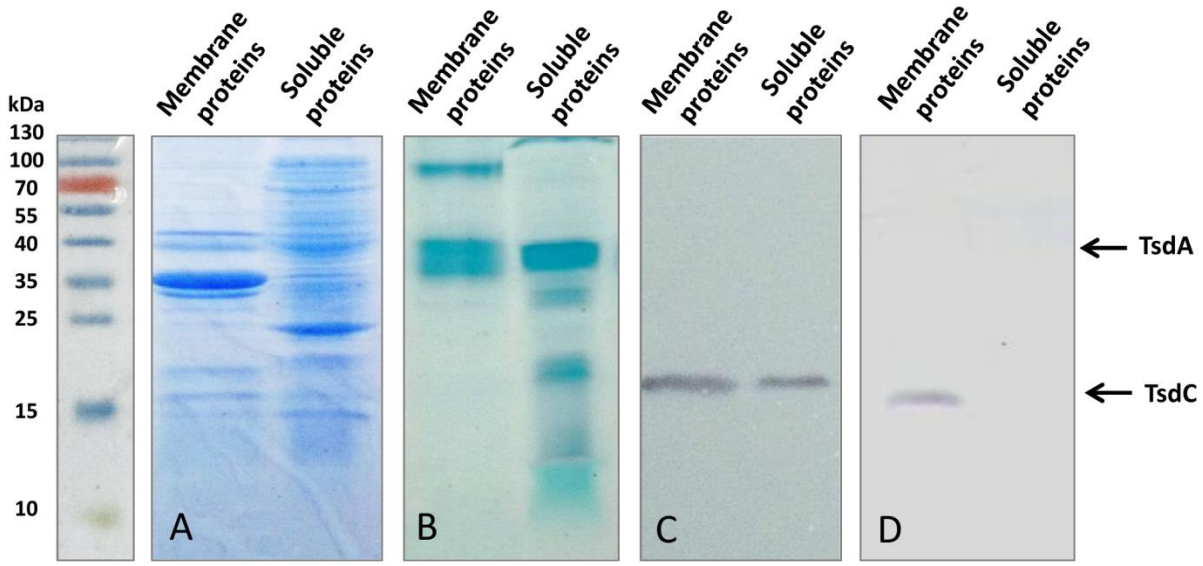
kDa
130
100
70
55
40
35
25
15
10
Membrane proteins
Soluble proteins
Membrane proteins
Soluble proteins
Membrane proteins
Soluble proteins
Membrane proteins
Soluble proteins
A
B
C
D
TsdA
TsdC

Figure 4

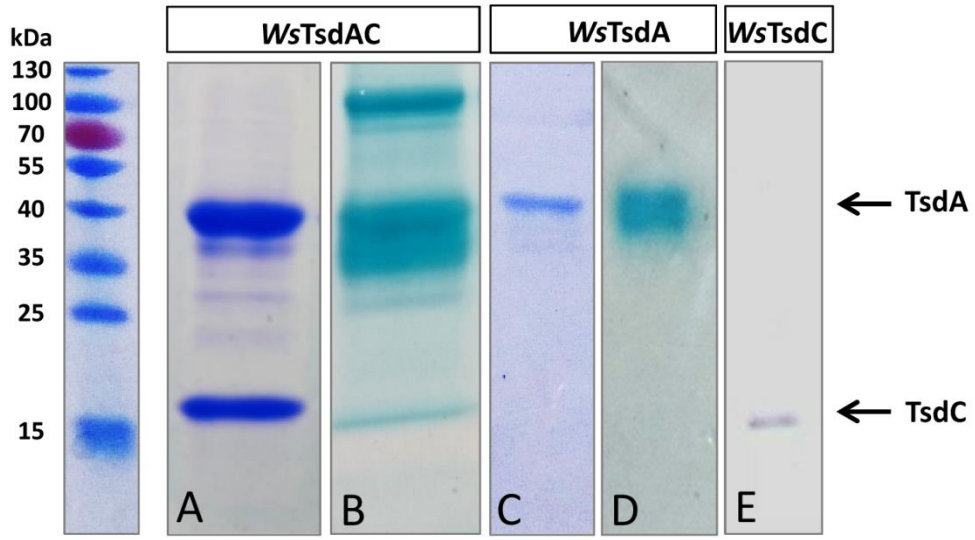
kDa
130
100
70
55
40
35
25
15
WsTsdAC
WsTsdA
WsTsdC
TsdA
TsdC
A
B
C
D
E

Figure 5

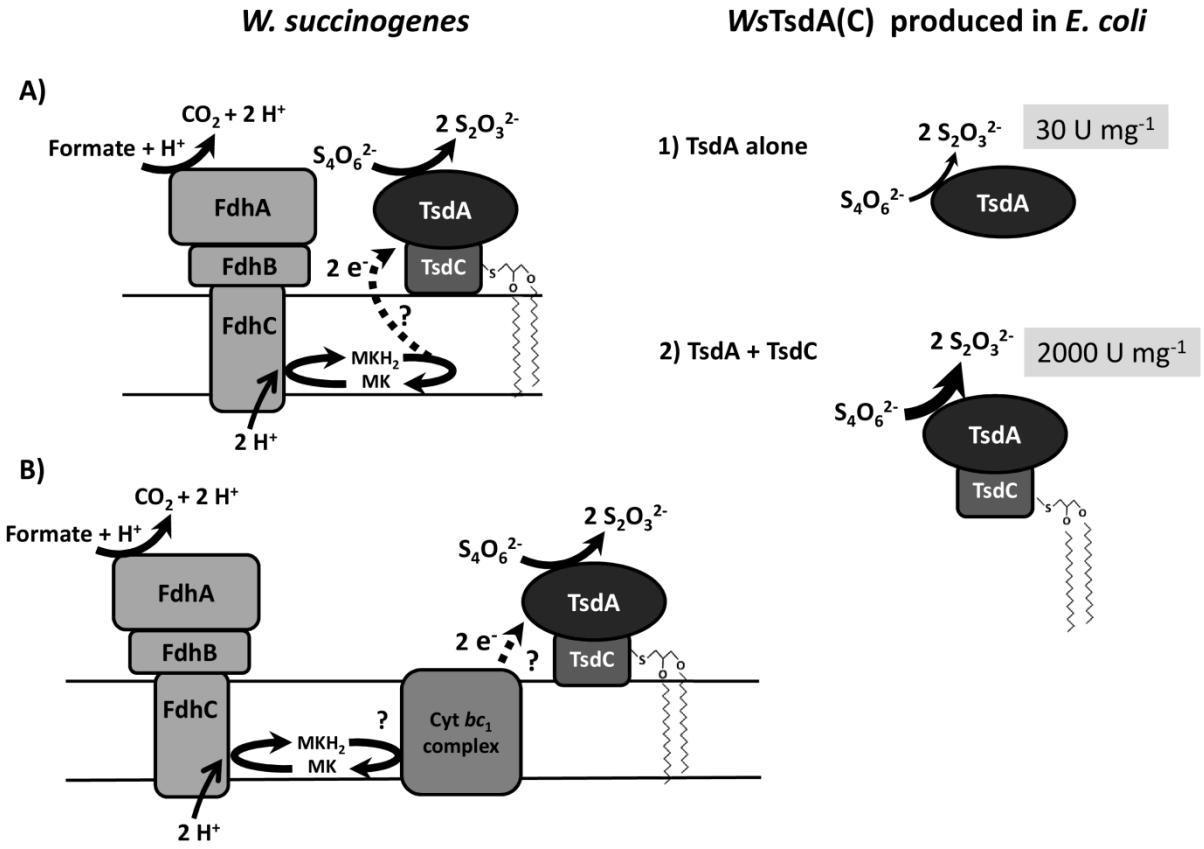
W. succinogenes
WsTsdA(C) produced in E. coli
A)
CO2 + 2 H+
Formate + H+
S4O6 2-
2 S2O3 2-
FdhA
FdhB
FdhC
TsdA
TsdC
2 e-
?
MKH2
MK
2 H+
1) TsdA alone
30 U mg-1
2) TsdA + TsdC
2000 U mg-1
B)
Cyt bc1 complex

Supporting Information

TsdC, a unique membrane-bound lipoprotein from *Wolinella succinogenes* that enhances tetrathionate reductase activity of TsdA

Julia M. Kurth[1], Anja Schuster[1], Waldemar Seel[1], Stefanie Herresthal[1], Jörg Simon[2], Christiane Dahl[1]

[1] Institut für Mikrobiologie & Biotechnologie, Rheinische Friedrich Wilhelms-Universität Bonn, Bonn, Germany

[2] Microbial Energy Conversion and Biotechnology, Fachbereich Biologie, Technische Universität Darmstadt, Darmstadt, Germany

Preparation and analysis of the TsdAC complex from *Wolinella succinogenes*

Cells of *W. succinogenes* DSM 1740 were grown under anoxic conditions in medium with formate as electron donor and polysulfide as electron acceptor (Klimmek *et al.* 1991). Cells were harvested in the late exponential growth phase using a tangential filtration system (Pellicon, Millipore, Eschborn, Germany, 0.2 µm pore size) and subsequent centrifugation (15 min, 10,000 × *g*, 4 °C). Sedimented cells were resuspended in 50 mM anoxic potassium phosphate buffer (pH 7.5) with 1 mM DTT (0.05 - 0.1 g cells per ml). The cell suspension was passed through a high-pressure cell disruption system (Constant Systems) at 135 MPa and ultracentrifuged for 1 h at 100,000 × *g*. Sedimented membranes were resuspended in anoxic 50 mM potassium phosphate buffer (pH 7.5) containing 1 mM DTT, followed by addition of 1 g Triton X-100 per mg protein and incubation for 1 h at 4 °C under gentle stirring. The supernatant of a second ultracentrifugation step (100,000 *g*, 45 min, 4°C) was separated by anion exchange chromatography on DEAE Sepharose CL-6B (column volume 60 ml, equilibration buffer 50 mM potassium phosphate, pH 7.5 containing 1 mM DTT and 0.05 % Triton X-100, flow rate 45 ml h^{-1}). After washing the column, a linear gradient from 0 to 0.4 M NaCl in equilibration buffer (four column volumes) was applied. A hemoprotein of 40 kDa eluted at 180 mM NaCl. Further dissection of the proteins present in this preparation was achieved by two-dimensional gel electrophoresis (Schägger *et al.* 1994). First, the proteins (100 - 150 µg) were separated by native PAGE in a 4 - 8% gradient polyacrylamide gel with 0.1 % Triton X-100 (Schägger *et al.* 1991) revealing the presence of two heme-staining bands. Separation in the second dimension (12.5 % SDS-PAGE) showed that the slower migrating heme-containing band in the native gel contained the 40-kDa cytochrome *c* and an additional Coomassie-stainable polypeptide of 16 kDa.

Both polypetides were electroblotted onto PVDF membranes (Immobilon, Millipore, Eschborn, Germany) using a discontinuous buffer system (Khyse-Andersen 1984). Protein bands were visualized with Coomassie, excised and extracted with 80 % formic acid. For bromcyan cleavage, 1 µg BrCN was added per µg of protein, followed by incubation at room temperature in the dark for 16 h. Liquid was removed by exsiccation over KOH. The obtained polypeptide fragments were separated by SDS-PAGE, transferred to PVDF membranes and subjected to Edman degradation (performed by Hermann Schägger, Gustav-Embden-Zentrum für Biologische Chemie, Johann Wolfgang Goethe-Universität Frankfurt am Main, Germany), applying a gas phase sequenator (473A, Applied Biosystems) equipped with a phenylthiohydantoin detector. While the 16-kDa protein was found to be N-terminally blocked, the N-terminal amino acid sequence of the 40-kDa hemoprotein was determined as FERWTLEARGKSGYDAPKE. Bromcyan cleavage yielded internal amino acid sequences for the 16-kDa (QSPALSGK) as well as for the 40-kDa polypeptide (YKVGPYKGIIKQ and PKGAPTLFDKDVAAFIN).

Construction of expression plasmids

The plasmids and primers used in this study are listed in supplementary Table S1. The *tsdC* gene (WS0008) from *W. succinogenes* (DSM 1740^T) was amplified from genomic DNA by PCR using primers WS0008-fw and WS0008-rev. Primers included BsaI restriction sites and the digested PCR product was cloned into BsaI-digested pASK-IBA3plus (IBA, Göttingen) resulting in pET-WS0008. The plasmid encodes *Ws*TsdC with a carboxy-terminal Strep tag extension that is thought to be transported across the cytoplasmic membrane on the basis of its own leader peptide.

The vector pET-N-2strep-tsdAWs was produced as follows: First, the Twin-Strep-tag encoding sequence from pASG-IBA103 (IBA, Göttingen) was amplified with primers pET-2xS-TsdA_fw and pET-2xS-TsdA_rev. Then, the PCR product was digested with BamHI and NcoI and cloned into pET-N-Strep-TsdACj. This plasmid had before been cut with BamHI and NcoI, thereby excising the existing DNA fragment encoding a conventional Strep tag. The resulting vector was termed pET-N-2strep-tsdACj. The *tsdA* (WS0009) sequence from *W. succinogenes* was amplified from chromosomal DNA with primers pET-N-TsdAWs_fw and pET-N-TsdAWs_rev, digested with BglII and HindIII and inserted into pET-N-2strep-tsdACj from which the existing Cj*tsdA* gene had been removed by digestion with BamHI and HindIII. The resulting vector was named pET-N-2strep-tsdAWs and encodes *Ws*TsdA with an N-terminal Twin-Strep tag and a PelB leader peptide.

Plasmid pET-C-2strep-WS0009+0008 was constructed by amplifying *tsdA* (WS0009) from *W. succinogenes* chromosomal DNA with primers WS0009-HindIII-fw and WS0009-XhoI-rev, digesting the PCR product and the pET-22b (+) vector (Novagen) with HindIII and XhoI and ligating both, resulting in pET-WS0009. Afterwards the Twin-Strep-tag encoding sequence from pASG-IBA103 (IBA, Göttingen) was amplified with primers tsdAWs-C-2xstrep_fw and tsdAWs-C-2xstrep_rev, digested with XhoI and BlpI and cloned into pET-WS0009 from which the His tag-encoding sequence had been removed with XhoI and BlpI. The resulting plasmid (pET-C-2strep-tsdAWs) was digested with XhoI and EcoRI, thereby removing the W*stsdA* gene. The XhoI and MunI digested PCR product generated with primers C-2S-WS8+9-fw and C-2S-WS8+9-rev comprising the *tsdA* (WS0009) and *tsdC* (WS0008) genes from *W. succinogenes* was inserted into the vector backbone, resulting in pET-C-2strep-WS0009+0008. This plasmid encodes *Ws*TsdA with 11 vector-derived amino acids at its N-terminus and *Ws*TsdC carrying a carboxy-terminal Twin-Strep tag. Transport of the proteins across the cytoplasmic membrane is mediated by the vector-encoded PelB leader peptide or by the original signal peptide for *Ws*TsdA and *Ws*TsdC, respectively.

The *tsdA* gene (Slit_1878), the *tsdB* gene (Slit_1877) and the *tsdBA* gene combination (Slit_1877-Slit1878) from *Sideroxydans lithotrophicus* ES-1 (ATCC 700298^T) were amplified from genomic DNA and cloned as described in (Kurth *et al.* 2016).

Assay of thiosulfate dehydrogenase activity with ferricyanide

Thiosulfate-dependent ferricyanide reduction was measured by following the decrease of absorbance at 420 nm (ε = 1.09 μM cm^{-1}) with 1 mM ferricyanide. Enzyme activity measurements with *Sl*TsdA(B) were run at 20°C in 100 mM ammonium acetate buffer (pH 5). Assays with *Ws*TsdA(C) were performed at 39°C in 100 mM ammonium acetate buffer (pH 5.5). Assays were started by addition of Tsd(B)A(C) and data were recorded in a Specord 210 spectrophotometer (Analytik Jena, Jena, Germany). Activity is expressed as μmol tetrathionate produced per min and mg protein on the basis of one molecule tetrathionate formed per two molecules ferricyanide reduced. In the case of enzymes that use two molecules of the same substrate (here thiosulfate) primary *v* versus *[S]* plots

provide the best way to examine the data (Segel 1993). Data were fitted to the empirical Hill Eqn 1 using Graph Pad Prism (version 6; Graph Pad).

Eqn 1 $$v = \frac{V_{\max}[S]^{n}}{K + [S]^{n}}$$

The Hill equation resembles the classical Henri–Michaelis–Menten equation; however, the *n* term allows accounting for non-hyperbolic shapes. A substrate concentration $[S]_{0.5}$ can be reported that yields half maximal velocity and is characteristic of the process. The constant *K*, which is not equivalent to K_m, characterizes enzyme–substrate interaction. The relationship between *K* and $[S]_{0.5}$ is $K = [S]_{0.5}{}^{n}$.

Assay of tetrathionate reductase activity with reduced methyl viologen

Methyl viologen-linked tetrathionate reductase assays were carried out in a 1 ml quartz glass cuvette closed with a rubber stopper and purged with N_2 for 10 min after buffer addition. All solutions were made anaerobic by sparging with N_2. The final assay mixture contained the appropriate buffer, 0.3 mM methyl viologen reduced with 1 to 3 µl of 2% titanium (III) citrate oxygen scavenger solution (Zehnder, Wuhrman 1976) and different final concentrations of tetrathionate. Enzyme solutions were injected after a relatively stable absorbance at 585 nm was achieved (below 2.0). The rate before addition of enzyme was subtracted from rate after enzyme addition. The specific activity for tetrathionate reductase was calculated using an extinction coefficient for methyl viologen of 11.8 mM^{-1} cm^{-1} at 585 nm. Enzyme assays with with *Sl*TsdA(B) and *Ws*TsdA(C) were carried out at 20°C in 100 mM ammonium acetate buffer (pH 5) and at 39°C in 100 mM ammonium acetate buffer (pH 6.5), respectively. Activity is expressed as µmol tetrathionate reduced min^{-1} mg $protein^{-1}$ on the basis of a 1:2 molar ratio of tetrathionate reduced to methyl viologen oxidized. Enzyme activity measurements were analyzed by non-linear regression with michaelis menten kinetic or with substrate inhibition using Graph Pad Prism (version 6; Graph Pad). Substrate inhibition analysis was used for K_i determination and curve fitting, Michaelis Menten kinetic was used to determine all other kinetic parameters.

The activity of TsdA is inhibited as substrate concentration increases. The K_i values given in Table S2 and S3 were derived from fitting complete data sets to the general equation for substrate inhibition (Eqn 2) (Cleland 1979) using Graph Pad Prism (version 6; Graph Pad).

Eqn 2 $$v = \frac{V_{\max}[S]}{K_m + [S] + \frac{[S]^2}{K_i}}$$

Kinetic constants other than K_i can be derived from Eqn 1. In that case V_{max} is the maximum enzyme velocity if the substrate did not also inhibit enzyme activity.

Table S1. Strains, plasmids and primers used in this study.

Strains, plasmids, primers	Description	Reference or source
Strains		
E. coli DH5α	F^- φ80d *lacZ*ΔM15 Δ(*lacZYA-argF*)*U169 recA1 endA1hsdR17* (rk^- mk^+) *supE44* λ^-*thi-1 gyrA relA1*	(Hanahan 1983)
E. coli BL21 (DE3)	F^- *ompT hsdS*$_B$ ($r_B^-m_B^-$) *gal dcm met*(DE3)	Novagen
E. coli C43 (DE3)	F^- *ompT hsdS*$_B$ ($r_B^-m_B^-$) *gal dcm* (DE3)	(Miroux *et al.* 1996)
Wolinella succinogenes DSM 1740^T	Type strain	(Tanner *et al.* 1981; Wolin *et al.* 1961)
Plasmids		
pEC86	Cm^r, product from pEC66 and pACYC184 with *E. coli ccmABCDEFGH* genes	(Arslan *et al.* 1998)
pET-22b(+)	Ap^r, T7 promoter, lac operator, C-terminal His tag, pelB leader	Novagen
pASK-IBA3 plus	Ap^r, *tetA* promoter/operator, C-terminal Strep tag	IBA (Göttingen)
pASG-IBA103	Ap^r, allows the expression of Twin-Strep-tag-fusion-proteins in *E.coli*	IBA (Göttingen)
pASK-IBA3plus-*slit1877*	Ap^r; *tsdB* from *S. lithotrophicus* (Slit_1877) cloned into pASK-IBA3 plus with BsaI, C-terminal Strep tag	(Kurth *et al.* 2016)
pASK-IBA3plus-*slit1878*	Ap^r; *tsdA* from *S. lithotrophicus* (Slit_1878) cloned into pASK-IBA3 plus with BsaI, C-terminal Strep tag	(Kurth *et al.* 2016)
pASK-IBA3plus-*slit1877-slit1878*	Ap^r; *tsdBA* from *S. lithotrophica* (Slit_1877-Slit_1878) cloned into pASK-IBA3 plus with BsaI, C-terminal Strep tag	(Kurth *et al.* 2016)
pET-WS0009	Ap^r, *tsdA* from *W. succinogenes* (WS0009*)* between HindIII and XhoI of pET-22b (+), C-terminal His tag	This study
pET-N-Strep-TsdACj	Apr; N-terminal Strep-tag, f1 origin, T7 Promoter, NcoI-HindIII fragment of PCR amplified tsdA in digested pETStrepDsrJ	(Kurth *et al.* 2015)
pET-N-2strep-tsdACj	Ap^r, sequence for Twin-Strep-tag was cloned into pET-N-strep-TsdACj with BamHI and NcoI, N-terminal Twin-Strep-tag	This study
pET-N-2strep-tsdAWs	Ap^r, *tsdA* from *C. jejuni* was removed from pET-N-2strep-tsdACj with BamHI and HindIII and W*stsdA* (WS0009*)* was cloned into the vector backbone using BglII and HindIII, N-terminal Twin-Strep-tag	This study
pET-C-2strep-tsdAWs	Ap^r, sequence for Twin-Strep-tag was cloned into pET-WS0009 with XhoI and BlpI after excision of the His tag encoding sequence	This study
pET-C-2strep-WS0009+0008	Ap^r, *tsdA* (WS0009) and *tsdC* (WS0008) from *W. succinogenes* cloned into the vector pET-C-2strep-tsdAWs with XhoI and MunI after excision of W*stsdA* with XhoI and EcoRI, C-terminal Twin-Strep-tag	This study
Primers		
WS0009-HindIII-fw	CAGCACCAAGCTTTTTGAGCGTTGGACGC	This study
WS0009-XhoI-rev	GCTCCTCGAGCTTCGCGGCG	This study
pET-N-TsdAWs_fw	CCAGATCTTTTGAGCGTTGGACGCT	This study
pET-N-TsdAWs_rev	ATAAGCTTTCACTTCGCGGCGGGTT	This study
pET-2xS-TsdA_fw	ATCCATGGGGAGCGCTTGGAGCCA	This study
pET-2xS-TsdA_rev	CCGGATCCTTTCTCGAACTGCGGGT	This study
tsdAWs-C-2xstrep_fw	ATCTCGAGAGCGCTTGGAGCCACC	This study
tsdAWs-C-2xstrep_rev	ATGCTCAGCGGAAAGCCGGCGAAC	This study
C-2S-WS8+9-fw	CCCAATTGTTTTGAGCGTTGGACGC	This study
C-2S-WS8+9-rev	ATCTCGAGCCTTAGGAGCCCCCTT	This study

Table S2. Tetrathionate reduction and thiosulfate oxidation catalyzed by recombinant *Ws*TsdA or TsdAC. Tetrathionate reduction was measured under anoxic conditions with 0.3 mM methyl viologen. V_{max} is given as µmol min^{-1} mg $protein^{-1}$. For thiosulfate oxidation, *v* versus [S] plots were fitted to the Hill equation and for tetrathionate reduction data sets were fitted to the general equation for substrate inhibition (Cleland 1979). n, Hill coefficient.

		$V_{max\ measured}$ [U/mg]	V_{max} [U/mg]	K_m [mM]	K_i [mM]
Tetrathionate reduction	*Ws*TsdA	28 ± 1	28 ± 1	0.01 ± 0.00	-
	*Ws*TsdAC	1975 ± 35	2208 ± 217	0.07 ± 0.02	13.4 ± 28.5
		V_{max} [U/mg]	$S_{0.5}$ [mM]	n	
Thiosulfate oxidation	*Ws*TsdA	27 ± 2	9.80 ± 1.23	1.45 ± 0.18	
	*Ws*TsdAC	310 ± 15	6.29 ± 0.79	0.99 ± 0.08	

Table S3. Tetrathionate reduction and thiosulfate oxidation catalyzed by TsdA(B) from *S lithotrophicus*. V_{max} is given in µmol min^{-1} mg $protein^{-1}$. For thiosulfate oxidation, *v* versus [S] plots were fitted to the Hill equation and for tetrathionate reduction data sets were fitted to the general equation for substrate inhibition (Cleland 1979). n, Hill coefficient.

	TsdA	$V_{max\ measured}$ **[U/mg]**	V_{max} **[U/mg]**	K_m **[mM]**	K_i **[mM]**
Tetrathionate reduction	*Sl*TsdA	39 ± 1	62 ± 16	0.30 ± 0.13	2.6 ± 2.1
	*Sl*TsdAB	50 ± 1	132 ± 47	1.13 ± 0.50	1.7 ± 1.4
	TsdA	V_{max} **[U/mg]**	$S_{0.5}$ **[mM]**	**n**	
Thiosulfate oxidation	*Sl*TsdA	835 ± 82	0.52 ± 0.14	0.89 ± 0.14	
	*Sl*TsdAB	1515 ± 188	0.45 ± 0.17	0.79 ± 0.14	

REFERENCES

Arslan E, Schulz H, Zufferey R *et al*. Overproduction of *Bradyrhizobium japonicum c*-type cytochrome subunits of the cbb_3 oxidase in *Escherichia coli*. *Biochem Biophys Res Commun* 1998;**251:**744-7.

Cleland WW. Substrate inhibition. *Meth Enzymol* 1979;**63:**500-13.

Hanahan D. Studies on transformation of *Escherichia coli* with plasmids. *J Mol Biol* 1983;**166:**557-80.

Khyse-Andersen J. Electroblotting of multiple gels: A simple apparatus without buffer-tank for rapid transfer of proteins. *J Biochem Biophys Meth* 1984;**10:**203-9.

Klimmek O, Kröger A, Steudel R *et al*. Growth of *Wolinella succinogenes* with polysulfide as terminal acceptor of phosphorylative electron transport. *Arch Microbiol* 1991;**155:**177-82.

Kurth JM, Dahl C, Butt JN. Catalytic protein film electrochemistry provides a direct measure of the tetrathionate/thiosulfate reduction potential. *J Am Chem Soc* 2015;**137:**13232-5.

Kurth JM, Brito JA, Reuter J *et al*. Electron accepting units of the diheme cytochrome *c* TsdA, a bifunctional thiosulfate dehydrogenase/tetrathionate reductase. *J Biol Chem* 2016; 10.1074/jbc.M116.753863 [Epub ahead of print].

Miroux B, Walker JE. Over-production of proteins in *Escherichia coli*: Mutant hosts that allow synthesis of some membrane proteins and globular proteins at high levels. *J Mol Biol* 1996;**260:**289-98.

Schägger H, Cramer WA, von JG. Analysis of molecular masses and oligomeric states of protein complexes by blue native electrophoresis and isolation of membrane protein complexes by two-dimensional native electrophoresis. *Anal Biochem* 1994;**217:**220-30.

Schägger H, von Jagow G. Blue native electrophoresis for isolation of membrane protein complexes in enzymatically active form. *Anal Biochem* 1991;**199:**223-31.

Segel IH (1993) Enzyme kinetics: behaviour and analysis of rapid equilibrium and steady-state enzyme systems. Wiley-Interscience, New York.

Tanner ACR, Badger S, Lai C-H *et al*. *Wolinella* gen. nov., *Wolinella succinogenes* (*Vibrio succinogenes* Wolin et al.) comb. nov., and description of *Bacteroides gracilis* sp. nov., *Wolinella recta* sp. nov., *Campylobacter concisus* sp. nov., and *Eikenella corrodens* from humans with peridontal disease. *Int J Syst Bacteriol* 1981;**31:**432-45.

Wolin MJ, Wolin EA, Jacobs NJ. Cytochrome-producing anaerobic *Vibrio succinogenes*, sp. n. *J Bacteriol* 1961;**81:**911-7.

V. Additional results

Chapter 5

Reaction mechanism of TsdA from *Campylobacter jejuni* revealed by structural, spectroscopic, electrochemical and spectroelectrochemical experiments

Introduction & Summary:

TsdA enzymes are diheme cytochromes *c* with an unusual His/Cys ligation at the active site heme. A rhodanese-like reaction cycle has been discussed for the enzyme. The crystal structure of the TsdBA enzyme from *Marichromatium vinosum* revealed that thiosulfate is covalently bound to Sγ of the heme-ligating cysteine of the active site heme and thereby proves that catalysis of thiosulfate oxidation by Tsd(B)A enzymes involves formation of a covalent adduct between the sulfane sulfur atom of thiosulfate and the Sγ of the active site cysteine.

This work focuses on gaining further insight into the *Cj*TsdA reaction mechanism. The formation of a covalent bond between thiosulfate and Sγ of the active site cysteine, most probably the rate-defining step in the TsdA reaction cycle, was supported by UV-vis spectroscopy, spectroelectrochemical and electrochemical experiments of TsdA in the presence of the thiosulfate mimic sulfite. This covalent bond can only be formed when the TsdA hemes are oxidized and formation of the cysteine S-thiosulfonate group is assumed to lead to immediate reduction of the TsdA hemes. Moreover, the *Cj*TsdA redox properties were analysed: Heme 1 was identified as the heme with the more negative reduction potential and Heme 2 was proven to be the heme with the more positive reduction potential. An important finding clarifying the TsdA reaction mechanism is that the reduction potential of Heme 1 becomes more positive after binding of a sulfur species to Sγ of the heme-ligating cysteine. Thus, electron transfer from thiosulfate to Heme 1 is facilitated in the thiosulfate-oxidizing direction while electron transfer from Heme 2 to Heme 1 is promoted in the reductive direction.

Chapter 5

Reaction mechanism of TsdA from *Campylobacter jejuni* revealed by structural, spectroscopic, electrochemical and spectroelectrochemical experiments

This chapter is in preparation to be published:

Kurth, J.M., Jenner, L.P., Dahl, C., Cheesman, M.R., Bradley, J.M., Butt, J.N.: Reaction mechanism of TsdA revealed by study of interaction between TsdA and sulfite. *J Biol Chem* **in preparation**

Jenner, L.P., Kurth, J.M., van Helmont, S., Dahl, C., Butt, J.N., Cheesman, M.R., Bradley, J.M.: Heme ligation and redox chemistry in thiosulfate dehydrogenase (TsdA) enyzmes. *Biochem J* **in preparation**

Brito, J.A., Kurth, J.M., Dahl, C., Archer, M.: Structural insight into TsdA from *Campylobacter jejuni*. *J Biol Chem* **in preparation**

Author contributions

- JMK performed all experiments except of protein crystallization, structure analysis and MCD spectroscopy

- JMK wrote this chapter

Introduction

Enzymes belonging to the widespread TsdA family are bifunctional thiosulfate dehydrogenases/tetrathionate reductases (Denkmann *et al.*, 2012; Liu *et al.*, 2013; Brito *et al.*, 2015; Kurth *et al.*, 2015). In contrast to TsdA from the purple sulfur bacteria *Allochromatium vinosum* (*Av*TsdA) (Denkmann *et al.*, 2012; Brito *et al.*, 2015) and *Marichromatium purpuratum* (*Mp*TsdBA) (Kurth *et al.*, 2015; Kurth, Brito *et al.*, 2016), TsdA from the human intestinal pathogen *Campylobacter jejuni* (*Cj*TsdA) is biased to tetrathionate reduction (Liu *et al.*, 2013; Kurth, Butt *et al.*, 2016). *Cj*TsdA represents a new type of tetrathionate reductase as this enzyme is distinct from the iron-sulfur molybdoenzyme TtrABC from *Salmonella typhimurium* (Hinojosa-Leon *et al.*, 1986; Hensel *et al.*, 1999) and the octaheme Otr enzyme from *Shewanella oneidensis* (Mowat *et al.*, 2004).

TsdA enzymes are diheme cytochromes *c* with an unusual His/Cys axial ligand set at the active site heme, Heme 1 (Brito *et al.*, 2015). The His/Cys-ligated heme equivalent to TsdA Heme 1 has been shown to participate in the SoxXA catalyzed reaction (Cheesman *et al.*, 2001; Dambe *et al.*, 2005; Kilmartin *et al.*, 2011). The SoxA subunit shows high sequence similarity to TsdA (Denkmann *et al.*, 2012) and the SoxXA enzyme catalyzes the formation of a sulfur-sulfur bond between thiosulfate and a cysteine residue (Friedrich *et al.*, 2001). A rhodanese-like reaction cycle has been depicted and discussed for the SoxXA protein (Bamford *et al.*, 2002; Hensen *et al.*, 2006). Our study on the *Mp*TsdBA structure (Chapter 2) revealed that a thiosulfate ion is covalently bound to Sγ of the heme-ligating cysteine in the active site and thereby unambiguously proved that catalysis of thiosulfate oxidation by Tsd(B)A enzymes and very probably also that by SoxXA proteins involves formation of a covalent adduct between the sulfane sulfur atom of thiosulfate and the Sγ of the active site cysteine (Kurth, Brito *et al.*, 2016). As sulfite is structurally very similar to thiosulfate and is known to be a strong inhibitor of various thiosulfate dehydrogenases (Lyric and Suzuki, 1970; Schook and Berk, 1979; Meulenberg *et al.*, 1993; Hensen *et al.*, 2006) this sulfur compound was used to obtain a better understanding of the TsdA reaction mechanism using UV-vis spectroscopy, spectroelectrochemical experiments and protein film electrochemistry (PFE).

Before getting a closer insight into the TsdA reaction mechanism, it is important to understand the heme iron ligation of the two *Cj*TsdA hemes. In a previous work (Chapter 3), analysis of *Cj*TsdA heme ligation was initiated by UV-vis spectroscopy of several enzyme variants with altered heme environment (Kurth, Butt *et al.*, 2016). UV-vis spectra of a *Cj*TsdA C138G variant revealed appearance of a 622 nm peak. Such a low-intensity spectral feature in the oxidized spectrum is indicative of the presence of high-spin heme either with water as a sixth ligand or with five-coordinate iron (Moore and Pettigrew, 1990; Miles *et al.*, 1993). High-spin heme generation in *Cj*TsdA C138G is caused by absence of the sixth heme ligand

in at least one of the two TsdA hemes. Thus cysteine is the sixth heme iron ligand of the active site heme, Heme 1, in *Cj*TsdA being in accordance with Heme 1 ligation in *Av*TsdA (Brito *et al.*, 2015) and *Mp*TsdBA (Kurth, Brito *et al.*, 2016). This finding was supported and Heme 1 ligation further analysed by nIR-MCD spectroscopy and X-ray diffraction described in this chapter. UV-vis spectra of *Cj*TsdA M255G also show a similar 622 nm charge transfer band indicative of high-spin ferrous heme, implying that Met^{255} is a heme ligand in the oxidized wildtype enzyme (Kurth, Butt *et al.*, 2016). Moreover, spectra of *Cj*TsdA feature a 700 nm peak indicative of methionine as heme iron ligand (Miles *et al.*, 1993). This peak is absent in the oxidized spectrum of the *Cj*TsdA M255G variant consistent with the assignment of Met^{255} as the sixth heme iron ligand of the *Cj*TsdA electron transfer heme, Heme 2, at least in the oxidized state. This is in contrast to *Av*TsdA Heme 2 where lysine is the sixth ligand in the oxidized protein and a ligand change to methionine occurs upon heme reduction (Brito *et al.*, 2015). His/Met ligation at Heme 2 of *Cj*TsdA was confirmed and further analyzed by nIR-MCD spectroscopy and X-ray diffraction included in this chapter. The sixth heme iron ligand of each of the two hemes was shown to be indispensable for efficient enzyme function *in vitro* and *in vivo* (Kurth, Brito *et al.*, 2016).

Next to Met^{255} there are two amino acids with the potential to interact with *Cj*TsdA Heme 2 iron, namely Asn^{254} and Lys^{252}. Indeed, these amino acid residues are located in close vicinity of Heme 2 iron as revealed by the crystal structures of *Cj*TsdA wildtype and variant proteins presented in this chapter. Exchange of Asn^{254} by glycine or lysine, the latter mimicing the ligand situation at Heme 2 in *Av*TsdA, and Lys^{252} by glycine did not lead to altered UV-vis spectroscopic characteristics in comparison to the wildtype protein (Kurth, Butt *et al.*, 2016). Exchange of Cys^{138} by methionine and histidine, led to an increase in the Soret peak intensity (Kurth, Butt *et al.*, 2016) consistent with replacement of Cys^{138} with these established stronger field ligands (Girvan *et al.*, 2007). In addition, a high-spin heme feature was not observed. This indicates that histidine and methionine can indeed ligate Heme 1 iron. In the previously described experiments dithionite was used to record spectra of fully reduced protein. As dithionite is a sulfur compound and TsdA catalyzes oxidation and reduction of sulfur compounds, this reducing agent is not optimal for recording UV-vis spectra with TsdA. For this reason the non-sulfur compound $EuCl_2$ in combination with EGTA was used for TsdA reduction in the experiments presented in this chapter. $Eu^{III/II}$-EGTA was shown to be a powerful reducing agent of protein active sites with a redox potential of about -0.88 V at pH 8 (Vincent *et al.*, 2003). Moreover, all UV-vis spectra depicted in this chapter were recorded under anoxic conditions to avoid the interaction of oxygen with heme ligands or heme iron itself.

As a detailed analysis of the redox properties of TsdA enzymes has not been performed so far, but is indispensable for understanding of TsdA catalysis and reaction mechanism, the

heme ligation of *Cj*TsdA was analyzed in more detail and complemented by research on the redox properties of the hemes. *Av*TsdA was found to be redox active between -300 mV and +150 mV (Kurth, Brito *et al.*, 2016). For a first insight into the redox properties of *Cj*TsdA the mild reducing agent ascorbate was used in nIR-MCD spectroscopy and UV-vis spectroscopy. As the reduction potential of ascorbic acid at pH 7 and 25°C is known to be -81 mV (Fruton, 1934), ascorbate can only partly reduce TsdA and therefore reveals which of the two hemes possesses the more positive and which the more negative redox potential. A detailed study of the *Cj*TsdA redox properties was performed by spectroelectrochemical experiments with TsdA bound on optically transparent SnO_2 electrodes. As we have previously shown that, structural differences in the immediate environment of *Cj*TsdA Heme 2 contribute to defining the reaction directionality of the enzyme (Kurth, Butt *et al.*, 2016), it was important to analyze the impact of the heme redox properties of the *Cj*TsdA variants on the reaction directionality of these enzymes. For this reason the catalytic properties of *Cj*TsdA wildtype and variant proteins were set in relation to their redox properties.

In conclusion, this study aimed at obtaining further insight into the *Cj*TsdA reaction mechanism. The heme environment of the two TsdA hemes was analysed in detail and the redox properties of the two hemes were elucidated. Moreover, the interaction of substrate and protein was studied by using sulfite as a substrate mimic and analyzing alteration of TsdA heme ligation, redox properties and catalysis. For this purpose X-ray crystallization, UV-vis spectroscopy, nIR-MCD spectroscopy, spectroelectrochemical experiments and protein film voltammetry were performed.

Material & Methods

Protein production

Construction of expression plasmids as well as protein production and purification of *Cj*TsdA wildtype and variant proteins was performed as described in Kurth, Butt *et al.*, 2016.

UV-vis spectroscopy with TsdA in solution

UV-vis spectra were recorded with an Analytik Jena Specord 210. Spectra were recorded in a 0.5 mL quartz glass cuvette filled with 50 mM Bis Tris buffer pH 6.5/100 mM ammonium acetate buffer pH 5 plus 8 µM protein, closed with a rubber stopper and purged with N_2 for 10 min. All solutions for protein oxidation and reduction were made anoxic by sparging with N_2. For oxidized protein spectra up to 30 µM ferricyanide were added if necessary. The proteins were partly reduced with up to 8 mM ascorbate until no further reduction could be detected. For full reduction of the proteins up to 0.9 mM $EuCl_2$ (1:1 mixture with EGTA) were added to the protein solution until no further reduction could be observed. In the case of spectra with imidazole up to 7.5 mM imidazole were added to the oxidized protein and in case of spectra with sulfite up to 5 mM sulfite were used.

Spectroelectrochemistry with TsdA adsorbed on a mesoporous nanocrystalline SnO_2 electrode

This method was performed by Julia Kurth in the laboratory of Julea Butt at the University of East Anglia (Norwich, U.K). An optically transparent mesoporous nanocrystalline SnO_2 electrode coated with *Cj*TsdA wildtype or variant protein was prepared using the previously described method (Marritt *et al.*, 2008) with adsorption from a solution of 80 to 105 µM *Cj*TsdA, 50 mM NaCl, 50 mM HEPES, pH 7. A three electrode system with a SnO_2 working electrode, a Ag/AgCl reference electrode and a platinum counter electrode was used as shown in Figure 1.

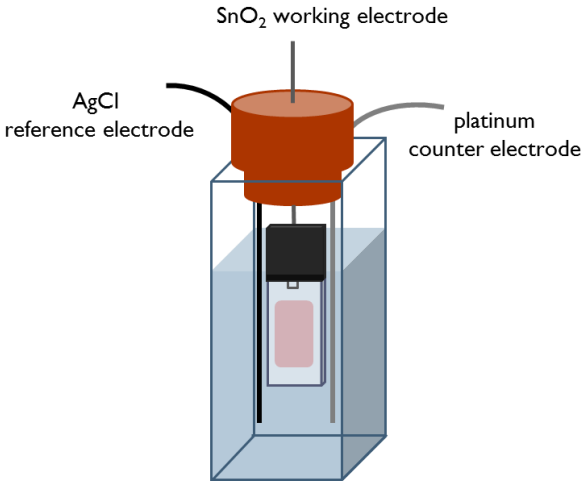

Figure 1: Set-up for spectroelectrochemistry experiments. An optically transparent mesoporous nanocrystalline SnO_2 working electrode coated with *Cj*TsdA, a platinum electrode and a Ag/AgCl electrode were placed in 100 mM ammonium acetate buffer pH 5 with 50 mM NaCl and closed with a rubber stopper in a N_2-filled chamber under anoxic conditions. The cuvette was placed in a spectrophotometer and the electrodes were connected to a potentiostat so that the redox-state of the bound protein could be altered by changing the potential.

The enzyme-coated electrode was rinsed with 100 mM ammonium acetate buffer pH 5 with 50 mM NaCl to remove unbound protein, taken into a N_2-filled chamber (atmospheric O_2 < 2 ppm) and immersed in an anaerobic solution of the same composition within a previously described spectroelectrochemical cell (Marritt *et al.*, 2008). The cell was sealed, removed from the anaerobic chamber and inserted into a JASCO V650 UV-visible spectrophotometer thermostated at 4°C and flushed with argon to maintain anaerobicity. Spectral contributions from light scattering by the electrode were minimized by placing a bare SnO_2 electrode (i.e., having no adsorbed enzyme) in the reference beam of the spectrophotometer. The electrode had been poised at approximately +380 mV (Autolab PGSTAT20 Potentiostat) for up to 30 min until the UV-vis spectrum revealed that the enzyme was completely oxidized. To determine the redox activity of TsdA increasingly negative potentials were applied to the electrode until the protein was fully reduced and then increasingly positive potentials were applied to the electrode until the protein was maximally oxidized. The electrode potential was swept from approximately +380 to -700 mV at a scan rate of 5 mV s^{-1} with a pause of 180 s every 50 mV. After each pause a spectrum was recorded (software: Jasco Spectra Manager) before the scan continued. Reoxidation of the sample was performed in a similar manner. Spectra are presented after equating absolute absorbance at 600 nm in order to account for potential dependent changes in the spectral contributions that arise from scattering by the electrode material. Absorbance at 553 nm, corresponding to the maximum of the α-peak of *Cj*TsdA, was used for indication of the redox state of the protein. In the plots shown in this chapter the maximal absorbance at 553 nm, indicative of fully reduced protein, was set to one and the minimal absorbance at 553 nm, indicative of fully oxidized protein, was set to zero. At 553 nm mainly absorbance changes of low-spin hemes can be observed.

Near-infrared Magnetic Circular Dichroism (nIR-MCD)

By CD spectroscopy the difference in intensity between left and right circularly polarized light is measured. In MCD spectroscopy this measurement is performed with the sample placed in a strong magnetic field parallel to the direction of propagation of the circularly polarized light. The MCD spectrometer consists of a spectropolarimeter and the detector. The sample is placed in the field of a superconducting magnet positioned between the light source and detector. It has been shown by Stephens and colleagues (Cheng *et al.*, 1973; Stephens *et al.*, 1976; Rawlings *et al.*, 1977) that MCD spectroscopy in the near-infrared region (800-2000 nm) can be used to study axial ligation of cytochromes (Simpkin *et al.*, 1989). MCD in the visible and ultraviolet region is dominated by porphyrin π-π* transitions whose energies depend only weakly on the axial ligands. In contrast, the electronic transitions of low-spin ferric hemes in the near-infrared region can be assigned to porphyrin (π) to metal (d) charge-transfer excitations, the energies of which are determined by the chemical identities of the axial heme ligands. Thus it is possible to identify the axial ligation of hemes by fingerprinting using the position and shape of signals in the nIR region compared to previously recorded spectra of known ligation. Some charge transfer bands exhibit a vibrational shoulder to shorter wavelength. Because water also has absorbance features at 1450 nm and 2000 nm which can obscure heme charge transfer bands, nIR MCD samples are usually prepared in D_2O.

NIR-MCD spectroscopy was performed as described in Bradley *et al.*, 2012 by Myles Cheesman at the University of East Anglia (Norwich, U.K). Proteins were produced and nIR-MCD samples prepared by Julia Kurth. Samples of *Cj*TsdA wildtype (~147 µM), *Cj*TsdA M255G (~115 µM) and *Cj*TsdA C138H (~150 µM) were prepared in 50 mM HEPES, 100 mM NaCl, D_2O, pH*7 (where pH* is the apparent pH of the D_2O solution determined using a standard glass pH electrode). UV-vis spectroscopy revealed all proteins to be fully oxidized before nIR-MCD spectroscopy. After recording the oxidized nIR-MCD-spectrum of the wildtype protein excess of ascorbate was added for analysis of the *Cj*TsdA redox properties. Before performing nIR-MCD spectroscopy, the UV-vis spectrum of this sample was recorded and showed that the protein was partly reduced.

Protein film electrochemistry (PFE)

Protein film electrochemistry (PFE) was performed by Julia Kurth in the laboratory of Julea Butt at the University of East Anglia (Norwich, U.K) using the method described in Kurth *et al.*, 2015. Cyclic voltammograms were measured under identical conditions using a graphite electrode coated with enzyme prior to placement in the buffer solution (100 mM ammonium acetate buffer with 50 mM NaCl, pH 5). Aliquots of thiosulfate or tetrathionate were then added as indicated. Catalytic currents (i_{cat}) due to the activity of the enzyme were defined by

subtraction of the response of the bare electrode from that of the enzyme coated electrode. The dependence of i_{cat} on potential was independent of whether the scan was to more negative, or more positive, potentials. For analysis of TsdA inhibition by sulfite, either 8 mM thiosulfate or 0.3 mM tetrathionate (maximal enzyme activity can be measured at those concentrations) were added to the buffer solution before PFE was performed and during cyclic voltammetry increasing amounts of sulfite were added. For detailed studies of sulfite inhibition the electrode coated with TsdA was placed in buffer containing varying concentrations of sulfite. Afterwards increasing amounts of thiosulfate or tetrathionate were added. The change in catalytic current was measured at a constant potential of 0.2 V vs. SHE (Standard hydrogen electrode) in the case of thiosulfate oxidation and 0 V vs. SHE in the case of tetrathionate reduction (Chronoamperometry).

Enzyme activity assays with *Cj*TsdA M255G in the presence of imidazole

Tetrathionate reduction and thiosulfate oxidation catalyzed by *Cj*TsdA M255G were performed as described in Kurth, Butt *et al.*, 2016. In activity assays with imidazole the 60 µM protein was pre-incubated for 10 min with 11 mM imidazole before addition to the reaction mixture. For comparison enzyme activity without imidazole addition was measured immediately prior to this.

Crystallization, structure determination and refinement

Crystallization, structure determination and refinement were performed by José Brito (Universidade Nova de Lisboa, Portugal) applying methods described for *Av*TsdA in Brito *et al.*, 2015. Proteins were supplied by Julia Kurth.

Results

Heme ligation

The amino acid sequence of *Cj*TsdA is similar to that of *Av*TsdA (Liu *et al.*, 2013) with 42 % sequence identity. In addition, X-ray crystallization of *Cj*TsdA revealed high structural similarity to *Av*TsdA (Figure 2A). Especially the N-terminal Heme 1-containg domains overlay quite well (Figure 2A, Figure 2B blue domain). This finding is not surprising as this domain contains the active site of TsdA (Brito *et al.*, 2015).

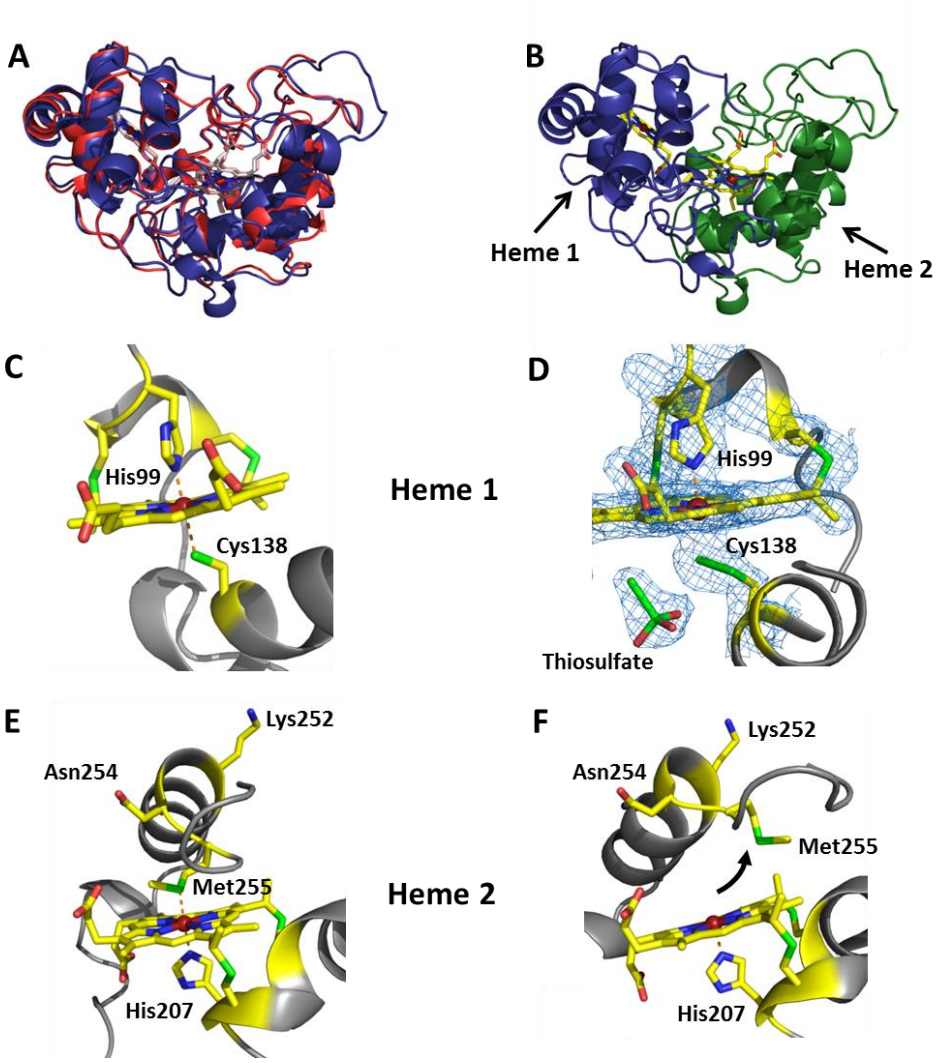

Figure 2: Crystal structure of *Campylobacter jejuni* TsdA. A) Structural superposition of *Campylobacter jejuni* TsdA (red) with *Allochromatium vinosum* TsdA (blue) with *Av*TsdA hemes shown in pink and *Cj*TsdA hemes in white. B) *Cj*TsdA overall fold with N-terminal Heme 1-containing domain represented in blue and C-terminal Heme 2-containing domain in green. C) Heme 1 is coordinated by His^{99} and Cys^{138}. D) The crystal structure of *Cj*TsdA K252G incubated with thiosulfate revealed Heme 1 to be coordinated by His^{99} and a persulfurated Cys^{138} with a thiosulfate molecule in close vicinity to the heme iron. Electron density map is shown. E) Heme 2 of *Cj*TsdA wt is coordinated by His^{207} and Met^{255}. F) In some crystals there is no amino acid ligating Heme 2 iron, but Met^{255}, Asn^{254} and Lys^{252} are in close vicinity to Heme 2. With the exception of the *Cj*TsdA K252G structure all structures show *Cj*TsdA in the "as isolated" state. Cartoon representation is shown in pale grey with heme moieties and coordinating amino acid residues colored by atom type (yellow for carbon, blue for nitrogen, red for oxygen, dark red for iron and green for sulfur). Crystallization, structure determination and refinement were performed by José Brito (Universidade Nova de Lisboa, Portugal).

In contrast, there are some structural differences in the Heme 2-containing C-terminal domains of *Cj*TsdA and *Av*TsdA. This might be due to the fact that Heme 2 is the electron transfer heme and the electron acceptor/donor interacting with this C-terminal domain is different in case of *Cj*TsdA and in case of *Av*TsdA: The most likely electron acceptor of *Av*TsdA is a high potential iron-sulfur protein HiPIP (Kurth, Brito *et al.*, 2016) whilst the most likely electron donor of *Cj*TsdA is a monoheme cytochrome *c* (Liu *et al.*, 2013). Similar to *Av*TsdA there is only a short distance between the two *Cj*TsdA hemes enabling fast electron transfer. Moreover, the heme ligation of *Cj*TsdA Heme 1 is similar to that in *Av*TsdA (Brito *et al.*, 2015) and *Mp*TsdBA (Kurth, Brito *et al.*, 2016): *Cj*TsdA Heme 1 is ligated by His^{99} and Cys^{138} (Figure 2C). In addition, Cys^{138} was found to be persulfurated and a thiosulfate molecule was observed in close vicinity of Heme 1 iron in some *Cj*TsdA crystal structures after incubation with thiosulfate (Figure 2D). Persulfuration of the Heme 1-ligating cysteine in a distinct portion of TsdA and a thiosulfate molecule in close vicinity to Heme 1 iron were also found to be present in crystals of *Av*TsdA (Brito *et al.*, 2015). Thus, Heme 1 was unambiguously identified as the active site heme not only in *Av*TsdA but also in *Cj*TsdA. In contrast to the His/Cys-ligated Heme 1, heme ligation of Heme 2 iron differs in *Cj*TsdA and in *Av*TsdA (Brito *et al.*, 2015): Heme 2 iron is ligated by Met^{255} in “as isolated” *Cj*TsdA (Figure 2E). The sixth heme iron ligand of *Av*TsdA is lysine in the oxidized state being replaced by methionine upon reduction. Interestingly, one crystal structure of *Cj*TsdA revealed Heme 2 iron not to be ligated by any amino acid residue (Figure 2F). The loop containing Met^{255} is twisted indicating a surprising flexibility of this loop. Similar to the ligand change observed in *Av*TsdA, movement of the Heme 2-ligating methionine out of the heme iron coordination sphere appears to be possible in *Cj*TsdA. The flexible loop at Heme 2 exhibits two further amino acids with the potential to interact with heme iron that are located in close vicinity of Heme 2 iron: Asn^{254} and Lys^{252}. However, so far there is no crystal structure indicating that one of those amino acids is able to ligate Heme 2 iron.

To analyze the impact of Cys^{138} on Heme 1 and Met^{255}, Asn^{254}, Lys^{252} on Heme 2, *Cj*TsdA variants were produced with those amino acids exchanged by glycine which does not have the potential to ligate heme iron. Those *Cj*TsdA variants were used for X-ray crystallization (Table 1 and Figure 3).

Table 1: The sixth heme iron ligands of *Cj*TsdA wildtype and variants. The heme coordination of *Cj*TsdA wt and variants was revealed by X-ray crystallography. In *Cj*TsdA N254G and some crystals of the M255G variant an imidazole-like molecule was observed in vicinity of Heme 2 iron. In case of *Cj*TsdA M255G some crystals exhibited His/H_2O ligation and some His/imidazole ligation at Heme 2. In case of *Cj*TsdA wildtype the sixth heme iron ligand of Heme 2 was either Met^{255} or no ligand was present.

	***Cj*TsdA**	**Heme 1**	**Heme 2**
	wildtype	Cys^{138}	Met^{255} or no ligand
Heme 1 ligation affected	C138G	H_2O	Met^{255}
	M255G	Cys^{138}	H_2O or imidazole
Heme 2 ligation affected	N254G	Cys^{138}	imidazole
	K252G	Cys^{138}	Met^{255}

In *Cj*TsdA C138G, where Cys^{138} is replaced by glycine, Heme 1 is found to exhibit a water molecule ligating Heme 1 iron (Table 1 and Figure 3A) in place of Cys^{138} as in *Cj*TsdA wt (Figure 2C). Similarly, In *Cj*TsdA M255G, where Met^{255} is replaced by glycine, Heme 2 is found to exhibit a water molecule ligating Heme 2 iron (Table 1 and Figure 3B) in place of Met^{255} as in *Cj*TsdA wt (Figure 2D). Hemes that do not exhibit a proteinaceous sixth heme iron ligand as observed for *Cj*TsdA C138G and M255G are referred to as high-spin hemes.

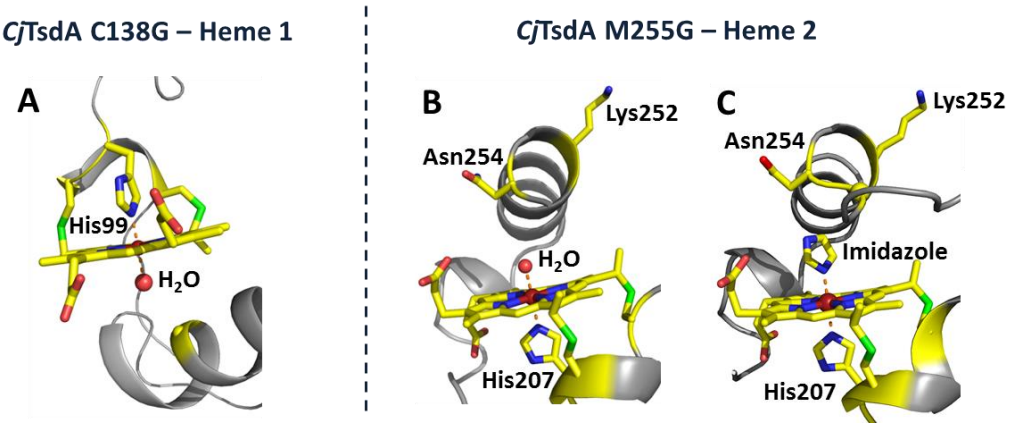

Figure 3: Heme coordination in *Cj*TsdA variants. In the *Cj*TsdA C138G "as isolated" structure Heme 1 is coordinated by His^{99} and a water molecule (A). In case of the *Cj*TsdA M255G "as isolated" structure Heme 2 is coordinated by His^{207} and either a water molecule (B) or an imidazole-like molecule (C). Cartoon representation is shown in pale grey with heme moieties and coordinating amino acid residues shown as sticks and colored by atom type (yellow for carbon, blue for nitrogen, red for oxygen, dark red for iron and green for sulfur). Crystallization, structure determination and refinement were performed by José Brito (Universidade Nova de Lisboa, Portugal).

*Cj*TsdA N254G as well as several crystal structures of *Cj*TsdA M255G revealed an imidazole-like molecule to ligate Heme 2 iron instead of Met^{255} (Table 1 and Figure 3C). This

indicates that in a certain population of *Cj*TsdA proteins an imidazole-like molecule is present. In *Cj*TsdA K252G heme ligation is not altered at Heme 2 in comparison to the wildtype protein (Table 1). Moreover, high flexibility in the amino acid environment of Heme 2 is shown as Met^{255} can be replaced by an imidazole-like molecule when Asn^{254} is exchanged by glycine.

The study of *Cj*TsdA heme ligation was extended using nIR-MCD spectroscopy with TsdA wildtype and variant proteins. It has been shown by Stephens and colleagues (Cheng *et al.*, 1973; Stephens *et al.*, 1976; Rawlings *et al.*, 1977) that MCD spectroscopy in the near-infrared region (800-2000 nm) is a good method to study axial ligation of cytochromes. This method was performed with *Cj*TsdA wildtype, *Cj*TsdA C138G and *Cj*TsdA M255G.

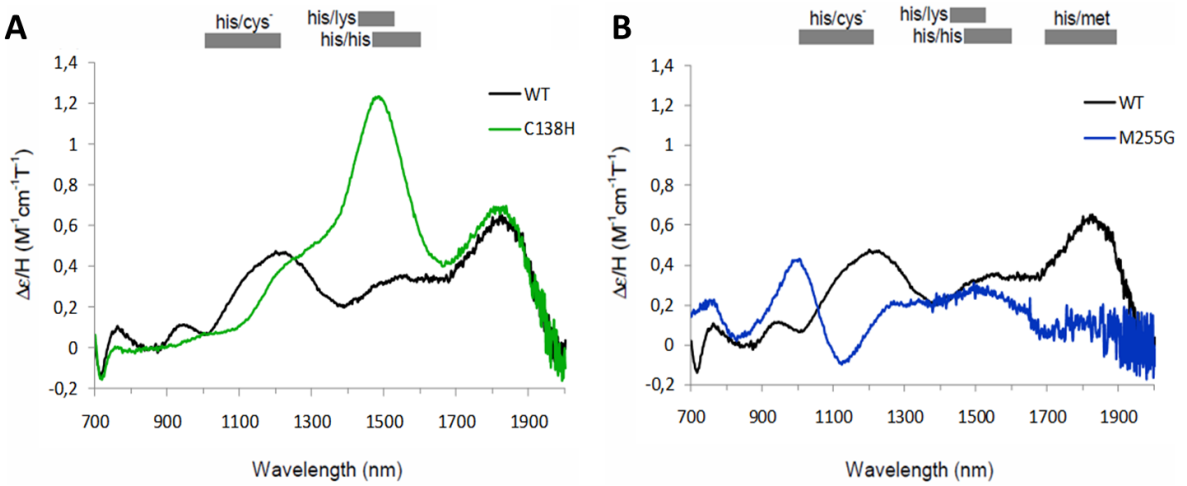

Figure 4: NIR-MCD spectra of TsdA wt and TsdA derivatives. Approximately 150 µM *Cj*TsdA wt, *Cj*TsdA M255G and *Cj*TsdA C138H were used for nIR-MCD in 50 mM HEPES and 50 mM NaCl in D_2O pH^*7. The nIR-MCD spectrum of the wildtype protein is shown in comparison to that of *Cj*TsdA C138H (A) and *Cj*TsdA M255G (B). The observed charge transfer bands were compared to those described for hemes with His/Lys ligation (1480-1550 nm), His/His or His/imidazole ligation (1500-1630 nm), His/Met ligation (1740-1950 nm) and His/thiolate ligation (1035-1200 nm) (Gadsby and Thomson, 1990). NIR-MCD was performed by Myles Cheesman in Norwich.

The nIR-MCD spectrum of *Cj*TsdA wildtype (Figure 4) shows a band at 1200 nm that is characteristic for His/Cys ligation (Gadsby and Thomson, 1990). In case of *Cj*TsdA C138H this band is replaced by a band at 1480 nm characteristic for bis-nitrogenous ligation, which is presumed to be His/His (Figure 4A; Gadsby and Thomson, 1990) as no lysine residues are nearby in the crystal structures. Thus Cys^{138} was identified as the sixth heme iron ligand of *Cj*TsdA Heme 1 confirming that the observations from X-ray crystallography (Figures 2C and 3A) are also present in solution. Moreover, the nIR-MCD spectrum of *Cj*TsdA wildtype shows a band at 1820 nm that is characteristic for His/Met-ligation (Gadsby and Thomson, 1990) with a vibrational shoulder at 1400-1700 nm. In case of *Cj*TsdA M255G the 1820 nm band disappears and a positive band at 900 nm as well as a negative band at 1100 nm appear that are characteristic for high-spin Fe^{III} population and indicative of His/H_2O ligation

(Figure 4B) (Eglinton *et al.*, 1983). This proves that Met^{255} is the sixth heme iron ligand of *Cj*TsdA Heme 2, at least in the oxidized state, confirming results from X-ray crystallography (Figures 2D and 3B). There is a small band at 1400-1700 nm indicative of bis-nitrogenous ligation (Gadsby and Thomson, 1990) indicating that there might be some heme population with His/Lys ligation from Lys^{252} at Heme 2 or an imidazole-like molecule as observed in some crystal structures (Figure 2E, 2F and 3C). His/His ligation can be excluded, as there are no histidine residues in close vicinity of Heme 1 or Heme 2 iron. Another important observation is that the 1200 nm His/Cys$^-$ band disappears in the *Cj*TsdA M255G nIR-MCD spectrum in contrast to the crystal structure where Cys^{138} remains ligated (Table 1). If changes in Heme 2 ligation can influence the ligation at Heme 1 this may indicate some level of cooperativity between the two hemes.

Redox properties

For a first insight into the redox properties of *Cj*TsdA nIR-MCD spectroscopy was performed with the *Cj*TsdA wildtype protein in presence and absence of the mild reducing agent ascorbate. The UV-vis spectrum of this sample revealed ascorbate to generate semi-reduced protein (data not shown). With the nIR-MCD spectroscopy of *Cj*TsdA in the presence of ascorbate we aimed to elucidate which of the two TsdA hemes can be reduced by asorbate pointing to a more positive reduction potential and which heme cannot be reduced by ascorbate pointing to a more negative reduction potential.

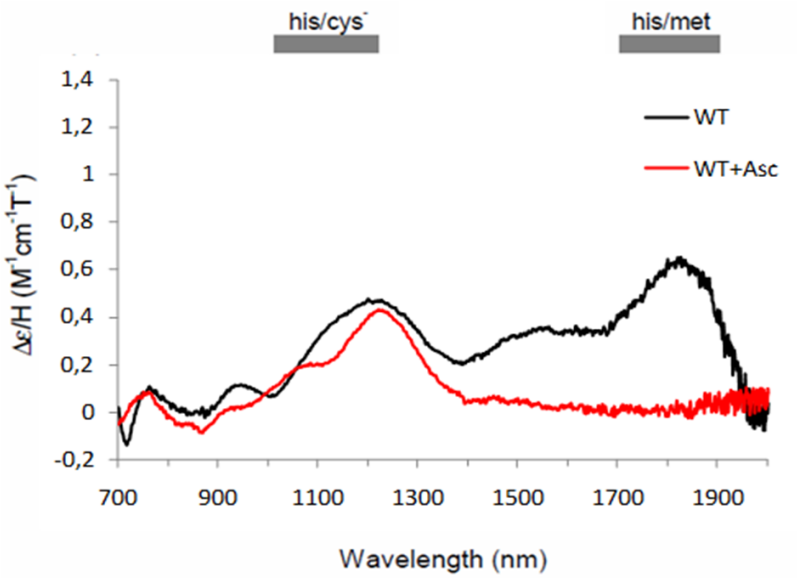

Figure 5: NIR-MCD spectra of TsdA wt and TsdA derivatives. Approximately 150 µM *Cj*TsdA wt were used for nIR-MCD in 50 mM HEPES and 50 mM NaCl in D_2O pH*7. *Cj*TsdA wt was partly reduced with excess of ascorbate to identify the positive potential heme ligand. The observed charge transfer bands were compared to those described for hemes with His/Lys ligation (1480-1550 nm), His/His or His/imidazole ligation (1500-1630 nm), His/Met ligation (1740-1950 nm), His/thiolate ligation (1035-1200 nm) (Gadsby and Thomson, 1990). NIR-MCD was performed by Myles Cheesman in Norwich.

Incubation with ascorbate led to a disappearance of the His/Met band in the nIR-MCD spectrum (Figure 5) indicating reduction of Heme 2. Thus, Heme 2 can be identified as the *Cj*TsdA heme with the more positive reduction potential. As ascorbate has a reduction potential of -81 mV at pH 7 (Fruton, 1934), the reduction potential of Heme 2 is assumed to be more positive than this value and the reduction potential of Heme 1 more negative.

The redox properties of *Cj*TsdA wildtype and variant proteins were further analyzed by UV-vis spectroscopy at pH 6.5 with ascorbate as a mild reducing agent and $Eu^{III/II}$-EGTA as strong reducing agent. The reduction potential of ascorbic acid at pH 6.5 and 25°C is -51 mV (Fruton, 1934). Spectra of ascorbate reduced proteins were compared to those of oxidized proteins and proteins fully reduced by $EuCl_2$-EGTA. $Eu^{III/II}$-EGTA has a reduction potential of -0.88 V at pH 8 (Vincent *et al.*, 2003), i.e. about -0.79 V at pH 6.5 as an increase of 59 mV per decreasing pH unit is predicted (Vincent *et al.*, 2003). Unless the reduction potential of the His/Cys^- heme is unusually low, $EuCl_2$-EGTA should be able to fully reduce *Cj*TsdA.

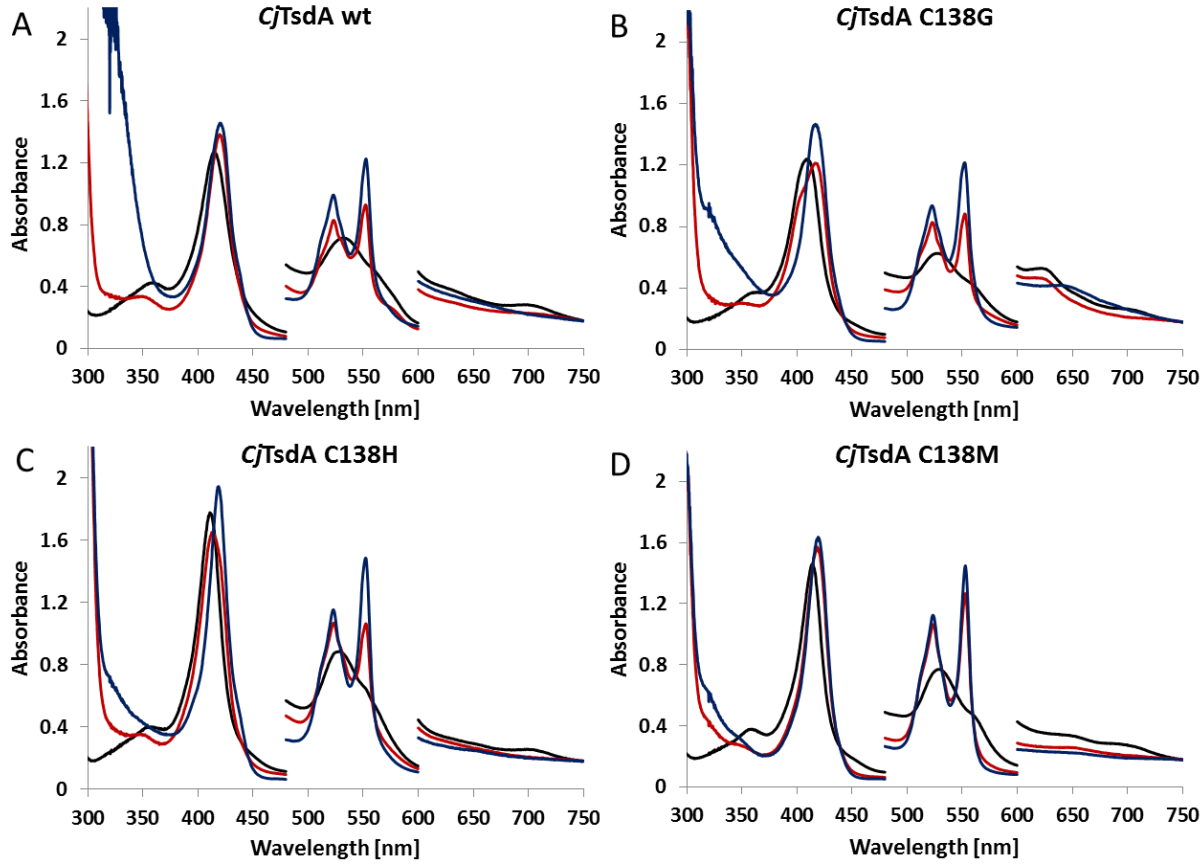

Figure 6: UV-vis spectra of *Cj*TsdA wt and variants with differing Heme 1 ligation in the presence of ascorbate. Spectra were recorded under anoxic conditions with 8 µM TsdA in 50 mM Bis Tris buffer pH 6.5. For oxidation of the enzymes up to 30 µM ferricyanide were used (black line). For protein reduction up to 7.5 mM ascorbate (red line) and subsequently up to 0.7 mM $EuCl_2$-EGTA-solution (blue line) were added until no further reduction was observed. Spectra were normalized to 280 nm and 750 nm. Absorbance values in the region between 480 and 600 nm are scaled by a factor of 5 and values between 600 and 750 nm by a factor of 15.

UV-vis spectra of ascorbate reduced *Cj*TsdA wildtype and Heme 1 ligation-affected variants are shown in Figure 6. The intensities of α- β- and γ-peak of *Cj*TsdA wildtype reduced with ascorbate are lower than those observed for $Eu^{III/II}$-EGTA-reduced protein (Figure 6A). This indicates partial reduction of TsdA by ascorbate consistent with the nIR-MCD spectrum of ascorbate reduced *Cj*TsdA (Figure 5). For *Cj*TsdA C138G the 622 nm peak indicative of high-spin heme is seen for oxidized as well as for ascorbate reduced protein. This is consistent with His/H_2O ligation at Heme 1 (Figure 3A) and Heme 1 having a lower reduction potential than Heme 2. Spectra of *Cj*TsdA C138H and C138M do not show high-spin features consistent with histidine ligation at Heme 1 in the case of *Cj*TsdA C138H and methionine in case of *Cj*TsdA C138M (Kurth, Butt *et al.*, 2016). *Cj*TsdA C138G and C138H are reduced in a similar manner as seen for the wildtype protein indicating that exchange of cysteine by glycine or histidine does not increase the reduction potential of Heme 1 enough for it to become reduced by ascorbate. In contrast, *Cj*TsdA C138M is fully reduced by ascorbate. These observations are consistent with the His/Met-ligated Heme 2 having a reduction potential above -51 mV regardless of the ligation at Heme 1. Likewise this is also consistent with the His/Cys-ligated Heme 1 not being reduced by ascorbate and having a reduction potential below -51 mV. The observed results are in accordance with the results received from nIR-MCD spectroscopy with ascorbate reduced *Cj*TsdA.

UV-vis spectra of ascorbate reduced *Cj*TsdA wildtype and Heme 2 ligation affected variants are shown in Figure 7. *Cj*TsdA N254G, N254K and K252G are reduced in a similar manner as seen for *Cj*TsdA wt (Figures 7A and 7C-E) indicating that exchange of Asn^{254} and Lys^{252} does not have a strong impact on the redox state of Heme 2. In contrast, spectra of *Cj*TsdA M255G strongly deviate from those of the wildtype protein: The 622 nm feature in the oxidized and ascorbate reduced spectrum shows that the Met^{255} exchange by glycine results in five-coordinated high-spin heme (Figure 7B) as also seen in the crystal structure (Figure 3B). in the nIR-MCD spectrum (Figure 4B) and in UV-vis spectra (Kurth, Butt *et al.*, 2016) of this variant. The intensities of α- and β-peak are much lower and the shift of the Soret peak smaller for *Cj*TsdA M255G reduced with ascorbate in comparison to the equivalent spectrum of the wildtype protein indicating that this variant can only slightly be reduced by ascorbate. The exchange of the Heme 2 iron-ligating methionine leads to impaired reducibility by ascorbate indicating a more negative reduction potential of Heme 2 than the wildtype protein and thus confirming the His/Met-ligated Heme 2 to be the positive potential heme supporting the nIR-MCD results (Figure 5).

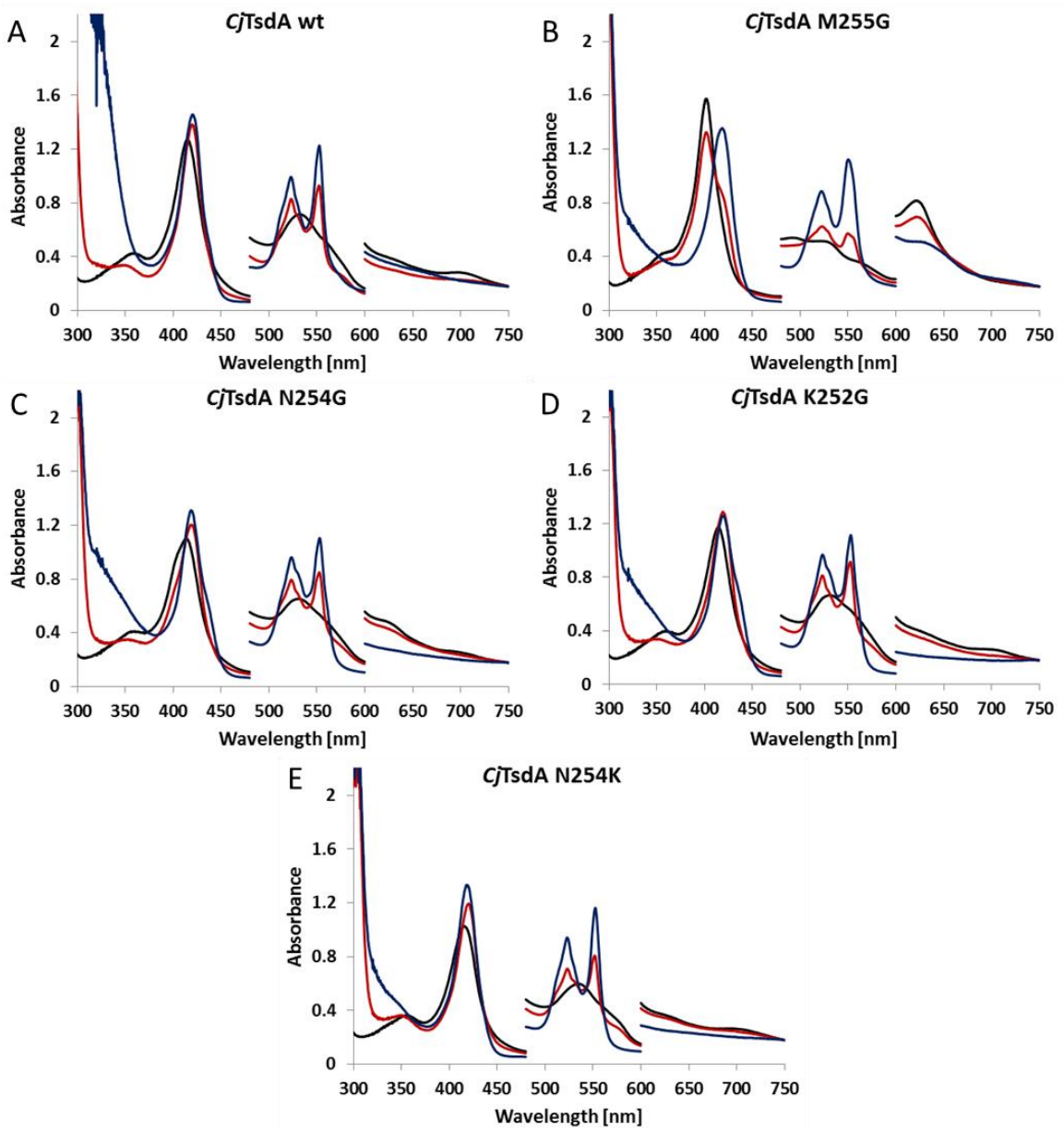

Figure 7: UV-vis spectra of *Cj*TsdA wt and variants with differing Heme 2 ligation in the presence of ascorbate. Spectra were recorded under anoxic conditions with 8 µM *Cj*TsdA in 50 mM Bis Tris buffer pH 6.5. For oxidation of the enzymes up to 30 µM ferricyanide were used (black line). For protein reduction up to 7.5 mM ascorbate (red line) and subsequently up to 0.7 mM $EuCl_2$-EGTA-solution (blue line) were added until no further reduction was observed. Spectra were normalized to 280 nm and 750 nm. Absorbance values in the region between 480 and 600 nm are scaled by a factor of 5 and values between 600 and 750 nm by a factor of 15.

As indicated by nIR-MCD spectroscopy (Figure 4) and revealed by X-ray crystallization (Figure 3C) of *Cj*TsdA an imidazole-like molecule is present in a distinct portion of *Cj*TsdA proteins. For this reason the impact of imidazole on heme ligation and redox properties of *Cj*TsdA wildtype and variants was analyzed by UV-vis spectroscopy (Figure 8).

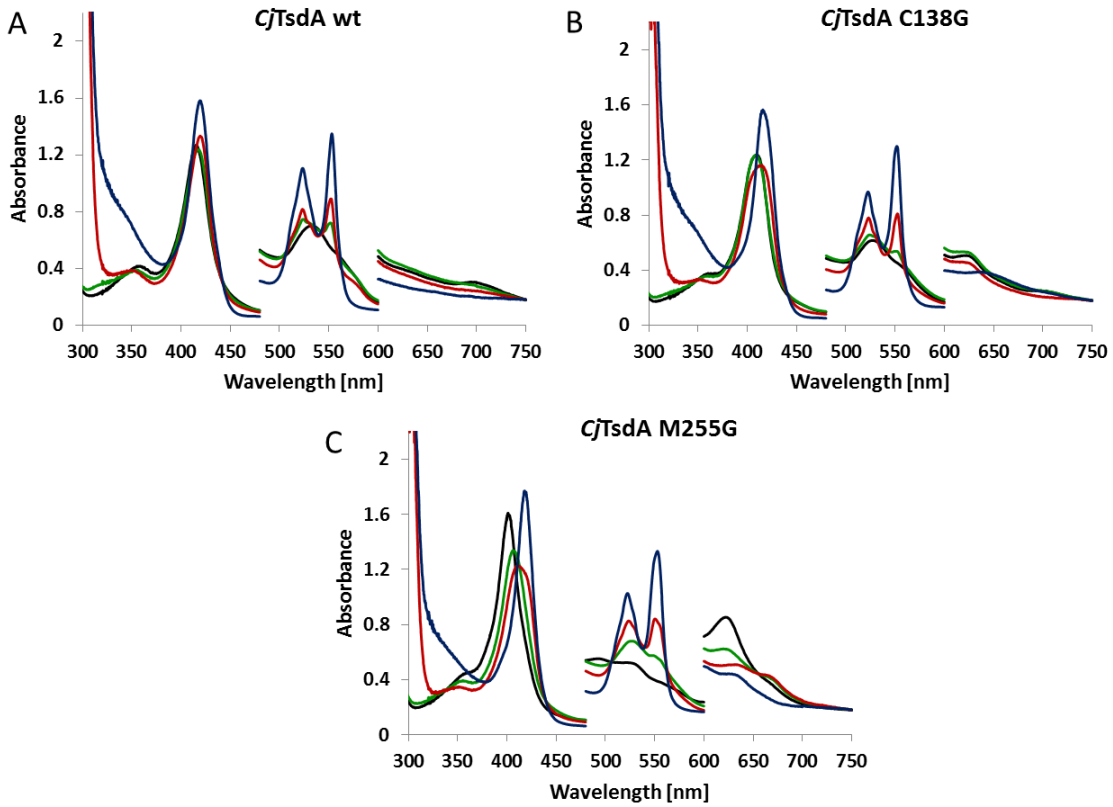

Figure 8: UV-vis spectra of *Cj*TsdA wt (A) as well as the C138G (B) and M255G (C) variant in the presence of imidazole. Spectra were recorded under anoxic conditions with 8 µM TsdA in 50 mM Bis Tris buffer pH 6.5. For oxidation of the enzymes up to 30 µM ferricyanide were used (black line). After recording the oxidized spectra up to 7.5 mM imidazole were added (green line) and subsequently the proteins were first reduced with up to 15 mM ascorbate (red line) and then with 0.7 mM EuCl2-EGTA-solution (blue line) until no further reduction could be observed. Spectra were normalized to 280 nm and 750 nm. Absorbance values in the region between 480 and 600 nm are scaled by a factor of 5 and values between 600 and 750 nm by a factor of 15.

*Cj*TsdA wildtype just shows slight reduction by imidazole, but no other changes are observed in the oxidized, ascorbate reduced and $EuCl_2$-EGTA reduced spectra (Figures 8A) in comparison to spectra without imidazole (Figure 6). The same is observed for *Cj*TsdA C138G (Figure 8B). As the *Cj*TsdA C138G variant still exhibits a high-spin feature at 622 nm it is obvious that imidazole cannot ligate Heme 1 iron. In contrast, imidazole addition strongly affects UV-vis spectra of *Cj*TsdA M255G (Figure 8C). Spectra of the oxidized variant show that the 622 nm high-spin feature decreases, the Soret band shifts to a higher wavelength and the combined α- and β-peak increases. The changes indicate that Heme 2 is not in the high-spin state anymore. Similar alterations of UV-vis spectral features were observed for a His39Ser derivative of cytochrome b_5 in the presence of imidazole (Wang *et al.*, 2003). UV-vis spectra of this variant revealed that the single heme of this cytochrome, which is in the high-spin state in absence of imidazole, resembles the spectrum of the wildtype protein after imidazole addition indicating hexa-coordinated, low-spin heme. The explanation for the observed changes in the UV-vis spectrum of *Cj*TsdA M255G in presence of imidazole is that imidazole has become the sixth heme iron ligand of Heme 2, because imidazole cannot

ligate Heme 1 iron as mentioned above. The slight 622 nm high-spin feature that is still observed is probably caused by the fact that cysteine is not ligating Heme 1 iron in a significant portion of this variant as revealed by nIR-MCD spectroscopy (Figure 4B). The increase of α- and β-peak in the ascorbate reduced spectrum of *Cj*TsdA M255G with imidazole in comparison to the equivalent spectrum without imidazole (Figure 7B) indicates that ascorbate leads to a stronger reduction of this variant in the presence of imidazole. Thus, the ligation of Heme 2 iron by imidazole results in a more positive reduction potential of Heme 2 in comparison to that of Heme 2 in the high-spin state observed for *Cj*TsdA M255G without imidazole. Previous experiments have shown that exchange of Met^{255} by glycine strongly impairs the specific activity of this *Cj*TsdA variant in comparison to the wildtype protein (Kurth, Butt *et al.*, 2016). Addition of imidazole to this variant and subsequent His/imidazole ligation at Heme 2 instead of high-spin heme led to the hypothesis that specific activity of *Cj*TsdA M255G increases in the presence of imidazole. Contrary to this hypothesis, enzymatic activity of the M255G variant did not improve in either catalytic direction after incubation of the enzyme with imidazole. One reason might be that cysteine is not ligating Heme 1 iron in a significant portion of the protein as mentioned before and thus enzyme activity cannot be regained when only heme iron ligation at Heme 2 is changed. Alternatively or additionally, the reduction potential of His/imidazole-ligated heme, which should be similar to His/His-ligated heme, is assumed to be more negative than that of His/Met-ligated heme (Reedy *et al.*, 2008) and this might cause impaired activity in comparison to the wildtype protein. In general, the capability of imidazole to act as sixth Heme 2 iron ligand supports the finding that some *Cj*TsdA crystal structures exhibit an imidazole-like substance in close vicinity of Heme 2 iron and that such an imidazole-like molecule has the potential to ligate Heme 2 iron.

To analyze the *Cj*TsdA redox properties in more detail spectroelectrochemical experiments with *Cj*TsdA wildtype and variants bound on a SnO_2 electrode were performed to determine the range of redox activity for each protein. During such experiments, the application of increasingly negative and then increasingly positive potentials to the electrode resulted in the complete reduction and then partial re-oxidation of the adsorbed wildtype enzyme (Figure 9A). The reductive and oxidative absorbance values, reflecting the concentrations of oxidised or reduced hemes of the protein upon reduction differ from those observed upon re-oxidation, i.e. hysteresis is found to be present for *Cj*TsdA. The reduced protein is slower re-oxidized and cannot be fully oxidized in this experiment. Hysteresis was also observed in spectroelectrochemical experiments with *Av*TsdA bound on a SnO_2 electrode (Kurth, Brito *et al.*, 2016). It was assumed that hysteresis is mainly caused by the ligand change occurring at *Av*TsdA Heme 2. In case of *Cj*TsdA there is no evidence for a ligand change from Met^{255} to another amino acid. The hysteresis, which is observed for *Cj*TsdA wildtype and also the

analysed variants, precluded fits to the Nernst equation. As a consequence, true E_m values could not be deduced. Nevertheless, clear trends were observed from which conclusions can be drawn.

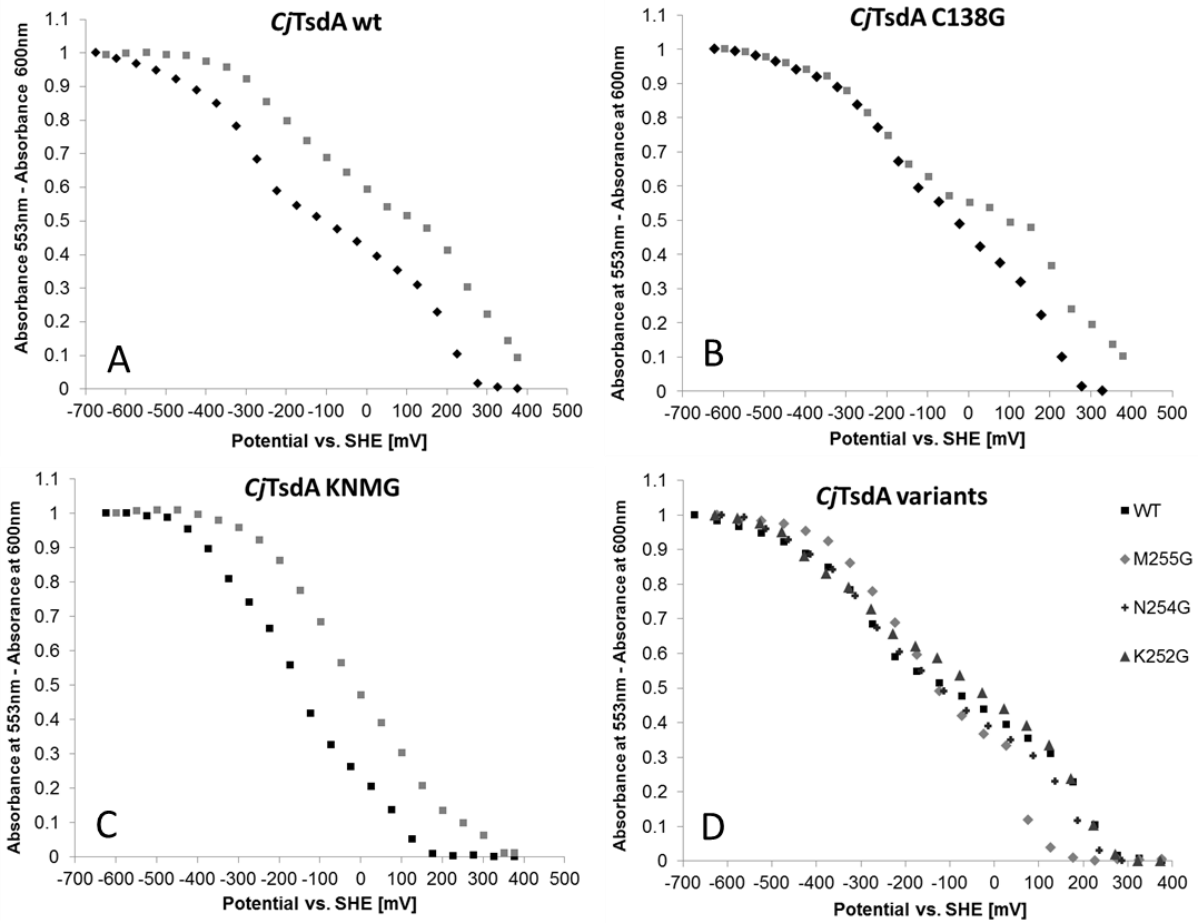

Figure 9: Spectroelectrochemistry with *Cj*TsdA wt and variants bound on a SnO_2 electrode. Absorbance at 553 nm is plotted against the potential with TsdA wt and variants bound on a SnO_2 electrode. Data collected uppon reduction (black diamonds) and oxidation (grey squares) of *Cj*TsdA wt (A), *Cj*TsdA C138G (B) and the *Cj*TsdA KNMG triple mutant (C) exhibits hysteresis. Redox behavior of TsdA variants with Heme 2 affected ligands upon reduction are compared to that of the wildtype protein (D). 100 mM ammonium acetate buffer pH 5 with 50 mM NaCl was used as Cl^- addition minimises any shifts in potential of the Ag/AgCl wire reference electrode. Experiments were performed by Julia Kurth in the laboratory of Julea Butt at the University of East Anglia (Norwich, U.K).

The redox activity of TsdA wildtype spans from approximately -650 mV to +300 mV (Figure 9A and Table 2). When Cys^{138} was exchanged by glycine, the reductive events observed below -100 mV changed (Figure 9B). Decreased hysteresis is observed caused by better reducibility of the protein in this potential range in comparison to the wildtype protein. The fact that reductive events observed below -100 mV changed in this Heme 1 ligation affected variant and the range of redox activity becomes less negative than for the wildtype protein (Figure 9B and Table 2) confirms Heme 1 to exhibit the more negative reduction potential. That hysteresis is reduced in the *Cj*TsdA C138G variant indicates that changes in Heme 1 ligation mainly cause the hysteresis. In the TsdA C138G variant Heme 1 is in the high-spin state as explained before. In vicinity of Heme 1 no other amino acids with the

potential to ligate heme iron are present besides Cys^{138} (Figure 2C). As Heme 1 is expected to be in the high-spin state in the oxidised as well as in the reduced state, no changes are expected at this heme which would complicate re-oxidation of Heme 1. In contrast the presence of Cys^{138} as Heme 1 ligand might complicate re-oxidation as Sγ of this residue has been shown to move out of the heme iron coordination sphere (Brito *et al.*, 2015). Moreover, protonation of Cys^- might occur upon reduction of the protein.

Table 2: Impact of alteration in Heme 1 and Heme 2 environment of *Cj*TsdA on range of redox activity. The range of redox activity of the *Cj*TsdA wildtype and variant proteins was determined by spectroelectrochemistry with the proteins bound on a SnO_2 electrode (Figure 9) upon reduction of the protein.

		***Cj*TsdA variant**					
		wildtype	**C138G**	**K252G**	**N254G**	**M255G**	**KNMG**
Range of redox activity [mV]	**minimum**	-650	-520	-620	-600	-500	-480
	maximum	+300	+300	+300	+280	+180	+180

In contrast to *Cj*TsdA C138G, the Heme 2 ligation affected variant *Cj*TsdA M255G showed notable differences in redox behaviour above -100 mV (Figure 9D) confirming Heme 2 as the positive potential heme. The range of redox activity of this variant is less positive than that of the wildtype protein (Figure 9D and Table 2). This finding is consistent with the results obtained by UV-vis spectroscopy when this variant was reduced by ascorbate (Figure 7B) indicating that an exchange of Met^{255} by glycine results in a more negative reduction potential of Heme 2. Interestingly, *Cj*TsdA M255G exhibits a less negative range of redox activity than observed for the wildtype protein (Figure 9D and Table 2) similar as seen for *Cj*TsdA C138G. This finding is in accordance with the nIR-MCD results which show that a significant portion of TsdA M255G Heme 1 is not ligated by cysteine anymore.

When amino acids other than Met^{255} in the vicinity of Heme 2 iron (Figure 9D) were changed, this had only a small impact on the redox behaviour of the enzyme and the range of redox activity of *Cj*TsdA N254G and K252G is quite similar to that of the wildtype protein (Figure 9D and Table 2). This indicates, that there is no ligand switch from Met^{255} to neither Asn^{254} nor Lys^{252}.

The KNMG triple mutant shows redox properties similar to the TsdA M255G variant (Figure 9C and Table 2) indicating that the exchange of Met^{255} has the greatest impact on the redox properties of *Cj*TsdA Heme 2. This is not surprising as an exchange of Asn^{254} and Lys^{252} by glycine did not alter the redox properties of Heme 2 and Met^{255} is assumed to be the only amino acid of those three residues acting as sixth ligand of Heme 2 iron. Besides

those three amino acids there are no amino acids in the vicinity of Heme 2 iron capable of ligating the iron atom. Thus, Heme 2 cannot be ligated by any proteinaceous ligand in the KNMG triple mutant. Only minimal absorbance at 553 nm arises from high-spin heme in comparison to low-spin heme, which can be seen for example in UV-vis spectra of the monoheme cytochrome *c*' from *Methylococcus capsulatus* exhibiting a high-spin heme center (Zahn *et al.*, 1996). The most straight forward explanation for the observed changes in absorbance at 553 nm would be the presence of low-spin heme. The absorbance changes which can be seen above -100 mV therefore can only be caused either by Heme 1 or by the presence of a non-proteinaceous ligand at Heme 2 like an imidazole-like molecule which is similar to a histidine ligand. In those cases low-spin heme would change absorbance at 553 nm.

Reaction mechanism

For a detailed study of the *Cj*TsdA reaction mechanism several experiments were performed with sulfite added to the protein. Sulfite is a substrate analogue to thiosulfate and has been reported to be a strong inhibitor of various thiosulfate dehydrogenases (Lyric and Suzuki, 1970; Schook and Berk, 1979; Meulenberg *et al.*, 1993; Hensen *et al.*, 2006). In a first approach, the impact of sulfite on the UV-vis spectroscopic characteristics of *Cj*TsdA was analyzed (Figure 10).

UV-vis spectra of the *Cj*TsdA wildtype protein (Figure 10A and 10B) show a blue shift of the soret band, a decrease of the combined α- and β-peak and a 622 nm high-spin feature after sulfite addition. As those features are indicative for the presence of high-spin heme (Moore and Pettigrew, 1990; Miles *et al.*, 1993; Girvan *et al.*, 2007) it can be concluded that sulfite causes the generation of high-spin heme in the *Cj*TsdA wildtype enzyme. To determine which of the two TsdA hemes interacts with sulfite, this sulfur compound was added to the Heme 1 ligation affected *Cj*TsdA variants C138G and C138H. Sulfite does not have an effect on the UV-vis spectra of those proteins (Figure 10C and 10D) in comparison to the spectra without sulfite (Figure 6B and 6C). This indicates that sulfite neither interacts with Heme 2 nor with Heme 1 when this heme is not ligated by cysteine. Thus, interaction of sulfite with Cys^{138} causes generation of high-spin heme in the *Cj*TsdA wildtype protein. The most probable explanation for this observation is that sulfite must cause a movement of Cys^{138} Sγ out of the Heme 1 iron coordination sphere and a strong interaction between sulfite and the Cys^{138} thus was proven.

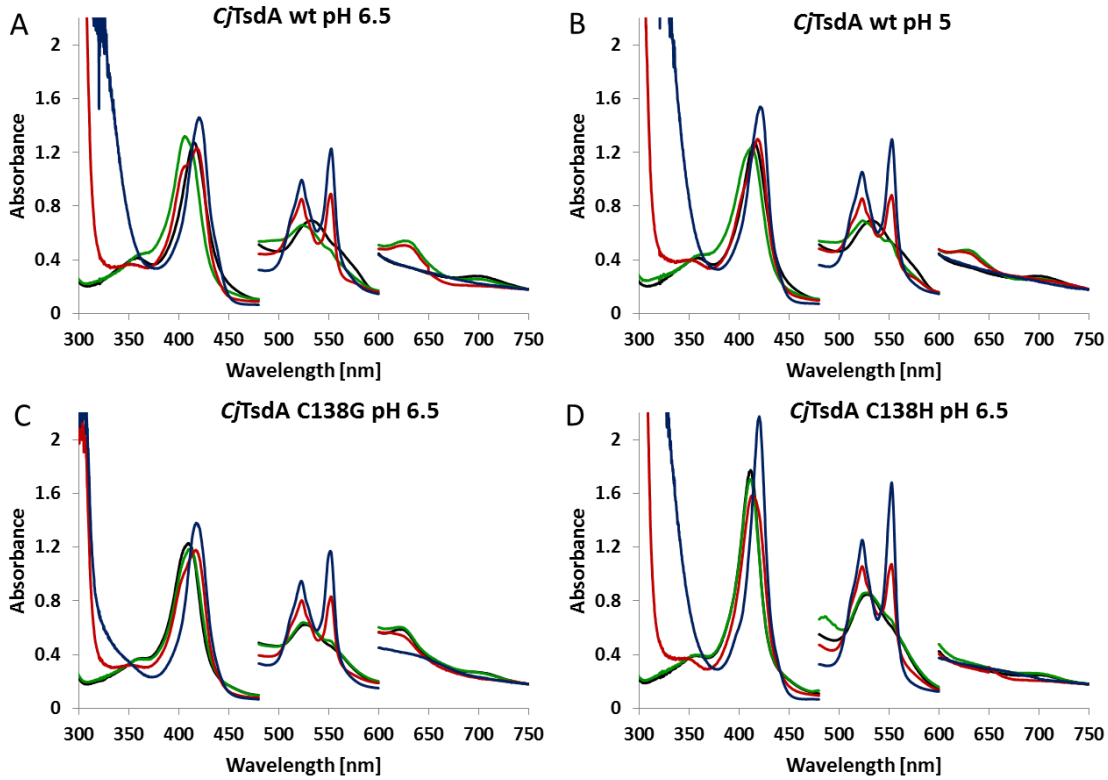

Figure 10: UV-vis spectra with *Cj*TsdA wt and Heme 1 ligation affected variants plus sulfite. Spectra were recorded under anoxic conditions with 8 µM TsdA in 50 mM Bis Tris buffer pH 6.5 (A, C, D) or in 100 mM ammonium acetate buffer pH 5 (B). For oxidation of the enzymes up to 30 µM ferricyanide were used (black line). After recording the oxidized spectra up to 5 mM sulfite were added (green line) and subsequently the proteins were first reduced with up to 17.5 mM ascorbate (red line) and then with 0.7 mM EuCl2-EGTA-solution (blue line) until no further reduction could be observed. Spectra were normalized to 280 nm and 750 nm. Absorbance values in the region between 480 and 600 nm are scaled by a factor of 5 and values between 600 and 750 nm by a factor of 15.

A covalent linkage of sulfite to Cys^{138} Sγ should cause heme reduction as generation of a sulfur-sulfur bond is a two electron transfer process. It has to be considered that ferricyanide was added for *Cj*TsdA oxidation. Ferricyanide can be used as electron acceptor in thiosulfate oxidation assays (Liu *et al.*, 2013; Brito *et al.*, 2015) and can oxidize the TsdA hemes. The electrons from the formation of a sulfur-sulfur bond might transfer first to the TsdA hemes and then be delivered to the artificial electron acceptor ferricyanide and the two TsdA hemes would not persist in the reduced state. Therefore, it is not possible to verify TsdA reduction by sulfite in this experiment when ferricyanide is present. Moreover, it was shown that the observed high-spin features are more pronounced at pH 6.5 than at pH 5 (Figures 10A and 10B). This might indicate that a protonation of Cys^{138} Sγ, which occurs most likely at low pH values, makes movement of Cys^{138} Sγ out of the Heme 1 iron coordination sphere and possibly also interaction with sulfite more difficult.

The effect of sulfite on the redox properties of TsdA was analyzed by spectroelectrochemical experiments with *Cj*TsdA wildtype protein bound on a SnO_2 electrode (Figure 11).

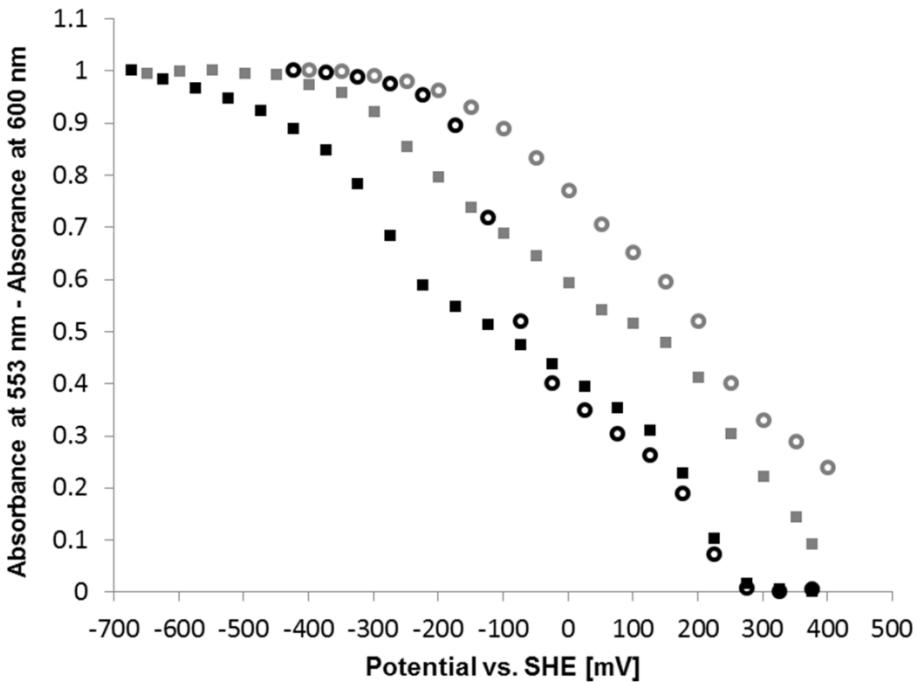

Figure 11: Impact of sulfite on reduction and oxidation of *Cj*TsdA wt bound on a SnO_2 electrode. Absorbance at 553 nm is plotted against the potential. The plot shows a comparison between *Cj*TsdA with 20 mM sulfite (circles) and without sulfite (squares; this data is also shown in Figure 9) upon reduction (black symbols) and re-oxidation (grey symbols). 100 mM ammonium acetate buffer pH 5 with 50 mM NaCl was used. Experiments were performed by Julia Kurth in the laboratory of Julea Butt at the University of East Anglia (Norwich, U.K).

In the presence of sulfite, reduction of the high potential His/Met-ligated Heme 2 above -100 mV is unchanged compared to the behavior in the absence of sulfite (Figure 11). However, reduction of Heme 1 occurs at significantly more positive potentials in the presence of sulfite. This is consistent with the assumption that sulfite binds very close to Heme 1 iron and therefore has an impact on the redox properties of this heme. As shown before by UV-vis spectroscopy (Figure 10A and 10B) sulfite causes a movement of Cys^{138} Sγ out of the Heme 1 iron coordination sphere and may interact directly with the Sγ of Cys^{138}, most probably by covalent linkage resulting in a cysteine S-sulfate group.

In a next step the influence of sulfite on *Cj*TsdA catalysis was analyzed. For this approach protein film electrochemistry (PFE) was used. *Cj*TsdA was adsorbed on a graphite electrode and placed in an electrochemical cell containing buffer solution. To analyse catalytic properties of TsdA increasing amounts of tetrathionate or thiosulfate were added. Sulfite inhibition was studied by adding increasing amounts of sulfite to TsdA in presence of either thiosulfate or tetrathionate. The change in catalytic current was measured over a potential window of -0.2 V and 0.3 V in case of tetrathionate reduction (Figures 12A and 12C) or 0 V to 0.3 V in case of thiosulfate oxidation (Figures 13A and 13C). For a detailed analysis of TsdA catalysis inhibited by sulfite the electrode coated with *Cj*TsdA was placed in an electrochemical cell containing buffer solution with a distinct amount of sulfite. Afterwards

increasing amounts of tetrathionate or thiosulfate were added. The resulting change in current was determined at a constant potential of 0 V in case of tetrathionate reduction (Figures 12D, 14B, 14D and 15) or 0.2 V in case of thiosulfate oxidation (Figures 13D, 14A, 14C and 15).

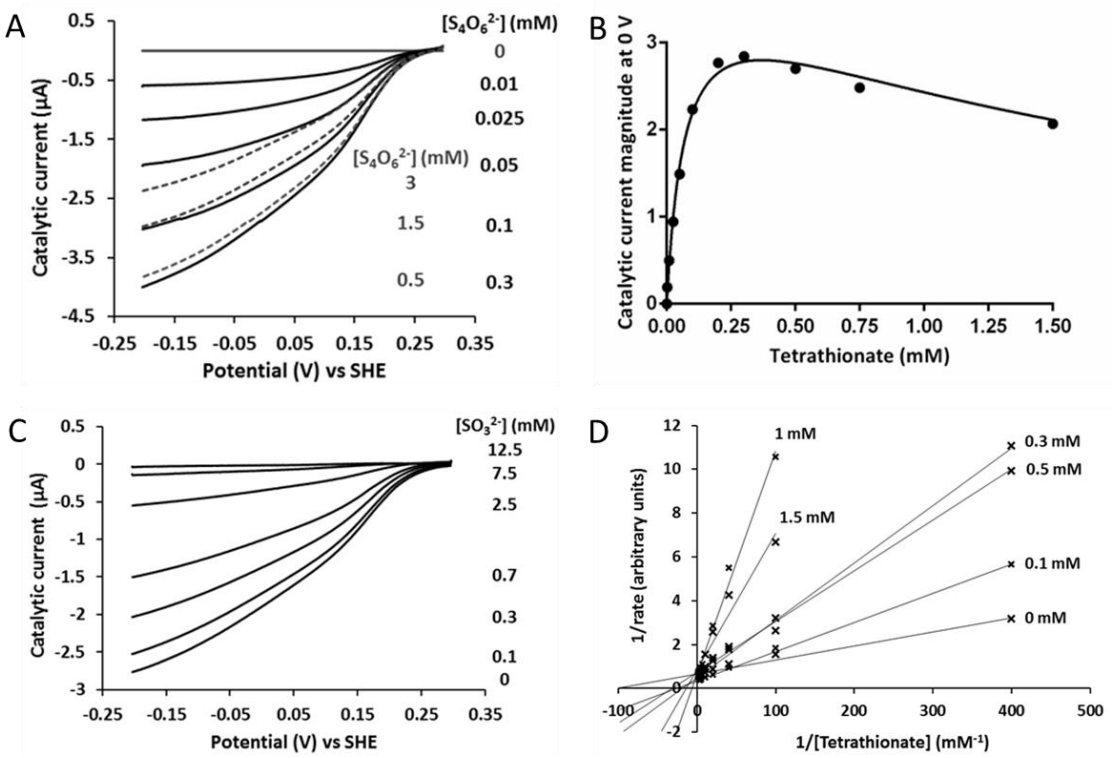

Figure 12: Tetrathionate reductase activity of *Cj*TsdA and its inhibition by sulfite as revealed by PFE. A) Representative cyclic voltammetry at the indicated tetrathionate concentrations. Tetrathionate concentrations above 0.3 mM led to a decrease of catalytic current (dotted lines) indicating substrate inhibition. B) Kinetic analysis of tetrathionate reduction. Values of catalytic current magnitude at 0 V were taken from A). Line shows the behavior predicted for general substrate inhibition with K_m = 0.072 mM and K_i = 1.89 mM. C) Representative cyclic voltammetry of *Cj*TsdA in 0.3 mM tetrathionate and the indicated sulfite concentrations. The IC_{50} value is 0.88 mM sulfite. D) Lineweaver-Burk plots for the indicated sulfite concentrations. For measurement of catalytic current values *Cj*TsdA adsorbed on a graphite electrode was placed in a sulfite containing solution and increasing amounts of tetrathionate were added. The change in catalytic current was measured at a constant potential of 0 V. Cyclic voltammetry was performed with a scan rate of 10 mV s^{-1}, an electrode rotation of 500 rpm in 100 mM ammonium acetate buffer plus 50 mM NaCl, pH 5 at 42°C. Experiments were performed by Julia Kurth in the laboratory of Julea Butt at the University of East Anglia (Norwich, U.K).

The tetrathionate reductase activity of *Cj*TsdA measured by cyclic voltammetry revealed negative catalytic currents below 0.25 V vs. SHE that quantify the rate of tetrathionate reduction for each substrate concentration (Figure 12A). The magnitude of the catalytic wave increased as the tetrathionate concentration was raised to 0.3 mM, but decreased in response to the addition of higher tetrathionate concentrations indicating substrate inhibition. For determination of catalytic parameters the catalytic current (i_{cat}) magnitude at 0 V vs. SHE was plotted against the tetrathionate concentration (Figure 12B). The data was fitted to the general equation for substrate inhibition (Cleland, 1979). By PFE a K_m value of 71 ± 10 µM

(n = 4) and a K_i value of 1770 ± 320 μM (n = 2) was determined. Those values are in good agreement with values determined in spectrophotometric assays with reduced methyl viologen as electron donor (Kurth, Butt *et al.*, 2016).

Inhibition of tetrathionate reduction was revealed by the decrease in catalytic currents upon sulfite addition (Figure 12C). This inhibition is reversible (data not shown). By measuring steady-state catalytic currents at 0 V with varying sulfite concentrations and increasing amounts of tetrathionate (Figure 12D) i_{cat} varied with substrate concentration in the manner predicted by the Michaelis-Menten equation. The corresponding Lineweaver-Burk plots intercept on the y-axis revealing sulfite as a competitive inhibitor with a value of 400 ± 80 μM sulfite for the dissociation constant K_i.

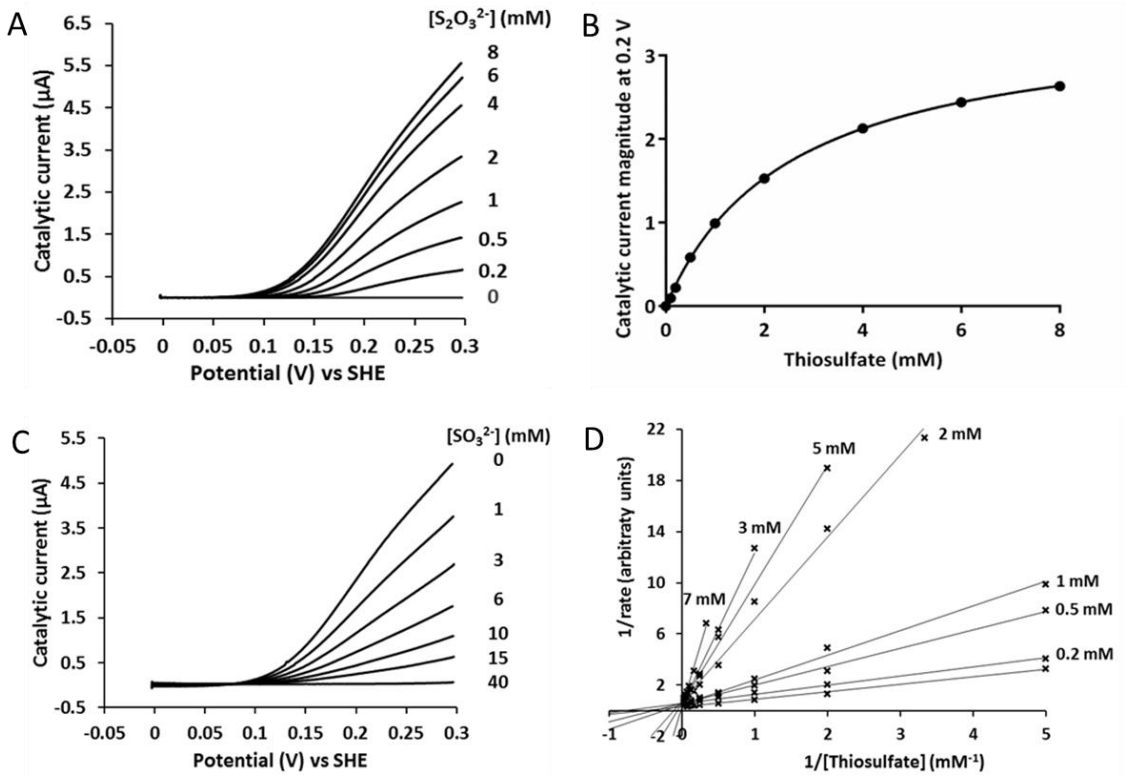

Figure 13: Thiosulfate oxidase activity of *Cj*TsdA and its inhibition by sulfite as revealed by PFE. A) Representative cyclic voltammetry at the indicated thiosulfate concentrations. B) Kinetic analysis of tetrathionate reduction. Values of catalytic current at 0.2 V were taken from A). Data was fitted to the Michaelis-Menten equation giving a K_m-value of 2.53 mM. C) Representative cyclic voltammetry of *Cj*TsdA in 8 mM thiosulfate and the indicated sulfite concentrations. The IC_{50} value is 4.21 mM sulfite. D) Lineweaver-Burk plots for the indicated sulfite concentrations. For measurement of catalytic current values *Cj*TsdA adsorbed on a graphite electrode was placed in a sulfite containing solution and increasing amounts of thiosulfate were added. The change in catalytic current was measured at a constant potential of 0.2 V. Cyclic voltammetry was performed with a scan rate of 10 mV s^{-1}, an electrode rotation of 500 rpm in 100 mM ammonium acetate buffer plus 50 mM NaCl, pH 5 at 42°C. Experiments were performed by Julia Kurth in the laboratory of Julea Butt at the University of East Anglia (Norwich, U.K).

The thiosulfate oxidase activity of *Cj*TsdA was analyzed by PFE and positive catalytic currents were detected above 0.1 V vs. SHE (Figure 13A). On raising the thiosulfate concentration the catalytic waves increased in magnitude up to a limiting thiosulfate

concentration of about 10 mM. The catalytic current magnitude at 0.2 V vs. SHE was plotted against the thiosulfate concentration (Figure 13B) and data was fitted to the Michaelis-Menten equation resulting in K_m = 2108 ± 329 μM (n = 3). As thiosulfate oxidation catalyzed by TsdA is a bimolecular reaction data obtained from spectroscopic assays of thiosulfate oxidation coupled to cytochrome *c* reduction were interpreted through the Hill equation (Kurth, Butt *et al.*, 2016). The results revealed the Hill coefficient n to be approximately one and as the rate equation in this case is equivalent to the standard Michaelis-Menten equation, data obtained by PFE was fitted to this equation. The K_m value determined by PFE is tenfold higher than the value obtained from spectroscopic assays, most probably because of complexities due to the nature of the redox partner.

Inhibition of thiosulfate oxidation by sulfite was revealed by the decrease in catalytic currents upon sulfite addition (Figure 13C) and was shown to be reversible (data not shown). By measuring steady-state catalytic currents at 0.2 V with varying sulfite concentrations and increasing amounts of thiosulfate (Figure 13D) i_{cat} varied with substrate concentration in the manner predicted by the Michaelis-Menten equation. The corresponding Lineweaver-Burk plots intercept on the y-axis revealing sulfite as a competitive inhibitor with a K_i value of 600 ± 70 μM sulfite. Very similar K_i values, describing sulfite binding to *Cj*TsdA, were determined for both catalytic directions. Comparing K_i to the K_m values for tetrathionate reduction (70 μM) and thiosulfate oxidation (2110 μM) leads to the conclusion that the affinity of *Cj*TsdA for these species increases in the order thiosulfate < sulfite < tetrathionate.

The catalytic response of TsdA on sulfite addition at a constant potential is shown in Figure 14 for both catalytic directions. Without sulfite each substrate addition leads to an immediate increase or decrease in catalytic current (Figures 14A and 14B). In presence of sulfite a biphasic release of sulfite is detected upon substrate addition: There is an immediate increase of catalytic current magnitude after substrate addition that is followed by a slow change in catalytic current until a limiting current value is reached (Figures 14C and 14D). A significant difference in sulfite inhibition of thiosulfate oxidation (Figure 14C) and that of tetrathionate reduction (Figure 14D) is that in case of tetrathionate reduction immediately a strong catalytic activity is observed after the first substrate addition, but this immediate tetrathionate reductase activity then slowly is inhibited by sulfite (Figure 14D). When the electrode potential is set to 0 V as in case of the tetrathionate reduction PFE experiments Heme 2 being redox active up to 0.3 V (Figure 9A and Table 2) should be reduced. The slow inhibition of tetrathionate reductase activity by sulfite might be caused by the fact that sulfite can only bind to TsdA after addition of tetrathionate which causes short-term oxidation of the TsdA hemes. It is supposed that sulfite can only react with oxidized TsdA but not TsdA containing reduced Heme 2, because electron transfer from sulfite to TsdA would be

impossible in this case. By contrast, no evidence for slow inhibition by sulfite was observed in the thiosulfate-oxidizing direction when TsdA was poised at 0.2 V (Figure 14C). As TsdA is redox active up to 0.3 V vs. SHE both hemes should be predominantly oxidized at 0.2 V. In this case sulfite can immediately bind to the oxidized enzyme.

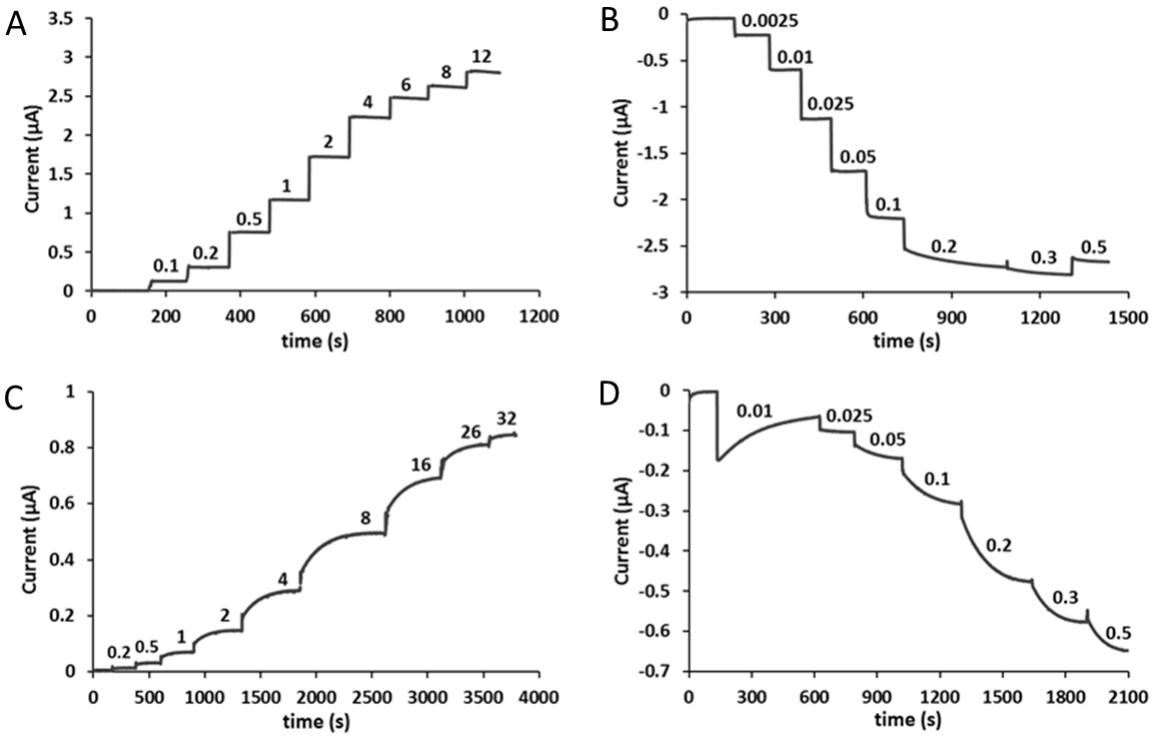

Figure 14: Thiosulfate oxidase activity and tetrathionate reductase activity of *Cj*TsdA inhibited by sulfite as revealed by PFE. *Cj*TsdA adsorbed on a graphite electrode was placed in buffer with 1.5 mM sulfite (D), 3 mM sulfite (C) or without (A, B) sulfite. Afterwards increasing amounts of thiosulfate (A, C) or tetrathionate (B, D) were added, as indicated. The change in catalytic current was measured at a constant potential of 0.2 V in case of thiosulfate oxidation (A, C) and 0 V in case of tetrathionate reduction (B, D). PFE was performed with a scan rate of 10 mV s^{-1}, an electrode rotation 500 rpm in 100 mM ammonium acetate buffer plus 50 mM NaCl, pH 5 at 42°C. Experiments were performed by Julia Kurth in the laboratory of Julea Butt at the University of East Anglia (Norwich, U.K).

The slow release of sulfite is shown in Figure 15 in detail. The catalytic current resulting from slow sulfite release can be fitted to a first order reaction in case of both catalytic directions (Figures 15A and 15B). The rate constant for first order release of sulfite is independent of substrate (Figure 15C).

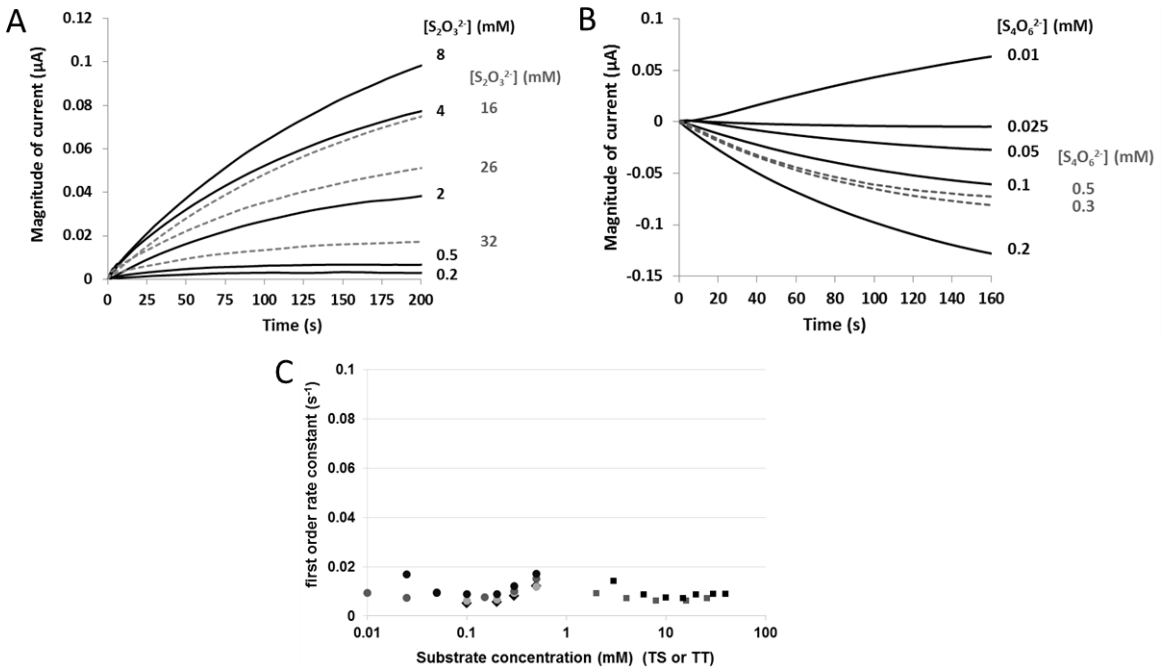

Figure 15: Variation in 1st order rate constant for sulfite release from *Cj*TsdA. PFE was performed with *Cj*TsdA adsorbed on a graphite electrode placed in buffer with 1.5 mM sulfite (B) or 3 mM sulfite (A) sulfite. Afterwards increasing amounts of thiosulfate (A) or tetrathionate (B) were added. The change in catalytic current was measured at a constant potential of 0.2 V in case of thiosulfate oxidation (A) and 0 V in case of tetrathionate reduction (B). Sulfite release of data shown in Figure 14 can be fitted to first order exponential decay (A and B). Values for first order rate constant (C) are shown for thiosulfate oxidation inhibited by 3 mM sulfite (grey squares) and 7 mM sulfite (black squares) and tetrathionate reduction inhibited by 0.3 mM sulfite (black diamonds), 0.5 mM sulfite (light grey circles), 1 mM sulfite (dark grey circles) and 1.5 mM sulfite (black circles). PFE was performed with a scan rate of 10 mV s^{-1}, an electrode rotation of 500 rpm in 100 mM ammonium acetate buffer plus 50 mM NaCl, pH 5 at 42°C. Experiments were performed by Julia Kurth in the laboratory of Julea Butt at the University of East Anglia (Norwich, U.K).

Discussion

TsdA enzymes from various organisms have been shown to differ in their reaction directionality (Kurth *et al.*, 2015). Not only is there variation in the catalytic bias of those TsdA enzymes, but their heme ligation also varies: Whereas the heme-ligating cysteine is conserved in TsdAs from different organisms (Denkmann *et al.*, 2012) and indeed serves as sixth heme iron ligand of the active site heme in *Av*TsdA (Brito *et al.*, 2015), *Mp*TsdBA (Kurth, Brito *et al.*, 2016) and *Cj*TsdA (Kurth, Butt *et al.*, 2016 and this chapter), the ligand constellation of the electron transfer heme of TsdA differs depending on the source organism. For *Cj*TsdA it has been shown previously by UV-vis spectroscopy (Kurth, Butt *et al.*, 2016) as well as by nIR-MCD spectroscopy and X-ray crystallization described in this chapter, that methionine is ligating Heme 2 iron in the oxidized state. A ligand change as shown for *Av*TsdA where lysine serves as the sixth ligand of Heme 2 iron in the oxidized state and is replaced by methionine upon reduction (Brito *et al.*, 2015) has not been observed for *Cj*TsdA. The sixth heme iron ligand of both *Cj*TsdA hemes has been shown to

be indispensable for efficient function of *Cj*TsdA *in vitro* and *in vivo* (Kurth, Butt *et al.*, 2016). Interestingly, a surprising flexibility in the amino acid environment of Heme 2 was revealed by X-ray crystallography of *Cj*TsdA (Figures 2E and 2F).

Analysis of the redox behavior of *Cj*TsdA wildtype and variants by spectroelectochemical approaches gave rise to the assumption that a non-proteinaceous ligand might play a role as transient Heme 2 ligand. NIR-MCD spectroscopy and X-ray crystallization suggest that an imidazole-like molecule is present in close vicinity of Heme 2 iron (Figure 3C and Figure 4). In addition it was shown that imidazole is capable to act as sixth iron ligand of *Cj*TsdA Heme 2 but not of Heme 1 (Figure 8). So far it is not known if the imidazole-like molecule observed at Heme 2 in some of the *Cj*TsdA crystal structures is only present in recombinantly produced protein or if such a molecule is also present *in vivo*. But although such a molecule might be present in *Cj*TsdA M255G as seen in several X-ray structures, this mutant exhibits a significant high-spin heme population which can only be minimized after addition of imidazole (Figure 8C). Thus the imidazole-like molecule present in this variant is likely to be only present in a very small portion of this variant. Moreover, the UV-vis spectrum of the wildtype protein with added imidazole looks very similar to that recorded in absence of imidazole. Those results indicate that even if an imidazole-like structure is present in close vicinity to *Cj*TsdA Heme 2, this molecule does not have a large impact on the heme ligation.

For a better understanding of TsdA catalysis and reaction mechanism analysis of the redox properties of TsdA enzymes is crucial. By nIR-MCD and UV-vis spectroscopy of *Cj*TsdA in the presence of the mild reductant ascorbate it was shown that Heme 1 exhibits the more negative potential and Heme 2 the more positive potential. The redox potential of Heme 1 was shown to be below -81 mV (Figure 5) and its redox activity spans down to -650 mV (Figure 9A; Table 2). In general His/Cys-ligated hemes are characterized by a very negative midpoint potential which has been shown for the corresponding heme in SoxA and DsrJ (Pires *et al.*, 2006; Reijerse *et al.*, 2007; Kappler *et al.*, 2008; Bradley *et al.*, 2012). Values of -400 mV and -432 mV have been reported for the SoxXA His/Cys-ligated active site heme (Reijerse *et al.*, 2007; Bradley *et al.*, 2012). Thus the redox properties observed for TsdA Heme 1 fit to those of other His/Cys-ligated hemes. The redox potential of Heme 2 was shown to be more positive than -81 mV (Figure 5) and the heme was redox active up to +300 mV (Figure 9A; Table 2). Heme 2 indeed is predicted to exhibit a quite positive reduction potential as soft ligands such as methionine stabilize reduced iron, which results in a positive E_m value (Reedy and Gibney, 2004; Reedy *et al.*, 2008).

The knowledge about the redox properties of the *Cj*TsdA wildtype and variant proteins with altered Heme 1 and Heme 2 amino acid environment facilitated connection of catalytic properties of each *Cj*TsdA protein to its range of redox activity.

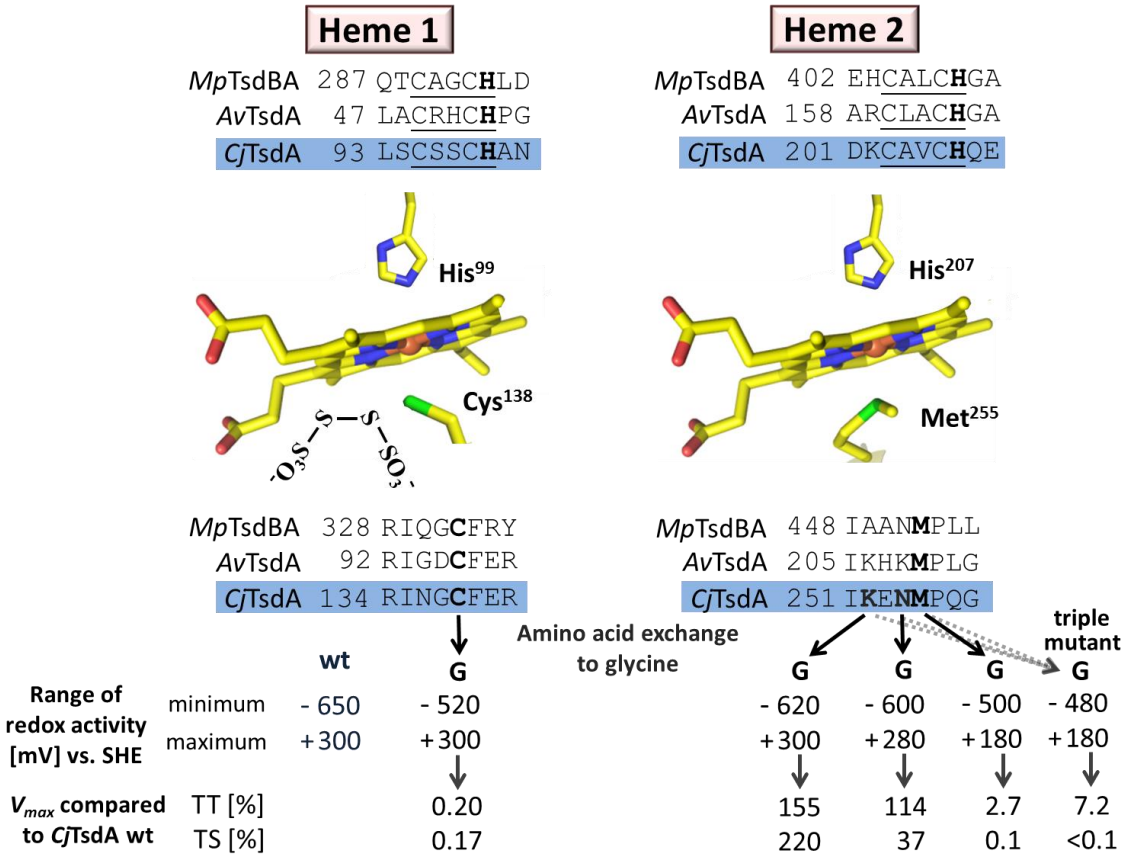

Figure 16: Impact of changes in *Cj*TsdA Heme 1 and Heme 2 environment on redox properties and catalytic activity. Relevant sequence alignments are shown for TsdA from *C. jejuni* (*Cj*TsdA), *A. vinosum* (*Av*TsdA) and the TsdBA fusion protein from *M. purpuratum* (*Mp*TsdBA). Amino acid numbers are given for the recombinant proteins without signal peptides. In case of *Cj*TsdA the sequence of the N-terminal Strep tag is included. In the central left panel a tetrathionate molecule is shown in vicinity of the active site Heme 1 iron-ligating cysteine, based on the *Av*TsdA crystal structure (Brito *et al.*, 2015). Amino acid numbers in the central panels refer to *Cj*TsdA. In the lower part of the figure, changes in the environments of Heme 1 and Heme 2 are indicated that were introduced by site directed mutagenesis. The effects of these changes on the range of redox activity in comparison to that of the wildtype protein are shown. The range of redox activity of *Cj*TsdA wt and variants was determined by spectroelectrochemistry with the proteins bound on SnO_2 electrodes (Figure 9; Table 2) upon reduction of the protein. The effects of these changes on maximal reaction velocity are listed as percent of V_{max} for the wildtype enzyme in the tetrathionate-reducing (TT) and the thiosulfate-oxidizing (TS) direction. Figure modified after Kurth, Butt *et al.*, 2016.

An exchange of the active site heme-ligating cysteine led to strong impairment in enzyme activity in both catalytic directions which was observed for all Heme 1 ligation affected variants. But changes in Heme 1 environment did not influence the catalytic bias of the protein. In case of the *Cj*TsdA C138G variant the reduction potential of Heme 1 has become more positive (Figure 16), which might facilitate electron transfer from thiosulfate to Heme 1 as a more positive reduction potential correlates with higher electron accepting power. However, this variant is not stronger biased to thiosulfate oxidation than the wildtype protein. This finding supports the statement that the reaction directionality of redoxenzymes is largely not determined by the redox properties of the active site (Abou Hamdan *et al.*, 2012; Hexter *et al.*, 2014).

In contrast to the *Cj*TsdA C^{138} derivatives the Heme 2 ligation affected variants showed higher catalytic activities (Figure 16). Structural differences in the immediate environment of *Cj*TsdA Heme 2 were shown to contribute to defining the reaction directionality of the enzyme (Kurth, Butt *et al.*, 2016). This observation rised the question if those changes are due to altered redox properties of the relevant *Cj*TsdA variants. In case of *Cj*TsdA M255G and the KNMG triple mutant the reduction potential of Heme 2 has become more negative, which has also become clear by the impaired reducibility of *Cj*TsdA M255G Heme 2 by ascorbate (Figure 7B). But simultaneously the Heme 1 ligation is affected when Met^{255} is exchanged by glycine as revealed by nIR-MCD spectroscopy (Figure 4) resulting in a more positive reduction potential of Heme 1. The replacement of Met^{255} by glycine leads to a stronger impairment of thiosulfate oxidation than of tetrathionate reduction (Kurth, Butt *et al.*, 2016; Figure 16). The reason might be that electron transfer between Heme 2 and Heme 1 should be facilitated in the tetrathionate-reducing direction due to the more negative reduction potential of Heme 2 resulting in a higher reducing power and the more positive reduction potential of Heme 1 resulting in a higher electron accepting power. Consequently electron transfer between Heme 1 and Heme 2 should be hindered in the thiosulfate-oxidizing direction and thus might cause the strong impairment of thiosulfate oxidation seen for the *Cj*TsdA M255G variant (Figure 16).

When amino acids other than Met^{255} in the vicinity of Heme 2 iron like Asn^{254} and Lys^{252} (Figures 9D; Table 2) were changed, this had only a slight impact on the redox behavior of the enzyme. Nevertheless, enzyme activity assays have revealed that *Cj*TsdA N254G has a stronger bias toward tetrathionate reduction and *Cj*TsdA K252G toward thiosulfate oxidation in comparison to the wildtype protein (Kurth, Butt *et al.*, 2016). Thus, differences in the reaction directionality of TsdA enzymes cannot in general be correlated to altered redox properties of Heme 2. For hydrogenases it has been described that the reaction directionality of those enzymes is not mainly determined by redox properties of the active site, but rather by steps which occur on sites of the proteins that are remote from the active site, such as proton transfer, intramolecular electron transfer, reorganization energy, substrate release or lid opening (Abou Hamdan *et al.*, 2012; Hexter *et al.*, 2014). This might be the case for TsdA as well.

In our previous study on the effect of the *Cj*TsdA heme environment on catalysis (Kurth, Butt *et al.*, 2016) and in the study on *Av*TsdA heme ligation (Brito *et al.*, 2015) alteration of the Heme 2 environment was shown to influence catalysis at the active site Heme 1. For example an exchange of Lys^{252} in vicinity of *Cj*TsdA Heme 2 led to significant increase in substrate inhibition by tetrathionate (Kurth, Butt *et al.*, 2016). For *Cj*TsdA as well as for *Av*TsdA changes at Heme 2 were shown to affect affinity of the enzyme to tetrathionate and thiosulfate (Brito *et al.*, 2015; Kurth, Butt *et al.*, 2016). Those observations indicate strong

cooperativity between the two TsdA hemes. This statement is confirmed by nIR-MCD spectroscopy (Figure 4B) and analysis of the redox properties (Figures 9C and 9D) described in this chapter: Those experiments revealed that an exchange of the Heme 2 iron ligand Met^{255} by glycine has an influence on Heme 1 iron ligation and its redox properties. The strong cooperativity between the TsdA hemes might be due to structural changes. X-ray crystallization of *Av*TsdA revealed that each TsdA heme is embedded in one of two very similar typical class I *c*-type cytochrome domains (Brito *et al.*, 2015). There might be some flexibility between those domains resulting in structural changes and rearrangement of the heme groups. Such structural changes might also influence the reaction directionality of the enzymes discussed before.

Regardless of the reaction directionality of TsdA enzymes general features of the TsdA reaction mechanism apply to all TsdA enzymes. One important finding regarding the TsdA reaction cycle is that a covalent bond is formed between thiosulfate and Sγ of the active site heme-ligating cysteine as shown by a crystal structure of *Mp*TsdBA (Kurth, Brito *et al.*, 2016). A covalent linkage between thiosulfate and the Sγ atom is supported by UV-vis spectroscopy (Figure 10), spectroelectrochemical experiments (Figure 11) and PFE (Figure 14) with *Cj*TsdA in presence of the substrate mimic sulfite indicating that such a bond is not an artefact resulting from protein crystallization but also occurs in solution. Formation of a cysteine S-thiosulfonate intermediate involved in the TsdA reaction mechanism has already been proposed by Grabarczyk *et al.*, 2015. This intermediate is assumed to be formed when the first thiosulfate molecule is positioned in the substrate binding pocket (Grabarczyk *et al.*, 2015; Kurth, Brito *et al.*, 2016). Positively charged amino acid side chains in the active site are supposed to stabilize this cysteine S-thiosulfonate group. The two electrons released in course of cysteine S-thiosulfonate formation reduce the iron atoms of the two TsdA hemes to the Fe^{II} state. After re-oxidation of the hemes by an external electron acceptor a thiol-disulfide exchange reaction most likely occurs that involves an attack of the sulfane atom of a second thiosulfate molecule on the thiosulfonate group (Grabarczyk *et al.*, 2015). In course of tetrathionate reduction the central sulfur-sulfur bond of the tetrathionate molecule first has to be cleaved by attack of Sγ of the active site cysteine (Kurth, Butt *et al.*, 2016). This reaction is assumed to release the first thiosulfate molecule and to create a cysteine S-thiosulfonate group. The second thiosulfate is reductively released from this intermediate after heme reduction by an external electron donor.

This reaction mechanism can be extended by findings shown in this chapter. To get a further insight into the TsdA reaction mechanism sulfite was used as a substrate mimic. Sulfite is known to be a strong inhibitor of thiosulfate-oxidizing enzymes (Lyric and Suzuki, 1970; Schook and Berk, 1979; Meulenberg *et al.*, 1993; Hensen *et al.*, 2006) and is a competitive inhibitor of TsdA in both catalytic directions (Figures 12D and 13D). Sulfite was shown to

cause a movement of Cys^{138} Sγ out of the Heme 1 iron coordination sphere as already described for thiosulfate (Brito *et al.*, 2015). In addition, a strong interaction between sulfite and the Cys^{138} has been proven, most likely a covalent linkage as stated previously for thiosulfate (Kurth, Brito *et al.*, 2016). Moreover, it has been shown by PFE experiments with *Cj*TsdA in the presence of sulfite (Figures 14C and 14D) that sulfite can only react with oxidized TsdA but not TsdA containing reduced Heme 2 as electron transfer from sulfite to TsdA would be impossible in this case. This finding supports the assumption described in Grabarczyk *et al.*, 2015 that binding of thiosulfate, in this case sulfite, to Sγ of the active site heme-ligating cysteine results in immediate reduction of the TsdA hemes. If the TsdA hemes are reduced, electrons cannot be transferred and the covalent bond cannot be formed. Another interesting observation is that the presence of sulfite causes an immediate increase in catalytic current magnitude after substrate addition that is followed by a slow phase of increase in catalytic current magnitude (Figures 14C and 14D). It is considered that the immediate increase in catalytic current magnitude arises from the population of *Cj*TsdA without sulfite covalently bound to Cys^{138} Sγ, whereas the slow increase in catalytic current magnitude, following first order reaction kinetics, arises from cleavage of this bond in the remaining population. This slow sulfite release suggests that the covalent linkage of a sulfur species to Cys^{138} Sγ might be the rate-defining step in TsdA catalysis. Furthermore, thiosulfate-oxidation can be well-described by Michaelis-Menten kinetics (Figure 13B) and data fitting to the Hill equation resulted in a Hill coefficient that is approximately one (Kurth, Butt *et al.*, 2016). This indicates that one step in the TsdA reaction cycle is rate defining. The finding supports the assumption that the rate-defining step in thiosulfate oxidation by TsdA is the redox reaction involving covalent linkage between thiosulfate and Sγ of the Heme 1 iron-ligating cysteine (Figure 17). In contrast, the thiol-disulfide exchange is assumed to occur quite fast.

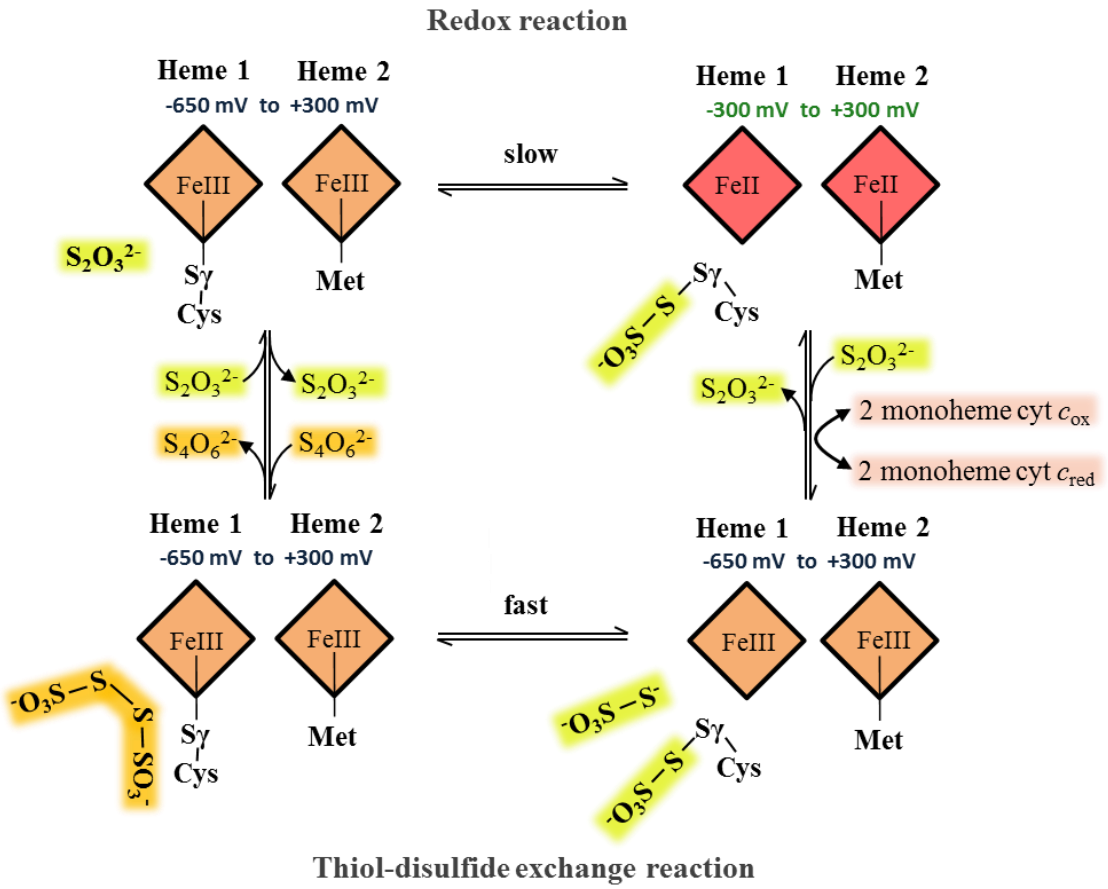

Figure 17: Model of *Cj*TsdA reaction mechanism. In case of *Cj*TsdA the sixth axial heme ligand of the active site heme, Heme 1, is Cys[138] and of the electron transfer heme, Heme 2, Met[255] as shown by nIR-MCD- and UV-vis spectroscopy. The range of redox activity was determined by spectroelectrochemistry with protein bound on a SnO_2 electrode (Figure 9) upon reduction of the protein. Sulfite addition led to a clear change of the *Cj*TsdA redox properties resulting in a less negative range of redox activity (Figure 11). Therefore, it is assumed that covalent linkage of thiosulfate to the Cys[138] Sγ, which has been established by the *Mp*TsdBA crystal structure including thiosulfate (Kurth, Brito *et al.*, 2016) as well as the reaction between sulfite and *Cj*TsdA shown in this chapter, might alter the redox properties of Heme 1 in a similar manner. Moreover, the catalytic behavior of *Cj*TsdA in the thiosulfate-oxidizing direction which can be described by Michaelis-Menten kinetics despite being a bimolecular reaction and the slow sulfite release from the enzyme indicate that the redox reaction involving Cys[138] S-thiosulfonate formation might be the rate-determining step in *Cj*TsdA catalysis. The thiol- disulfide exchange is assumed to occur fast. A monoheme cytochrome has been shown to be the most likely electron acceptor/donor of *Cj*TsdA (Liu *et al.*, 2013).

Our findings regarding TsdA redox properties helped us especially in understanding the reaction mechanism of this enzyme. *Cj*TsdA exhibits a range of redox activity between -650 mV and +300 mV. *Av*TsdA was found to be redox active in a narrower range between -300 mV and +150 mV (Kurth, Brito *et al.*, 2016). However, the reduction potential of Heme 1 appears to be quite negative in both proteins as expected for His/Cys-ligated hemes. Considering the E_m of +198 mV for the thiosulfate/tetrathionate couple (Kurth *et al.*, 2015), it is quite interesting that TsdA Heme 1 possesses a reduction potential below -81 mV (Figure 5). Thus, electron transfer from thiosulfate oxidation to the active site heme appears quite difficult. The study on impact of sulfite on the *Cj*TsdA redox properties (Figure 11) has

solved this problem: The reduction potential of Heme 1 becomes more positive after binding of a sulfur species to Sγ of the Heme 1 iron-ligating cysteine (Figure 17). Thiosulfate is assumed to have a similar effect on the reduction potential of Heme 1 as sulfite: The predicted modifications of the heme-ligating cysteine Sγ after sulfite addition resulting in a cysteine S-sulfate group and those after thiosulfate or tetrathionate addition resulting in a cysteine S-thiosulfonate group are structurally very similar. Thus, a comparable positive shift of the reduction potential of TsdA Heme 1 is expected in the presence of thiosulfate or tetrathionate. This positive increase in the Heme 1 reduction potential is assumed to occur during movement of the heme-ligating cysteine Sγ out of the Heme 1 iron coordination sphere and formation of a cysteine S-thiosulfonate group. The increase in redox potential might facilitate electron transfer from thiosulfate to Heme 1 before passing electrons to an external electron acceptor via Heme 2 (Figure 17). In the tetrathionate-reducing direction an increase in the Heme 1 reduction potential might facilitate electron transfer from Heme 2 to Heme 1 as the redox potential of the negative potential Heme 1 converges to that of the positive potential Heme 2.

In conclusion, the reaction mechanism already proposed for TsdA enzymes (Grabarczyk *et al.*, 2015; Kurth, Brito *et al.*, 2016) was strengthened and extended by some findings described in this chapter. Our results indicate that formation of a covalent bond between thiosulfate and Sγ of the active site cysteine, most probably the rate-defining step in the TsdA reaction cycle, can indeed be formed in solution. This covalent bond can only be formed when the TsdA hemes are oxidized resulting in immediate reduction of the TsdA hemes. Furthermore, a first detailed analysis of TsdA redox properties was provided. Heme 1 was identified as the heme with the more negative reduction potential and Heme 2 as the heme with the more positive reduction potential. Interestingly, the reduction potential of Heme 1 becomes more positive after binding of a sulfur species to Sγ of the heme-ligating cysteine. Thus, electron transfer from thiosulfate to Heme 1 is facilitated in the thiosulfate-oxidizing direction and in the reductive direction electron transfer from Heme 2 to Heme 1.

VI. Overview article

Chapter 6

Ein altes Paar in neuem Glanz: Thiosulfat und Tetrathionat

Introduction & Summary:

Thiosulfate and tetrathionate can be interconverted in a reversible redox reaction. Both compounds are used in the metabolism of some bacteria. To understand the role of these sulfur ions in bacterial bioenergetics, exact knowledge of the reduction potential of the tetrathionate/thiosulfate couple $E_{TT/TS}$ is required. The experimentally determined value of $E_{TT/TS}$ is +198 mV, which is much more positive than the calculated value of +24 mV most widely cited in the field of microbial bioenergetics. Thus tetrathionate respiration is probably much more prevalent in tetrathionate containing environments like the marine sediment or the human gut than previously thought. A well-studied enzyme that catalyzes thiosulfate oxidation and tetrathionate reduction is the bifunctional enzyme TsdA. The reaction directionality of this diheme cytochrome *c* varies in dependence of the source organism. This widespread enzyme enables the purple sulfur bacteria *Allochromatium vinosum* and *Marichromatium purpuratum* to use thiosulfate as electron donor for phototrophic growth or aerobic respiration. In contrast, the human gut pathogen *Campylobacter jejuni* is enabled by TsdA to use tetrathionate as additional electron acceptor. TsdA contains a His/Cys-ligated active site heme and an either His/Met- or His/Lys-coordinated electron transfer heme depending on the source organism. The heme environment of the electron transfer heme was shown to contribute to the reaction directionality of TsdA. The rare His/Cys ligation of the active site heme was shown to be indispensable for the TsdA reaction cycle as the cysteine can form a covalent bond with a thiosulfate molecule. This covalent linkage between thiosulfate and the active site cysteine involving heme reduction or oxidation in addition to a thiol-disulfide exchange reaction are the essential steps in the TsdA reaction cycle.

Chapter 6

Ein altes Paar in neuem Glanz: Thiosulfat und Tetrathionat

This article was accepted by BIOspektrum:

Kurth, J.M. and Dahl, C. (2017) Ein altes Paar in neuem Glanz: Thiosulfat und Tetrathionat. *BIOspektrum* **in press**

http://link.springer.com/article/10.1007/s12268-017-0761-0

Author contributions

- JMK wrote this article together with CD

Themenstichwort: Bakterieller Schwefelstoffwechsel

Ein altes Paar in neuem Glanz: Thiosulfat und Tetrathionat

JULIA M. KURTH, CHRISTIANE DAHL

INSTITUT FÜR MIKROBIOLOGIE & BIOTECHNOLOGIE, UNIVERSITÄT BONN

Thiosulfate dehydrogenase (TsdA) enzymes represent a phylogenetically widespread family of periplasmic *c* type diheme cytochromes. They catalyze both thiosulfate oxidation and tetrathionate reduction. The reaction directionality of TsdA enzymes varies in dependence of the source organism. Currently, the best characterized TsdA enzymes are the thiosulfate-oxidizing enzyme from the purple sulfur bacterium *Allochromatium vinosum* and the tetrathionate-reducing enzyme from the human gut pathogen *Campylobacter jejuni*.

Die anorganischen Schwefelverbindungen Thiosulfat ($^-$S-SO$_3^-$) und Tetrathionat ($^-$O$_3$S-S-S-SO$_3^-$) können in einer einfachen, reversiblen Redoxreaktion ineinander umgewandelt werden (2 $S_2O_3^{2-}$ ↔ $S_4O_6^{2-}$ + 2 e^-). Spätestens seit Mitte des vorigen Jahrhunderts ist bekannt, dass beide Verbindungen im Schwefelkreislauf in der Natur von herausragender Bedeutung sind. Insbesondere im marinen Bereich spielen sie nicht nur als Intermediate bei der bakteriellen Oxidation von Sulfid zu Sulfat durch schwefeloxidierende Prokaryonten eine wichtige Rolle, sondern dienen auch als Elektronenakzeptoren für anaerobe respiratorische Prozesse. Erst vor wenigen Jahren wurde nachgewiesen, dass Thiosulfat und Tetrathionat nicht nur in der Umwelt, sondern auch im Gastrointestinaltrakt von Säugetieren vorkommen, wo Thiosulfat im Zuge der Detoxifizierung hochgiftiger Thiole entsteht. Die Bildung von Tetrathionat aus Thiosulfat wird im menschlichen Darm durch reaktive Sauerstoffspezies angetrieben, die bei Entzündungsreaktionen entstehen, hervorgerufen durch humanpathogene Durchfallerreger wie *Salmonella typhimurium* [1]. *S. typhimurium* und weitere krankheiterregende Bakterien im Intestinaltrakt, z. B. das durch ungenügend erhitztes Hühnerfleisch übertragene Bakterium *Campylobacter jejuni*, besitzen die Fähigkeit, Tetrathionat als Elektronenakzeptor zu nutzen und erhalten hierdurch einen Wachstumsvorteil gegenüber anderen Darmbakterien. Trotz ihrer offensichtlich immensen Bedeutung war bis vor kurzem wenig über den genauen Reaktionsablauf der Umsetzung zwischen Thiosulfat und Tetrathionat sowie die Eigenschafen der wichtigsten beteiligten Enzyme bekannt.

Ein Redoxpotenzial in neuem Kleid

Die Kenntnis des Standardpotenzials einer Redoxreaktion, hier also die des Tetrathionat/Thiosulfat-Paares ($E_{TT/TS}$), ist unerlässlich, um ihre Bedeutung im bakteriellen Stoffwechsel einordnen zu können. Für $E_{TT/TS}$ wurden in den letzten Jahrzehnten allerdings viele unterschiedliche Werte publiziert, die einen Bereich von mehr als 250 mV abdecken. Dies ist vor allem dadurch begründet, dass die Thiosulfat/Tetrathionat-Umsetzung an inerten Elektroden irreversibel und einer Bestimmung über die Nernst-Gleichung nicht zugänglich ist. Alle älteren Werte wurden daher aus den freien Bildungsenergien für Thiosulfat und Tetrathionat berechnet, die aber ebenfalls wiederholter Neubewertung unterlagen. Wir haben $E_{TT/TS}$ erstmals experimentell ermittelt [2] und zwar mit Hilfe von Proteinfilmelektrochemie mit Enzymen aus der TsdA-Familie der Thiosulfatdehydrogenasen. Wir ermittelten für $E_{TT/TS}$ einen Wert von +198 ± 4 mV. Dies ist deutlich positiver als das in Publikationen und Lehrbüchern zur mikrobiellen Bioenergetik weithin zitierte Potential von +24 mV, das aus den 1970er Jahren stammt [3]. Die wichtigste Erkenntnis aus dieser Neubewertung ist, dass die Reduktion von Tetrathionat energetisch deutlich günstiger ist als bisher angenommen und dass deren Bedeutung an anoxischen Standorten wahrscheinlich deutlich unterschätzt wurde.

Oxidation von Thiosulfat zu Tetrathionat

Bislang wurden zwei Enzymklassen beschrieben, die die Oxidation von Thiosulfat zu Tetrathionat katalysieren: Lösliche Thiosulfat:Ferricytochrom *c*-Oxidoreduktasen sowie membrangebundene Thiosulfat:Chinon-Oxidoreduktasen (TQO) (**Abb. 1A**). Eine genaue molekularbiologische Analyse erfolgte für die Enzyme aus der ersten Klasse bislang nur für das periplasmatische Dihäm Cytochrom *c* TsdA. Besonders gut untersucht sind die Enzyme aus den Schwefelpurpurbakterien *Allochromatium vinosum* und *Marichromatium purpuratum* (**Abb. 1**) [2, 4-6].

TsdA befähigt schwefeloxidierende Bakterien dazu, bei phototrophen Wachstum oder aerober Atmung Thiosulfat als Elektronendonor zu verwenden [4, 6] (**Abb. 1A**). Chemoorganotrophen Bakterien wie einigen Pseudomonaden [4] kann es dazu verhelfen, Thiosulfat neben organischen Verbindungen als zusätzlichen Elektronendonor zu nutzen. In *M. purpuratum* ist TsdA unmittelbar mit einem weiteren Dihäm-Cytochrom *c*, TsdB, verbunden (**Abb. 2A**), das als Elektronenakzeptor für TsdA dient [6]. Strukturanalysen belegen eine effektive Elektronentransportkette von Häm 3, dem aktiven Zentrum in der TsdA-Domäne über Häm 4 zu den Hämen 1 und 2 in der TsdB-Domäne (**Abb. 2B**). TsdB ähnelt dem Cytochrom c_4 und kann bei aerobem Wachstum möglicherweise Elektronen direkt an die terminale Cytochrom cbb_3-Oxidase übertragen. In Organismen ohne TsdB leitet wahrscheinlich HiPIP (high potential iron-sulfur protein) die Elektronen entweder ebenfalls an

die terminale Oxidase oder in phototrophen Organismen an das photosynthetische Reaktionszentrum weiter [6].

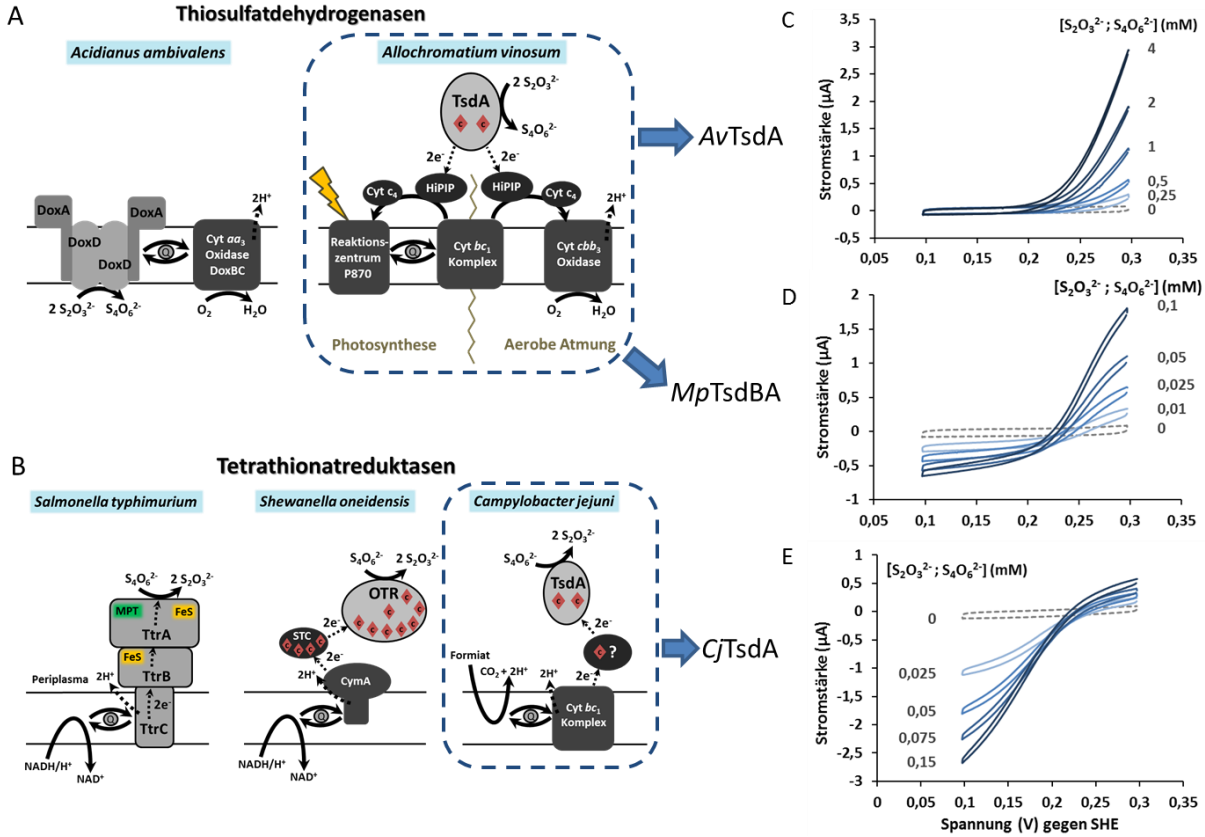

Abb. 1: A, Thiosulfatdehydrogenasen: das membrangebundene Thiosulfat-oxidierende und Chinon-reduzierende Enzym DoxAD aus *Acidianus ambivalens* [12] und die periplasmatische Thiosulfatdehydrogenase TsdA aus *A. vinosum*. In *A. vinosum* ist HiPIP (high-potential iron-sulfur protein) der wahrscheinlichste Elektronenakzeptor von TsdA [6]. **B**, Tetrathionatreduktase-Typen: das Eisen-Schwefel-Molybdoenzym Ttr [10], die Octahäm Tetrathionatreduktase OTR [9] und TsdA aus *C. jejuni* [7]. STC ist ein kleines Cytochrom *c*, das Elektronen vom Tetrahäm Cytochrom *c* CymA akzeptiert und an verschiedene terminale Oxidoreduktasen weiterleitet. **C-E**, Zyklische Proteinfilmvoltammetrie beweist die Bifunktionalität von TsdA Enzymen. Die katalytische Ausrichtung der Enzyme wurde bei einer äquimolaren Konzentration von Thiosulfat und Tetrathionat (wie angegeben) bestimmt. Positiver Stromfluss indiziert Thiosulfatoxidation, negativer Tetrathionatreduktion. TsdA aus *C. jejuni* (*Cj*TsdA) ist somit in Richtung Tetrathionatreduktion ausgerichtet und die Enzyme aus *M. purpuratum* (*Mp*TsdBA) sowie vor allem *A. vinosum* (*Av*TsdA) in Richtung Thiosulfatoxidation. Abbildungen C-E aus [2].

Reduktion von Tetrathionat zu Thiosulfat

TsdA ist bifunktional und fungiert in manchen Organismen als Tetrathionatreduktase. So wird die Fähigkeit bestimmter *C. jejuni*-Stämme, Tetrathionat zu reduzieren, einzig durch TsdA vermittelt [7, 8]. Damit stellt TsdA einen neuen Enzym-Typ innerhalb der Tetrathionatreduktasen dar, zu denen neben der Octahäm-Tetrathionatreduktase OTR aus *Shewanella oneidensis* [9] auch das Eisen-Schwefel-Molybdoenzym TTR aus *Salmonella typhimurium* [10] zu zählen ist (**Abb. 1B**).

Der Reaktionsmechanismus: kein direktes „Shake hands“

Das katalytisch aktive Häm von TsdA-Enzymen weist eine bei prokaryontischen Cytochromen seltene, axiale Ligation des zentralen Eisenatoms durch Histidin und Cystein auf [5]. Strukturanalysen zeigten, dass der Cystein-Ligand kovalent Thiosulfat binden kann (**Abb. 2C)**.

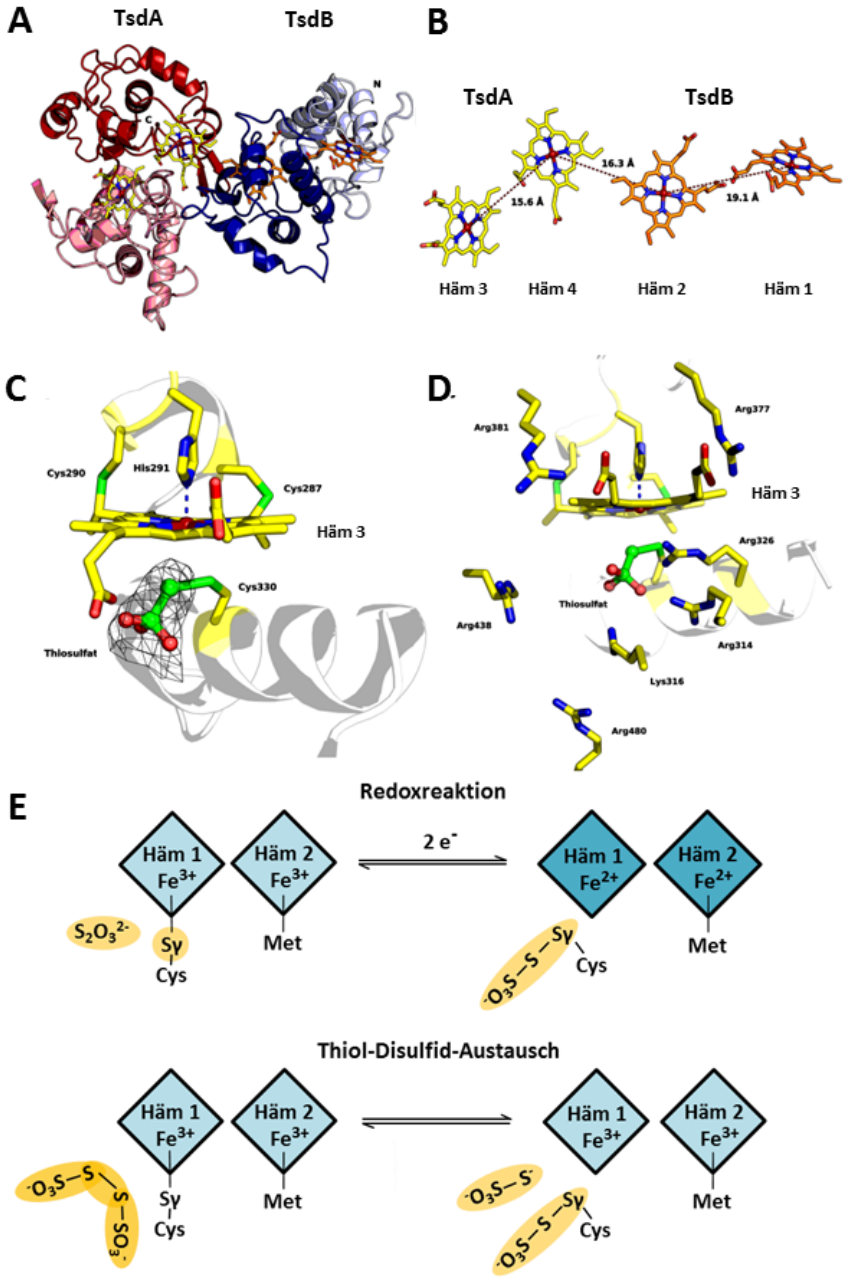

Abb. 2: A, Struktur von TsdBA aus *M. purpuratum*, **B,** Elektronen werden vom Häm 3 im aktiven Zentrum über die Häme 4, 2 und 1 abgeleitet. **C,** Kovalente Bindung von Thiosulfat an das Cystein Sγ-Atom des aktiven Zentrums. **D,** Positiv geladene Aminosäuren in der Substratbindetasche. Farben der Atome: orange: C, rot: O, blau: N, dunkelrot: Fe, grün: S. Abbildungen aus [6]. **E,** Reaktionsmechanismus von Tsd(B)A: Die zwei wichtigsten Schritte des Reaktionszyklus von TsdA-Enzymen sind eine Redoxreaktion, bei der Thiosulfat an das Cysteine Sγ-Atom des aktiven Zentrums gebunden wird, und zum anderen der Thiol-Disulfid-Austausch, bei dem keine Elektronen übertragen werden.

Es kommt also nicht zu einem direkten „Shake hands“ zwischen zwei Thiosulfatmolekülen (**Abb. 2E**). Stattdessen wird intermediär ein Cystein-S-Thiosulfonat gebildet, sobald das erste Thiosulfat-Molekül die Substratbindetasche erreicht hat. Dort befinden sich mehrere positiv geladene Aminosäurereste (**Abb. 2D**), die das Reaktionsintermediat stabilisieren [6, 11]. Dessen Bildung setzt zwei Elektronen frei, die die beiden Häme reduzieren. Nach deren Reoxidation erfolgt ein Thiol-Disulfid-Austausch mit einem zweiten Thiosulfat und damit Bildung von Tetrathionat.

Wie geht es in die richtige Richtung?

Es ist leicht vorstellbar, wie die beschriebene Reaktion auch umgekehrt, also in Richtung der Reduktion von Tetrathionat erfolgt. Bei gleichem Aufbau des aktiven Zentrums fällt es aber schwer zu verstehen, warum TsdA-Enzyme abhängig vom Organismus unterschiedliche katalytische Ausrichtungen haben. Tatsächlich katalysieren die Enyzme aus Schwefeloxidierern *in vitro* bevorzugt die Oxidation von Thiosulfat, während das Enzym aus *Campylobacter* eine verhältnismäßig höhere Tetrathionatreduktase-Aktivität aufweist (**Abb. 1C-E**). Ein erster Erklärungsansatz ergibt sich aus der strukturellen Situation um das zweite Häm in TsdA. Hier gibt es nämlich signifikante Unterschiede: Im *A. vinosum*-Enzym ist das Eisen des zweiten TsdA-Häms im oxidierten Zustand durch Histidin und Lysin ligiert. Das Lysin wird im reduzierten Zustand durch ein unmittelbar daneben liegendes Methionin ersetzt [5]. Im *C. jejuni*-Enzym sitzt anstelle des Lysins ein Asparagin. Methionin dient schon im oxidierten Zustand der Häm-Koordination. Detaillierte Analyse dieser und weiterer Aminosäuren am zweiten TsdA-Häm ergab, dass sie tatsächlich einen Einfluss auf die Reaktionsausrichtung haben [8]. Da aber die einfache Angleichung der Situation in den Enzymen aus *C. jejuni* und *A. vinosum* durch Austausch von Asparagin zu Lysin nicht dazu führt, dass *Cj*TsdA zu einer besseren Thiosulfatdehydrogenase wird [8], tragen auch noch andere Faktoren als das zweite Redoxzentrum selbst dazu bei, die Reaktionsausrichtung des Enzyms festzulegen.

Die verbleibende Frage, welche weiteren Faktoren die Reaktionsausrichtung von TsdA-Enzymen beeinflussen, soll in zukünftigen Experimenten mit TsdA aus *A. vinosum* und *C. jejuni* geklärt werden. Von herausragender Bedeutung ist es zudem in Zukunft zu klären, wie sich die Fähigkeit bestimmter Darmbakterien, Tetrathionat als Elektronenakzeptor zu nutzen, auf die Besiedlung des menschlichen Darms durch pathogene Bakterien auswirkt.

Literatur

[1] Winter SE, Thiennimitr P, Winter MG et al. (2010) Gut inflammation provides a respiratory electron acceptor for *Salmonella*. Nature 467: 426-429

[2] Kurth JM, Dahl C, Butt JN (2015) Catalytic protein film electrochemistry provides a direct measure of the tetrathionate/thiosulfate reduction potential. J Am Chem Soc 137: 13232-13235

[3] Thauer RK, Jungermann K, Decker K (1977) Energy conservation in chemotrophic anaerobic bacteria. Bacteriol Rev 41: 100-180

[4] Denkmann K, Grein F, Zigann R et al. (2012) Thiosulfate dehydrogenase: a wide-spread unusual acidophilic *c*-type cytochrome. Environ Microbiol 14: 2673-2688

[5] Brito JA, Denkmann K, Pereira IAC et al. (2015) Thiosulfate dehydrogenase (TsdA) from *Allochromatium vinosum*: Structural and functional insights into thiosulfate oxidation. J Biol Chem 290: 9222-9238

[6] Kurth JM, Brito JA, Reuter J et al. (2016) Electron accepting units of the diheme cytochrome *c* TsdA, a bifunctional thiosulfate dehydrogenase/tetrathionate reductase. J Biol Chem 291: 24804-24818

[7] Liu Y-W, Denkmann K, Kosciow K et al. (2013) Tetrathionate stimulated growth of *Campylobacter jejuni* identifies TsdA as a new type of bi-functional tetrathionate reductase that is widely distributed in bacteria. Mol Microbiol 88: 173-188

[8] Kurth JM, Butt JN, Kelly DJ et al. (2016) Influence of heme envionment on the catalytic properties of tetrathionate reductase (TsdA) from *Campylobacter jejuni*. Biosci Rep DOI: 10.1042/BSR20160457:

[9] Mowat CG, Rothery E, Miles CS et al. (2004) Octaheme tetrathionate reductase is a respiratory enzyme with novel heme ligation. Nat Struct Mol Biol 11: 1023-1024

[10] Hensel M, Hinsley AP, Nikolaus T et al. (1999) The genetic basis of tetrathionate respiration in *Salmonella typhimurium*. Mol Microbiol 32: 275-287

[11] Grabarczyk DB, Chappell PE, Eisel B et al. (2015) Mechanism of thiosulfate oxidation in the SoxA family of cysteine-ligated cytochromes. J Biol Chem 290: 9209-9221

[12] Müller FH, Bandeiras TM, Urich T et al. (2004) Coupling of the pathway of sulphur oxidation to dioxygen reduction: characterization of a novel membrane-bound thiosulphate:quinone oxidoreductase. Mol Microbiol 53: 1147-1160

Autoren

Julia Kurth

2011 B.Sc. in Biologie an der Universität Bonn, dort Masterstudium Mikrobiologie bis 2013 seitdem Doktorandin am Institut für Mikrobiologie & Biotechnologie, Bonn, 2014-2016 Hoechst Doktorandenstipendium der Aventis Foundation (vergeben von der Stiftung Stipendienfonds des Verbandes der Chemischen Industrie e.V)

Christiane Dahl

Biologiestudium in Bonn, hier 1992 Promotion am Institut für Mikrobiologie & Biotechnologie, 1991 Forschungsaufenthalt Duke University, Durham, NC, USA, 1999 Habilitation Universität Bonn, seitdem Arbeitsgruppenleiterin am Institut für Mikrobiologie & Biotechnologie, Bonn

Korrespondenzadresse

Priv.-Doz. Dr. Christiane Dahl, Institut für Mikrobiologie & Biotechnologie, Rheinische Friedrich-Wilhelms-Universität Bonn, Meckenheimer Allee 168, 53115 Bonn, Tel.: 0228-732119, Fax: 0228-737576, E-Mail: ChDahl@uni-bonn.de

VII. References

Abou Hamdan, A., Dementin, S., Liebgott, P.P., Gutierrez-Sanz, O., Richaud, P., Lacey, A.L. De, *et al.* (2012) Understanding and tuning the catalytic bias of hydrogenase. *J Am Chem Soc* **134**: 8368–8371.

Afonine, P. V., Grosse-Kunstleve, R.W., Echols, N., Headd, J.J., Moriarty, N.W., Mustyakimov, M., *et al.* (2012) Towards automated crystallographic structure refinement with phenix.refine. *Acta Crystallogr* **68**: 352–367.

Alric, J., Tsukatani, Y., Yoshida, M., Matsuura, K., Shimada, K., Hienerwadel, R., *et al.* (2004) Structural and functional characterization of the unusual triheme cytochrome bound to the reaction center of *Rhodovulum sulfidophilum*. *J Biol Chem* **279**: 26090–26097.

Alves, M.N., Neto, S.E., Alves, A.S., Fonseca, B.M., Carrêlo, A., Pacheco, I., *et al.* (2015) Characterization of the periplasmic redox network that sustains the versatile anaerobic metabolism of *Shewanella oneidensis* MR-1. *Front Microbiol* **6**: 665.

Anderson, L.J., Richardson, D.J., and Butt, J.N. (2001) Catalytic protein film voltammetry from a respiratory nitrate reductase provides evidence for complex electrochemical modulation of enzyme activity. *Biochemistry* **40**: 11294–11307.

Appia-Ayme, C., Little, P.J., Matsumoto, Y., Leech, A.P., and Berks, B.C. (2001) Cytochrome complex essential for photosynthetic oxidation of both thiosulfate and sulfide in *Rhodovulum sulfidophilum*. *J Bacteriol* **183**: 6107–6118.

Arai, H., Kawakami, T., Osamura, T., Hirai, T., Sakai, Y., and Ishii, M. (2014) Enzymatic characterization and *in vivo* function of five terminal oxidases in *Pseudomonas aeruginosa*. *J Bacteriol* **196**: 4206–4215.

Armstrong, F.A. (1990) Probing metalloproteins by voltammetry. In *Structure and Bonding*. Springer-Verlag, Berlin. pp. 137–230.

Armstrong, F.A., Butt, J.N., and Sucheta, A. (1993) Voltammetric studies of redox-active centers in metalloproteins adsorbed on electrodes. *Methods Enzymol* **227**: 479–500.

Armstrong, F.A., Heering, H.A., and Hirst, J. (1997) Reaction of complex metalloproteins studied by protein-film voltammetry. *Chem Soc Rev* **26**: 169–179.

Arnold, B. (1999) *Die* c-*Cytochrome von Wolinella succinogenes*. Diplomarbeit, Johann Wolfgang Goethe-Universität Frankfurt.

Arslan, E., Schulz, H., Zufferey, R., Künzler, P., and Thöny-Meyer, L. (1998) Overproduction of the *Bradyrhizobium japonicum c*-type cytochrome subunits of the cbb_3 oxidase in *Escherichia coli*. *Biochem Biophys Res Commun* **251**: 744–747.

Atkinson, S.J., Mowat, C.G., Reid, G.A., and Chapman, S.K. (2007) An octaheme *c*-type cytochrome from *Shewanella oneidensis* can reduce nitrite and hydroxylamine. *FEBS Lett* **581**: 3805–3808.

Aylmore, M.G., and Muir, D.M. (2001) Thiosulfate leaching of gold - a review. *Miner Eng* **14**: 135–174.

Baar, C., Eppinger, M., Raddatz, G., Simon, J., Lanz, C., Klimmek, O., *et al.* (2003) Complete genome sequence and analysis of *Wolinella succinogenes*. *Proc Natl Acad Sci U S A* **100**: 11690–11695.

Babu, M.M., Priya, M.L., Selvan, A.T., Madera, M., Gough, J., Aravind, L., and Sankaran, K. (2006) A database of bacterial lipoproteins (DOLOP) with functional assignments to predicted lipoproteins. *J Bacteriol* **188**: 2761–2773.

Bamford, V.A., Bruno, S., Rasmussen, T., Appia-Ayme, C., Cheesman, M.R., Berks, B.C., and Hemmings, A.M. (2002) Structural basis for the oxidation of thiosulfate by a sulfur cycle enzyme. *EMBO J* **21**: 5599–5610.

Barco, R.A., Emerson, D., Sylvan, J.B., Orcutt, B.N., Jacobson Meyers, M.E., Ramirez, G.A., *et al.* (2015) New insight into microbial iron oxidation as revealed by the proteomic profile of an obligate iron-oxidizing chemolithoautotroph. *Appl Environ Microbiol* **81**: 5927–5937.

Bard, A.J., Parsons, R., and Jordan, J. (1985) *Standard potentials in aqueous solution*. Marcel Dekker, New York.

Barrett, E.L., and Clark, M.A. (1987) Tetrathionate reduction and production of hydrogen sulfide from thiosulfate. *Microbiol Rev* **51**: 192–205.

Barrett, E.L., and Kwan, H.S. (1985) Bacterial reduction of trimethylamine oxide. *Ann Rev Microbiol* **39**: 131–149.

Bartsch, R.G. (1978) Purification of $(4Fe\text{-}4S)^{1\text{-}2\text{-}}$ ferrodoxins (high-potential iron-sulfur proteins) from bacteria. *Methods Enzymol* **53**: 329–340.

Bartsch, R.G. (1991) The distribution of soluble metallo-redox proteins in purple phototrophic bacteria. *Biochim Biophys Acta* **1058**: 28–30.

Beckwith, C.R., Edwards, M.J., Lawes, M., Shi, L., Butt, J.N., Richardson, D.J., and Clarke, T.A. (2015) Characterization of MtoD from *Sideroxydans lithotrophicus*: a cytochrome *c* electron shuttle used in lithoautotrophic growth. *Front Microbiol* **6**: 332.

Bengtsson, J., Rivolta, C., Hederstedt, L., and Karamata, D. (1999) *Bacillus subtilis* contains two small *c*-type cytochromes with homologous heme domains but different types of membrane anchors. *J Biol Chem* **274**: 26179–26184.

Bengtsson, J., Tjalsma, H., Rivolta, C., and Hederstedt, L. (1999) Subunit II of *Bacillus subtilis* cytochrome *c* oxidase is a lipoprotein. *J Bacteriol* **181**: 685–688.

Berry, E.A., and Trumpower, B.L. (1987) Simultaneous determination of hemes *a*, *b*, and *c* from pyridine hemochrome spectra. *Anal Biochem* **161**: 1–15.

Blanc, E., Roversi, P., Vonrhein, C., Flensburg, C., Lea, S.M., and Bricogne, G. (2004) Refinement of severely incomplete structures with maximum likelihood in BUSTER-TNT. *Acta Crystallogr* **60**: 2210–2221.

Blaser, M.J., and Engberg, J. (2008) Clinical aspects of *Campylobacter jejuni* and *Campylobacter coli* infections. In *Campylobacter*. Nachamkin, I., Szymanski, G., and Blaser, M.J. (eds). ASM Press, Washington, DC. pp. 99–121.

Bonora, P., Principi, I., Monti, B., Ciurli, S., Zannoni, D., and Hochkoeppler, A. (1999) On the role of high-potential iron-sulfur proteins and cytochromes in the respiratory chain of two facultative phototrophs. *Biochim Biophys Acta* **1410**: 51–60.

Bradley, J.M., Marritt, S.J., Kihlken, M.A., Haynes, K., Hemmings, A.M., Berks, B.C., *et al.* (2012) Redox and chemical activities of the hemes in the sulfur oxidation pathway enzyme SoxAX. *J Biol Chem* **287**: 40350–40359.

Branca, R.M.M., Bodo, G., Várkonyi, Z., Debreczeny, M., Ősz, J., and Bagyinka, C. (2007) Oxygen and temperature-dependent structural and redox changes in a novel cytochrome c_4 from the purple sulfur photosynthetic bacterium *Thiocapsa roseopersicina*. *Arch Biochem Biophys* **467**: 174–184.

Brito, J.A., Denkmann, K., Pereira, I.A.C., Archer, M., and Dahl, C. (2015) Thiosulfate dehydrogenase (TsdA) from *Allochromatium vinosum*: structural and functional insights into thiosulfate oxidation. *J Biol Chem* **290**: 9222–9238.

Brune, D.C. (1989) Sulfur oxidation by phototrophic bacteria. *Biochim Biophys Acta* **975**: 189–221.

Brüser, T., Trüper, H.G., and Dahl, C. (1997) Cloning and sequencing of the gene encoding the high potential iron-sulfur protein (HiPIP) from the purple sulfur bacterium *Chromatium vinosum*. *Biochim Biophys Acta* **1352**: 18–22.

Chang, H.-Y., Ahn, Y., Pace, L.A., Lin, M.T., Lin, Y.-H., and Gennis, R.B. (2010) The diheme cytochrome c_4 from *Vibrio cholerae* is a natural electron donor to the respiratory cbb_3 oxygen reductase. *Biochemistry* **49**: 7494–7503.

Cheesman, M.R., Little, P.J., and Berks, B.C. (2001) Novel heme ligation in a *c*-type cytochrome involved in thiosulfate oxidation: EPR and MCD of SoxAX from *Rhodovulum sulfidophilum*. *Biochemistry* **40**: 10562–10569.

Chen, V.B., Arendall, W.B., Headd, J.J., Keedy, D.A., Immormino, R.M., Kapral, G.J., *et al.* (2010) MolProbity: All-atom structure validation for macromolecular crystallography. *Acta Crystallogr* **66**: 12–21.

Cheng, J.C., Osborne, G.A., and Stephens, P.J. (1973) Infrared magnetic circular dichroism in the study of metalloproteins. *Nature* **241**: 193–194.

Clark, W.M. (1960) *Oxidation-reduction potentials of organic systems*. Williams & Wilkins, Baltimore.

Cleland, W.W. (1979) Substrate inhibition. *Methods Enzymol* **63**: 500–513.

Cobble, J.W., Stephens, H.P., McKinnon, I.R., and Westrum, E.F. (1972) Thermodynamic properties of oxygenated sulfur complex ions. *Inorg Chem* **11**: 1669–1674.

Cusanovich, M.A., and Bartsch, R.G. (1969) A high potential cytochrome *c* from *Chromatium chromatophores*. *Biochim Biophys Acta* **189**: 245–255.

Dahl, C. (1999) Deposition and oxidation of polymeric sulfur in prokaryotes. In *Biochemical principles and mechanisms of biosynthesis and biodegradation of polymers*. Steinbüchel, A. (ed.). Wiley-VCH, Weinheim. pp. 27–34.

Dahl, C., Engels, S., Pott-Sperling, A.S., Schulte, A., Sander, J., Lübbe, Y., *et al.* (2005) Novel genes of the *dsr* gene cluster and evidence for close interaction of Dsr proteins during sulfur oxidation in the phototrophic sulfur bacterium *Allochromatium vinosum*. *J Bacteriol* **187**: 1392–1404.

Dahl, C., Friedrich, C.G., and Kletzin, A. (2008) Sulfur oxidation in prokaryotes. In *Encyclopedia of Life Sciences*. John Wiley & Sons, Ltd, Chichester.

Dahl, C., and Prange, A. (2006) Bacterial sulfur globules: occurrence, structure and metabolism. In *Inclusions in prokaryotes*. Shively, J.M. (ed.). Springer-Verlag, Heidelberg. pp. 21–51.

Dahl, C., Schulte, A., Stockdreher, Y., Hong, C., Grimm, F., Sander, J., *et al.* (2008) Structural and molecular genetic insight into a widespread sulfur oxidation pathway. *J Mol Biol* **384**: 1287–1300.

Dam, B., Mandal, S., Ghosh, W., Gupta, S.K. Das, and Roy, P. (2007) The S4-intermediate pathway for the oxidation of thiosulfate by the chemolithoautotroph *Tetrathiobacter kashmirensis* and inhibition of tetrathionate oxidation by sulfite. *Res Microbiol* **158**: 330–338.

Dambe, T., Quentmeier, A., Rother, D., Friedrich, C., and Scheidig, A.J. (2005) Structure of the cytochrome complex SoxXA of *Paracoccus pantotrophus*, a heme enzyme initiating chemotrophic sulfur oxidation. *J Struct Biol* **152**: 229–234.

DeLano, W.L. (2002) *The PyMOL molecular graphics system*. DeLano Scientific, San Carlos, California, USA.

Denkmann, K., Grein, F., Zigann, R., Siemen, A., Bergmann, J., van Helmont, S., *et al.* (2012) Thiosulfate dehydrogenase: A widespread unusual acidophilic *c*-type cytochrome. *Environ Microbiol* **14**: 2673–2688.

van Driessche, G., Devreese, B., Fitch, J.C., Meyer, T.E., Cusanovich, M.A., and van Beeumen, J.J. (2006) GHP, a new *c*-type green heme protein from *Halochromatium salexigens* and other proteobacteria. *FEBS J* **273**: 2801–2811.

Drozd, J.W. (1977) Energy conservation in *Thiobacillus neapolitanus* C: sulphide and sulphite oxidation. *J Gen Microbiol* **98**: 309–312.

Du, J., Sono, M., and Dawson, J.H. (2011) The H93G myoglobin cavity mutant as a versatile scaffold for modeling heme iron coordination structures in protein active sites and their characterization with magnetic circular dichroism spectroscopy. *Coord Chem Rev* **255**: 700–716.

Eglinton, D.G., Gadsby, P.M.A., Sievers, G., Peterson, J.I.M., and Thomson, A.J. (1983) A comparative study of the low-temperature magnetic circular dichroism spectra of horse heart metmyoglobin and bovine liver catalase derivatives. *Biochim Biophys Acta* **742**: 648–658.

Eisenthal, R., Danson, M.J., and Hough, D.W. (2007) Catalytic efficiency and k_{cat}/K_M: a useful comparator? *Trends Biotechnol* **25**: 247–249.

Emsley, P., Lohkamp, B., Scott, W.G., and Cowtan, K. (2010) Features and development of Coot. *Acta Crystallogr* **66**: 486–501.

Evans, P. (2006) Scaling and assessment of data quality. *Acta Crystallogr* **62**: 72–82.

Evans, P.R. (2011) An introduction to data reduction: space-group determination, scaling and intensity statistics. *Acta Crystallogr* **67**: 282–292.

Evans, P.R., and Murshudov, G.N. (2013) How good are my data and what is the resolution? *Acta Crystallogr* **69**: 1204–1214.

Fava, A., and Bresadola, S. (1955) Kinetics of the catalytic rearrangement of tetrathionate. *J Am Chem Soc* **77**: 5792–5794.

Feng, D., and van Deventer, J.S.J. (2010) Effect of thiosulphate salts on ammoniacal thiosulphate leaching of gold. *Hydrometallurgy* **105**: 120–126.

Friedrich, C.G., Rother, D., Bardischewsky, F., Quentmeier, A., and Fischer, J. (2001) Oxidation of reduced inorganic sulfur compounds by bacteria: emergence of a common mechanism? *Appl Environ Microbiol* **67**: 2873–2882.

Frigaard, N.-U., and Dahl, C. (2009) Sulfur metabolism in phototrophic sulfur bacteria. *Adv Microb Physiol* **54**: 103–200.

Fruton, J.S. (1934) Oxidation-reduction potentials of ascorbic acid. *J Biol Chem* **105**: 79–85.

Fujiwara, Y., Oka, M., Hamamoto, T., and Sone, N. (1993) Cytochrome *c*-551 of the thermophilic bacterium PS3, DNA sequence and analysis of the mature cytochrome. *Biochim Biophys Acta* **1144**: 213–219.

Fukumori, Y., and Yamanaka, T. (1979) A high-potential nonheme iron protein (HiPIP)-linked, thiosulfate-oxidizing enzyme derived from *Chromatium vinosum*. *Curr Microbiol* **3**: 117–120.

Furne, J., Springfield, J., Koenig, T., DeMaster, E., and Levitt, M.D. (2001) Oxidation of hydrogen sulfide and methanethiol to thiosulfate by rat tissues: a specialized function of the colonic mucosa. *Biochem Pharmacol* **62**: 255–259.

Gadsby, P.M.A., and Thomson, A.J. (1990) Assignment of the axial ligands of ferric ion in low-spin hemoproteins by near-infrared magnetic circular dichroism and electron paramagnetic resonance spectroscopy. *J Am Chem Soc* **112**: 5003–5011.

van Gelder, B.F., and Slater, E.C. (1962) The extinction coefficient of cytochrome *c*. *Biochim Biophys Acta* **58**: 593–595.

Girvan, H.M., Seward, H.E., Toogood, H.S., Cheesman, M.R., Leys, D., and Munro, A.W. (2007) Structural and spectroscopic characterization of P450 BM3 mutants with unprecedented P450 heme iron ligand sets: new heme ligation states influence conformational equilibria in P450 BM3. *J Biol Chem* **282**: 564–572.

Grabarczyk, D.B., Chappell, P.E., Eisel, B., Johnson, S., Lea, S.M., and Berks, B.C. (2015) Mechanism of thiosulfate oxidation in the SoxA family of cysteine-ligated cytochromes. *J Biol Chem* **290**: 9209–9221.

Grein, F., Venceslau, S.S., Schneider, L., Hildebrandt, P., Todorovic, S., Pereira, I.A.C., and Dahl, C. (2010) DsrJ, an essential part of the DsrMKJOP transmembrane complex in the purple sulfur bacterium *Allochromatium vinosum*, is an unusual triheme cytochrome *c*. *Biochemistry* **49**: 8290–8299.

Grosse, A.C., Dicinoski, G.W., Shaw, M.J., and Haddad, P.R. (2003) Leaching and recovery of gold using ammoniacal thiosulfate leach liquors (a review). *Hydrometallurgy* **69**: 1–21.

Hall, M.R., and Berk, R.S. (1972) Thiosulfate oxidase from an *Alcaligenes* grown on mercaptosuccinate. *Can J Microbiol* **18**: 235–245.

Hanahan, D. (1983) Studies on transformation of *Escherichia coli* with plasmids. *J Mol Biol* **166**: 557–580.

Harding, C., Janes, R., and Johnson, D. (2002) *Elements of the P Block*. Royal Society of Chemistry, Cambridge.

Havelaar, A.H., Ivarsson, S., Löfdahl, M., and Nauta, M.J. (2012) Estimating the true incidence of campylobacteriosis and salmonellosis in the European Union, 2009. *Epidemiol Infect* **141**: 293–302.

Hayashi, S., and Wu, H.C. (1990) Lipoproteins in Bacteria. *J Bioenerg Biomembr* **22**: 451–471.

Hensel, M., Hinsley, A.P., Nikolaus, T., Sawers, G., and Berks, B.C. (1999) The genetic basis of tetrathionate respiration in *Salmonella typhimurium*. *Mol Microbiol* **32**: 275–287.

Hensen, D., Sperling, D., Trüper, H.G., Brune, D.C., and Dahl, C. (2006) Thiosulphate oxidation in the phototrophic sulphur bacterium *Allochromatium vinosum*. *Mol Microbiol* **62**: 794–810.

Hermann, B., Kern, M., Pietra, L. La, Simon, J., and Einsle, O. (2015) The octahaem MccA is a haem *c*-copper sulfite reductase. *Nature* **520**: 706–710.

Hexter, S. V, Esterle, T.F., and Armstrong, F.A. (2014) A unified model for surface electrocatalysis based on observations with enzymes. *Phys Chem Chem Phys* **16**: 11822–11833.

Hinojosa-Leon, M., Dubourdieu, M., Sanchez-Crispin, J.A., and Chippaux, M. (1986) Tetrathionate reductase of *Salmonella typhimurium*: a molybdenum containing enzyme. *Biochem Biophys Res Commun* **136**: 577–581.

Hirst, J., Sucheta, A., Ackrell, B.A.C., and Armstrong, F.A. (1996) Electrocatalytic voltammetry of succinate dehydrogenase: direct quantification of the catalytic properties of a complex electron-transport enzyme. *J Am Chem Soc* **118**: 5031–5038.

Hochkoeppler, A., Jenney, F.E., Lang, S.E., Zannoni, D., and Daldal, F. (1995) Membrane-associated cytochrome c_y of *Rhodobacter capsulatus* is an electron carrier from the cytochrome bc_1 complex to the cytochrome *c* oxidase during respiration. *J Bacteriol* **177**: 608–613.

Hochkoeppler, A., Kofod, P., and Zannoni, D. (1995) HiPIP oxido-reductase activity in membranes from aerobically grown cells of the facultative phototroph *Rhodoferax fermentans*. *FEBS Lett* **375**: 197–200.

Holm, L., and Rosenström, P. (2010) Dali server: conservation mapping in 3D. *Nucleic Acids Res* **38**: W545–W549.

Horton, R.M. (1995) PCR-mediated recombination and mutagenesis: SOEing together tailor-made genes. *Mol Biotechnol* **3**: 93–99.

Igarashi, N., Moriyama, H., Fujiwara, T., Fukumuri, Y., and Tanaka, N. (1997) The 2.8 Å structure of hydroxylamine oxidoreductase from a nitrifying chemoautotrophic bacterium, *Nitrosomonas europaea*. *Nat Struct Biol* **4**: 276–284.

Jacobs, B.C., van Belkum, A., and Endtz, H.P. (2008) Guillain-Barré syndrome and *Campylobacter* infection. In *Campylobacter*. Nachamkin, I., Szymanski, G., and Blaser, M.J. (eds). ASM Press, Washington, DC. pp. 245–261.

Janiczek, O., Zemanova, J., and Mandl, M. (2007) Purification and some properties of thiosulfate dehydrogenase from *Acidithiobacillus ferrooxidans*. *Prep Biochem Biotechnol* **37**: 101–111.

Jones, C.W. (1982) *Bacterial respiration and photosynthesis*. Thomas Nelson and Sons, Ltd., Walton-on-Thames.

Kabsch, W. (2010) XDS. *Acta Crystallogr* **66**: 125–132.

Kämpf, C., and Pfennig, N. (1980) Capacity of Chromatiaceae for chemotrophic growth. Specific respiration rates of *Thiocystis violacea* and *Chromatium vinosum*. *Arch Microbiol* **127**: 125–135.

Kappler, U., Aguey-Zinsou, K.-F., Hanson, G.R., Bernhardt, P. V., and McEwan, A.G. (2004) Cytochrome c_{551} from *Starkeya novella*: characterization, spectroscopic properties, and phylogeny of a diheme protein of the SoxAX family. *J Biol Chem* **279**: 6252–6260.

Kappler, U., Bernhardt, P. V., Kilmartin, J., Riley, M.J., Teschner, J., McKenzie, K.J., and Hanson, G.R. (2008) SoxAX cytochromes, a new type of heme copper protein involved in bacterial energy generation from sulfur compounds. *J Biol Chem* **283**: 22206–22214.

Kappler, U., and Maher, M.J. (2013) The bacterial SoxAX cytochromes. *Cell Mol life Sci* **70**: 977–992.

Kaprálek, F. (1972) The physiological role of tetrathionate respiration in growing *Citrobacter*. *J Gen Microbiol* **71**: 133–139.

Karplus, P.A., and Diederichs, K. (2012) Linking crystallographic model and data quality. *Science* **336**: 1030–1033.

Kashino, Y., Inoue-Kashino, N., Roose, J.L., and Pakrasi, H.B. (2006) Absence of the PsbQ protein results in destabilization of the PsbV protein and decreased oxygen evolution activity in cyanobacterial photosystem II. *J Biol Chem* **281**: 20834–20841.

Kennel, S.J., Bartsch, R.G., and Kamen, M.D. (1972) Observations on light-induced oxidation reactions in the electron transport system of *Chromatium*. *Biophys J* **12**: 882–896.

Kern, M., Eisel, F., Scheithauer, J., Kranz, R.G., and Simon, J. (2010) Substrate specificity of three cytochrome *c* haem lyase isoenzymes from *Wolinella succinogenes*: unconventional haem *c* binding motifs are not sufficient for haem *c* attachment by NrfI and CcsA1. *Mol Microbiol* **75**: 122–137.

Kern, M., Klotz, M.G., and Simon, J. (2011) The *Wolinella succinogenes mcc* gene cluster encodes an unconventional respiratory sulphite reduction system. *Mol Microbiol* **82**: 1515–1530.

Kern, M., and Simon, J. (2009) Electron transport chains and bioenergetics of respiratory nitrogen metabolism in *Wolinella succinogenes* and other Epsilonproteobacteria. *Biochim Biophys Acta* **1787**: 646–656.

Kikumoto, M., Nogami, S., Kanao, T., Takada, J., and Kamimura, K. (2013) Tetrathionate-forming thiosulfate dehydrogenase from the acidophilic, chemolithoautotrophic bacterium *Acidithiobacillus ferrooxidans*. *Appl Environ Microbiol* **79**: 113–120.

Kilmartin, J.R., Maher, M.J., Krusong, K., Noble, C.J., Hanson, G.R., Bernhardt, P. V., *et al.* (2011) Insights into structure and function of the active site of SoxAX cytochromes. *J Biol Chem* **286**: 24872–24881.

Klimmek, O., Dietrich, W., Dancea, F., Lin, Y.-J., Pfeiffer, S., Löhr, F., *et al.* (2004) Sulfur respiration. In *Respiration in Archaea and Bacteria*. Zannoni, D. (ed.). Springer, Dordrecht. pp. 217–232.

Klimmek, O., Kröger, A., Steudel, R., and Holdt, G. (1991) Growth of *Wolinella succinogenes* with polysulphide as terminal acceptor of phosphorylative electron transport. *Arch Microbiol* **155**: 177–182.

Knobloch, K., Schmitt, W., Schleifer, G., Appelt, N., and Müller, H. (1981) On the enzymatic system thiosulfate-cytochrome *c*-oxidoreductase. In *Biology of Inorganic Nitrogen and Sulfur*. Bothe, H., and Trebst, A. (eds). Springer-Verlag, Berlin. pp. 359–365.

Kröger, A., Biel, S., Simon, J., Gross, R., Unden, G., and Lancaster, C.R.D. (2002) Fumarate respiration of *Wolinella succinogenes*: enzymology, energetics and coupling mechanism. *Biochim Biophys Acta* **1553**: 23–38.

Kurek, E.J. (1985) Properties of an enzymatic complex active in sulfite and thiosulfate oxidation by *Rhodotorula sp*. *Arch Microbiol* **143**: 277–282.

Kurth, J.M., Brito, J.A., Reuter, J., Flegler, A., Koch, T., Franke, T., *et al.* (2016) Electron accepting units of the diheme cytochrome *c* TsdA, a bifunctional thiosulfate dehydrogenase/tetrathionate reductase. *J Biol Chem* **291**: 24804–24818.

Kurth, J.M., Butt, J.N., Kelly, D.J., and Dahl, C. (2016) Influence of heme environment on the catalytic properties of the tetrathionate reductase TsdA from *Campylobacter jejuni*. *Biosci Rep* **36**: e00422.

Kurth, J.M., Dahl, C., and Butt, J.N. (2015) Catalytic protein film electrochemistry provides a direct measure of the tetrathionate/thiosulfate reduction potential. *J Am Chem Soc* **137**: 13232–13235.

Kurth, J.M., Schuster, A., Seel, W., Herresthal, S., Simon, J., and Dahl, C. (2016) TsdC, a unique lipoprotein from *Wolinella succinogenes* that enhances tetrathionate reductase activity of TsdA. *FEMS Microbiol Lett* **submitted**.

Kusai, K., and Yamanaka, T. (1973) The oxidation mechanisms of thiosulphate and sulphide in *Chlorobium thiosulphatophilum*: roles of cytochrome c_{551} and cytochrome c_{553}. *Biochim Biophys Acta* **325**: 304–314.

Kyhse-Andersen, J. (1984) Electroblotting of multiple gels: a simple apparatus without buffer tank for rapid transfer of proteins from polycrylamide to nitrocellulose. *J Biochem Biophys Methods* **10**: 203–209.

La Fortelle, E. de, and Bricogne, G. (1997) Maximum-likelihood heavy-atom parameter refinement for multiple isomorphous replacement multiwavelength anomalous diffraction methods. *Methods Enzymol* **276**: 472–494.

Laemmli, U.K. (1970) Cleavage of structural proteins during the assembly of the head of bacteriophage T4. *Nature* **227**: 680–685.

Latimer, W.M. (1952) *Oxidation potentials*. 2nd ed., Prentice-Hall, New York.

Léger, C., Jones, A.K., Albracht, S.P.J., and Armstrong, F.A. (2002) Effect of a dispersion of interfacial electron transfer rates on steady state catalytic electron transport in [NiFe]-hydrogenase and other enzymes. *J Phys Chem* **106**: 13058–13063.

Lieutaud, C., Nitschke, W., Verméglio, A., Parot, P., and Schoepp-Cothenet, B. (2003) HiPIP in *Rubrivivax gelatinosus* is firmly associated to the membrane in a conformation efficient for electron transfer towards the photosynthetic reaction centre. *Biochim Biophys Acta* **1557**: 83–90.

Liu, Y.W., Denkmann, K., Kosciow, K., Dahl, C., and Kelly, D.J. (2013) Tetrathionate stimulated growth of *Campylobacter jejuni* identifies a new type of bi-functional tetrathionate reductase (TsdA) that is widely distributed in bacteria. *Mol Microbiol* **88**: 173–188.

Liu, Y.W., and Kelly, D.J. (2015) Cytochrome *c* biogenesis in *Campylobacter jejuni* requires cytochrome c_6 (CccA; Cj1153) to maintain apocytochrome cysteine thiols in a reduced state for haem attachment. *Mol Microbiol* **96**: 1298–1317.

Lovell, S.C., Davis, I.W., Adrendall, W.B., Bakker, P.I.W. de, Word, J.M., Prisant, M.G., *et al.* (2003) Structure validation by C_α geometry: Φ, Ψ and C_β deviation. *Proteins* **50**: 437–450.

Lu, W.-P., and Kelly, D.P. (1988) Cellular location and partial purification of the “thiosulphate-oxidizing enzyme” and “trithionate hydrolyase” from *Thiobacillus tepidarius*. *J Gen Microbiol* **134**: 877–885.

Lyric, R.M., and Suzuki, I. (1970) Enzymes involved in the metabolism of thiosulfate by *Thiobacillus thioparus*. III. Properties of thiosulfate-oxidizing enzyme and proposed pathway of thiosulfate oxidation. *Can J Biochem* **48**: 355–363.

Marritt, S.J., Kemp, G.L., Xiaoe, L., Durrant, J.R., Cheesman, M.R., and Butt, J.N. (2008) Spectroelectrochemical characterization of a pentaheme cytochrome in solution and as electrocatalytically active films on nanocrystalline metal-oxide electrodes. *J Am Chem Soc* **130**: 8588–8589.

Mason, J., and Kelly, D.P. (1988) Thiosulfate oxidation by obligately heterotrophic bacteria. *Microb Ecol* **15**: 123–134.

Masuda, K., Matsuyama, S., and Tokuda, H. (2002) Elucidation of the function of lipoprotein-sorting signals that determine membrane localization. *Proc Natl Acad Sci USA* **99**: 7390–7395.

Matsuyama, S., Tajima, T., and Tokuda, H. (1995) A novel periplasmic carrier protein involved in the sorting and transport of *Escherichia coli* lipoproteins destined for the outer membrane. *EMBO J* **14**: 3365–3372.

Matsuyama, S.I., Yokota, N., and Tokuda, H. (1997) A novel outer membrane lipoprotein, LolB (HemM), involved in the LolA (p20)-dependent localization of lipoproteins to the outer membrane of *Escherichia coli*. *EMBO J* **16**: 6947–6955.

Matthews, B.W. (1968) Solvent content of protein crystals. *J Mol Biol* **33**: 491–497.

Mel, H.C., Hugus, Z.Z., and Latimer, W.M. (1956) The thermodynamics of thiosulfate ion. *J Am Chem Soc* **78**: 1822–1826.

Meulenberg, R., Pronk, J.T., Hazeu, W., van Dijken, J.P., Frank, J., Bos, P., and Kuenen, J.G. (1993) Purification and partial characterization of thiosulphate dehydrogenase from *Thiobacillus acidophilus*. *J Gen Microbiol* **139**: 2033–2039.

Meyer, B., Imhoff, J.F., and Kuever, J. (2007) Molecular analysis of the distribution and phylogeny of the *soxB* gene among sulfur-oxidizing bacteria – evolution of the Sox sulfur oxidation enzyme system. *Environ Microbiol* **9**: 2957–2977.

Miki, K., and Lin, E.C.C. (1975) Anaerobic energy-yielding reaction associated with transhydrogenation from glycerol 3-phosphate to fumarate by an *Escherichia coli* system. *J Bacteriol* **124**: 1282–1287.

Miles, C.S., Manson, F.D.C., Reid, G.A., and Chapman, S.K. (1993) Substitution of a haem-iron axial ligand in flavocytochrome b_2. *Biochim Biophys Acta* **1202**: 82–86.

Miroux, B., and Walker, J.E. (1996) Over-production of proteins in *Escherichia coli*: mutant hosts that allow synthesis of some membrane proteins and globular proteins at high levels. *J Mol Biol* **260**: 289–298.

Moore, G., and Pettigrew, G.W. (1990) *Cytochromes* c*: evolutionary, structural and physicochemical aspects*. Springer-Verlag, Heidelberg.

Mowat, C.G., Rothery, E., Miles, C.S., McIver, L., Doherty, M.K., Drewette, K., *et al.* (2004) Octaheme tetrathionate reductase is a respiratory enzyme with novel heme ligation. *Nat Struct Mol Biol* **11**: 1023–1024.

Müller, F.H., Bandeiras, T.M., Urich, T., Teixeira, M., Gomes, C.M., and Kletzin, A. (2004) Coupling of the pathway of sulphur oxidation to dioxygen reduction: characterization of a novel membrane-bound thiosulphate:quinone oxidoreductase. *Mol Microbiol* **53**: 1147–1160.

Nagashima, K.V.P., Matsuura, K., Shimada, K., and Verméglio, A. (2002) High-potential iron-sulfur protein (HiPIP) is the major electron donor to the reaction center complex in photosynthetically growing cells of the purple bacterium *Rubrivivax gelatinosus*. *Biochemistry* **41**: 14028–14032.

Nakamura, K., Nakamura, M., Yoshikawa, H., and Amano, Y. (2001) Purification and properties of thiosulfate dehydrogenase from *Acidithiobacillus thiooxidans* JCM7814. *Biosci Biotechnol Biochem* **65**: 102–108.

Nakayama, H., Kurokawa, K., and Lee, B.L. (2012) Lipoproteins in bacteria: Structures and biosynthetic pathways. *FEBS J* **279**: 4247–4268.

Newell, D.G., McBride, H., and Pearson, A.D. (1984) The identification of outer membrane proteins and flagella of *Campylobacter jejuni*. *J Gen Microbiol* **130**: 1201–1208.

Nissum, M., Karlsson, J.-J., Ulstrup, J., Jensen, P.W., and Smulevich, G. (1997) Resonance raman characterization of the di-heme protein cytochrome c_4 from *Pseudomonas stutzeri*. *J Biol Inorg Chem* **2**: 302–307.

Oelkers, E.H., Helgeson, H.C., Shock, E.L., Sverjensky, D.A., Johnson, J.W., and Pokrovskii, V.A. (1995) Summary of the apparent standard partial molal Gibbs free energies of formation of aqueous species, minerals, and gases at pressures 1 to 5000 bars and temperatures 25 to 1000 °C. *J Phys Chem Ref Data* **24**: 1401–1560.

Ohmine, M., Matsuura, K., Shimada, K., Alric, J., Verméglio, A., and Nagashima, K.V.P. (2009) Cytochrome c_4 can be involved in the photosynthetic electron transfer system in the purple bacterium *Rubrivivax gelatinosus*. *Biochemistry* **48**: 9132–9139.

Oltmann, L.F., Claassen, V.P., Kastelein, P., Reijnders, W.N.M., and Stouthamer, A.H. (1979) Influence of tungstate on the formation and activities of four reductases in *Proteus mirabilis*. Identification of two new molybdo-enzymes: chlorate reductase and tetrathionate reductase. *FEBS Lett* **106**: 43–46.

Oltmann, L.F., Schoenmaker, G.S., and Stouthamer, A.H. (1974) Solubilization and purification of a cytoplasmic membrane bound enzyme catalyzing tetrathionate and thiosulphate reduction in *Proteus mirabilis*. *Arch Microbiol* **98**: 19–30.

Oltmann, L.F., and Stouthamer, A.H. (1975) Reduction of tetrathionate, trithionate and thiosulphate, and oxidation of sulphide in *Proteus mirabilis*. *Arch Microbiol* **105**: 135–142.

Papavassiliou, J., Samaraki-Lyberopoulou, V., and Piperakis, G. (1969) Production of tetrathionate reductase by *Salmonella*. *Can J Microbiol* **15**: 238–240.

Parkin, A., Seravalli, J., Vincent, K.A., Ragsdale, S.W., and Armstrong, F.A. (2007) Rapid and efficient electrocatalytic CO_2/CO interconversions by *Carboxydothermus hydrogenoformans* CO dehydrogenase I on an electrode. *J Am Chem Soc* **129**: 10328–10329.

Pichinoty, F., and Bigliardi-Rouvier, J. (1962) Etude et mise au point d'une methode permettant de mesurer l'activite des tetrathionate-reductases d'origine bacterienne. Inhibition par l'oxygene de la biosynthese et de l'activite de l'enzyme d'*Escherichia intermedia*. *Antonie van Leeuwenhoek* **28**: 134–140.

Pichinoty, F., and Bigliardi-Rouvier, J. (1963) Recherches sur la tétrathionate-réductase d'une bactérie anaérobie facultative. *Biochim Biophys Acta* **67**: 366–378.

Pires, R.H., Venceslau, S.S., Morais, F., Teixeira, M., Xavier, A. V., and Pereira, I.A.C. (2006) Characterization of the *Desulfovibrio desulfuricans* ATCC 27774 DsrMKJOP complex - a membrane-bound redox complex involved in the sulfate respiratory pathway. *Biochemistry* **45**: 249–262.

Pittman, M.S., Elvers, K.T., Lee, L., Jones, M.A., Poole, R.K., Park, S.F., and Kelly, D.J. (2007) Growth of *Campylobacter jejuni* on nitrate and nitrite: electron transport to NapA and NrfA via NrfH and distinct roles for NrfA and the globin Cgb in protection against nitrosative stress. *Mol Microbiol* **63**: 575–590.

Podgorsek, L., and Imhoff, J.F. (1999) Tetrathionate production by sulfur oxidizing bacteria and the role of tetrathionate in the sulfur cycle of baltic sea sediments. *Aquat Microb Ecol* **17**: 255–265.

Pollock, M.R., and Knox, R. (1943) Bacterial reduction of tetrathionate. *Biochem J* **37**: 476–481.

Pollock, M.R., Knox, R., and Gell, P.G.H. (1942) Bacterial reduction of tetrathionate. *Nature* **150**: 94.

Postgate, J.R. (1951) The reduction of sulphur compounds by *Desulphovibrio desulphuricans*. *J Gen Microbiol* **5**: 725–738.

Pourbaix, M., and Pourbaix, A. (1992) Potential-pH equilibrium diagrams for the system S-H_2O from 25 to 150°C: influence of access of oxygen in sulphide solutions. *Geochim Cosmochim Acta* **56**: 3157–3178.

Price-Carter, M., Tingey, J., Bobik, T.A., and Roth, J.R. (2001) The alternative electron acceptor tetrathionate supports B12-dependent anaerobic growth of *Salmonella enterica* serovar Typhimurium on ethanolamine or 1,2-propanediol. *J Bacteriol* **183**: 2463–2475.

Rawlings, J., Stephens, P.J., Nafie, L.A., and Kamen, M.D. (1977) Near-infrared magnetic circular dichroism of cytochrome *c*'. *Biochemistry* **16**: 1725–1729.

Reedy, C.J., Elvekrog, M.M., and Gibney, B.R. (2008) Development of a heme protein structure - Electrochemical function database. *Nucleic Acids Res* **36**: 307–313.

Reedy, C.J., and Gibney, B.R. (2004) Heme Protein Assemblies. *Chem Rev* **104**: 617–649.

Reijerse, E.J., Sommerhalter, M., Hellwig, P., Quentmeier, A., Rother, D., Laurich, C., *et al.* (2007) The unusal redox centers of SoxXA, a novel *c*-type heme-enzyme essential for chemotrophic sulfur-oxidation of *Paracoccus pantotrophus*. *Biochemistry* **46**: 7804–7810.

Reuter, M., and van Vliet, A.H.M. (2013) Signal balancing by the CetABC and CetZ chemoreceptors controls energy taxis in *Campylobacter jejuni*. *PLoS One* **8**: e54390.

Roose, J.L., Kashino, Y., and Pakrasi, H.B. (2007) The PsbQ protein defines cyanobacterial Photosystem II complexes with highest activity and stability. *Proc Natl Acad Sci U S A* **104**: 2548–2553.

Roy, A.B., and Trudinger, P.A. (1970) *The biochemistry of inorganic compounds of sulphur*. Cambridge University Press, Cambridge.

Schägger, H., Cramer, W.A., and Vonjagow, G. (1994) Analysis of molecular masses and oligomeric states of protein complexes by blue native electrophoresis and isolation of membrane protein complexes by two-dimensional native electrophoresis. *Anal Biochem* **217**: 220–230.

Schägger, H., and von Jagow, G. (1991) Blue native electrophoresis for isolation of membrane protein complexes in enzymatically active form. *Anal Biochem* **199**: 223–231.

Schleifer, G., Schmitt, W., and Knobloch, K. (1981) The enzymatic system thiosulfate:cytochrome *c* oxidoreductase from photolithoautotrophically grown *Rhodopseudomonas palustris*. *Arch Microbiol* **130**: 328–333.

Schmitt, W., Schleifer, G., and Knobloch, K. (1981) The enzymatic system thiosulfate:cytochrome *c* oxidoreductase from photolithoautotrophically grown *Chromatium vinosum*. *Arch Microbiol* **130**: 334–338.

Schnorf, U. (1966) *Der Einfluß von Substituenten auf Redoxpotential und Wuchsstoffeigenschaften von Chinonen*. ETH, Zürich.

Schook, L.B., and Berk, R.S. (1979) Partial purification and characterization of thiosulfate oxidase from *Pseudomonas aeruginosa*. *J Bacteriol* **140**: 306–308.

Schumacher, W., Kroneck, P.M.H., and Pfennig, N. (1992) Comparative systematic study on "Spirillum" 5175, *Campylobacter* and *Wolinella* species. *Arch Microbiol* **158**: 287–293.

Segel, I.H. (1993) *Enzyme kinetics: behavior and analysis of rapid equilibrium and steady-state enzyme systems*. Wiley-Interscience, New York.

Sellars, M.J., Hall, S.J., and Kelly, D.J. (2002) Growth of *Campylobacter jejuni* supported by respiration of fumarate, nitrate, nitrite, trimethylamine-N-oxide, or dimethyl sulfoxide requires oxygen. *J Bacteriol* **184**: 4187–4196.

Sievert, S.M., Heidorn, T., and Kuever, J. (2000) *Halothiobacillus kellyi* sp. nov., a mesophilic obligately chemolithoautotrophic, sulfur-oxidizing bacterium isolated from a shallow-water hydrothermal vent in the Aegean Sea, and emended description of the genus *Halothiobacillus*. *Int J Syst Evol Microbiol* **50**: 1229–1237.

Silver, M., and Lundgren, D.G. (1968) The thiosulfate-oxidizing enzyme of *Ferrobacillus ferrooxidans* (*Thiobacillus ferrooxidans*). *Can J Biochem* **46**: 1215–1220.

Simon, J. (2002) Enzymology and bioenergetics of respiratory nitrite ammonification. *FEMS Microbiol Rev* **26**: 285–309.

Simon, J., Einsle, O., Kroneck, P.M.H., and Zumft, W.G. (2004) The unprecedented *nos* gene cluster of *Wolinella succinogenes* encodes a novel respiratory electron transfer pathway to cytochrome *c* nitrous oxide reductase. *FEBS Lett* **569**: 7–12.

Simon, J., Kern, M., Hermann, B., Einsle, O., and Butt, J.N. (2011) Physiological function and catalytic versatility of bacterial multihaem cytochromes *c* involved in nitrogen and sulfur cycling. *Biochem Soc Trans* **39**: 1864–1870.

Simpkin, D., Palmer, G., Devlin, F.J., McKenna, M.C., Jensen, G.M., and Stephens, P.J. (1989) The axial ligands of heme in cytochromes: a near-infrared magnetic circular dichroism study of yeast cytochromes *c*, c_1, and *b* and spinach cytochrome *f*. *Biochemistry* **28**: 8033–8039.

Smith, A.J. (1966) The role of tetrathionate in the oxidation of thiosulphate by *Chromatium* sp. strain D. *J Gen Microbiol* **42**: 371–380.

Sorokin, D.Y. (1970) Experimental investigation of the rate and mechanism of oxidation of hydrogen sulfide in the Black Sea using S-35. *Oceanology* **10**: 37–46.

Sorokin, D.Y. (1992) Oxidation of thiosulfate to tetrathionate by heterotrophic bacteria from aquatic environments. *Microbiology* **61**: 524–529.

Sorokin, D.Y. (1996) Oxidation of sulfide and elemental sulfur to tetrathionate by chemoorganoheterotrophic bacteria. *Microbiology* **65**: 1–5.

Sorokin, D.Y., Lysenko, A.M., and Mityushina, L.L. (1996) Isolation and characterization of alkaliphilic chemoorganoheterotrophic bacteria oxidizing reduced inorganic sulfur compounds to tetrathionate. *Microbiology* **65**: 326–338.

Sorokin, D.Y., Teske, A., Robertson, L.A., and Kuenen, J.G. (1999) Anaerobic oxidation of thiosulfate to tetrathionate by obligately heterotrophic bacteria, belonging to the *Pseudomonas stutzeri* group. *FEMS Microbiol Ecol* **30**: 113–123.

Sorokin, D.Y., Tourova, T.P., and Muyzer, G. (2005) Oxidation of thiosulfate to tetrathionate by an haloarchaeon isolated from hypersaline habitat. *Extremophiles* **9**: 501–504.

Starkey, R.L. (1950) Relations of microorganisms to transformations of sulfur in soils. *Soil Sci* **70**: 55–65.

Stephens, P.J., Sutherland, J.C., Cheng, J.C., and Eaton, W.A. (1976) *The excited states of biological molecules*. Wiley, New York.

Suga, M., Lai, T.L., Sugiura, M., Shen, J.R., and Boussac, A. (2013) Crystal structure at 1.5 Å resolution of the PsbV2 cytochrome from the cyanobacterium *Thermosynechococcus elongatus*. *FEBS Lett* **587**: 3267–3272.

Tanner, A.C.R., Badger, S., Lai, C.-H., Listgarten, M.A., Visconti, R.A., and Socransky, S.S. (1981) *Wolinella* gen. nov., *Wolinella succinogenes* (*Vibrio succinogenes* Wolin et al.) comb. nov., and description of *Bacteroides gracilis* sp. nov., *Wolinella recta* sp. nov., *Campylobacter concisus* sp. nov., and *Eikenella corrodens* from humans with periodontal disease. *Int J Syst Bacteriol* **31**: 432–445.

Taylor, P., Pealing, S.L., Reid, G.A., Chapman, S.K., and Walkinshaw, M.D. (1999) Structural and mechanistic mapping of a unique fumarate reductase. *Nat Struct Biol* **6**: 1108–1112.

Thauer, R.K., Jungermann, K., and Decker, K. (1977) Energy conservation in chemotrophic anaerobic bacteria. *Bacteriol Rev* **41**: 100–180.

Then, J., and Trüper, H.G. (1981) The role of thiosulfate in sulfur metabolism of *Rhodopseudomonas globiformis*. *Arch Microbiol* **130**: 143–146.

Thomas, P.E., Ryan, D., and Levin, W. (1976) An improved staining procedure for the detection of the peroxidase activity of cytochrome P-450 on sodium dodecyl sulfate polyacrylamide gels. *Anal Biochem* **75**: 168–176.

Tilton, R.C., Cobet, A.B., and Jones, G.E. (1967) Marine thiobacilli. I. Isolation and distribution. *Can J Microbiol* **13**: 1521–1528.

Trudinger, P.A. (1961) Thiosulphate oxidation and cytochromes in *Thiobacillus X*. 2. Thiosulphate-oxidizing enzyme. *Biochem J* **78**: 680–686.

Trudinger, P.A. (1967) Metabolism of thiosulfate and tetrathionate by heterotrophic bacteria from soil. *J Bacteriol* **93**: 550–559.

Tuttle, J.H. (1980) Thiosulfate oxidation and tetrathionate reduction by intact cells of marine pseudomonad strain 16B. *Appl Environ Microbiol* **39**: 1159–1166.

Tuttle, J.H., and Jannasch, H.W. (1972) Occurence and types of *Thiobacillus*-like bacteria in the sea. *Limnol Oceanogr* **17**: 532–543.

Tuttle, J.H., and Jannasch, H.W. (1973a) Sulfide and thiosulfate-oxidizing bacteria in anoxic marine basins. *Mar Biol* **20**: 64–70.

Tuttle, J.H., and Jannasch, H.W. (1973b) Dissimilatory reduction of inorganic sulfur by facultatively anaerobic marine bacteria. *J Bacteriol* **115**: 732–737.

Tuttle, J.H., and Jannasch, H.W. (1976) Microbial utilization of thiosulfate in the deep sea. *Limnol Oceanogr* **21**: 697–701.

Tuttle, J.H., Schwartz, J.H., and Whited, G.M. (1983) Some properties of thiosulfate-oxidizing enzyme from marine heterotroph 16B. *Appl Environ Microbiol* **46**: 438–445.

Urban, P.J. (1961) Colorimetry of sulphur anions. I. An improved colorimetric method for the determination of thiosulphate. *Z Anal Chem* **179**: 415–422.

Varga, D., Horváth, A.K., and Nagypál, I. (2006) Unexpected formation of higher polythionates in the oxidation of thiosulfate by hypochlorous acid in a slightly acidic medium. *J Phys Chem B* **110**: 2467–2470.

Verméglio, A., Li, J., Schoepp-Cothenet, B., Pratt, N., and Knaff, D.B. (2002) The role of high-potential iron protein and cytochrome c_8 as alternative electron donors to the reaction center of *Chromatium vinosum*. *Biochemistry* **41**: 8868–8875.

Vincent, K.A., Tilley, G.J., Quammie, N.C., Streeter, I., Burgess, B.K., Cheesman, M.R., and Armstrong, F.A. (2003) Instantaneous, stoichiometric generation of powerfully reducing states of protein active sites using Eu(II) and polyaminocarboxylate ligands. *Chem Commun* 2590–2591.

Visser, J.M., Jong, G.A.H. de, Robertson, L.A., and Kuenen, J.G. (1997) Purification and characterization of a periplasmic thiosulfate dehydrogenase from the obligately autotrophic *Thiobacillus* sp. W5. *Arch Microbiol* **166**: 372–378.

Vonrhein, C., Blanc, E., Roversi, P., and Bricogne, G. (2007) Automated structure solution with autoSHARP. *Methods Mol Biol* **364**: 215–230.

Vonrhein, C., Flensburg, C., Keller, P., Sharff, A., Smart, O., Paciorek, W., *et al.* (2011) Data processing and analysis with the autoPROC toolbox. *Acta Crystallogr* **67**: 293–302.

Wagman, D.D., Evans, W.H., Parker, V.B., Schumm, R.H., Halow, I., Bailey, S.M., *et al.* (1982) The NBS tables of chemical thermodynamic properties: selected values for inorganic and C_1 and C_2 organic substances in SI units. *Phys Chem Ref Data* **11**: Supplement No. 2, 2.1-2.392.

Wang, W.-H., Lu, J.-X., Yao, P., Xie, Y., and Huang, Z.-X. (2003) The distinct heme coordination environments and heme-binding stabilities of His39Ser and His39Cys mutants of cytochrome b_5. *Protein Eng* **16**: 1047–1054.

Weingarten, R.A., Taveirne, M.E., and Olson, J.W. (2009) The dual-functioning fumarate reductase is the sole succinate:quinone reductase in *Campylobacter jejuni* and is required for full host colonization. *J Bacteriol* **191**: 5293–5300.

Weyer, K.A., Lottspeich, F., Gruenberg, H., Lang, F., Oesterhelt, D., and Michel, H. (1987) Amino acid sequence of the cytochrome subunit of the photosynthetic reaction centre from the purple bacterium *Rhodopseudomonas viridis*. *Embo J* **6**: 2197–2202.

Whited, G.M., and Tuttle, J.H. (1983) Separation and distribution of thiosulfate-oxidizing enzyme, tetrathionate reductase, and thiosulfate reductase in extracts of marine heterotroph strain 16B. *J Bacteriol* **156**: 600–610.

Williamson, M.A., and Rimstidt, J.D. (1992) Correlation between structure and thermodynamic properties of aqueous sulfur species. *Geochim Cosmochim Acta* **56**: 3867–3880.

Winter, S.E., Thiennimitr, P., Winter, M.G., Butler, B.P., Huseby, D.L., Crawford, R.W., *et al.* (2010) Gut inflammation provides a respiratory electron acceptor for *Salmonella*. *Nature* **467**: 426–429.

Wolin, M.J., Wolin, E.A., and Jacobs, N.J. (1961) Cytochrome-producing anaerobic *Vibrio succinogenes*, sp. n. *J Bacteriol* **81**: 911–917.

Wood, P.M. (1981) The redox potential for dimethyl sulphoxide reduction to dimethyl sulphide. *FEBS Lett* **124**: 11–14.

Xu, L., and Horváth, A.K. (2014) A possible candidate to be classified as an autocatalysis-driven clock reaction: kinetics of the pentathionate−iodate reaction. *J Phys Chem A* **118**: 6171–6180.

Yakushi, T., Masuda, K., Narita, S., Matsuyama, S., and Tokuda, H. (2000) A new ABC transporter mediating the detachment of lipid-modified proteins from membranes. *Nat Cell Biol* **2**: 212–218.

Zahn, J.A., Arciero, D.M., Hooper, A.B., and Dispirito, A.A. (1996) Cytochrome *c*' of *Methylococcus capsulatus* Bath. *Eur J Biochem* **240**: 684–691.

Zehnder, A.J., and Wuhrmann, K. (1976) Titanium (III) citrate as a nontoxic oxidation-reduction buffering system for the culture of obligate anaerobes. *Science* **194**: 1165–1166.

Zhang, H., and Jeffrey, M.I. (2010) A kinetic study of rearrangement and degradation reactions of tetrathionate and trithionate in near-neutral solutions. *Inorg Chem* **49**: 10273–10282.

Zopfi, J., Ferdelman, T.G., and Fossing, H. (2004) Thiosulfate, and elemental sulfur in marine sediments. *Geol Soc Am* **379**: 97–116.

Zu, Y., Shannon, R.J., and Hirst, J. (2003) Reversible, electrochemical interconversion of NADH and NAD^+ by the catalytic (Iλ) subcomplex of mitochondrial NADH:Ubiquinone oxidoreductase (complex I). *J Am Chem Soc* **125**: 6020–6021.

VIII. List of Publications

Kurth, J.M., Brito, J.A., Reuter, J., Flegler, A., Koch, T., Franke, T., Klein E.-M., Rowe S.F., Butt J.N., Denkmann K., Pereira I.A.C., Archer M., Dahl C. (2016) Electron accepting units of the diheme cytochrome *c* TsdA, a bifunctional thiosulfate dehydrogenase/tetrathionate reductase. *J Biol Chem* **291**: 24804–24818.

Kurth, J.M., Butt, J.N., Kelly, D.J., and Dahl, C. (2016) Influence of heme environment on the catalytic properties of the tetrathionate reductase TsdA from *Campylobacter jejuni*. *Biosci Rep* **36**: e00422.

Kurth, J.M., Dahl, C., and Butt, J.N. (2015) Catalytic protein film electrochemistry provides a direct measure of the tetrathionate/thiosulfate reduction potential. *J Am Chem Soc* **137**: 13232–13235.

Kurth, J.M., Schuster, A., Seel, W., Herresthal, S., Simon, J., and Dahl, C. (2016) TsdC, a unique lipoprotein from *Wolinella succinogenes* that enhances tetrathionate reductase activity of TsdA. *FEMS Microbiol Lett* **364**: fnx003.

Kurth, J.M. and Dahl, C. (2017): Ein altes Paar in neuem Glanz: Thiosulfat und Tetrathionat. *BIOspektrum* **23**: 25-27.